UNIVERSITY OF
BIRMINGHAM

MILLING/ROUTING OF CARBON FIBRE REINFORCED PLASTIC (CFRP) COMPOSITES

by

MOHAMED HASSAN EL-HOFY

A thesis submitted to
The University of Birmingham
For the degree of
DOCTOR OF PHILOSOPHY

School of Mechanical Engineering
College of Engineering and Physical Sciences
University of Birmingham
May 2014

ABSTRACT

A literature review has been carried out to identify factors affecting the machinability of fibre reinforced plastics (FRP) composites in general and carbon fibre reinforced plastics (CFRP) in particular. This includes the use of different cutting tool materials, tool geometry, and process variables together with aspects such as cutting forces, tool wear/life, cut quality/defects, cutting temperature, and surface integrity in both experimental and modelling approaches.

The experimental work was divided into 3 phases. The first phase dealt with the effect of cutting parameters such as tool material including different polycrystalline diamond (PCD) grades, cutting speed, feed rate, and cutting environment (dry/chilled air). The first phase aimed to identify the preferred range of parameters for the process. This was followed by 3 sub phases to benchmark PCD grades, and chemical vapour deposition (CVD) diamond tools, to identify the possible wear mechanisms in physical vapour deposition (PVD) and CVD diamond coated Tungsten carbide (WC) tools and finally to study the use of PVD and CVD coated burr tools in terms of tool life and workpiece surface quality.

The second phase of experiments dealt with the effects of varying the workpiece lay-up configuration on tool wear/life, cutting forces, and surface quality. This phase incorporated 3 different workpiece lay-up configurations namely Type-1 [25/50/25], Type-2 [44/44/11], and Type -3 [15/70/15]. A full factorial experimental design was employed involving 12 tests. In addition, a test using a thermocouple implanted router was performed to evaluate the effect of different lay-up configuration on cutting temperature.

The third and last phase investigated the influence of different tool geometry aspects (clearance angle, helix angle, and number of flutes) on measured responses in order to identify the most suitable geometry for the CFRP milling applications. Additionally, a sub phase focused on the effect of helix angle on various aspects including cutting temperature when milling CFRP.

The results of Phase-1 indicated that slotting of CFRP using PCD allows reasonable surface quality without compromising productivity. Surface damage was dependent on ply orientation and cutting parameters and was thermal, mechanical or a combination of both. Severe tool wear resulted in a serrated cutting edge when using diamond like carbon (DLC) coated WC. In some cases when feed rate was high, the high cutting forces caused plastic deformation of the WC tools. Workpiece fuzz and uncut fibres occurred mainly on the up milling side due to flexing of fibres. The use of chilled air prevented the accumulation of dust

in the cut slot, eliminated the burning hazard and avoided poor surface finish as well as short tool life. Coarse grain PCD (CTM-302) proved to be susceptible to chipping especially at high feed rates. The finer CTB-010 proved to be the best in terms of tool life better than DLC-coated WC especially at high cutting speed and high feed rates.

Low cutting speed and high feed rate (200 m/min and 0.15 mm /tooth) are recommended for better surface integrity/roughness. Feed rate was the most significant factor affecting surface roughness with a 57.47% percentage contribution (PCR). The highly abrasion resistant CTM-302 PCD grade was the best tool for workpiece surface quality.

None of the 2-fluted WC routers tested were suitable for the slotting operation. However, Dura-coated WC outperformed the DLC-coated and the uncoated WC in terms of tool wear due to its diamond structure. Moreover, workpiece surface roughness using Dura-coated tooling was better. Dura coated two fluted routers proved to be ideal for finishing.

Benchmarking of uncoated and Dura (diamond) coated WC Burr routers showed that the uncoated Burr router produced a rough surface with no fuzz on either side due to its down cutting action which makes it an ideal choice for roughing. Fracture of the coating and subsequent substrate wear added to its higher cost made the coated router uneconomical. The wavy surface and high surface roughness ~ 250 µm St produced with the uncoated router necessitate a finishing pass at 0.3-0.5 mm radial depth of cut to remove the damaged layer.

The results of Phase-2 showed that fibres at 0° were responsible for the highest cutting force (Fx), while those at 90° were responsible for the highest feed force (Fy). It was also possible to predict the maximum cutting force Fx for different layups with 2.5 -12% variation for 200 m/min cutting speed and 0.03 mm/tooth feed rate. Workpiece surface integrity was dominated by damage from 45° layer corresponding with the wavy surface. While Type-2 lay-up exhibited the lowest surface roughness owing to the larger number of 0° layers, Type-3 lay-up showed the highest surface roughness because of the larger number of 45° layers. The up-milling side had lower surface roughness compared to the down-milling side possibly because of the lower temperature on the former, hence it is recommended that any finishing pass adopt this mode for better quality. The layer at 45° was responsible for the highest cutting temperature and consequently high wear in these layers. Type-3 lay-up material generated greater levels of heat followed by Type-2 then Type-1. The use of neutral tool geometry generated the highest temperature. Down-cut router produced a ~5-8% temperature reduction while using the Up-cut was ~2.5-4%. Temperature during cutting ¾ engagement was ~ 85% of that in full engagement slotting. Moreover, dry cutting environment generated 100°C higher temperature, while using chilled air with a single-nozzle was 20°C lower than

with a twin-nozzle. Tool cutting edges prepared using WEDM were more prone to chipping due to high initial cutting force spikes. The most significant factor affecting tool life was workpiece lay-up with 61.3% PCR. Type-3 lay-up material was the most difficult to cut causing severe chipping at locations of 45° layers. Not surprisingly the most significant factor affecting feed force was the feed rate with 49.4% PCR. The most significant factor affecting delamination and fuzz length was feed rate with PCR's of 50.1% and 57.8% respectively. The use of chilled air applied through a single-nozzle did not affect uniform abrasion wear of the tool but caused an increase in cutting forces. Furthermore, it did not affect fuzz length but reduced the delamination factor. Twin nozzle operations were better in terms of workpiece surface integrity.

Phase-3 indicated that low helix angle (3°) did not affect tool life as PCD grade was the same. Down-cut geometry produced lower cutting temperature but the highest cutting force and workpiece surface roughness. The Neutral router produced the best surface roughness Sa owing to the high temperature that did not adversely affect the quality. Dynamic forces were observed using a single relief tool which appeared less stable however this improved with increasing tool wear while workpiece surface roughness using the twin relief angle was ~50% better than that using single relief.

DEDICATION

To my parents, my wife Walaa, my daughter Zaina and my son Hassan

ACKNOWLEDGEMENTS

The author would like to express his thanks and appreciation to the following people and organisations for their assistance and support over the duration of the project:

Dr. Sein Leung Soo (Senior Lecturer and Head of the Machining Research Group) and Prof. David Aspinwall, both from the School of Mechanical Engineering for their academic supervision and guidance.

Dr. Wei-Ming Sim, formerly Machining Technologist at Airbus Operations Ltd. (currently Lead Technologist at GKN Aerospace) for his guidance and motivation throughout the project. Special thanks to Airbus for the provision of CFRP workpiece material and financial support for the research.

Dr. Peter Harden and Dr. Neels Pretorius, both formerly of Element Six for providing PCD tool materials and related technical advice.

Mr. David Pearson and Mr. Mike Fleming of Seco Tools (UK) Ltd. for the supply of cutting tools and technical support. Additional thanks are due to Marcel Aarts, and Jeroen Huijs from Seco Jabro Netherlands and Dr. Rachid M'Saoubi from Seco Tools AB, Sweden for their help and support with regard to tooling.

The Overseas Research Student Award Scheme (ORSAS) and the School of Mechanical Engineering, University of Birmingham for the award of a research studentship.

Richard Fasham, Andy Loat and Alan Saywell, Technical Engineers within the School of Mechanical Engineering for their invaluable assistance during the experimental work.

Velnom Laurent from Actarus France, for his guidance, assistance and general advice relating to the temperature measurement trials.

Eike Hasselberg (intern from the University of Hannover), Kelvin Cobb, Timothy Frost, Hugh Muir, Ted Johnston, Chris Bristol, Leif Williams, Richard Middleton, Chris Harper, Stewart Gaffney, Jason Workman and John Stenning for their valuable time and attention during the author's internship period at Airbus-UK's Composite Structure Development Centre in Filton, Bristol.

Simon Groves from the National Composite Centre (NCC), Bristol for help and technical support with the lay-up, fabrication and sectioning of the CFRP samples used in the research.

Paul Simons for providing training on the Matsuura FX-5 and Dr. Saad Mahmoud for his continuous encouragement throughout the project.

Dr. Khalid Al-Ghamdi for his assistance and fruitful discussions relating to experimental design techniques.

Prof. Paul Cooper and Michele Holder from the School of Dentistry, University of Birmingham for access and help with using the X-ray scanning facilities.

Dr. Moataz Attallah and Dr. Khamis Essa for their help and support using the laser CMM at the School of Metallurgy and Materials, University of Birmingham.

Colleagues in the Machining Research Group (past and present), in particular Dr. Richard Hood, Dr. Islam Shyha, Dr. Juri Saedon, Dr. Mohammed Antar, Alex Kuo, Debajyoti Bhaduri, Dr. Sarmad Ali Khan, Raul Munoz, Maojun Li and Dr. Rattanachai Rattanakit for their unwavering moral support and encouragement.

Finally I would like to express my love and gratitude to my wife Walaa El-Kholy, my daughter Zaina, my son Hassan and my parents for their encouragement, support and motivation throughout this work.

TABLE OF CONTENTS

LIST OF FIGURES

LIST OF TABLES

LIST OF SYMBOLS

Symbol	Definition	Unit
ϕ	Angle between the resultant force and cutting force	Deg
φ_i	Instantaneous immersion angle	Deg
θ	Fibre angle	Deg
a_e	Radial depth of cut or width of cut	mm
a_c	Uncut chip thickness at laminate thickness	mm
aeff	Chip thickness removed by burr router	mm
a_p	Axial depth of cut/ depth per helical rotation	mm
a_t	Ply thickness	mm
C	Taylor constant	
CH	Chipping wear	mm
C_{new}	New tool cost	£
C_L	Labor cost	£
C_m	Machine cost	£
C_r	Tool regrinding cost	£
C_{scrap}	Worn tool selvage value	£
C_t	Tooling cost for a single product	£
C_T	Tooling cost for a single tool	£
D	Diameter	mm
Dc	Diameter of cutter	mm
DF	Delamination factor	
Dh	Helical path diameter	mm
Fx	Cutting force	N
Fy	Feed force	N
Fz	Axial force	N
Fm	Resultant force	N
f	Feed rate per tooth	mm/tooth
f	Feed rate per revolution	mm/rev
f_{za}	Axial feed rate	mm/tooth
f_{zt}	Tangential feed rate	mm/tooth
H	Height of profile	µm
h_m	Mean chip thickness	mm
Kc	Tangential specific cutting energy	N/mm^2
Ks	Specific cutting resistance	N/mm^2
Kt	Normal specific cutting energy	N/mm^2
MRR	Material removal rate	mm^3/min
n	Taylor exponent	
n_p	Number of plies being cut	
n_s	Number of tool regrinds	
Ra	Arithmetic average roughness	µm

Rq	Root mean square roughness	µm
Rt	Maximum peak to valley height	µm
Rz	Ten-point height	µm
Sa	Arithmetic average roughness (3D)	µm
St	Maximum peak to valley height (3D)	µm
t_{ct}	Tool change time	min
t_m	Machining time per product	min
T	Tool life	min
T_e	Tool life for minimum cost	min
Tg	Glass temperature	^oC
T_o	Tool life for maximum production rate	min
VB	Flank wear	mm
VBN	Notch wear	mm
Vc	Cutting speed	m/min
Vcr	Critical cutting speed	m/min
V_e	Cutting speed for minimum cost	min
V_f	Feed speed	mm/min
V_o	Cutting speed for maximum production rate	min
W	Nominal width	mm
Wmax	Width of damage	mm
z	Number of products in a tool life time	
Z	Number of cutter teeth	

LIST OF ACRONYMS

Acronym	Description
ACF	Auto correlation function
ACGIH	American Conference of Governmental Industrial Hygienists
ANOVA	Analysis of variance
ATL	Automatic tape laying
AWJ	Abrasive water jet
C	Ceiling
CA	Chilled air
CAMQL	A mixture of chilled refrigerated air and oil mist
CBN	Cubic boron nitride
CE	Cyanate easter
CFRP	Carbon fibre reinforced plastic composite
CHD	Cumulative height distribution
CMC	Ceramic matrix composite
CNC	Computer numerical control
CTE	Coefficient of thermal expansion
CVD	Chemical vapor deposition
CW	Continuous wave
DLC	Diamond like carbon
DOF	Degree of freedom
EDM	Electrodischarge machining
EDX	Energy-dispersive X-ray
EHM	Equivalent homogenous material
EP	Epoxies
FEA	Finite element analysis
FP	Fibre placement
FRP	Fibre reinforced plastic composites
GFRP	Glass fibre reinforced plastic composite
HAZ	Heat affected zone
HIPIC	Hot isostatic pressure impregnation carbonization
HLU	Hand lay-up
HM	High modulus
HSM	High speed machining
HSS	High speed steel
HT	High strength
HV	Hardness Vickers
IM	Intermediate modulus
IR	Infra-red
ISO	International Standards Organisation
IT	Tolerance grade

LPI	liquid phase impregnation
MD	Multidirectional
MIS	Manufacturing instruction sheet
MMC	Metal matrix composite
MQL	Minimum quantity lubricant
MS	Mean of squares
MSDS	Material safety data sheet
MSE	Mean square of error
N	Noise
NCF	Non-crimp fabrics
NDM	Nearly dry machining
NDT	Non-destructive test
ND-YAG	Neodymium-doped yttrium aluminum garnet
OSHA	Occupational Safety and Health Administration
P	Phenolics
PAN	Polyacrylonitrile
PCD	Polycrystalline diamond
PCR	Percentage of contribution
PEEK	Polyetheretherketone
PEI	Polyetherimide
PEL	Permissible limit of exposure
PES	Polyethersulfone
PI	Polyimide
PM	Pulsed mode
PMC	Polymer matrix composite
PMI	Besmaleimide
PPS	Polyphenylsulfide
PSDF	Power spectral density functions
PVD	Physical vapor deposition
RFI	Resin film infusion
RMS	Root mean square height
RTM	Resin transfer method
S	Signal
SEM	Scanning electron microscopy
SS	Sum of squares
SST	Sum of squares total
STEL	Short term exposure limits
Ta-C	Tetrahedral amorphous carbon
TLV	Threshold limit value
TRS	Transverse rupture strength
TWA	Time weighted average
UD	Unidirectional
UHM	Ultra-high modulus

UPR	Unsaturated Polyester Resin
USM	Ultrasonic machining
UV	Ultraviolet
VGCF	Vapour grown carbon fibre
WC	Tungsten carbide
WEDM	Wire electrodischarge machining
WJ	Water jet

1 INTRODUCTION

1.1 Background to project

Advances in composite materials technology have made composites a viable alternative to traditional lightweight alloys such as aluminium and titanium for aerospace applications. Indeed, most of the world's aircraft component manufacturers including Airbus and Boeing have indicated that future commercial and military aircraft will increasingly use composite components to provide strength to weight ratio, leading to improvements in aircraft operational efficiency and fuel savings. The annual research and development expenditure in Airbus is £1.6 billion, 90% of which is directed towards technologies for lowering the environmental impact of their products. For example, the latest A380 consumes only 3 litres of fuel per passenger per 100 kilometres (20% lower than their nearest competitor) while emissions of the next generation A350 XWB's are 99% below the permitted hydrocarbon limit according to the Committee on Aviation Environmental Protection [1].

Optimisation of aircraft design necessitates extensive use of advanced materials such as CFRP composites in primary aircraft structures for parts such as wing spars, stringers, ribs, skin panels etc. In the 1980's use of composites in an aircraft was limited to secondary structures such as interior panels/trims. Traditionally, the machining of composites is considered to be significantly more difficult than their metallic counterparts due to the formers' material properties such as workpiece heterogeneity, abrasive / tough reinforcement phase and anisotropic orientation. Machinability data and recommendations for high speed milling of such materials are limited, hence the motivation for this project.

During the R&D phase of the Airbus A350, Airbus needed to study the machinability of CFRP when end milling. Milling/routing processes are used to obtain the final shape of a panel produced to near-net-shape. The extent of literature concerning the milling of CFRP was limited compared to other processes such as drilling, which is very important for assembly process. It was also apparent that the process of identifying the best parameters/tools for milling carbon fibre panels is reliant on trial and error experimental approaches.

At the outset of the present work, published milling research essentially dealt with edge trimming process, with only a few articles discussing slot milling (slotting) operations. The literature review highlighted the absence of data on the use of high cutting speeds and high feed rates especially in slotting using polycrystalline diamond (PCD) together with the use of

different PCD grades (with cutting edges manufactured by different grinding techniques) or various diamond coatings in the slotting of CFRP. Furthermore, there was no data covering tool temperature during slot milling or the influence of material configuration. The effect of different chilled air flow rates on machined surface quality had not been studied, despite equipment and data for vortex operated chilled air delivery being available with reference to other materials. In addition, delamination assessment using laser techniques was limited. In relation to tool geometry, no details could be found concerning the effect of geometry either on stability of cutting or cutting temperature and consequent effects on surface integrity when milling FRP composites. Cost analysis with respect to tooling when slotting CFRP was similarly not discussed. The overall aim and objectives of the present research reflect the above shortcomings in machinability data/understanding.

1.2 Aim and objectives

The overall aim of the project was to evaluate the machinability and develop improved strategies for the end-milling/routing of carbon fibre reinforced plastic composites (CFRP) of the type used for aerospace applications. Specific objectives were to:

A- Undertake a comprehensive literature review on the machining of composite materials across different engineering applications, and in particular on the milling/routing of CFRP's.

B- Identify preferred/optimum tool material, operating parameters and the cutting environment for the machining of specified carbon fibre reinforced composite material. This work to include evaluation of the following:

- Effect of tool material, cutting speed, feed rate, cutting environment on machinability aspects such as cutting forces, cutting temperature, tool life and surface integrity when slotting CFRP.
- Benchmarking of PCD grades.
- Benchmarking of carbide tools and their coatings and identification of related wear types/modes with subsequent effects on workpiece surface quality.
- Identify suitable advanced cutting tool materials (polycrystalline diamond "PCD", WC, chemical vapour deposition "CVD" diamond etc.) to provide reasonable levels of productivity, tool life and workpiece quality.

C- Evaluate the effect of workpiece material variables (different unidirectional "UD", and multidirectional workpiece layups etc.) on machinability performance and specifically to study:
    - Effect of layup configuration on cutting forces, cutting temperature and surface integrity.
    - Effect of different tool geometries on cutting temperature when machining different layup configuration.
    - Effect of cutting environment on cutting temperature.

D- Evaluate the effect of varying tool geometry on the machinability of CFRP with reference to the effect of helix angle and secondary clearance on slot milling performance and surface integrity.

E- Identify operating approaches that minimise / eliminate workpiece surface defects such as delamination, fibre pull-out, matrix chipping / degradation, cracking etc. during milling/routing.

F- Perform a cost benefit analysis on the proposed machining approach.

The thesis is organised in 6 chapters. Chapter 1 provides a brief introduction to the background, aim and objectives in addition to project sponsors and collaborators. Chapter 2 presents a comprehensive literature review for milling/routing CFRP.

The experimental work is presented in Chapter 3 and covers work material, cutting tools, test equipment, and measuring devices. The chapter also details the experimental design/approaches taken, procedures and test arrays and outlines the experimental phases adopted to achieve the planned set of objectives.

Chapter 4 presents the result and discussion for each experimental phase. Data for tool wear, tool life, milling forces, slot quality measures as well as cut surface quality are presented. The effects of cutting speed, work feed, work material, tool material, etc. are discussed. Conclusions drawn from the experimental work are detailed in Chapter 5 while recommendations for future work are shown in Chapter 6.

1.3 Project sponsors and collaborators

The present research work was undertaken in the Machining Research Group laboratories, School of Manufacturing & Mechanical Engineering, University of Birmingham. Airbus UK initiated the project which was led by Dr. Wei-Ming Sim, who was employed as a Machining

Technologist at Airbus and was responsible for A350 XWB wing assemblies. Details of industrial supervisors/contacts and funding sources are given in Table 1.1.

Table 1.1 Project collaboration details

Collaborator	Contribution	Contact
Airbus Operations Ltd UK (Bristol, UK)	£30k Workpiece material Technical support	Dr. Wei-Ming Sim (Machining Technologist) Airbus operations Ltd UK New Filton House, Filton, Bristol, BS99 7AR, U.K. Tel: +44(0)7706997494 Email: WeiMing.Sim@airbus.com
Element Six (Shannon, Ireland)	£2k Tool materials Technical support	Dr Peter Harden (Manager at Market Support Centre) Element 6, Shannon, Ireland. Tel: + 353 (0)61 460 048 Email: peter.harden@e6.com
Seco Tools UK (Alcester, UK)	£2k Tool fabrication/supply Technical support	Mr David Pearson (Business Development Manager – Aerospace) Seco Tools (UK) Ltd, Arden Forest Industrial Estate, Alcester, Warks, B49 6EL, UK. Tel: +44(0) 7970 764433 Email: david.pearson@secotools.com
Overseas Research Student Award Scheme (ORSAS)	£ 27k (university fees) Scholarship support	http://www.orsas.ac.uk/
University of Birmingham	£39k Scholarship support Equipment/facilities	Dr. S. L. Soo (Senior Lecturer and Head of the Machining Research Group) & Prof. D. K. Aspinwall School of Mechanical Engineering University of Birmingham, Edgbaston, B15 2TT, UK. Tel: +44(0) 121 414 4196 Email : s.l.soo@bham.ac.uk

2 LITERATURE REVIEW

2.1 Composite material

Over the past 30 years there has been a significant increase in the use of composites in aerospace industry as a replacement for metal alloys owing to their high strength/stiffness-to-weight ratios (specific strength and specific stiffness) which has increased fuel efficiency and payload. The Airbus A380 jumbo airliner employs a central wing box made of carbon fibre reinforced plastic composite which provides ~1.5 tons reduction in component weight without compromising strength. The planned Airbus A350 XWB incorporates nearly 53% of composites in its body. An aircraft that is lighter can travel further and have less impact on the environment [1]. Composites can also provide stealth benefits [2] such as the skin of Lockheed Martin's F-35 jet.

Composite materials have existed since antiquity for example Japanese sword/blades made of soft iron sandwiched between steel have good resistance to flexure and impact [3]. There are some natural composites such as wood or bone [4] and other man made ones surrounding us in everyday life such as concrete or car tyres. Generally, a composite material is a mixture of two or more different constituents that are not soluble in each other and remain separate on the macro-scale. Each constituent is called a phase[4-6], the part that is continuous is called the matrix phase and surrounds and protects the dispersed phase (reinforcement) which provides enhanced mechanical properties.

There are many classifications of composite materials. One of the broadest classifications identifies the dispersed phase which can be particles in the case of particulate reinforced composites (e.g. concrete) or fibres in the case of fibre-reinforced-composites. Here fibres made from glass (GFRP) and carbon (CFRP) are commonly employed, see Figure 2.1. Properties of composites depend on the phase materials, concentrations, distribution, form, orientation and its fabrication process [3]. Composites can be also classified according to their matrix phase material. A matrix material can be metal in the case of metal matrix composites (MMC), ceramic as in ceramic matrix composites (CMC), or polymer (PMC) [6]. In this work, the emphasis is on fibre reinforced polymer/plastic composites. Figure 2.2 identifies property comparisons for composites and more traditional composites and other materials. Additionally, predetermined properties can be obtained to suit function and the cost of manufacturing large components can be relatively low [5]. Reinforcement can augment other properties - chemical, thermal, and electrical.

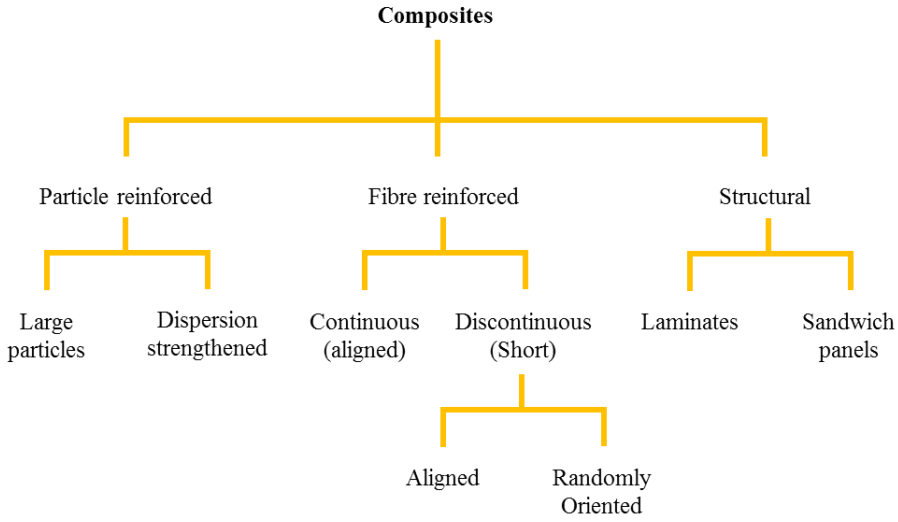

Figure 2.1: Composites classification [6]

Many areas/industries utilise composites including aerospace, defence, nuclear, automotive, marine (boats, yachts). Composites structures/components can be found in wind energy systems, machine tools, sports goods (golf clubs, tennis rackets, bicycles, arrows, surfing and skateboards) and biomedical products. Fibre reinforced polymer composites (FRP) and particularly those involving carbon fibre (CFRP) are the most widely used composite material in military and commercial aerospace systems, see Figure 2.3 for examples of FRP's in the Airbus A380 [7].

2.1.1 Particulate reinforced composites

There are two different types of particulate reinforced composites, based on particle size. The first involves large particles where matrix/particle interaction cannot be treated on the atomic or molecular level, examples include concrete and cemented carbide cutting tools. The second type is dispersion strengthened where the particle/matrix interface can be treated on the atomic or molecular level with particles down to 0.01 μm e.g. carbon black dispersed in rubber matrix of car tyres.

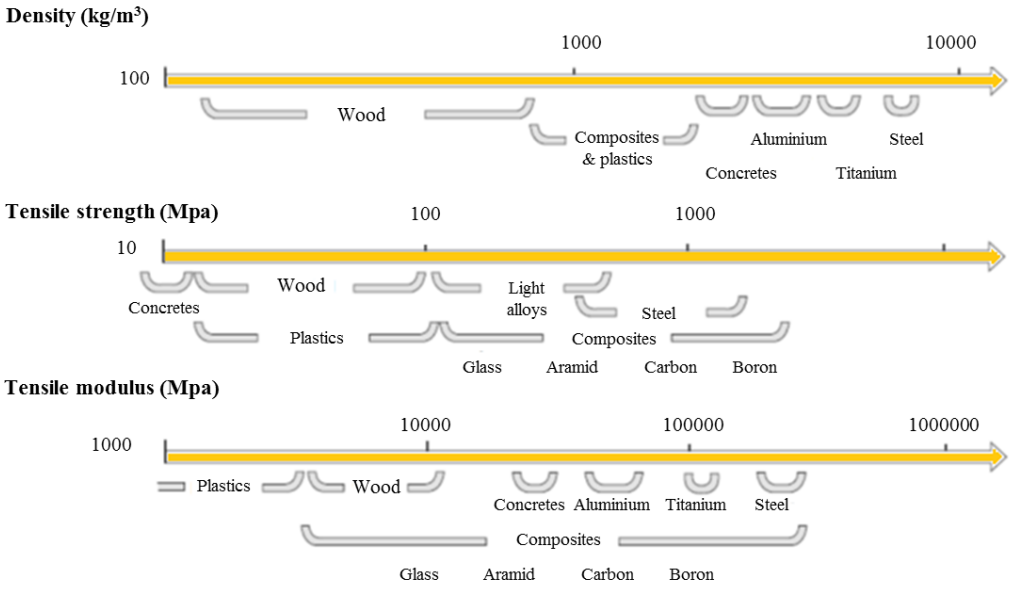

Figure 2.2: Fibre reinforced composite material properties in comparison to traditional composites and other materials [8]

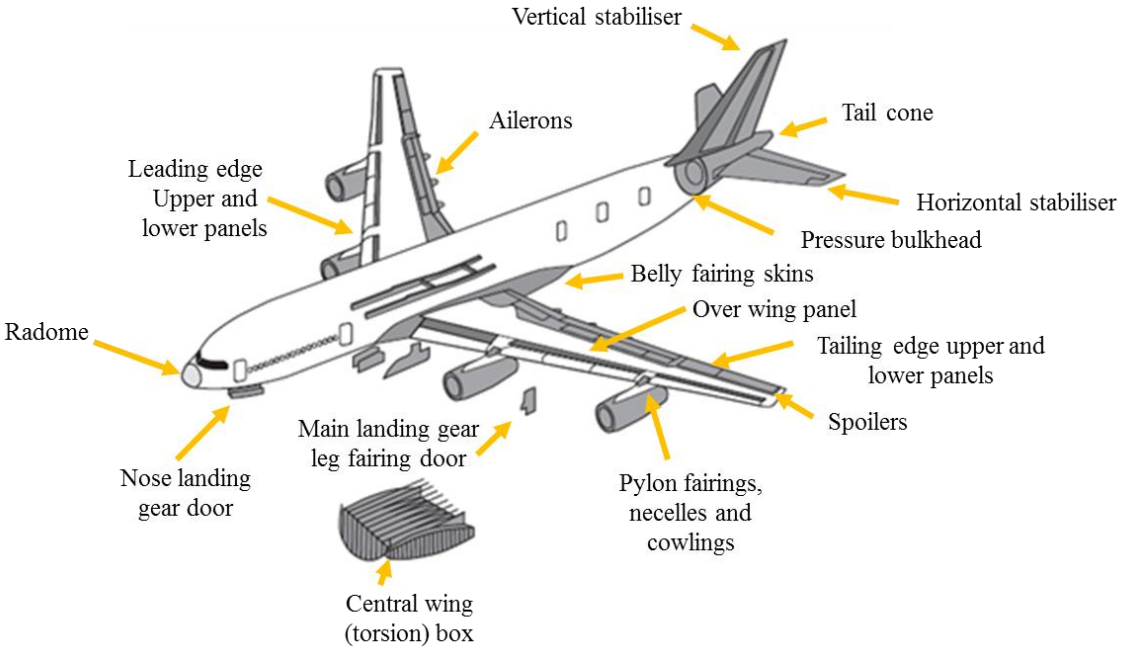

Figure 2.3: Use of fibre-reinforced polymer composites in the Airbus 380 [7]

2.1.2 Fibre reinforced composites

Composites are stronger than steel and lighter than aluminium, they are also "heterogeneous", and "anisotropic" which affect their machinability characteristics as will be discussed later. The whiskers or filaments within FRP composites are ~ 5-15 µm in diameter which is smaller than a human hair (40-120 µm) [4]. Fibres have an elongated form with

aspect ratios l/d of not more than 10 and a maximum cross-sectional area of 0.05 mm^2. The term whisker is used if the fibre is a single crystal. A material is said to have maximum strength when it takes the form of a filament or a whisker because of enhanced purity and fewer surface defects compared to the bulk material [5, 6]. Filaments can be either continuous or discontinuous fibres, Figure 4. Many filaments packed together are termed a bundle or tow (untwisted) and the number of filaments in a bundle is referred to as the tow size which normally contain 1000's of fibres e.g. 3k, 6k, 12k, 24k, 40k, 48, 80k,160k, 320k, 400k and 410k [9]. A smaller tow size provides easier formability of the composite to a complex shape with sharper corners/fillets. The smaller the tow size however the more expensive are the fibres [7, 9].

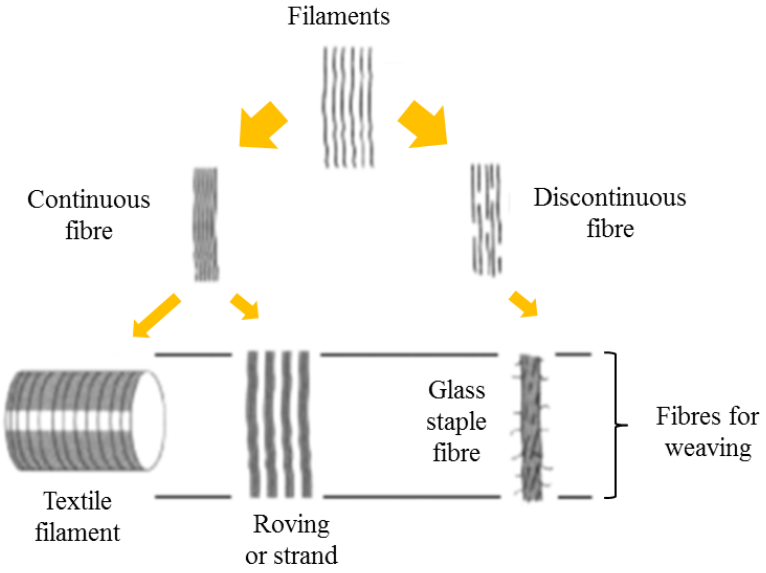

Figure 2.4: Filament and fibre [3]

Reinforcement not only offers a weight saving over metals but also provides enhanced mechanical properties such as strength and stiffness [5]. Therefore, fibres should be continuous and as long as possible because the load is carried only at the axial centre of fibres [6]. A combination of high strength and low modulus means the fibres are strong but flexible and can be used to obtain complex shapes. Figure 2.5 displays the difference between strength and modulus for a selection of the most common fibres used in industry [3]. The arrangement, orientation, concentration, and distribution of fibres affects the properties of fibre reinforced composites [6, 7]. For example, a 50% by volume unidirectional E-glass composite will have 1.37 GPa tensile strength (along fibres) although the individual fibres have a strength of 2.75

GPa. If the load is perpendicular to fibres the tensile strength depends on the bonding between fibre and matrix [5].

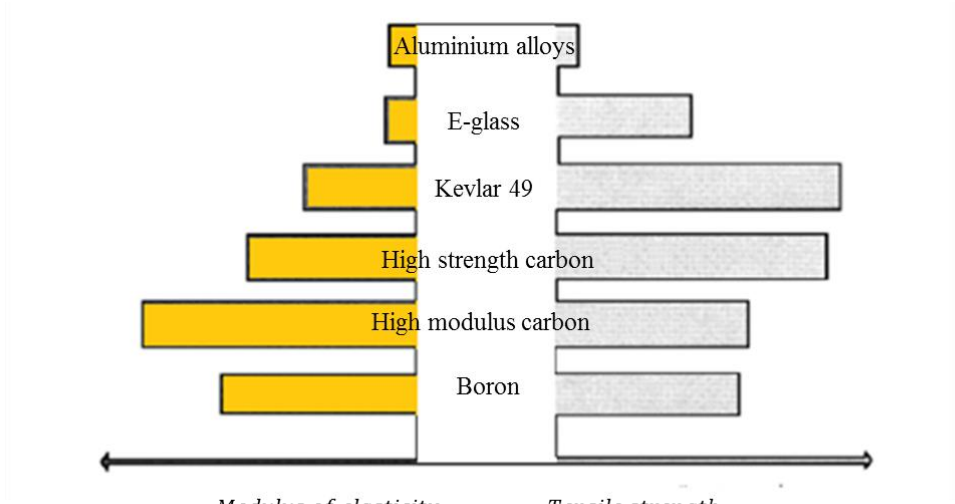

Figure 2.5: Modulus vs. strength [3]

There is an wide range of fibres including Alumina (Al_2O_3), Aramid (Ar), Boron (B) Carbon (C), D-Glass (DGl), E-Glass (EGl), Graphite (Gr), Lithium (Li), Polyacrylonitrile (PAN), Quartz (Q), Silicon (Si), Silicon carbide (SiC), S-Glass (SGl), Titanium (Ti) and Tungsten (W). Carbon, aramid and glass fibres are the most common. The properties/cost of different fibres are shown in Figure 2.6 while more fibre properties can be found in Appendix-A. Generally, fibres may require surface treatment to improve their adhesion to the matrix [3].

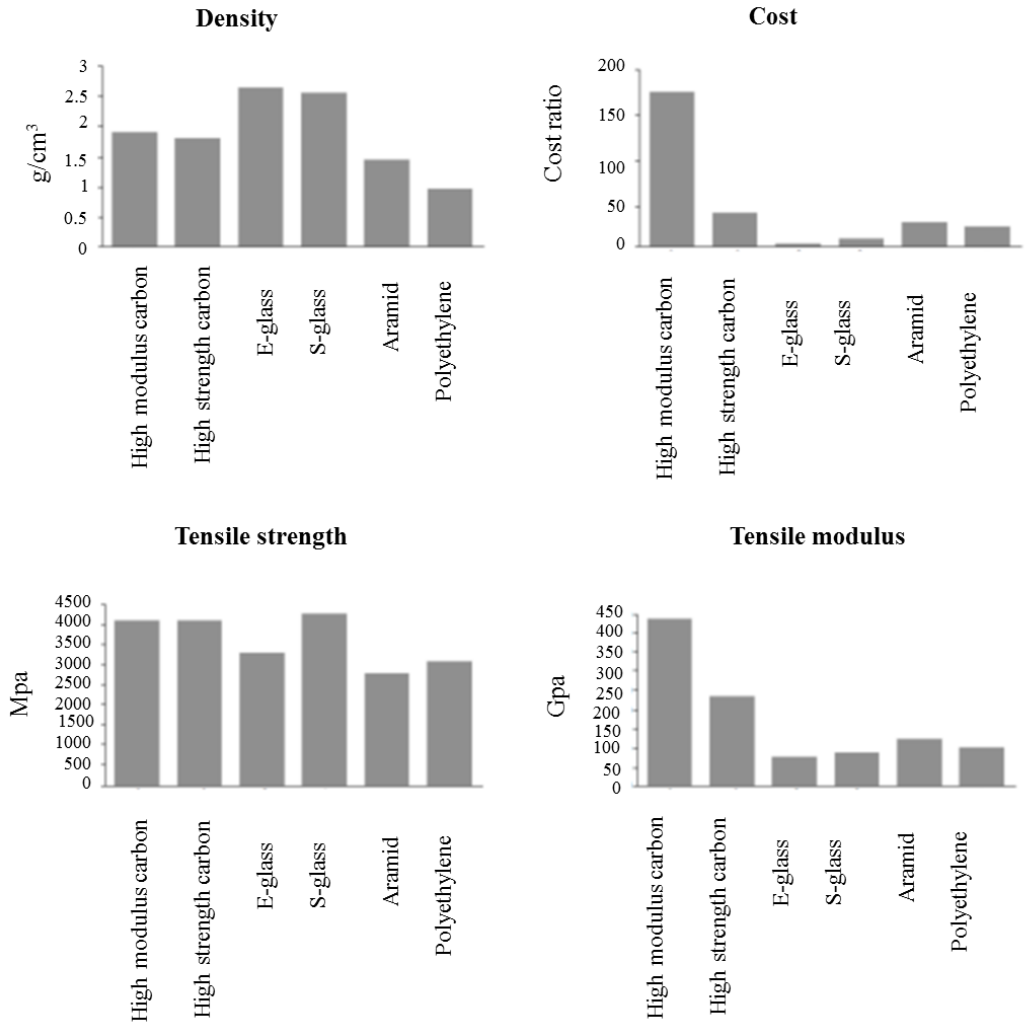

Figure 2.6: Properties and cost of different fibre materials [8]

2.1.2.1 Glass fibres

Glass fibres were first introduced in 1930's and are widely used as the reinforcement material for composites [5]. They are used in applications requiring high corrosion resistance and have diameters 10-20 µm [4]. They have enhanced mechanical properties and low cost but their limitation is service temperature which is below 200°C[6]. Additionally, they have higher density and lower tensile strength in comparison to carbon fibres [7]. Glass fibres are mostly used in polymer matrix composites. The most common types include E-glass (electrical), S-glass (high strength), and C-glass. S-glass fibres are used for aerospace applications while C-glass fibres are used in applications requiring corrosion resistance. The abrasiveness of glass fibre causes excessive tool wear during machining [4, 7].

2.1.2.2 Aramid fibres

Aramid fibres have high strength and modulus and were introduced early the 70's. These light-weight fibres are used to increase toughness and impact strength as well as creep and fatigue resistance [4, 6]. The limitation of Aramid fibres is their sensitivity to degradation by acids and, a temperature ceiling of 200 °C. They are used in a polymer matrix and the most common commercial names are Kevlar and Nomex. Typical applications of aramid fibres include breakes/clutch linings, and bullet proof vests [6]. Aramid fibres have the advantage of negative coefficient of thermal expansion (CTE) in the longitudinal direction and the disadvantage of low compressive strength and difficulty in being cut during machining operations [4, 7].

2.1.3 Carbon Fibres

Carbon fibre dates back to Thomas Edison who made a carbon filament for a bulb. The first high strength/modulus carbon fibre was developed in the 1960's [10]. It is considered the most important material for reinforcement because it possesses the highest specific strength/modulus among all fibre materials [6]. Its tensile modulus ranges from 207 GPa to 1035 GPa [7]. Fibres are produced by the pyrolysis of organic (hydrocarbon) precursor fibres such as rayon (cellulose), polyacrylonitrile (PAN), or pitch in an inert (non-reactive) atmosphere. Figure 7 shows the typical steps used in making polyacrylonitrile (PAN) based carbon fibre. Although a pitch precursor (raw material) is cheaper than PAN [7], the produced pitch based carbon fibres cost more than PAN based carbon fibres [11]. PAN carbon fibres have lower electrical and thermal conductivity than pitch based ones[7]. Short carbon fibres can be grown also by chemical vapour deposition from carbonaceous gas and are known as vapour grown carbon fibres (VGCF) [11].

2.1.3.1 Types of carbon fibre composite

Carbon fibre reinforced composites are classified according to their tensile strength and modulus into the following categories [11]:

- Ultra-high modulus (UHM) if tensile modulus is > 500 GPa
- High modulus (HM) fibre where modulus > 300 GPa and strength to modulus ratio < 0.01
- Intermediate modulus (IM) when fibres have modulus up to 300 GPa and strength –to – modulus ratio > 0.01
- Low-modulus Carbon fibres with modulus as low as 100 GPa and low strength

- High strength (HS) if strength is > 3GPa and Strength-to- modulus ratio (0.015 – 0.02)

The properties of different carbon fibres are shown in Table 2.1, see also Appendix-A for further data. Carbon filaments can be surface treated (sized or coated) in order to provide protection from the atmosphere and improve adhesion (bonding) to the matrix. The selection of the sizing material depends on the matrix material.

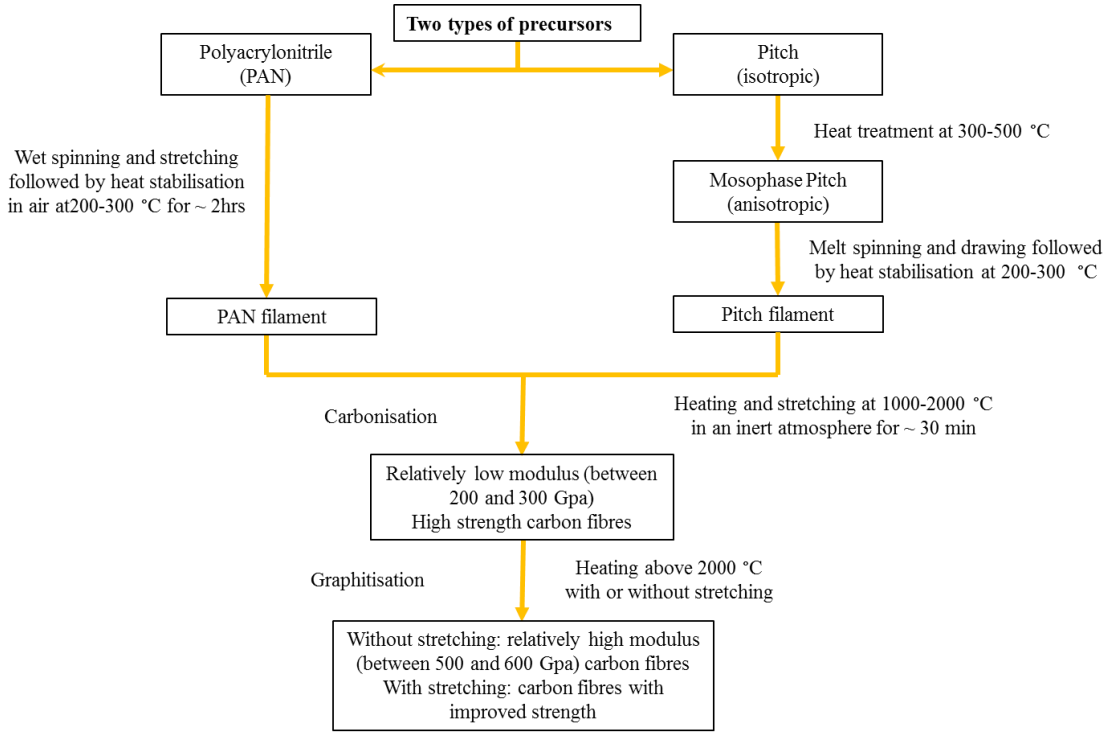

Figure 2.7: Making Carbon fibre from PAN or pitch [7]

Table 2.1: Properties of Carbon fibre, Kevlar, E-glass and S-glass [4]

Characteristic		**PAN-based carbons**		**Kevlar 49**	**E-glass**	**S-glass**
		High modulus (HM)	**High strength (HS)**			
Diameter (μm)		5-8	6-8	8-14	10-20	10-20
Density (kg/m3)		1.81	1.78	1.44	2.62	2.46-2.49
Young's modulus (Gpa)	**Parallel to fibre**	400	230	131	80-81	88-91
	Perpendicular	12	20	70		
Tensile strength (Gpa)		2.5-4.5	2.8-4.2	3.6-4.1	3.1-3.8	4.38-4.59
Strain to failure (%)		0.6	2.0	2.8	4.6	5.4-5.8
Coefficient of thermal expansion ($10^{-6}K^{-1}$)	**Parallel to fibre**	-0.5	-0.6	-4.3	6.0	2.9
	Perpendicular	7.0	10.0	41		
Thermal conductivity (W/m K)		70	11	0.04-1.4	10-13	1.1-1.4
Specific heat (kJ/kgk)		0.7-0.9		0.769	0.45	0.41

2.1.4 Matrix in FRP composites

The matrix material protects the reinforcement fibres from abrasion or chemical reactions, keeps the fibre in place, distributes the load and determines the service temperature of a composite material [6]. Matrix materials should provide good adhesion to the fibre surface and compatible stress strain behaviour with fibres [5]. Generally, composites can be classified according to matrix material: polymer matrix composites (PMC), metal matrix composites (MMC), Carbon matrix as in Carbon-Carbon composites, or hybrid composites.

Metal matrix composites have the advantage of high temperature resistance [6, 7, 11], high fire resistance, good transverse strength/modulus and high thermal/electrical conductivity [11]. Metals such as aluminium, copper, nickel, magnesium, steel, titanium or its alloys can be strengthened with carbon fibres. Carbon fibres are used in the metal matrix to reduce the density as well as the coefficient of thermal expansion (CTE). Fabrication of such composites is achieved by wetting fibres in the molten metal or infiltration of a preform by liquid metal under pressure [11]. The incorporation of carbon fibres in aluminium requires a high temperature of 500 °C, which may degrade the carbon fibres and necessitates the use of a coating [7].

Ceramic matrix composites (CMC) can be used for high temperature applications [6]. The ceramic can be either an oxide or non-oxide and typically exhibits low density, high temperature resistance, high thermal shock resistance, high modulus but poor crack resistance (brittle) [7]. Fracture toughness can increase up to 6 times because the particles or fibres act as crack stoppers[6]. They are used in high-temperature applications for aerospace and engine components [11]. Glass, MgO, $A1_2O_3$, SiC, Si_3N_4, and ZrO_2 are other ceramic materials that have been used as matrix materials for carbon fibre composites that are made mainly by hot pressing[11].

Carbon-Carbon composites possess the highest temperature resistance among composites. Furthermore, their coefficient of thermal expansion is near zero. The main disadvantages relate to high fabrication cost, poor oxidation resistance and poor interlaminar properties. Fabrication methods include liquid phase impregnation (LPI), hot isostatic pressure impregnation carbonization (HIPIC), and hot pressing. Applications for carbon-carbon composites include aircraft brakes, heat pipes and heat sinks, re-entry vehicles, rocket motor nozzles, hip replacements, biomedical implants, tools and dies, and engine pistons [6, 11].

Polymer matrix composites (PMC) (commonly plastics) comprise long chain molecules containing repeating units of atoms[7]. They are easier to fabricate than other types of

composite because of low processing temperatures. They can be either a thermoplastic or a thermoset. In thermoplastic polymers the atoms are not chemically joined and the molecules have weak Van-Der-Waals bonds [7]. For the common thermoplastics such as polyethersulfone (PES), polyetheretherketone (PEEK), polyetherimide (PEI), and polyphenylsulfide (PPS), the processing temperature typically ranges from 300°C to 400°C. Thermoplastics offer greater ductility and processing speed compared to thermosets, and can withstand high temperatures. The higher processing speed of thermoplastics is due to the low glass transition temperature (Tg) above which the material is softened and easily shaped. Subsequent cooling completes the fabrication process [4, 7, 11].

In thermosets the molecules are chemically joined together (cross liked) by strong covalent bonds [7]. For thermosets, such as epoxy and phenolic, the processing temperature typically ranges from room temperature to about 200°C. Thermosets (especially epoxy) have long been used as the polymer matrix for carbon fibre composites. During curing, usually performed in the presence of heat and pressure, a thermoset resin hardens gradually due to the completion of polymerization and the cross-linking of the polymer molecules. The curing of a thermoset resin is a reaction which occurs gradually. Thermoset resins in the liquid state quickly wet the surface of carbon fibre [11]. Heating of thermoset material causes disintegration and burning [4]. Thermoset limitations include a short shelf life, long fabrication times, and low strain to failure [7]. Thermosets in the liquid state require cross linking and solidification which takes from 7 hours to several days after adding the relevant agents. Partially cross-linked epoxies can be used where crosslinking is interrupted by storing the material at -18 °C [4]. The most commonly used thermoset polymer matrices include:

Epoxies (EP): Used for high quality high performance composites, normally a shiny amber/brown colour [12]. They exhibit excellent mechanical properties, toughness, and environmental resistance[13], however, their mechanical properties depend on the cure temperature of the epoxy (120 °C cure is used for moderate performance, while 180 °C cure is used in aerospace/military applications) with service temperature up to 155°C [8]. Nearly 95% of aerospace composites are epoxy based because of their inherent advantages such as the variety in mechanical properties achievable with different resins/hardeners and good adhesion to fibres. On the other hand, epoxy can suffer from moisture absorption and degradation, produce toxic fumes if burnt, and require painting to resist ultraviolet (UV)[14].

Vinyle Easter: Has balanced properties between epoxy and polyester.

Phenolic (P): Is a relatively cheaper thermoset resin used for secondary aircraft structures and interiors [13]. Its main advantage is fire resistance [12] with low smoke and toxic emissions [8].

Besmaleimide (BMI) and Polyimide (PI): Exhibit high mechanical properties at elevated temperatures[13]. They can withstand up to 260 °C and are mainly used in aero engines [8] but are relatively expensive.

CyanateEaster (CE): Exhibits temperature resistance up to 350 °C but absorbs moisture [13].

The term hybrid composites usually refers to composites containing more than one type of filler and/or more than one type of matrix [4, 11]. Hybrid composites can be cheaper than other types of composites depending on the required properties [6].

2.1.5 Fibre forms/architecture

Fibre type, volume fraction, length, and orientation affect the properties of a laminate in terms of density, tensile strength and modulus, compressive strength, thermal and electrical conductivities, fatigue strength and cost. Fibre form identifies the arrangement of fibres in the composite [7] which may involve unidirectional tows (strands), yarns (twisted), roving tapes in one-dimensional composites, (bi-dimensional or bi-directional) woven or nonwoven fabrics (felts or mats) and tri-dimensional fabrics or multidimensional fabrics with fibres oriented along many directions (>2)[3, 7], see Figure 2.8.

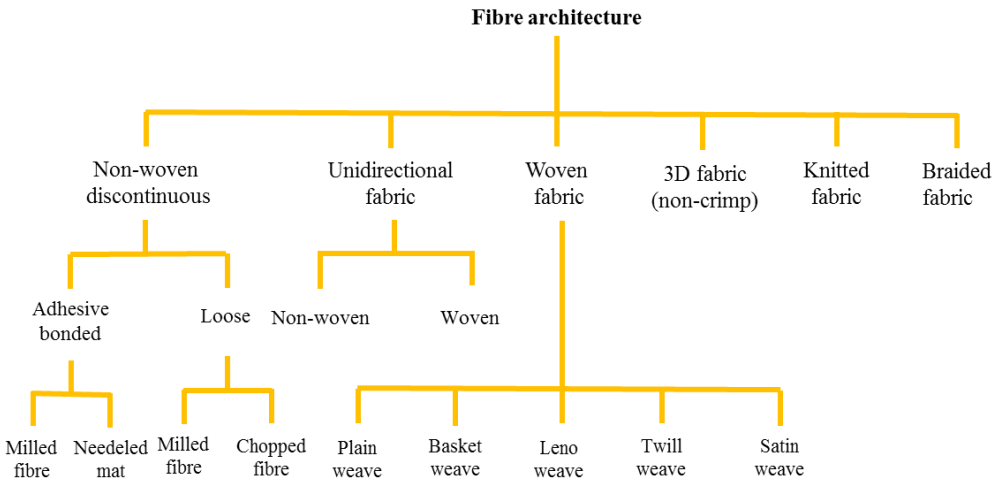

Figure 2.8: Fibre architecture

In unidirectional fabrics the fibres are held in place using an adhesive strip without weaving or fine weft to form non-woven UD fabrics alternatively the fibres can be woven [9]. Woven fabrics are more convenient for handling [11] see Figure 2.9. Fabric is made of fibres in two perpendicular directions namely warp and fill (weft). The fibres are woven together, which means the fill yarns pass over and under the warp yarns, following a fixed pattern of either plain weave or basket weave [4]. In 5-harness satin weave each fill yarn goes over 4 warp yarns before going under the fifth. A twill weave is done by passing the weft yarn over one or more warp yarns and then under two or more warp yarns and so on, with a "step" or offset between rows to create the characteristic diagonal pattern.

A drapeable fabric is easier to layup over complex shapes and drapeability is the ability of fibres to conform to the shape of the tool [4]. To obtain a fabric with maximum strength the fibres should be as straight as possible with minimum overlapping (i.e. low crimp). Knitting is a textile method used to obtain woven fabrics [7] but is not discussed in detail in this chapter.

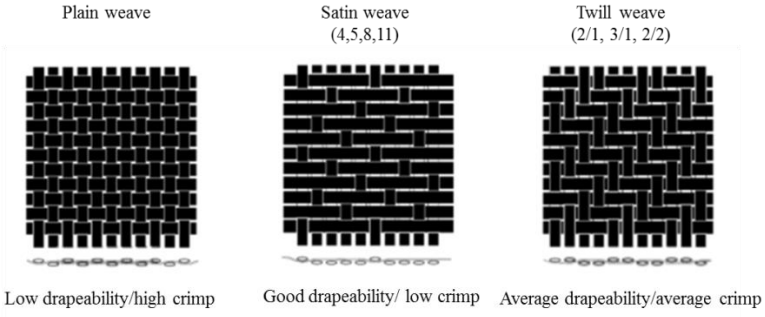

Figure 2.9: Weave patterns [8]

Non-crimp fabrics (NCF) are produced by assembling unidirectional layers and stitching them together to prevent fraying of fibre bundles. They can be unidirectional, bidirectional, Tri-axial, or quad-axial, see Figure 2.10. NCF flexibility in lay-up (drapeability) depends on material, angle, and the number of plies. Although NCF is cheap, it sometimes suffers from waviness and gaps [14].

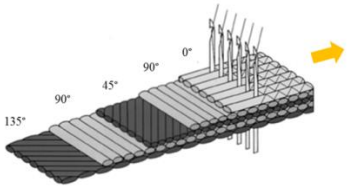

Figure 2.10: Non-crimp fabric [9]

Braiding is another textile weaving method [7] suitable for making composite tubes [11].

Prepregs (pre-impregnated fibres) are intermediate product consisting of fibres or tows aligned together in the form of sheet or tape coated with matrix (resin). The matrix material is usually not fully cured and is flexible enabling the laminate composite to be stored in a freezer and cured. The advantages of prepregs are as follows [15]:

- Reduced handling damage to dry fibres.
- Improved laminate properties by better dispersion of short fibres.
- Allows the use of hard-to-mix or proprietary resin systems.
- Allows more consistency because there is a chance for inspection before use.
- Subsequent heat curing provides more time for the proper laydown of fibres and for the resin to move and degas before cure.
- Enables increased curing pressure which reduces voids and improves fibre wetting.
- Enables optimisation of individual systems to improve processing.

2.1.6 Laminates

Lamina describes a layer of composite material in which fibres are oriented in one or more directions to reinforce the matrix. Laminae is the plural of lamina and a laminate is a stack of bonded Laminae [16]. Lamina usually ranges from 0.1-1 mm thick and consist of fibres, matrix, coupling agent or fibre surface coating, fillers, and other additives. Layers or plies are stacked and consolidated to form a laminate [7]. Lamina fibre configurations are shown in Figure 2.11 alternatively they can comprise a hybrid arrangement.

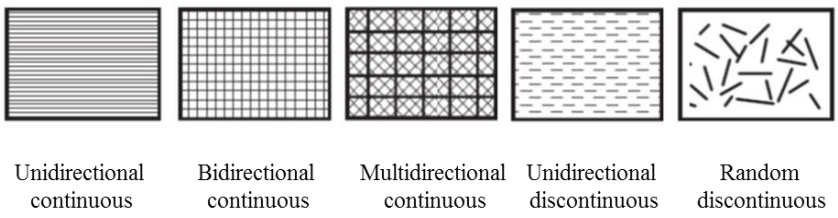

Figure 2.11: Lamina fibres configurations [7]

Figure 2.12 shows the anatomy of a laminated composite panel. Accordingly, the x axis represents the 0° and positive angles are counter clockwise while the negative angles are clockwise. In this case angles of 135° and -45° define the same fibre orientation. The laminate code provides a simple and easy description of a laminate ply orientation and the stacking

sequence. The simplest code describing a laminate consisting of fibres at different angles such as 0°, 45°, 90° and 135°, uses brackets to indicate the percentage of different ply orientation in the laminate. Consequently a designation of (25/50/25) means 25% of plies are in 0°, 50% at 45° and 135° or -45° and 25% at 90°. Alternatively, the code may indicate the percentage of 45° and 135° plies separately, such that (25/25/25/25) means every ply orientation equally represents 25% of the laminate. These codes are not descriptive enough for the stacking sequence.

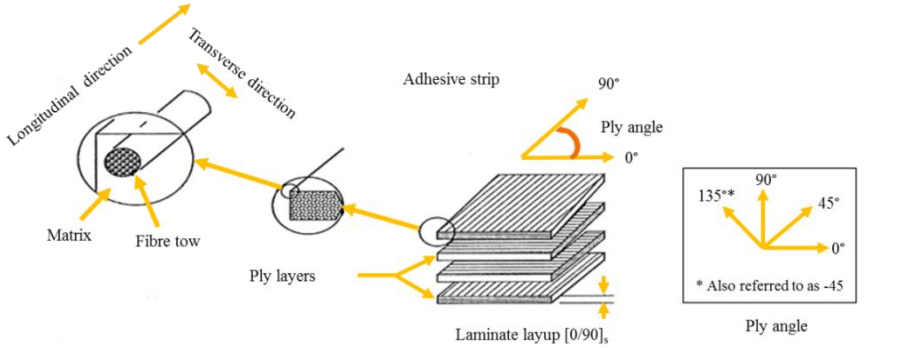

Figure 2.12: Anatomy of laminated composite panel [15]

In order to have a better description of the ply stack sequence, another code is used in which the orientation of each lamina is represented by the angle of orientation. The lamina code shows the order from the first ply to the last one between brackets. Orientation of successive layers is separated by a slanting line as long as they are of different orientation. If two or more adjacent plies are in the same direction, they will be put in parentheses and a number is indicated by a subscript. In the case of symmetric layups, a subscript of S is used while for non-symmetric laminates a subscript T outside the bracket denotes the total laminate definition code. If a layer is a weave fabric a subscript f is used. In hybrid composites, the ply material is represented by a subscript after the ply angle, see Figure 2.13 [17].

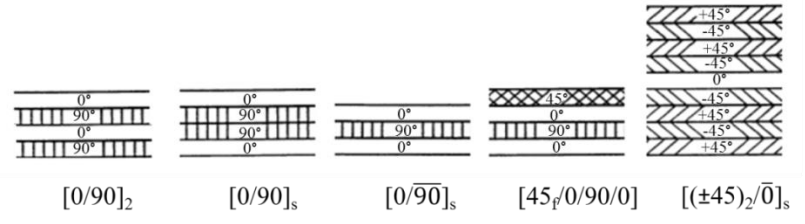

Figure 2.13: Example laminate codes [17]

For a quasi-isotropic laminate, there are three or more layers [15] with a middle plane that separates two half thicknesses of the laminate. Mid plane symmetry means stacking the plies on both sides starting from the middle plane. During cooling, the plies have a tendency to contract differently depending on their orientations causing thermal residual stresses, but using mid plane symmetry prevents deformation of the part [3], see Figure 2.14.

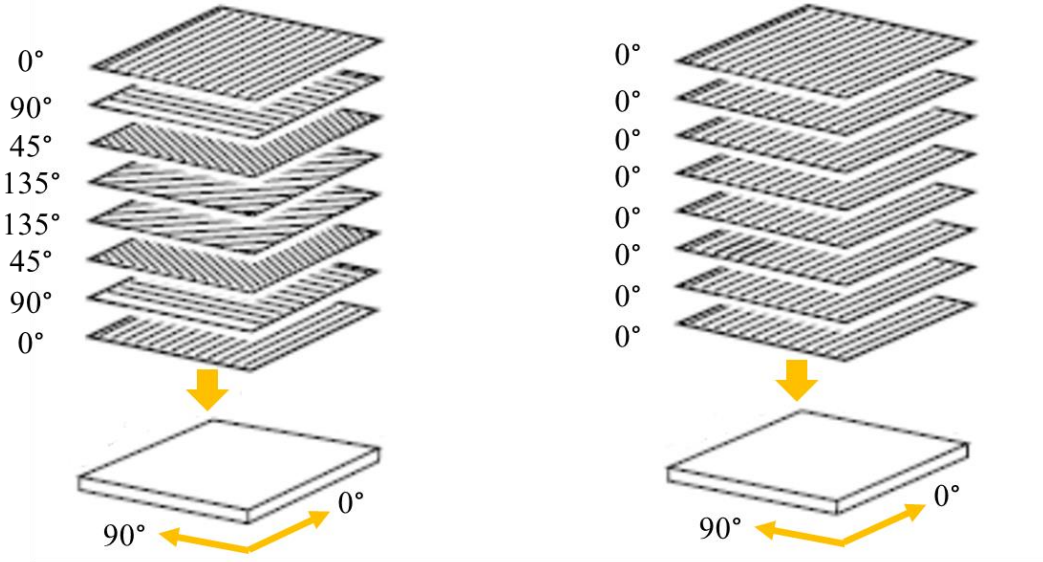

Figure 2.14: Quasi-isotropic vs. unidirectional lay-up [8]

2.1.7 Sandwich

A sandwich composite structure, see Figure 2.15, comprises a thin composite laminate skin bonded to a thicker core made from honeycomb, foam or balsa. The sandwich structure has very low weight, high stiffness, and typically production costs are low [8, 13].

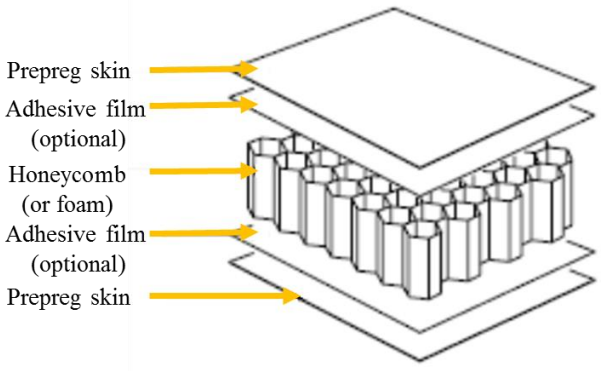

Figure 2.15: Honeycomb sandwich panel [13]

2.1.8 FRP composite fabrication methods

Generally, a composite component can have either monolithic, self-stiffened, sandwich structures or a combination of these. A monolithic component consists of parts or laminates without a core partly stiffened by stringers and stiffeners held together by fasteners [14] an example of which is the primary structure of an aircraft wing (shown in the next chapter). A self-stiffened component is designed to be stiffened by its own geometry and moulded as one part that may have stiffening features such as u-shaped elements [18]. A sandwich structure consists of two monolithic parts with a core (e.g. honeycomb or foam) between two surface layers [19].The most common fabrication methods are shown in Figure 2.16.

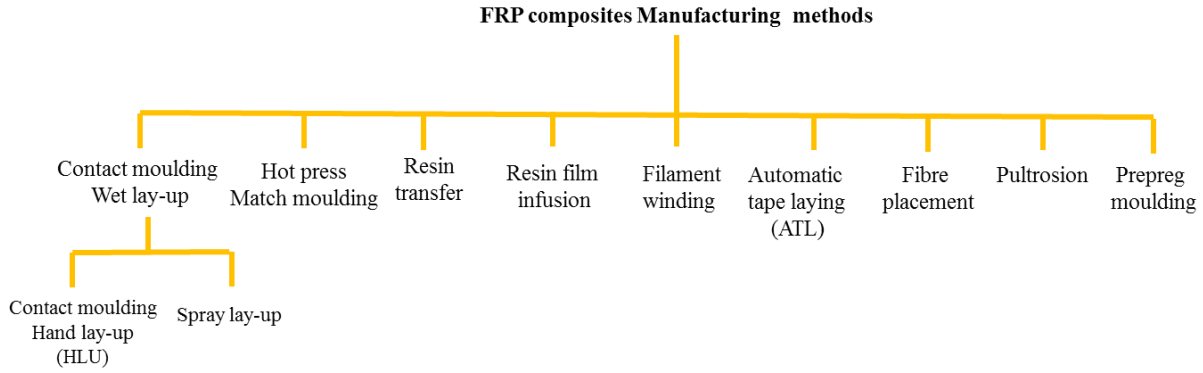

Figure 2.16: Most common fabrication methods of composites

Prepreg lay-up is used to produce high performance composites. The process can involve manual hand lay-up (HLU) or automatic layup using a robot or CNC machine as in the automatic tape laying (ATL) process. The prepregs require a vacuum bag and curing in an autoclave in order to harden the matrix. The curing process can be done in an oven for marine and railway applications while most high performance aerospace composites are cured in an autoclave [8]. Fabrication of material used in this research by HLU process is detailed in Appendix-B. A diagram summarising the process which is used for primary and secondary aircraft structure parts is shown in Figure 2.17 [14] .

Inspection of fibre reinforced composite parts typically focuses on the fibre arrangement and defects such as matrix cracks (voids, porosities), fibre cracks, interface cracks (debonding), delamination (splitting between laminae and a laminate) or inclusions which may significantly affect its properties [11]. Inspection methods include metallographic examination, X-ray analysis, infrared thermal imaging, and the C-scan techniques.

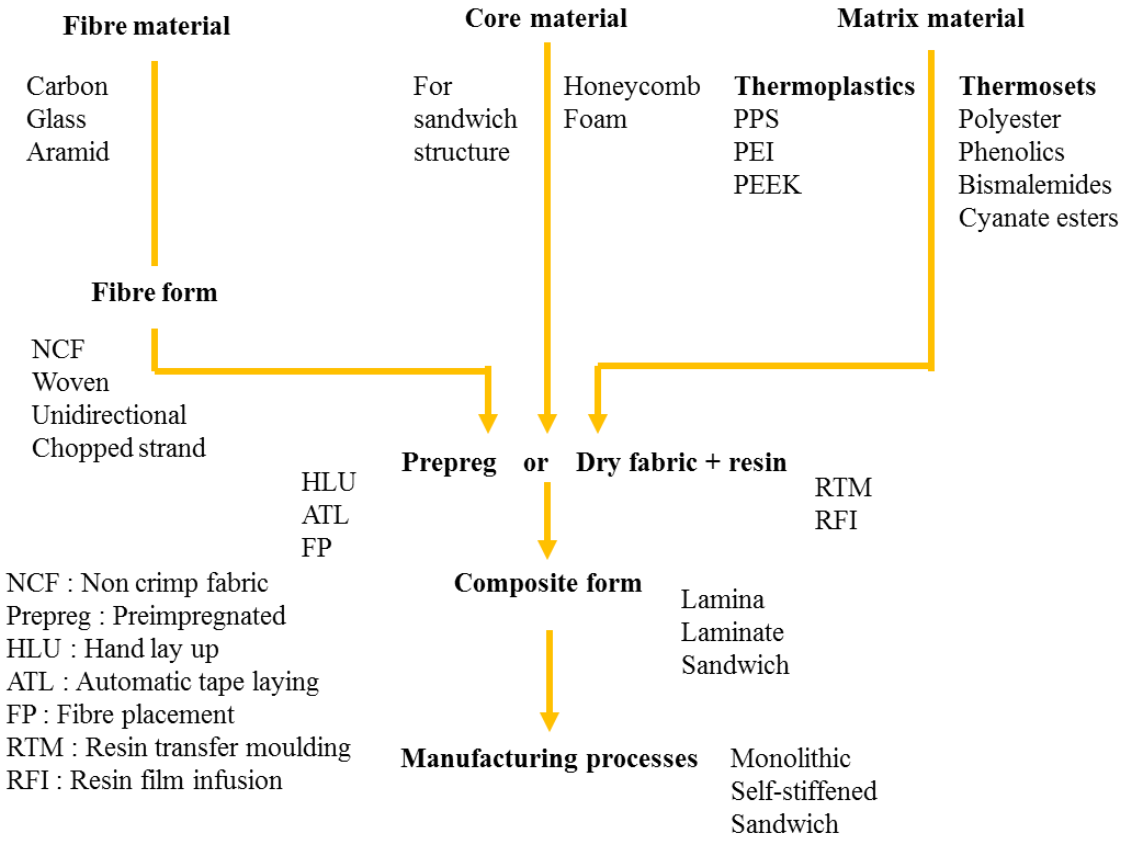

Figure 2.17 Composite material manufacturing methods [14]

2.1.9 Health and Safety

Machining carbon fibre can affect human health and machine condition. The person using composites can be exposed to hazardous material through skin and eyes by contact or inhalations of solvent fumes or dust, ingestion, or injection of fibres which enter the body by puncturing the skin. Skin protection requires the use of gloves while masks and extraction systems are required to remove dust and hazardous volatiles. Abrasive fibres cause wear to machine tool guideways, and conductive fibres cause short circuiting [4]. Abrasive dust may also cause spindle wear, hence, there is a need for dust extraction systems [12]. Material toxicity in relation to human health is a function of the exposure times. The probability of this hazard being harmful is called the risk. For every material which poses a hazard to human health there are permissible limits of exposure. Occupational Safety and Health Administration (OSHA's) permissible exposure limits (PEL) and ACGIH's threshold limit value (TLV) are the most common recommended exposure limits for airborne concentration of a material [15].

There are common terminologies to describe exposure limits which are time weighted average (TWA), short term exposure limits (STEL), and ceiling (C). The first is based on the 8 hr work period done by the majority of workers, the second is the exposure permitted for short times, while the third one is the exposure not to exceed a specific level. Data for each case appears as PEL-TWA or TLV-STEL etc.[15].

There are hazards which relate to the matrix material and the fibres. For example a carbon fibre/epoxy composite material may have some health effects as seen in Table 2.2 [15]. Normally, the material supplier provides a material safety data sheet (MSDS) which includes toxilogical information to be used for risk assessment of a material. The MSDS of the material used in this thesis can be found in Appendix-C.

Machining of composite materials is necessary to obtain accurate geometries and surfaces to facilitate a precision fit of components during assembly. It also improves surface quality and eliminates inherent shrinkage problems from previous composite processing.

Machining of composites represents a challenge owing to the inhomogeneous and anisotropic nature of the material. Machining of such materials depends largely on the cutting direction with respect to fibres. As a result, the large machinability database relating to metals, alloys and plastics are not appropriate/relevant for composite machining.

Table 2.2 Health effects associated with epoxy type [15]

Material	**Known health effects**	**Key notes**
Bisophenol A based	Possible skin senstiser; low order of acute toxicity; slightly to moderately irritating	Insufficient evidence to classify as a carcinogenic according to IARC. Considering the many studies as a whole, the evidence does not show the resins to be carcinogenic
Carbon or graphite fibres	Mechanical abrasion and irritation of the skin; possible dermatitis; physico-mechanical properties of the fibres rather than a toxico-chemical reaction. Possible reaction from the fibersising.	PEL-TWA is 15 mg/m^3 total dust, and PEL-TWA of 5 mg/m^3 for synthetic graphite respirable dust. ACGIH has a TLV-TWA of graphite except fibres. There are no limits for carbon fibre, through the US Navy has set 3 carbon fibres/cc. EPA did not classify the potential carcinogenic properties of carbon fibres due to insufficient data

2.2 Machinability of fibre reinforced plastic (FRP) composites

Machinability is not a single measureable characteristic of a material nor is it universally defined but it describes the level of difficulty encountered in cutting a material [19, 20]. The assessment of machinability involves measurement/evaluation of cutting tool performance (tool wear/life), cutting forces and power, cutting temperature, surface integrity (delamination/roughness etc.), and chip formation. Figure 2.18 shows factors affecting the machinability of FRP composites during cutting operations [20]. In the following sections, the machinability of FRP undergoing machining by various cutting processes with emphasis on milling will be discussed to highlight research trends.

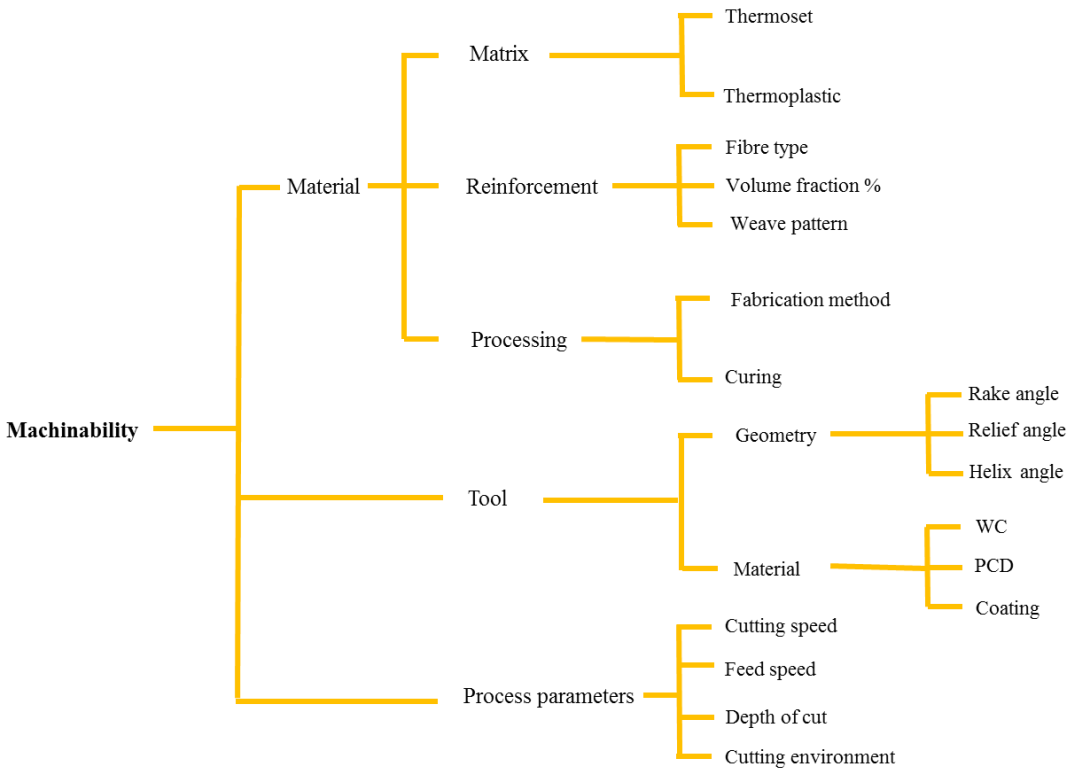

Figure 2.18: Factors/parameters affecting machinability of FRP composites [20]

2.2.1 Orthogonal cutting

Researchers have studied the orthogonal cutting of composites since the early 1980's to understand the behaviour of the composites when machined. Research on turning and drilling has increased with the increased application of composites in industry. Table 2.3 gives references relating to variables and responses. Research on drilling represents the majority of machinability literature. Despite the fact that in orthogonal cutting (two dimensional

arrangements) there are few cutting parameters compared with industrial machining (three dimensional), it is felt noteworthy to detail values and associated references, see Table 2.4.

Table 2.3: References relating to variables and responses studied in orthogonal, turning and drilling tests

Process	Variables	Responses
Orthogonal cutting	Tool geometry [21-33] Fibre orientation [21-25, 27-29, 32, 33] Depth of cut [21, 23-27, 29, 30, 32, 33] Tool material/coating [21, 33] Workpiece material [29] Cutting speed [21, 23-25]	Chip formation [21-25, 27-29, 33] Cutting force [21-25, 27-34] Tool performance [21, 22, 31] Surface roughness [21, 23-25, 29]
Turning	Feed rate [35-53] Cutting speed [35-40, 42-44, 47-54] Depth of cut [37, 39, 40, 43, 47, 49-53] Tool material/coating [38-44, 47, 48, 55, 56] Tool geometry [40, 41, 44, 45] Workpiece material [35, 36, 38, 39, 41, 45, 46, 57] Fibre orientation [37, 48-51]	Cutting force [35, 36, 39-43, 45-48, 58] Tool performance [38-41, 43, 44, 47-50, 55, 56]. Temperature [43, 47] Chip formation [43, 48] Surface roughness [37, 39-42, 44] [45, 48, 51-54, 56, 58]
Drilling	Feed rate [59-103], Cutting speed [59, 61-65, 67-70, 72, 74, 76-86, 88, 90-100, 102, 103], Tool geometry [59-61, 64, 65, 67-71, 73, 78-84, 87, 92, 94, 96, 97, 99, 104-114], Tool material performance [62, 82, 88, 91, 93, 95, 96, 99, 108, 113, 115, 116], Drill diameter [68, 71, 72, 95, 98, 101, 107, 117-119], Workpiece material [72, 74, 95, 100, 102, 107] Fibre orientation [60, 66],	Delamination [59-61, 64-67, 69-80, 86, 87, 90, 91, 93, 96-98, 100, 103, 106-111, 116-118, 120-126] Thrust force/torque [59-75, 82-93, 96, 99-111, 116-128] On surface roughness [68, 91, 93, 95, 100, 102, 103, 113, 114] On roundness / circularity size [60, 92, 93]

Table 2.4: Values and associated references for different machining process

Factor		**Orthogonal cutting**	**Turning**	**Drilling**
Material	CFRP	[21-29, 33, 34]	[36, 38, 39, 41, 43, 44, 47, 48, 55, 56, 58]	[59-64, 66-73, 76-79, 81-85, 96-99, 104-108, 112, 114, 116-118, 120-126, 128, 129] in epoxy, [100, 103] ABS matrix
	GFRP	[30-32, 130]	[35, 37, 40, 42, 45, 46, 49-51, 53, 57]	[74, 75, 80, 87-90, 94, 95, 101, 102, 114, 115, 119]
	Aramid	-		[72, 95, 114]
Tool geometry	Rake	-10° [27] to 40°[32]	-5° [47] to 20° [41]	-
	Relief	5° [21] to 30°[30]	5° [39] to 12° [56]	-
	Helix	-		-
Cutting speeds	m/min	0.46 m/min [31] to 48 m/min [21]	11 [48] to 800 [38]	1.9 m/min [100] to 877 m/min [88]
Feed rate	mm/min	---	0.025 mm/rev [38] to 0.5 mm/rev [49]	0.001 mm/rev (1.5 mm/min) [124] to 0.7 mm/rev 700 mm/min [117]
Depth of cut	mm	0.025 [29] to 0.4 [31]	0.05 [58] to 2 [41]	
Force components	N/ N.m	Fc, Ft	Fc, Ft, Fr	Fz, Mz

A large number of published papers dealing with the orthogonal cutting of composites focuses on chip formation using the quick-stop technique [21-26]. Accordingly it was found that when cutting unidirectional composites with fibres tilted towards the cutting direction at 45°, the fibres encounter compression and bending, and are broken by shear. In the case where fibres are tilted away at 135°, they encounter tension and bending and easily broken due to their brittle nature, the resulting fibre pull-out providing a smoother machined surface [22, 29]. When cutting multi-directional composites, the response of fibres at angles $\geq 90°$ is improved by the support of the adjacent layers yet material removal is governed by the most difficult to cut rigid layers [24] see Figure 2.19 [23] . Chip shape, cutting forces, and surface roughness are also dependent on fibre orientation.

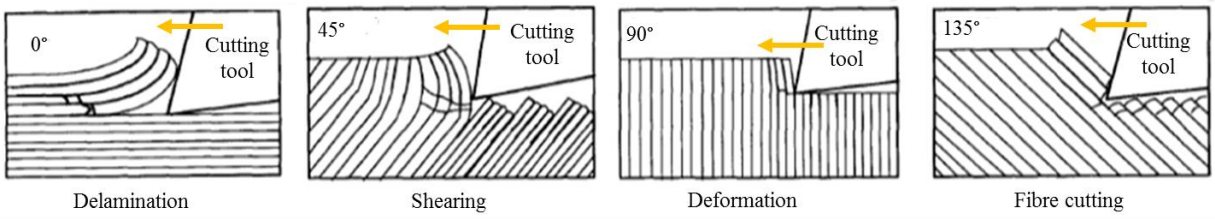

Figure 2.19: Different fracture modes occur at different fibre orientations and tool rake angles [23]

Arola et al. suggested that chip fracture occurs in two stages due to primary and secondary fractures [27, 28] as shown in Figure 2.20 (a). Wang and Zhang [29] reported a 'bounce-back' phenomena which tended to increrese rubbing between the tool and workpiece, see Figure 2.20 (b). However, there were no equations presented to describe neither the bouncing back nor the primary/secondary fractures phenomena. The coefficient of friction between a WC tool and CFRP composite is ~ 0.25 [21] compared to 0.5-0.8 in the case of WC with metals [131]. Only few researchers have compared the performance of different tool materials [21, 33] and there have been relatively few attempts to model the process using either Merchant's model [22] or FEA [27, 28, 32-34, 130].

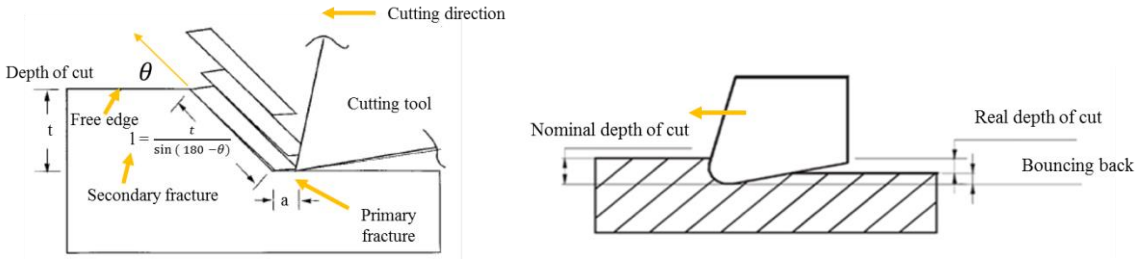

Figure 2.20: (a) Primary and secondary fractures [28], (b) Bouncing back after cutting [29]

Published research work on turning has covered the effect of fibre length (i.e. long or short) [39], the machining of an unreinforced matrix in comparison to a fibre reinforced one [41, 45], and the effect of different composite processing methods [57]. Reinforcing glass fibres were found to be responsible for the brittle behaviour and lowering of the cutting forces [46]. Testing has also included the use of brittle cutting tools like ceramics [39, 44]. The use of tools with a sharp corner is not recommended for achieving good surface roughness [45]. Vibration assited cutting helped minimise workpiece surface roughness even in the most difficult cutting conditions with fibres at 90˚ orientation.

Sreejith et al. reported a cutting temperature ranging from 200-450 °C depending on cutting speed and feed rate [43]. In the case of PCD tools, the temperature was less than WC due to the higher thermal conductivity of the PCD (~560 W/mK) compared to WC (85-100 W/mK) [56].

2.2.2 Turning of FRP composites

Turning research has highlighted operational aspects such as low dynamic forces which result mainly from the alternating fibre direction with workpiece rotation and provided an understanding of the effect of different parameters on workpiece quality with moderate levels data on tool performance and tool wear. Despite the good performance and long tool life reported, some of the tools detailed may not be applicable in milling as will be discussed later. Little or no data appears to have been published concerning tool temperature when using coolants.

2.2.3 Drilling of FRP composites

Hole making represents 90% of the carbon fibre machining in the aerospace industry [132]. Tool performance is characterised by the number of holes drilled. The effect of thrust force and torque have been extensively studied as they affect delamination and hole quality aspects. Delamination represents the main concern associated with drilling of composites as it affects the fatigue life due to splitting cracks [129] and is responsible for rejection of drilled parts which are very expensive [133]. Delamination in the top ply is typically lower than in the bottom ply which is why permitted drill damage at the entrance surface should be less than 1.5 mm measured from the edge of the hole, and be not deeper than 0.25 mm while the damage permitted at the exit surface depends on the diameter as specified in Figure 2.21.

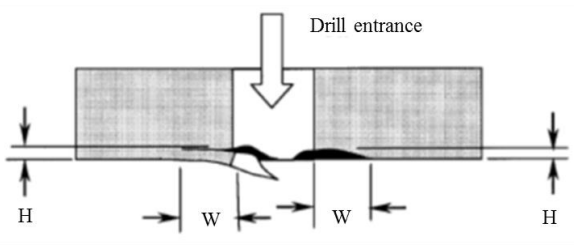

	Fabrics		UD tape	
Hole Diameter (Nominal)	**H (mm)**	**W (mm)**	**H (mm)**	**W (mm)**
3/16" (4.76 mm)	0.18	0.75	0.35	2.5
1/4" (6.35 mm)	0.18			2.5
5/16" (7.93mm), 3/8" (9.52mm)	0.18	1.0	0.35	3.0
7/16" (11.11mm)	0.18	1.0	0.35	4.0

Figure 2.21: Acceptable damage (courtesy of Airbus) [134]

Delamination can be quantitatively measured using different techniques such as ultra-sonic C-scan [59, 61, 62, 64, 65, 69, 118], imaging analysis [74, 76, 81, 82], radiography [97, 104, 120, 121] or, laser "Shadow Moire", as presented by Seif et al. [77]. Radiography (X-ray computerised tomography) and laser techniques have the capability of detecting surface and sub-surface defects, without contact or using liquid mediums compared to C-Scan which can affect the properties of composites [59].

Researchers have used different methods to obtain dimensional and non-dimensional delamination measures. Khashaba studied delamination size (Rmax-R) which was measured using imaging [74]. Tsao and Hocheng [59] calculated a delamination factor by dividing the diameter of the damaged zone by the hole diameter from C-Scan images. A more accurate delamination factor based on damage area was used by Davim et al. [76]. Delamination was found to be affected by drill diameter [59] and feed rate, and reduced with cutting speed [74, 77, 80, 81, 98], eccentricity [110], and point angle [81]. It was also noted that the chisel edge was responsible for more than 50% of the thrust force [101]. For optimum results, the use of special tool designs rather than the conventional twist drills have been adopted to minimise damage [97], see Figure 2.22.

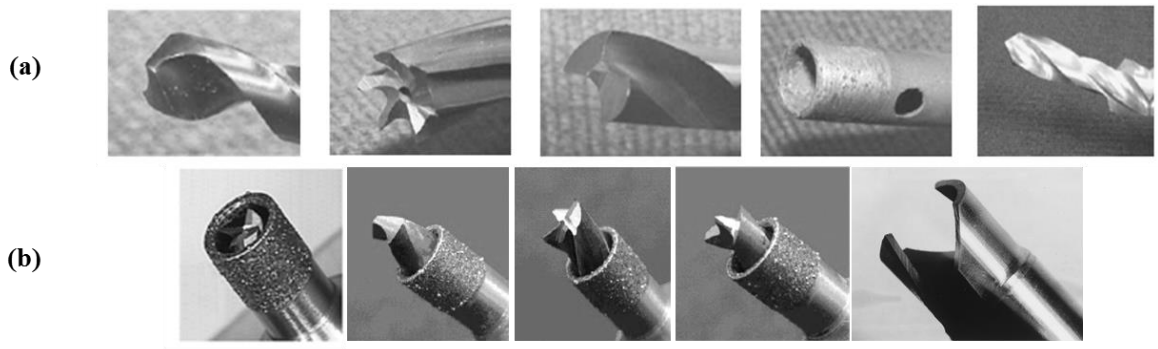

Figure 2.22: Drill geometries investigated (a) Conventional twist drill, saw, candle stick, core drill, and stepped drill, (b) Core-saw drill composed of the saw drill (inner) and core drill (outer), step core drills (twist, saw and candle-stick) drills [109], trepanning [119]

Delamination can be minimised or prevented using trepanning (16 times higher feeds, 50% less thrust and 10% less torque) [119], a woven or random fibre orientation compared to unidirectional laminates [74], a pilot hole to neutralise chisel edge effects [71, 72], backup[75, 77], peel ply layers [82, 96], variable feed rate (decaying feed) [60, 74, 122], vibration assisted drilling (small amplitude < 6 μ and high frequency > 300 Hz) to reduce the thrust force and torque by 20-30% [88-90], helical feed or orbital drilling (65% of conventional drill

force) [86, 108, 135], or by using hybrid process (ultrasonic assisted helical drilling)[136]. Most recently, an ingenious technique for minimizing both entry and exit delamination was developed by Schulz et. al [137] involving a 5-axis wobble milling technique where the material acts as self-backup as shown in Figure 2.23. Alternatively drilling can be replaced with moulded-in holes [115].

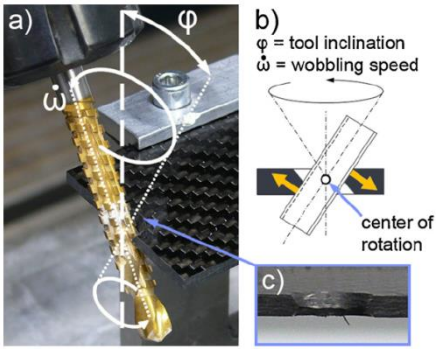

Figure 2.23: Kinematics of wobble milling [12]

With regard to modelling of the critical thrust force to onset of delamination in different situations, a summary of equations of critical thrust force and delamination factor can be found in Liu et al. [138]. Recently drilling hybrid structures or stacks (FRP and other materials such as Ti or aluminium) represent the current research focus [86, 91-93, 113]. Burr formation is a major challenge in the drilling of stacks.

2.3 Milling/routing of composites

Milling is one of the most frequently used machining processes for FRP composites. It can be used for deburring, slotting, and routing/edge trimming of composite components produced to near–net-shape [139]. Milling of FRP composites is characterised by low material removal rates as compared to metal cutting operations. The process is used to obtain the required level of surface quality and accuracy [140]. In addition to trimming and contouring operations, milling can also be used for producing 3D details.

There are two main types of milling operation namely face milling and peripheral milling. This section deals mainly with routing and slotting operations (which are milling processes most of the time). The main process parameters in milling are given in Table 2.5. Based on the shape of the surface required, a variety of milling operations can produce flat surfaces, shoulders, groves, edges, pockets, contours, slots, cut-offs or chamfers, see Figure 2.24. In

composite machining there is not as much material removal as when machining conventional materials/alloys because the material is already cured to near-net-shape. Milling operations such as shouldering, grooving, cutting-off and edge trimming represent the most common operations for composites, see Figure 2.25. In the following sections the machinability of composites using end milling is discussed.

Table 2.5: Milling process parameters

Spindle speed N (rpm)	Cutting speed $V = \frac{\pi \times D \times N}{1000}$ (m/min)
Feed per minute or feed speed V_f (mm/min	Feed per revolution (mm/rev)
Feed per tooth $f = \frac{V_f}{N \times Z}$ (mm/tooth)	Axial depth of cut a_p (mm)
Radial depth of cut or width of cut a_e (mm)	Material removal rate MRR (mm^3/min)

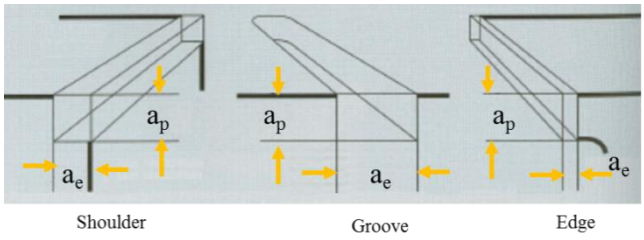

Figure 2.24: Shoulder, groove and edge cutting [19]

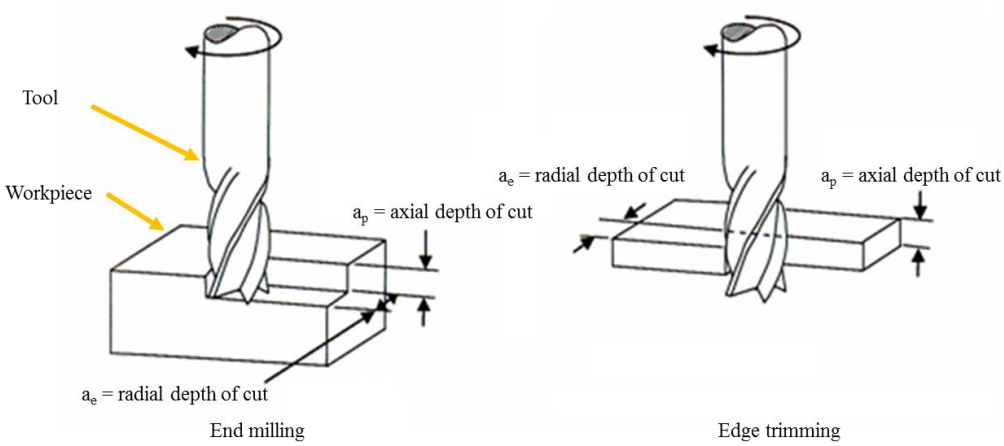

Figure 2.25: End mill in action performing end milling of a shoulder, and edge trimming [4]

There are two different modes of milling namely; up milling and down (climb) milling, see Figure 2.26. Climb milling is preferred because it does not require strong workpiece fixation but it may be affected by table feed backlash necessitating a backlash eliminator [141]. When milling composites there is controversy about which milling mode is best, as

different materials respond differently to the cutting action depending on fibre orientation. Generally, climb (down) milling helps prevent fibre separation.

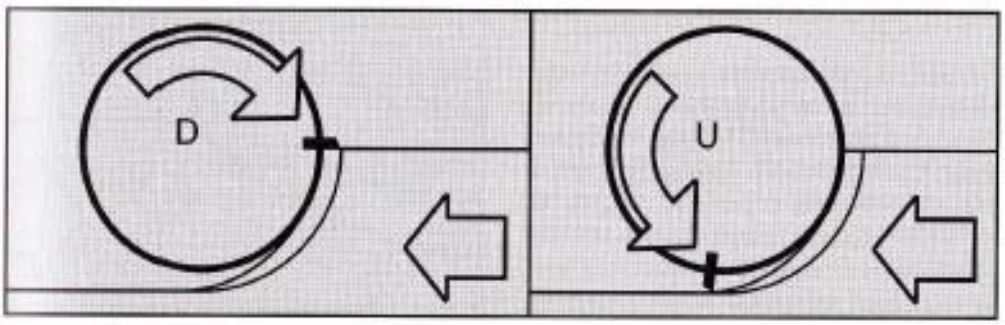

Figure 2.26 : Down (climb) milling, and up (conventional) milling [19]

2.3.1 Process requirements

Cutting CFRP requires high stiffness machine tools in order to avoid vibration and deflection resulting from the high cutting forces[142]. Machine requirements to provide efficient high quality machining of FRP are detailed in Figure 2.27 [140]. Milling CFRP requires control of the small particles of fibres and matrix material which are abrasive (harm slide ways) and conductive (harm electronic circuits). The hazardous and abrasive dust like chips together with any fumes produced during machining, necessitate the use of an extraction system [139].

High speed machining (HSM) can provide advantages in terms of reduced machining time and burr formation and increased productivity, improved accuracy and product quality. Schulz noted that the definition of HSM varies from one material to another as shown in Figure 2.28 [143]. HSM reduces cutting forces, tool deflection, and temperature, however, it requires operating higher skills, and greater control of tool balancing, and runout (restricted to $\leq$ 10 μm [144] compared to 30-50 μm in case of normal machining [145]). Runout causes a torchoidal motion of the cutter teeth that affects machining stability and produces increased surface roughness in end milling [146]. Additionally the machine tool requires appropriate rigidity, dynamic behaviour, and kinematics [147].

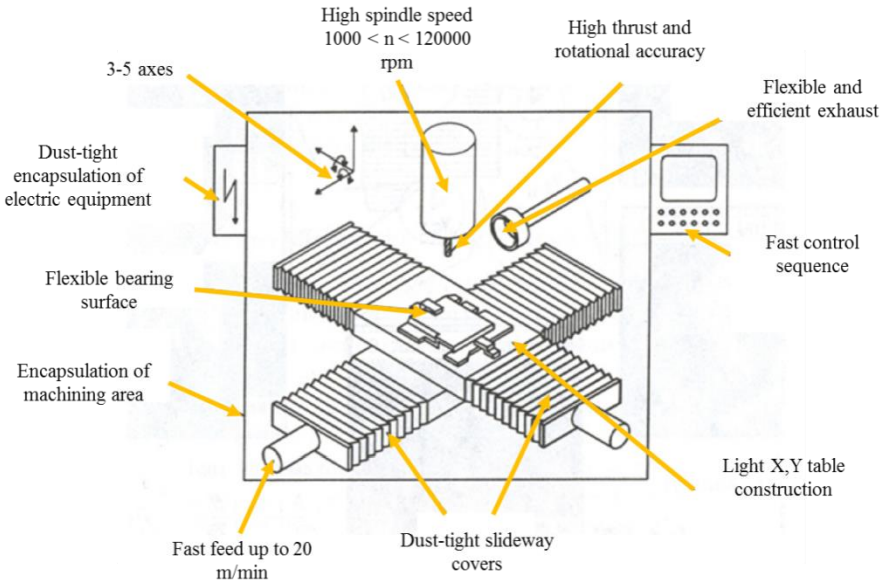

Figure 2.27: Machine requirements for reliable, high quality machining of FRP, proper clamping is required as FRP are sensitive to compressive stresses [140].

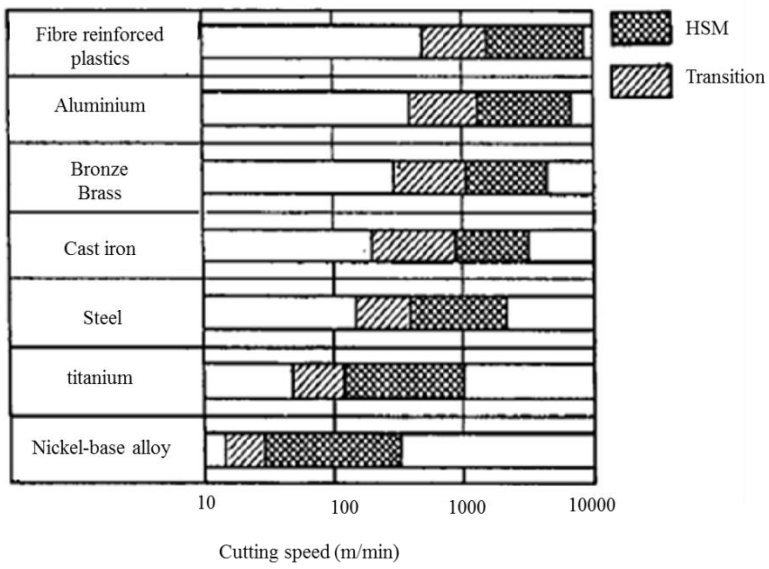

Figure 2.28: Cutting speeds for HSM of different materials [143]

2.3.2 Machinability study

Since the knowledge acquired in cutting metals/alloys cannot readily/easily be transferred to composites, studying the milling of composites becomes necessary. The majority of published research has addressed edge trimming operations, only a few papers have dealt with full immersion or slotting operations. Research work on milling of composites has involved a wide range of materials including aramid fibre reinforced plastics [140, 148-150], carbon

fibre reinforced plastics in a thermoset resin matrix [139, 140, 142, 148-174] or in thermoplastic resin [175], or even stacks [135], together with glass fibre reinforced plastics [140, 148-150, 176-178]. CFRP is the most common composite material used in military and commercial aerospace systems [152]. Relevant components are subject to specific requirements relating to surface roughness, edge angularity, size, and allowable top and bottom surface ply delamination. Table 2.6 presents variables and responses studied in milling together with sample references.

Table 2.6: Variables and responses studied in milling and sample references.

Variables	**Responses**
Parameters Cutting speed [139, 142, 150, 154, 160, 161, 165, 167-170, 172, 175-177, 179, 180] Feed rate [135, 139, 142, 151-153, 158, 160, 161, 165, 167-170, 172, 175-177, 179, 180] Radial depth of cut [142, 167-169, 171, 175, 179, 180] Axial depth of cut [173, 174] Up milling/down milling [151-153, 157, 171] Workpiece Material [140, 148, 176, 177] Fibre orientation [139, 140, 151, 152, 157, 164, 171, 173, 181] Tool diameter [155, 172] Tool geometry [140, 148, 150-153, 155, 156, 159, 160, 170, 172] Tool material [148-152, 154-156, 158, 159, 163, 172, 178] Cutting environment Coolant [151, 152, 175]	Chip formation [139, 140, 157] Cutting forces [135, 139, 140, 150, 153, 157, 161, 163, 165, 167, 168, 170, 172-176, 178-181] Delamination [139, 142, 150-153, 157, 163, 165, 169-171, 176, 177] Surface roughness [139, 140, 142, 153, 156-158, 160-165, 169, 170, 175-177, 179, 180] Tool performance [139, 140, 142, 148, 150, 154-156, 158, 159, 161-163, 165, 172, 175, 178-180] Cutting temperature [155, 161, 163, 175]

2.3.3 Chip formation

In milling CFRPs the fibre orientation with respect to the cutting edge, is always varying. Cutting mechanisms can be described with respect to different fibre orientation as shown in Figure 2.29. Accordingly, fibres of 0˚ orientation laminates are subjected to forces parallel to the fibre orientation causing buckling, material fails due to delamination in front of the cutting tool edge. At fibre angles between 0˚ and 90˚, fibres break as a result of bending and compression, fibre fracture extending beyond the surface such that surface quality is poor

(least favourable). Fibres at 90˚ are subjected to bending loads causing interfacial fractures extending under the surface. Fibres at approximately 135˚ are subjected to bending and tensile stresses and are removed in bundles. Fibres are sometimes ripped off where there is insufficient adhesion to the matrix [140]. The cutting mechanism also depends on fibre type such that glass and carbon fibres show brittle fracture failure when subjected to shearing, tension or bending stresses. In contrast, aramid fibres show resistance to bending or shearing but fail due to tension, producing some fuzz in the axial direction [140]. Tool life is reported to be dependent on fibre type [156]. The common chip form in milling of composites is 'powder like', however, when milling unidirectional composite the chip type can be either powder, ribbon, or brush-like depending on fibre orientation as shown in Figure 2.30.

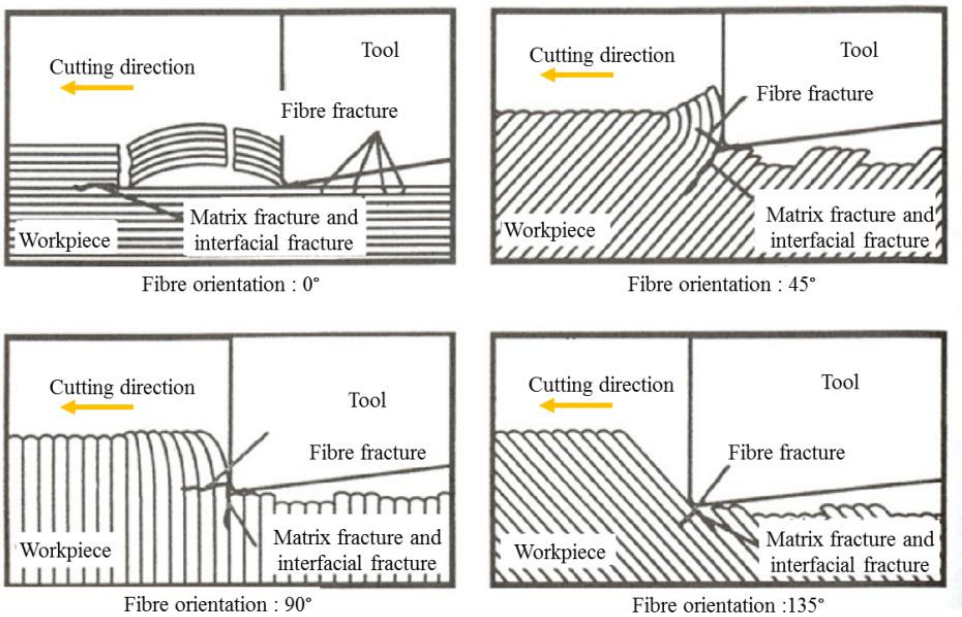

Figure 2.29: Cutting mechanisms for milling of CFRPs [140].

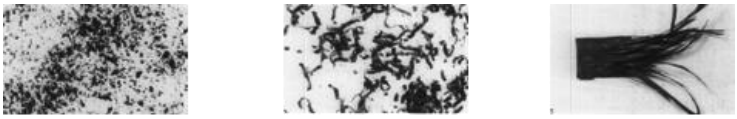

Powder Ribbon Brush

Figure 2.30: Chip characteristics (powder, ribbon, brush) 45˚, 90˚, 0˚ [139]

2.3.4 Cutting speed and workpiece feed

As previously detailed there are several machining techniques that can be used to generate surfaces on composite parts such as edge trimming, face milling, and Sturz milling (Sandvik Coromant), see Figure 2.31. Sturtz milling involves the use of an end mill to generate a complex surface by tilting the tool (2o-10o) relative to the component surface to create an elliptical cutter path. It can replace machining with ball end mills for profiling of CFRP workpiece and is 3 times faster than a ball nose tool as the number of passes per square meter are reduced [12]. In milling of CFRP composites using routers ranging from 6-12 mm diameter, the recommended cutting speeds and feed rates varied from manufacturer to another and also according to the application (i.e. slotting or edge trimming) and the suitable tool geometry and tool material. For example, SECO Tools recommended a 100-200 m/min cutting speed and a 0.018 to 0.036 mm/tooth feed rate for slotting using WC tooling. The use of higher cutting speeds and feed rates is favourable for higher productivity but however was still under feasibility investigation. Carbon fibre composites are normally cut at a cutting speed of 244-762 m/min using PCD [15]. Table 2.7 shows recommended cutting speeds and workpiece feeds for roughing and finishing of CFRP using PCD tooling. Researchers have used a wide range of cutting speeds from 25 m/min [153] to 1000 m/min [140], and feed rates from 0.01 mm/tooth [168] to 0.3 mm/tooth [157]. In the case of helical milling (mix between face milling and drilling) the tool has two feed parameters (axial and tangential). The helical path can be achieved using a CNC code with helical interpolation. The kinematics of the process are detailed by Denkena et al. [135].

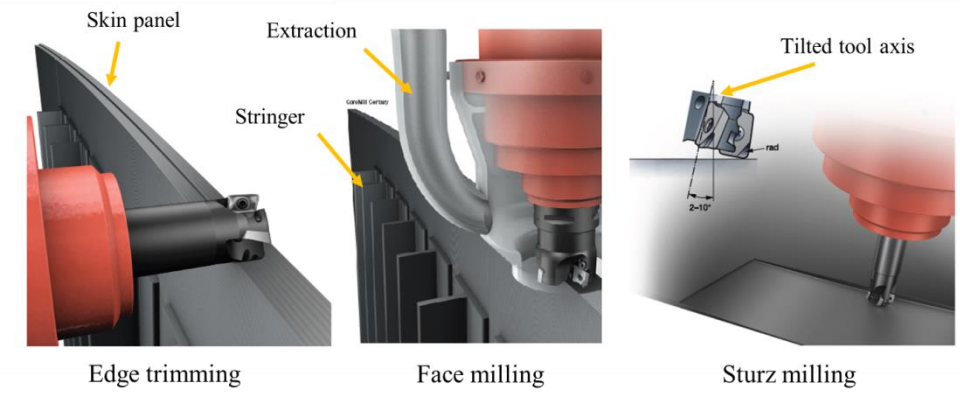

Figure 2.31: Edge routing, face milling, and Sturtz milling [12]

Table 2.7 :Recommended parameters for roughing and finishing (using PCD tooling) from Sandvik [12]

<table>
<tr><th colspan="2">Edge routing</th><th>Face milling</th><th>Sturtz milling</th></tr>
<tr><td rowspan="2">200 m/min , 0.15 mm/tooth
For high removal rate and good surface finish</td><td>Roughing
314 m/min
0.03-0.08 mm/tooth</td><td>Roughing
300 m/min
ap 0.1
0.16 mm/tooth</td><td rowspan="2">5 degrees Sturtz angle
2 mm depth of cut
1800 mm/min
0.2 mm/tooth</td></tr>
<tr><td>Finishing
314 m/min
0.02 – 0.04 mm/tooth</td><td>Finishing
300m/min
ap 0.5
0.1 mm/tooth</td></tr>
</table>

2.3.5 End mill geometry

A variety of cutter shapes/configurations are available for milling of FRP. The most commonly used geometries are fluted tools, burr routers, and diamond grit routers. The selection of router geometry can be material oriented such that some tools are recommended to deal with specific work materials. For example straight fluted tools are recommended for carbon fibre composites, burr tools are preferred for glass fibre, while serrated tools are best suited for aramid fibres or sandwich structures [19].

2.3.5.1 Fluted tools

Fluted tools have many detailed features, the most important of which are the relief angle, rake angle, and helix angle. The relief angle is required to reduce the friction between the tool and the machined surface, the rake angle facilitates chip flow, and the helix angle is beneficial in distributing the cutting load, reducing temperature or minimising tool damage. The cutting edge can have a secondary relief angle which is advantageous for material spring-back after cutting [155] and ensures machining stability [156]. When milling composites, helical flutes help reduce the heat input per unit length of the cutting edge [182]. However, cutting is more stable using a tool with low helix angles such that the tool life was longer with 2° resulting in 1800 m cut length compared to 850 m using 30° helix [183]. While more flutes reduces the pressure on the tool and keeps it cooler, Davim and Reis found that 2 flutes were better than 6 in relation to delamination [160]. End mill geometry is detailed in Figure 2.32 while the effects of different geometry features on machinability for different FRP machining process are tabulated in Table 2.8.

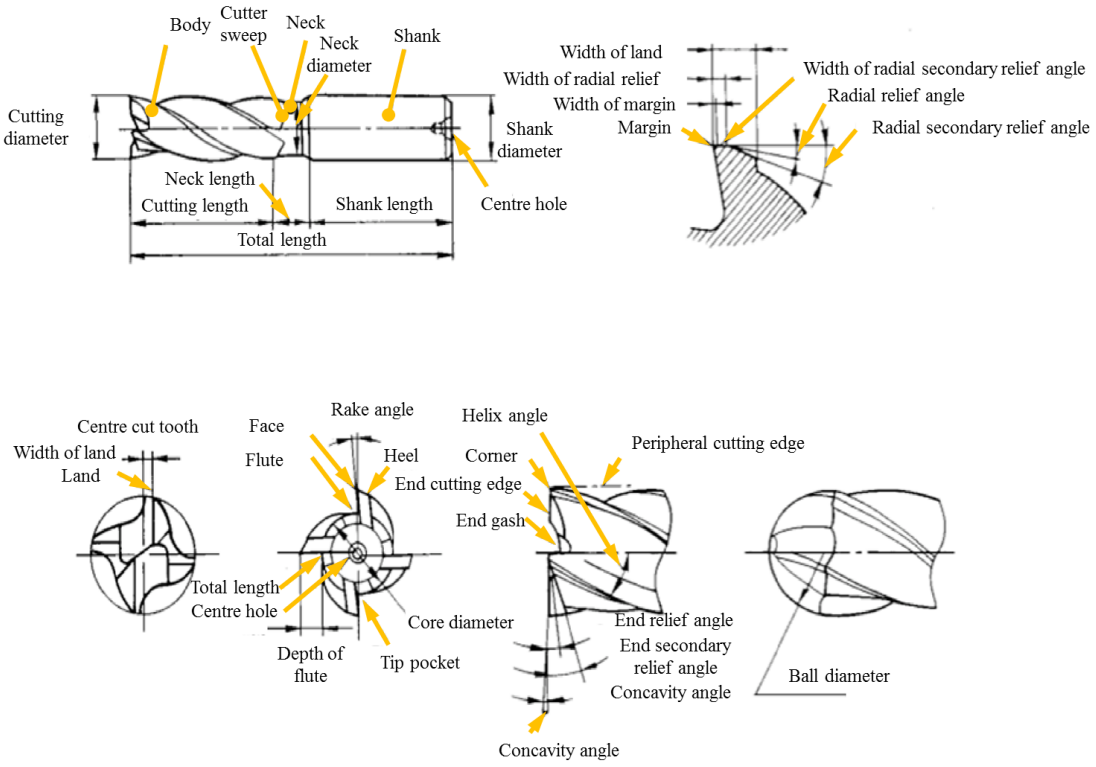

Figure 2.32: Geometry features of an end mill

2.3.5.2 Interlocking (burr) tools

Burr routers have teeth with a pyramidal shape (knurled shape) resulting from the interlocking between right hand and left hand helices. Burr routers are most commonly used with glass fibre composites [149]. The complex shaped teeth require special techniques to characterise tool wear. Tool geometry has been shown to have an impact on tool wear as the number of right/left helices change, open design 14-11 being better than 14-12 [178]. The powder like chips may fill the spaces between the teeth hence open teeth are recommended with such materials. Clogged teeth in the closed design reduces tool life [172]. In the case of small diameter tools which are prone to breakage due to deflection at high feed rates, Iliescu et al. introduced an optimised design that increased tool life by a factor of 10, see Figure 2.33 [172].

Figure 2.33: Tapered shank as a solution for small diameter tools [172]

Table 2.8: Effect of different geometry features on machinability responses

Geometry feature / Response	Relief angle	Rake angle	Helix angle
Tool wear	Flank wear generally decreased at larger relief angles [31, 184]	Higher positive rake angle tool makes the tool more fragile and susceptible to higher amount of wear [44]. Negative rake angles are not favourable in terms of tool life [184]	An increase in helix angle decreases the amount of heat per edge length [182]
Workpiece surface integrity/ roughness	Larger relief angle reduces/eliminates workpiece surface defects causes by tool wear.	Larger rake angles produce finer chips and promote high quality machined surfaces [26, 30, 31, 44]. For fibres at 90˚ and above, the dependency of surface quality on rake angle is high [29, 130]	The level of workpiece delamination decreases with larger helix angles while the position of greatest surface delamination (top or bottom) is dependent on helix direction. [151] Use of a double helix milling cutter reduces the occurrence of fuzzing and improves workpiece surface quality [151, 185]
Forces	Increasing the clearance angle reduced contact between the tool and workpiece and consequently reduces cutting forces [23, 24, 30] Specification of a secondary relief angle is recommended to reduce cutting forces because of bouncing back fibres [29]	Negative rake angle generally enhances tool strength and heat capacity but conversely leads to higher cutting forces [182] Forces are lower at larger positive tool edge rake angles due to easier chip flow [26-28, 30, 32].	Use of double helix tool directs axial cutting forces towards the centre of the workpiece , which in turn minimises surface damage [151, 185].
Recommended values	17˚ [23, 24, 30]	0˚ and 7˚ [140], 6˚-7˚ [26] 15˚ for low cutting forces, 10˚ for better surface [28] 0˚-20˚ [29]	10˚- 30˚ Smaller is better for tool life [183]

2.3.5.3 Abrasive grit tools

In abrasive machining of composites the tools are smaller (6-25 mm) than conventional applications where wheels can reach 1000 mm in diameter. The cutting speeds and feed rates when using abrasive tools are lower compared to grinding and moreover, the large effective chip thickness makes material removal higher than that in grinding [4]. The abrasive grit is typically held in a metal matrix. In this case tool geometry is represented by the grit mesh number. Figure 2.34 shows such tools with different grit sizes, used by Colligan and Ramulu [153]. In comparison to fluted tools, abrasive cutters are normally used at lower feed rates below 0.15 m/min [152]. Ideally, for higher productivity tools should be held in modular tool holders rather than jaw chuck holders to facilitate rapid tool change and reduced idle time. The most common modular tool holders are the SK (or ISO), BT, HSK (mostly in Europe) and CAT (most common in USA). The HSK, or the hollow shank, was developed in Germany in the 1980's and helped overcome the unbalance associated with higher rotational speeds. Adapters can help interchangeablity between different systems.

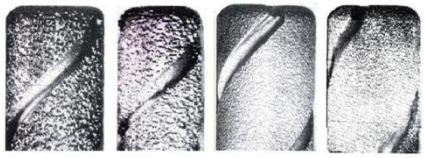

30 **50** **80** **125**

Figure 2.34: Abrasive grit tools with various grit numbers 30, 50, 80 and 125 [153]

2.3.6 Tool material

Unlike turning, milling is an intermittent machining process in which the cutting forces vary. Additionally, changes in fibre orientation with respect to cutting direction causes dynamic forces [22]. Such fluctuations of force cause flaking of cutting tool coatings by accelerated fatigue [186], which makes the milling of composites a challenging process. Generally, a cutting tool is subjected to mechanical loads and high temperature, with friction between chips as well as against the machined surface. A tool should possess special characteristics such as high toughness to resist fracture, high hardness at elevated temperature, chemical stability, and high wear resistance [187]. Tool materials suitable for machining composites [18, 154, 155, 159, 186, and 187] include the following:

Sintered carbides: The hardness of the material at room temperature depends on the carbide type such that tungsten carbide (WC) is ~ 2000 HV, titanium carbide TiC is ~ 3000

HV, tantalum carbide TaC is ~1700 HV, and niobium carbide NbC is ~ 2000 HV [19]. TiC and TiCN products are usually called cermets. The performance of WC is affected by:

- WC/cobalt ratio (typically 6–12%), increasing cobalt decreases hardness, but increases toughness and impact resistance. When testing three different substrates for coated and uncoated burr tools 6%, 8% and 12% Co micro grain, Lopez de Lacalle [178] found that the 6% cobalt was better in terms of tool life.
- Grain size can be <1µm , the smaller the grain the harder the WC

The most commonly used carbide is WC made as integral tools (for better balancing) or inserts (for rapid tool change). The different WC grades are P, M, K, H, S, and N and are intended for different applications. The most common commercial grades are P, M, and K. The P (1-50) grade is used for long chipping materials like steels, M (1-40) grade is used for more demanding alloys, while K (1-40) grades are recommended for short chipping materials such as cast iron or plastics [19]. A two digit number after the letter (1- 40) represent the hardness and toughness and the lower the number the harder the grade and the opposite for toughness. For example, in K grades which is the most common grade used in machining of composites the K10 is harder than K30 [187].

Diamond: Mono-crystalline or natural diamond is the hardest material on earth with hardness ~ 9000 HV. This single crystal diamond is normally used to obtain mirror surface machining required in high end applications [187].

Polycrystalline diamond (PCD): PCD provides 60 – 100 times the tool life of WC when machining composites [15]. The PCD segment thickness ranges from 0.2–2 mm bonded to a WC substrate [159]. The properties of PCD vary to some extent with grain size. Coarse products (50 µm) are more abrasion resistant than medium grades (10-25 µm) while fine (1-5 µm) or ultra-fine-grain (< 0.5 µm) products provide high sharpness and toughness [187]. PCD wear stabilises (longer uniform zone) compared to WC which results in longer tool life. Fine grain products (1-2 µm) have been shown to have lower wear resistance in milling of CFRP compared to 6-7 µm products as noted by Klocke and Wurtz [156]. At elevated cutting temperature, the brazing joint holding the PCD to any substrate material is susceptible to failure. In tests by Ramulu and Rogers [154] tool life for carbide tooling was less than 10 seconds as it sustained severe wear due to the interrupted cutting and repeated impacts resulting in a rough surface, PCD was more economical. It was found to be 10 times better than carbides in terms of tool life [155].

During fabrication of PCD tools use of wire EDM, electro-discharge grinding, or mechanical grinding will influence the surface roughness of the PCD and may affect performance of the tool. Mechanical grinding is extensively used in preparing cutting edges producing flank surfaces of 0.12 µm Ra compared to 0.53 µm Ra in the case of WEDM [188]. Laser cutting is reported to leave lower damage on PCD [189]. Veined PCD is made by packing the diamond powder into groves formed in the carbide body and sintering under high pressure and temperature to provide more complex geometries compared to the segmental PCD an added benefit is the elimination of braze joint failures [159].

2.3.7 Tool coatings

Towards the end of 1960's tool coatings were introduced which are applied using physical or chemical vapour deposition (PVD) or (CVD). One or more layers (usually 2-15 µm thick) are deposited and bonded to the substrate to provide a hard wear resistant surface capable of increasing performance and ensuring chemical stability [187]. The most common coating types are titanium carbide TiC (3000 HV), aluminium oxide Al_2O_3 (2300 HV) and titanium nitride TiN (2200 HV) [19]. A list of the commonly used coating materials and relevant references on milling CFRP are shown in Table 2.9.

Table 2.9: Common coating material

Coating Materials	**Colour**	**Thickness (µm)**	**Coefficient of friction**	**Max temperature (°C)**	**Reference**
TiN	Gold	1-7	0.55	600	[140, 155, 161]
TiCN	Blue-Grey	1-4	0.2	400	
CrN	Metal-Silver	1-7	0.3	700	
CBC	Grey	0.5	0.15	400	
AlTiN	Black	1-4	0.7	900	[150, 163, 172]
µAlTiN	Black	1-4	0.3	900	
TiAlCN	Burgundy-violet	1-4	0.3	500	
ZrN	White-gold	1-4	0.4	550	
AlCrN	Blue-grey	1-4	0.6	900	[150]
nACo	Violet-Blue	1-4	0.45	1200	

Milling of CFRP using Al2O3 coated carbide is detailed by Kauppinen [149] while CVD diamond was used by Sheikh-Ahmad and Sridhar [158] ,and Lopez de Lacalle et al. [178]. The smoothness of the coating surface affects the friction forces between the tool and the workpiece. The deposited coating layer may have a rough surface resulting from spattered

coating droplets. This can be removed or enhanced by surface treatment as shown in Figure 2.35.

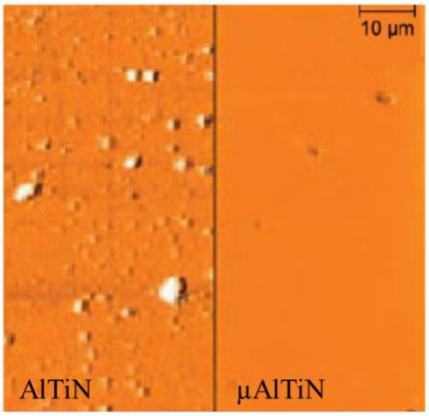

Figure 2.35: Difference between un-treated (left) and treated (right) AlTiN coating surface [187]

Coating performance depends on the coating material and its adhesion to the substrate. For example, when using an Al_2O_3 coated burr router tool life was ~ 10 min compared with 1 min in the case of a cermet coated router (at 1400 m/min cutting speed and 0.007 mm/tooth) [155]. A thicker coating retards tool wear, however, thicker coatings are prone to brittle fracture and flacking.

The rounding of the cutting edge with thicker coatings was noted by Wurtz et al. [155] who tested different coating materials and reported that coating performance was found to be a function of hardness and adhesive force. Chemical etching, ultrasonic scratching with diamond particles, and the use of an intermediate layer are possible means of surface treatment of the substrate material prior to coating. All these methods are used to improve adhesion and nucleation. Good adhesion permits predictable uniform abrasive wear [190-192]. Etching of the surface was reported as being helpful in roughing the surface and providing good adhesion thus preventing peeling of the coating [150]. Treating the surface with a chemical agent roughens the surface by removing cobalt to improve the adhesion of the coating [150]. The application of coatings using physical vapour deposition (PVD) has been the focus of research from 1980's. Table 2.10 is a comparison between PVD and CVD coating deposition techniques.

Table 2.10: Comparison between PVD and CVD coating deposition techniques

Coating deposition process	**PVD**	**CVD**
Process description	PVD process is atomisation or vaporisation of solid material and depositing on a substrate. No chemical reaction occurs between coating and substrate. Easily recoated and resharpened. Cracking resistant.	Condensing an element from a gas in reaction chamber. Interact with the substrates, and sometimes producing brittle carbides at the interfaces. Susceptible to cracking at impact.
Sharp edge	Possible	Difficult
Process temperature (°C)	400-500	900- 1000
Common substrates	HSS, WC	WC
Common coating material	• TiN • DLC	• Al_2O_3 • TiC • TiCN • Diamond

Forces are generally lower in the case of coated tools (low friction coefficient) [150]. Diamond coated carbides compete with polycrystalline diamond (PCD), the former being 30% lower in cost and easier to manufacture with complex geometries [41]. There are two types of diamond coating, the first is diamond like carbon (DLC) which has similar properties to natural diamond (optical, chemical, mechanical, and electrical) but does not have the crystalline lattice structure [192]. This type of coating is deposited using PVD techniques. Diamond like carbon contains less Sp3 and a mixture of Sp2/Sp which makes the structure amorphous. In contrast CVD diamond contains more Sp3 within the structure and may be the reason why CVD diamond is better than the amorphous DLC coating in terms of abrasion resistance [192].

Chemical vapour deposited diamond coatings were developed in the 1980's, the process involving precipitation of carbon atoms from a hydrocarbon gas onto a substrate [159]. Two distinct types of diamond coating based on coating thickness can be produced, namely "thin film" where the coating thickness is ~5- 50 μm, and "thick film" involving 0.5 μm layer CVD diamond. Both have polycrystalline structure [192] but contain no binder phase. Chemical vapour deposited diamond coatings have good properties such as high hardness (6000-9000 HV), low coefficient of friction (as low as 0.05), high thermal conductivity (up to 2200

W/mK), and moderate chemical stability. The polycrystalline structure of the CVD diamond makes it tougher than the mono-crystalline diamond (~5.5 compared to 3.4 MPa/m^2) [193]. The hardness of the CVD diamond (described as pure PCD) is higher than PCD because the later contains cobalt and porosity [194]. Horman et al. [159] compared WC, CVD diamond, and PCD when milling CFRP. Accordingly, the tool life ratio was 1:10:15 respectively. On the other hand the cost ratio was 1:7:13 which highlights the cost effectiveness of CVD diamond. The superior wear resistance of the CVD diamond may be because of the crystalline tetrahedral Sp3 covalent bond structure [192]. Improved CVD coatings were produced by Shen et al. [150]. They found that a modified hot filament CVD with a spiral heat source provide better and uniform thermal distribution of 2-3 μm grain diamond particles than the conventional horizontal filament CVD. In the case of thick film, edge preparation is not important as these CVD films are brazed to a substrate then ground to required geometry [194]. Stephan et al. found that thick film CVD had an advantage over WC 15:1 in terms of flank wear [194].

A new coating technique involves interlocking layers of polycrystalline and nano-crystalline diamond, see Figure 2.36. This provides high resistance to abrasion and is also capable of diverting the direction of crack growth [195]. Nanostructure coatings are said to be the future of coatings, being harder, tougher, and more chemically stable than previous/existing coatings [4]. Lopez de Lacalle et al. [178] found that a micro-grained carbide tool with a cobalt content of 6% coated with nanostructures had a cost advantage over PCD. A nano coating of AlTiN did not show any significant advantage in milling of CFRP [178]. Using a diamond interlocked tool, coating provides a barrier against high abrasion. Once the top of the pyramid shaped tooth is lost in the initial wear stage, it leaves behind exposed substrate. An improved composite coating described as naCo or nano-composite, was noted by Lopez De Lacalle. It was obtained by embedding nano-crystalline AlTiN or AlCrN grains in a $Si3N_4$ honeycomb matrix to improve the coating characteristics. Testing of AlCrN against AlTiN in milling CFRP showed that thicker layers of AlTiN (more than 4 μm) were advantageous [172, 178].

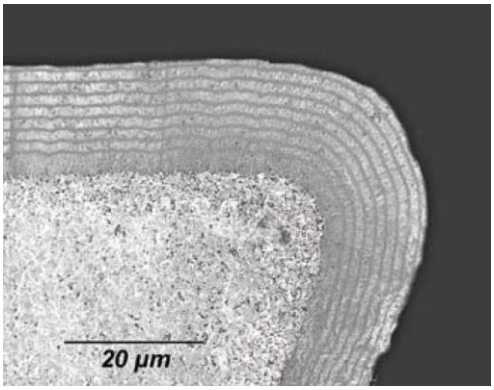

Figure 2.36: Interlocking layers of polycrystalline and nano-crystalline diamond [195].

2.3.8 Tool wear

Wurtz et al. [155] stated that the most suitable tools are determined by mechanical load from the abrasive fibres and thermal stresses due to insufficient thermal conductivity of the polymer matrix. Under such harsh conditions milling tools encounter various sorts of wear during cutting of FRP composites including; flank wear, rounding of edges, burns, cracks, pitting on cutting edges, chipping, failure of brazing joint, or deposited material on flank/rake faces. Additionally, milling of FRP composites expose the tool to dynamic forces. In order to understand the wear mechanisms in milling, a simulation of the router cutting action was introduced by Ramulu and Rogers [154]. It allowed differentiation between the wear caused by abrasion against that resulting from intermittent cutting. Because routing is an interrupted process, they used a CNC lathe programmed to maintain constant cutting speed to cut a 90˚ notched circular disc using a single insert as shown in Figure 2.37. They concluded that tool life in the case of interrupted cutting is shorter than that in continuous cutting as impact produced more damage.

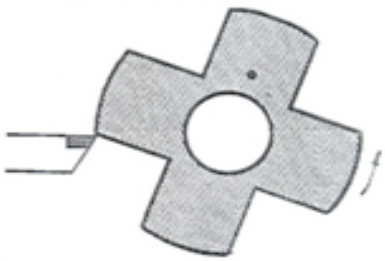

Figure 2.37: Interrupted cutting was simulated using a notched workpiece [154].

The main tool wear mechanisms in milling of FRP are abrasion, attrition, and micro fracture/ chipping. When using carbide tools, Santhanakrishnan et al. [11] noted that brittle

fracture was responsible for tool failure due to the carbon fibres reacting with cobalt and forming a harder compound which was subsequently pulled out. Energy-dispersive X-ray spectroscopy (EDX) analysis showed less cobalt content in the worn tools [155]. Sheikh-Ahmad and Sridhar [158] studied edge trimming of CFRP using uncoated and two CVD diamond coated carbide tools (thin 10 µm and thick film 20 µm). When using the CVD coated tools at high feed rates, chipping and delamination of the coating occurred due to the high cutting forces, while abrasion wear of both the coating film and the substrate was dominant at low feed rates. The thicker CVD coating showed better resistance to abrasion as shown in Figure 2.38 [158].

There is no common criterion used for judging the end of tool life, however, a tool is considered to warrant-replacement if adhesion of resin, flames or workpiece delamination is observed [150]. Tool life can be evaluated qualitatively, i.e. based on deterioration of workpiece quality and evidence of uncut tufts which result only if cutter sharpness decreases and/or rounding of the cutting edge increases [156]. When edge trimming, tool life is normally 100-200 m cut length depending on depth of cut and tool material. In contrast, slotting operations are generally subject to a shorter tool life of ~ 30m due to the harsh cutting action [150]. Tool wear takes many forms depending on tool geometry (fluted, burr, or abrasive), tool material, and cutting conditions. The following section describes the common tool wear phenomena associated with standard flute tools, as well as burrs and abrasive tools.

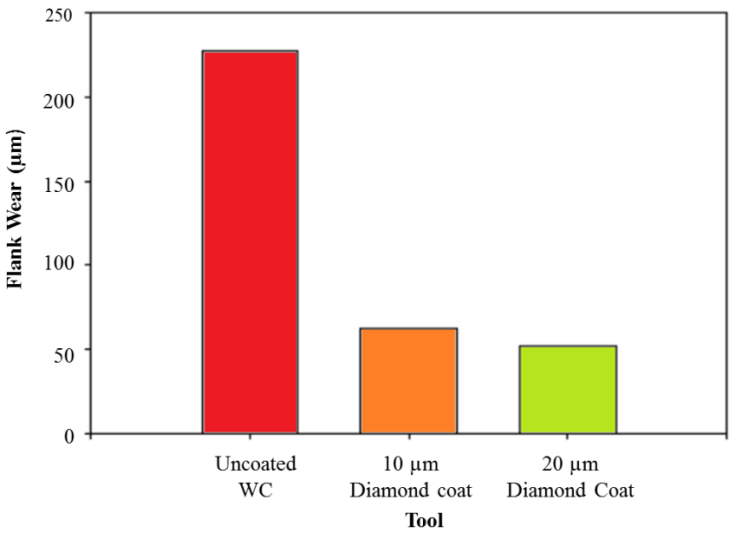

Figure 2.38: Flank wear compared after 338 m cut length (calculated total distance travelled by tool) at 62 m/min cutting speed, 1270 mm/min feed rate (0.127 mm/tooth) [158]

The ISO 8688 standard [145] describes the main wear patterns in milling and their locations on a fluted milling cutter. Figure 2.39 shows the most common wear types seen when milling composites. Wear such as crater wear, flacking, and cracking are not mentioned because they rarely occur. A mean flank wear size is the usual tool life criterion, due to it causing a change in tool dimension and therefore the size of the machined part. Values of 0.3 mm and 0.5 mm are the maximum accepted for finishing and roughing respectively. Chipping of greater than 0.5 mm is also a further tool life criterion. Flank wear (VB) is characterised by loss of particles along the cutting edge and is measured on the clearance face of end milling tools. Three different measurements are possible: uniform flank wear VB1 which is the mean wear, non-uniform flank wear VB2 which is irregular wear in several zones of the cutting edge, and the localized flank wear VB3, found at specific points. Notch wear (VBN) is located at the depth of cut line when cutting materials susceptible to mechanical hardening.

Chipping (CH) is said to occur when irregular flaking of the cutting edge occurs at random points, this is very difficult to measure and prevent. It consists of small tool portions breaking away from the cutting edge caused by mechanical impact and transient thermal stresses due to cyclic heating and cooling in interrupted machining operations. Two different measurements are possible: Uniform chipping CH1 which appears as small edge breaks of approximately equal size along the cutting edge engaged on material. Non-uniform chipping CH2 is random chipping located at some points of the cutting edge, but with no consistency from one edge to another, see Figure 2.39. Interlocked tools are not mentioned in the ISO standard. Recently Lopez de Lacalle et al. [150] used the measure "wear percentage" to evaluate the wear in pyramidal shaped teeth as follows :

Wear % = (Worn surface area/ area of the pyramid base) × 100 Equation 2.1

The wear associated with a burr or an interlocked tool is complex and results from superposition of tip fracture and flank wear. Prashanth [196] introduced a new technique based on image processing software to measure the complex tool wear with diamond interlocked tools. Fractures of the pyramids increased with a decrease of cutting speed and increase of feed rate, see Figure 2.40. Depth of cut affects tool life such that using a burr tool, Kauppinen [149] reported that tool life was only 5 min at a radial depth of cut a_e = 2 mm however this increased to 20 min by reducing the depth of cut to 1 mm. Surprisingly flank wear was found to decrease with the increase of the effective chip thickness and the

phenomena was explained as a possible result of self-grinding of such tools, see Figure 2.41 [162]. The wear phenomena associated with abrasive grit tools are similar to the grinding process. Figure 2.42 shows wear flats (abrasion), grit loss, and grit fracture [197].

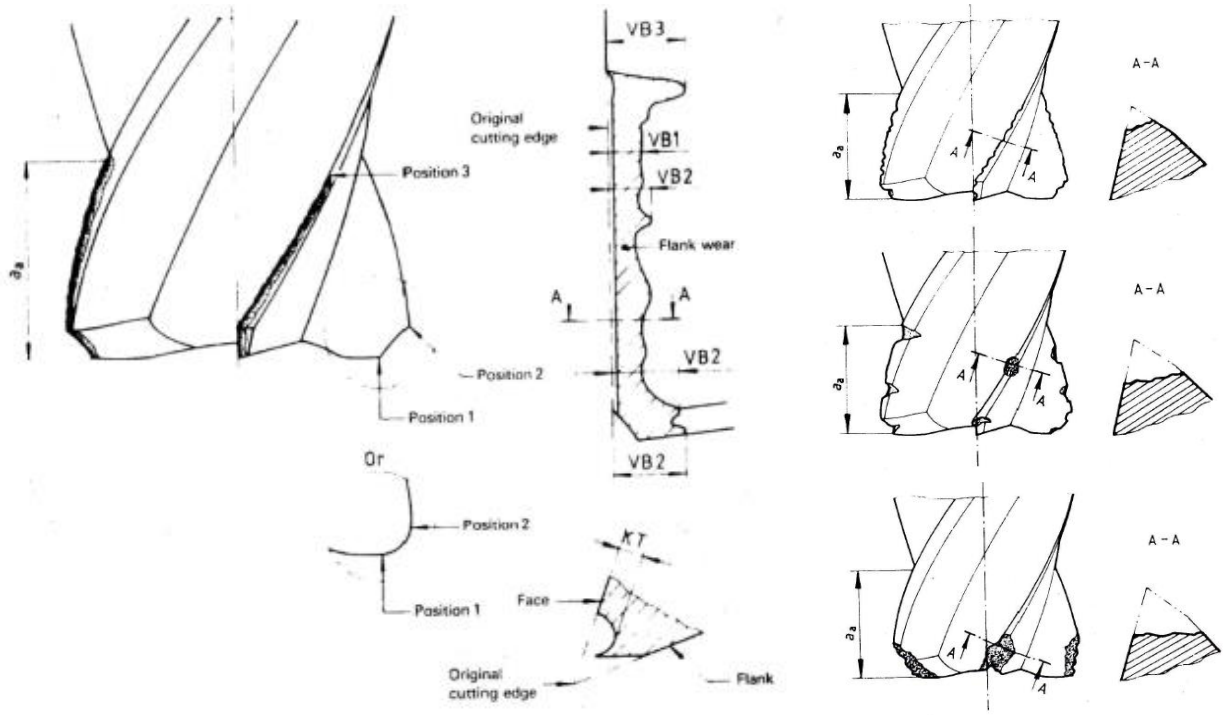

Figure 2.39: Flank wear, chipping and catastrophic failure [145]

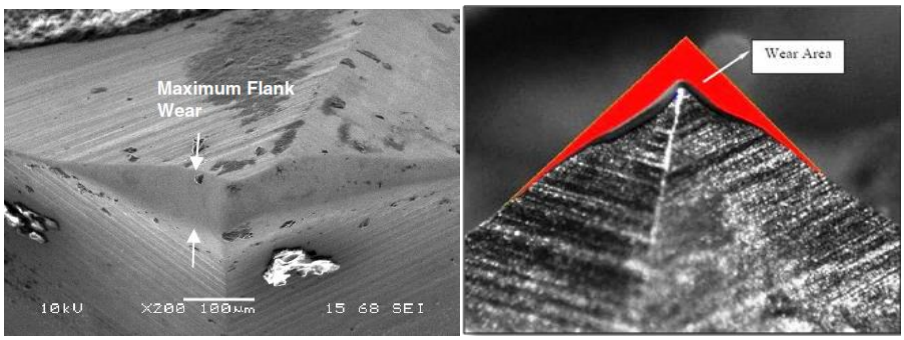

Figure 2.40: Flank wear and wear area method [196].

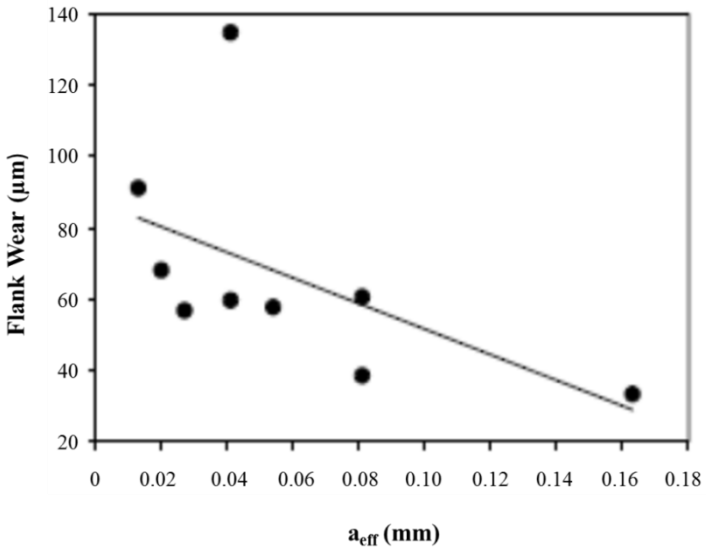

Figure 2.41: Variation of flank wear with effective chip thickness (after cut length of 26 m) [162]

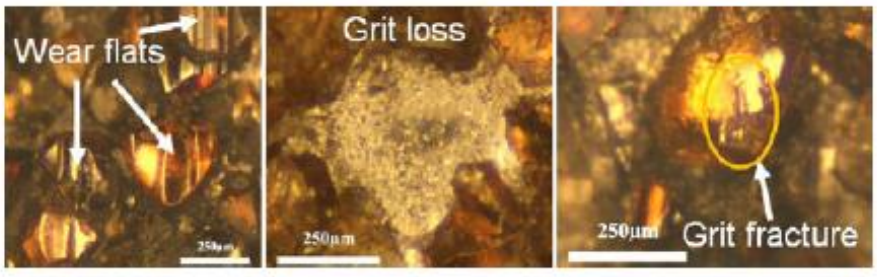

Figure 2.42: wear phenomena using abrasive grit tools [197]

2.3.9 Cutting forces

In milling, chip thickness is an important factor that determines cutting forces. Chip thickness varies with the radial immersion and the width of cut a_e as shown in Figure 2.43. Average chip thickness h_m is calculated using the following equation:

$$h_m = f\sqrt{\frac{a_e}{D}} \qquad \text{Equation 2.2}$$

Where f is the feed per tooth, and D is the cutter diameter. In case of slotting, full immersion occurs (i.e. a_e = D is equal to the maximum chip thickness). The chip size removed by the burr router is very small, similar to that in the grinding process, and is calculated using the following equation [162].

$$aeff = a_e \frac{V}{Vf}$$ Equation 2.3

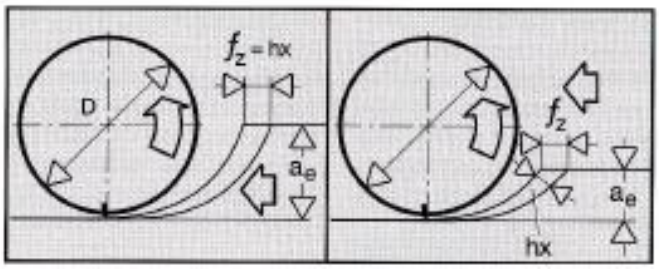

Figure 2.43: Chip thickness for two different widths of cut [19]

The milling forces include the main cutting force (tangential), the radial force (towards the centre of the cutter), and an axial component when using helical milling cutters. These are generally detailed as; Fx, Fy, Fz where Fz is the axial force. Davim and Reis [176] and Azmi et al. [179] used a resultant workpiece force Fm calculated by;

$$Fm = \sqrt{Fx^2 + Fy^2 + Fz^2}$$ Equation 2.4

Milling forces are affected by matrix material [176] however feed rate is the most significant factor affecting cutting forces, higher feed rates equating with higher forces [165]. When Sheikh Ahmad and Sridhar increased feed rate by 100%, forces increased by 78% causing premature tool failure in the form of chipping and thin coating delamination [158]. Forces, generally, decrease with cutting speed [175] then increase due to tool wear [165]. Cutting forces also increase with length of cut as a result of progressive tool wear [161]. Inoue et al. [163] studied slotting and face milling of CFRP using HSS, CVD coated, and TiAlN-coated tungsten carbide end mills, the effect of tool performance on cutting forces is shown in Figure 2.44.

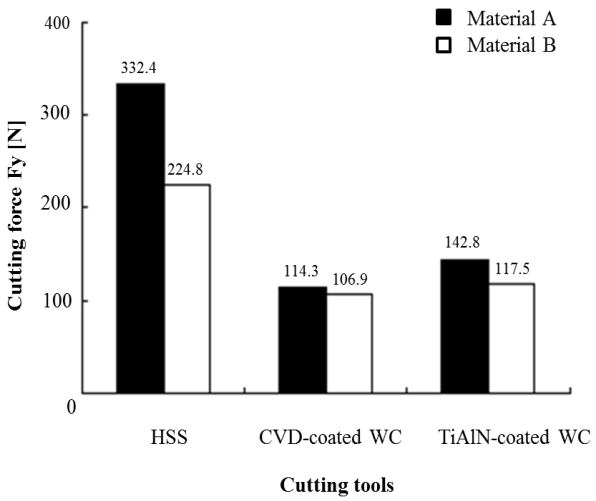

Figure 2.44: Effect of tool material on cutting forces [163]

Forces have been shown to be lower with coated tools due to their low friction coefficient. About 30% reduction in feed force (tangential) was reported by Shen et al. [150] which is significant in relation to tool wear. Comparison of specific cutting energy (Ks) for CFRP, aluminium, and steel, produced values of 300-600, 700-900, 2000-2200 N/mm2 for each material respectively, with tool wear occurring mainly by abrasion in the case of CFRP [178].

In recent work involving ultrasonic assisted milling, Li et al. [167] found that cutting forces decreased with increasing cutting speed. They reported a critical speed of 113 m/min at which the ultrasonic action had no effect. Forces increased with the increase of feed rate and depth of cut. Liu et al. [168] also observed similar results with maximum forces (at maximum feed rate and width of cut) of 460 N and 345 N respectively. In helical milling, the cutting forces were affected by axial and tangential feed rates f_{zt}, and f_{za}, such that increasing only axial feed increased forces, but increasing only tangential feed reduced forces, see Figure 2.45 [135].

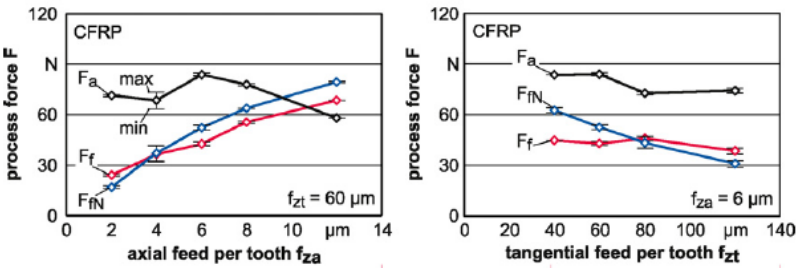

Figure 2.45: Left: increasing axial feed at constant tangential feed, right: increasing tangential feed at constant axial feed [135]

2.3.10 Temperature/cooling

Although fibre reinforced plastic composites, can be cut dry, stagnant heat represents a major concern due to the low thermal conductivity of the matrix, resulting in poor surface quality and higher thermal stresses on the cutting tool [156]. Typically 50% of the cutting temperature is absorbed by the tool, compared to 18% in the case of metal cutting due to the low thermal conductivity of matrix martial. Temperature, absorbed by the tool, necessitates the use of coolant [114]. Cutting fluids are used to reduce the adverse effects of heat and friction on the cutting tools and workpiece. The cutting fluid, required for cooling, lubrication, and evacuation of chips can be compressed air, a gas, or a liquid. The most common cutting fluids are oils, oil–water emulsions, pastes, gels, mists, and gases (liquid nitrogen and CO_2) [187].

Water soluble coolants are recommended for cutting composites but should be avoided when cutting hydrophilic composites since they damage the laminate if absorbed [159]. In such cases air cooling and an extraction system are preferable. Generally, the cooling medium can be fed internally through the tool which may require spindle modifications, alternatively cooling can be provided externally. Figure 2.46 shows the common cooling methods used in milling. Oil mist, minimum quantity lubricant (MQL), or nearly dry machining (NDM) were described by Astakhov as flexible, efficient, cost effective, and environment friendly cooling methods [198]. Nearly dry machining avoids the thermal fatiguing and cracking induced by flood coolants. Oil mist is preferred in the case of high speed end milling for longer tool life [199] and improved surface quality [200]. MQL showed better performance when intermittent cutting occurs as in end milling and should be supplied to the flank face of the tool [201]. The air stream carrying the oil can be cooled using the vortex flow principle [202]. In addition to the adverse effects of flood coolant on the workpiece, there are adverse environmental effects of using Freon (used by Ramulu [151]). In contrast chilled air (CA) of -30˚C has been shown to be effective in reducing tool wear and surface roughness [203] but there was no significant effect reported regarding cutting forces. A mixture of chilled refrigerated air and oil mist (CAMQL) showed a drastic reduction in temperature and improvement in tool life when compared to MQL alone [204]. Tool geometry and tool diameter affect the cutting temperature as noted by Wurtz et al. [155]. Here the use of a larger diameter cutter with a secondary clearance angle helped reduce cutting temperature, see Figure 2.47. The larger the cutter size, the higher the heat capacity of the tool, while a secondary clearance angle reduces tool rubbing from the bounce-back of fibres. In dry milling the temperature, generated in

cutting of CFRP, is normally 250-400 °C, which is higher than aluminium (~150°C) but lower than that for titanium (600°C) [205]. The tool should preferably have high heat capacity to absorb heat [156].

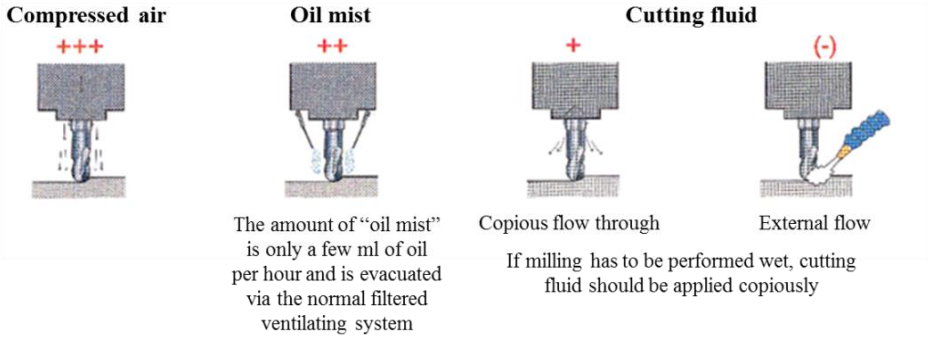

Figure 2.46: Different cooling options in milling [206]

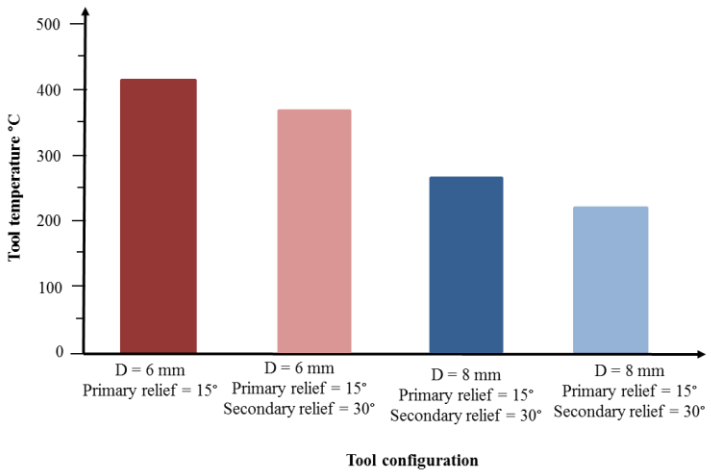

Figure 2.47: Effect of tool diameter and secondary clearance on temperature [155]

During cutting of FRP composites, there is a critical cutting speed Vcr beyond which the temperature increase to exceed the glass temperature of the matrix. Rahman et al. [175] measured temperature using an IR camera and mentioned that in the case of thermoplastic PEEK, the critical temperature was 150°C to 175°C while the glass temperature at which the matrix becomes leathery then rubbery is 143°C. Any further increase in temperature beyond the glass temperature may cause melting or burning of the matrix. Ucar and Wang [161] used a K type thermocouple to measure cutting temperature and found it to be no more than 44° C, possibly because of the very low cutting speed/feed rate used (35 m/min and 0.178 mm/min respectively) and the four fluted 11.11 mm diameter TiN-coated WC tool with 30 degree helix

angle. Matrix content can have an influence on cutting temperature. The effect of resin percentage and layup and tool material on temperature (measured using IR) is shown in Figure 2.48 [163]. The use of coolant in milling is not common, additionally there is very little published data on cutting temperature when slotting of CFRP. Compressed air can be helpful in cooling the cutting zone and evacuating the chips. A colder stream of air can be obtained from compressed air using a vortex tube. Here the compressed air is filtered to remove water and oil and the pressure is then regulated. As shown in Figure 2.49, clean air enters the vortex tube at point (A). The vortex tube splits the compressed air into a cold (B) and hot (C) stream of air. The hot air is vented to the atmosphere at point (D) after being muffled to reduce noise. Cold air enters into the muffler (E) and is then distributed through the hose (F) onto the tool being cooled. A strong magnet (G) is used to hold the unit onto the machine. The system is said to be capable of delivering a cold air stream 28 °C below the inlet air temperature [207]. Despite the advantage of the vortex tube being easy to operate, the author is not aware of it previously being used in the milling of composites.

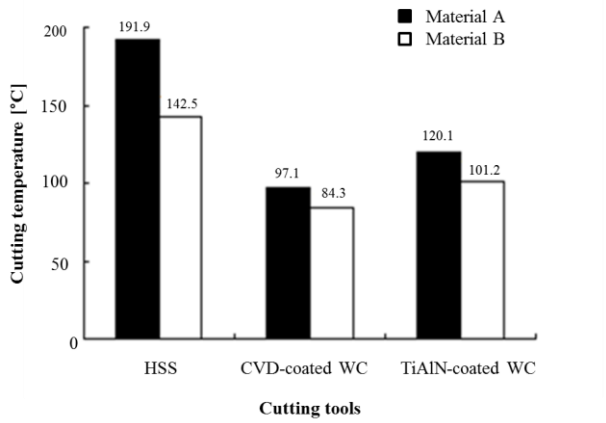

Figure 2.48: Relationship between tool material and cutting temperature [163]

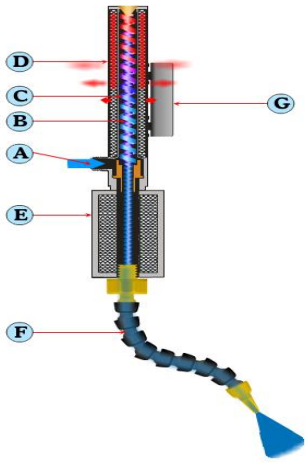

Figure 2.49: Schematic of the vortex tube [207]

2.3.11 Surface integrity

Surface integrity describes the inherent surface alterations from machining or any other surface generation operation [208]. Milling of inhomogeneous and anisotropic FRP composites is difficult and may result in some defects if the tool and the machining parameters are not selected properly. Common defects include the following:

- Small holes due to fibre pull out
- Edge fracture
- Fuzz, tufts, or extended fibres beyond cut surface
- Delamination (affects structural integrity & tolerance)
- Splintering
- Deep cracking
- Matrix smearing or burning

Appropriate selection of machining parameters is vital to avoid mechanical or thermal induced defects. For example, smearing of matrix material and deep cracking can result from excessive feeds [158] while burning is likely at high cutting speeds and low feeds [156]. Fracture of edges can be avoided by making a pre-cut to avoid weakening the edges at the tool exit [157].

2.3.11.1 Delamination

When milling composites there is a likelihood of delamination due to the action of machining forces [177]. Delamination reduces the strength of components, it is highly

dependent on fibre orientation relative to the machining direction, and is significantly affected by the feed rate [152]. For this reason milling of FRP is considered as a complex process [160]. Fibre orientation has a significant effect on the quality of cut. Cutting parallel to fibres is recommended for best cut quality. Forces in cutting fibres at 45˚, 90˚, are higher than that for fibres at 0˚ because the effort exerted in bending or shearing is higher than that for buckling [139]. Surface plies are not stabilised by neighbouring layers compared to internal plies, consequently, axial machining forces will cause damage. Colligan and Ramulu [151, 152] observed surface defects and classified them into 3 distinctive types (shown in Figure 2.50), namely Type 1 where fibres were broken some distance inward from the trimmed edge (missing fibres) at 90˚ fibre orientation, Type 2 where uncut fibres protruded from the edge (may be delaminated some distance from next ply) due to fibre movement away from the cutter due to bending and usually at 45°, and Type 3 involving loose fibres partially attached appearing fuzzing/frayed usually at 0˚, 5˚ and 175˚, the fibres being almost parallel to the cutting direction. Type 1 was the most frequent defect to occur. A lower tendency to delaminate was observed during cutting 0° fibres or fabric plies. They also recommended use a specific top ply placement around the workpiece edges in order to minimise surface damage, with unidirectional fibres used parallel to the edge in case of straight edges and fabric in the case of curved edges.

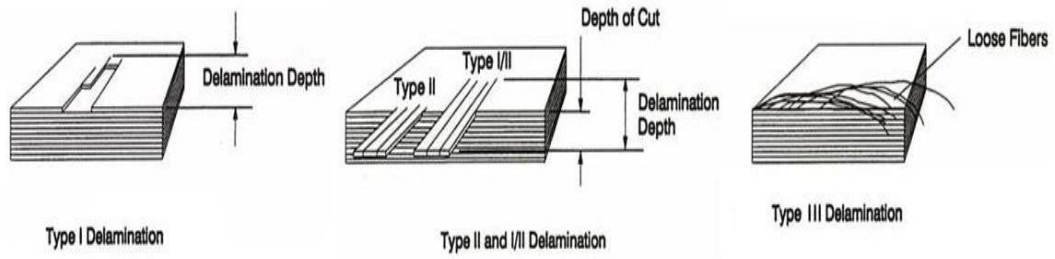

Figure 2.50: Types of surface ply delamination [151]

In edge trimming of different fibre orientations, the probability of damaged surface plies increases in the case of top plies. The use of a large helix angle has showed a lower incidence of delamination probably because of the smooth cutting action provided by the helix, see Figure 2.51 a,b. With helical tools, at any moment more than one tooth is engaged keeping the tool constantly loaded and avoiding harmonic interrupted bending [159]. The use of a double helix milling cutter, directs the axial cutting forces towards the centre, which in turn

minimises surface damage [151]. There is controversy about which cutting mode is better, up milling or down milling. It is difficult to decide which is better because it is affected by several parameters and their interactions. Colligan and Ramulu [151] found down milling was better as it produced less delamination, a fact also reported by Sheikh Ahmed et al. [158]. Figure 2.52 shows how down milling prevents fibre separation. Other researchers have found up milling preferable [161, 162]. A higher feed rate causes a rise in cutting forces, rapid tool wear and hence an increase in delamination. See Figure 2.51 c and d for effect of cutting mode and feed rate.

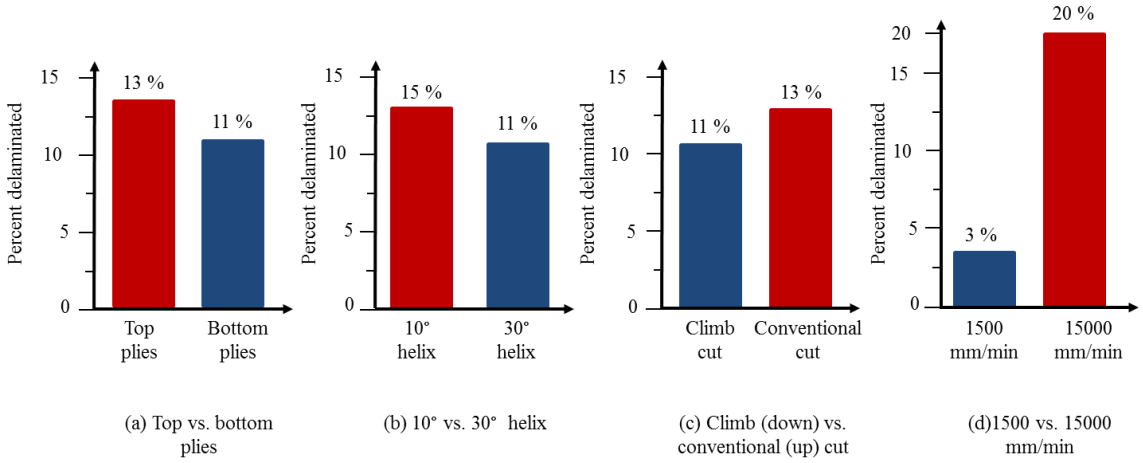

Figure 2.51: Factors affecting probability of delamination occurring [151]

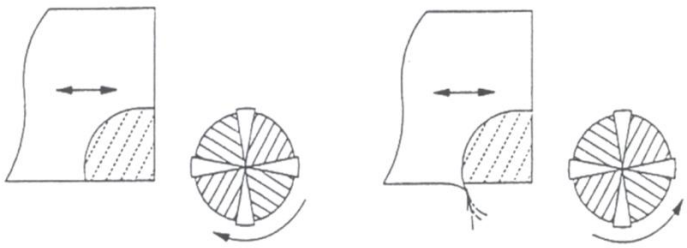

Figure 2.52: Down milling (left) prevents fibre separation [157].

Allowable damage varies from one manufacturer to other. It was noted by Coligan and Ramulu [152] that the maximum allowable delamination commonly used in the aerospace industry is 2.5 mm (based on Boeing data), although in their research they used a value of 1mm. Prashanth [196] used 1.5 mm as a conservative value. For Airbus, the allowable delamination value in drilling is 1.5 mm [134]. A dimensionless delamination factor of >1 can be calculated from an equation similar to the drilling equation shown in Figure 2.53. For this

slotting example Wmax is the maximum extent of damage and W is the actual slot width. The damage extent can be measured using a tool makers microscope, imaging techniques or most recently laser techniques as reported by Hintze et al. [171]. Matrix material has an effect on the delamination factor (DF), which is increased with both cutting speed and feed rate [176]. Delamination is also affected by cutting tool performance. Inoue et al. [163] studied slot and face milling of CFRP using HSS, CVD coated, and TiAlN-coated tungsten carbide tools. Uncut fibres (fuzzing) on the surface plies were observed mostly with HSS tools due to excessive tool wear.

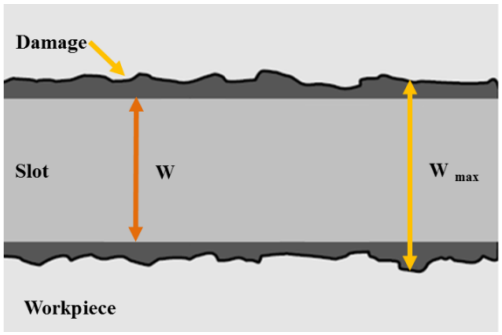

Figure 2.53: Calculation of delamination factor [176]

Hintze et al. [171] studied the causes of delamination during a slotting operation using fluted tools, they found that increasing the cutting edge radius (due to tool wear) was responsible for the occurrence of delamination especially in the top ply. For example, in milling 90° fibres the amount of uncut fibre (fuzz) increased when using a worn tool with 90 µm edge radius as shown in Figure 2.54.

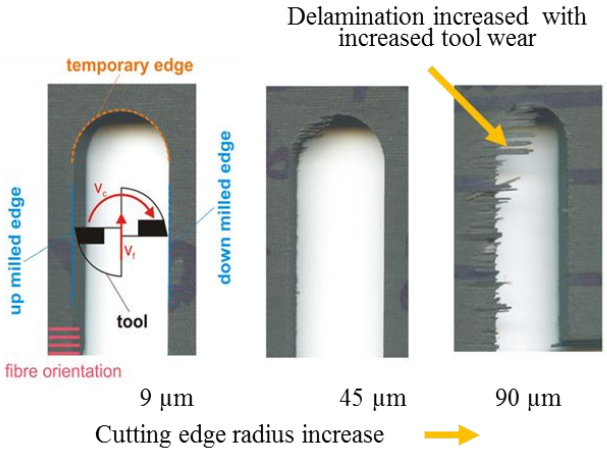

Figure 2.54: Delamination due to tool wear (V= 800 m/min, f = 0.03 mm/tooth, a_e = D, a_p = 4mm) [171]

The chance of delamination was higher in slotting compared to edge trimming and Hintze et al. pointed out that when the ratio ae/d < 0.13, there is little chance of delamination compared to when ae/d > 0.13. The delamination was most frequent on the up milling side. They highlighted the difference between the fibre angle and cutting angle (see Figure 2.55 and Figure 2.56) and stated that there are non-critical cutting angles $0°<\theta<90°$ and critical cutting angles $90°<\theta<180°$ (for fibres at 0°, 90°, and 135°) and $45°<\theta<180°$ (in case if 45°). They also divided the cutting into three distinct regions, see Figure 2.57. Region A is associated with a critical fibre cutting angle where delamination occurs, in Region B propagation of delamination occurs and in Region C no propagation occurs. They concluded that the length of the overhang fibres was equal to the distance from the edge to the point where the cutting edge cut the fibres at the critical cutting angle [171]. In case of burr routers, delamination increased with increasing effective chip thickness and cut length as shown in Figure 2.58.

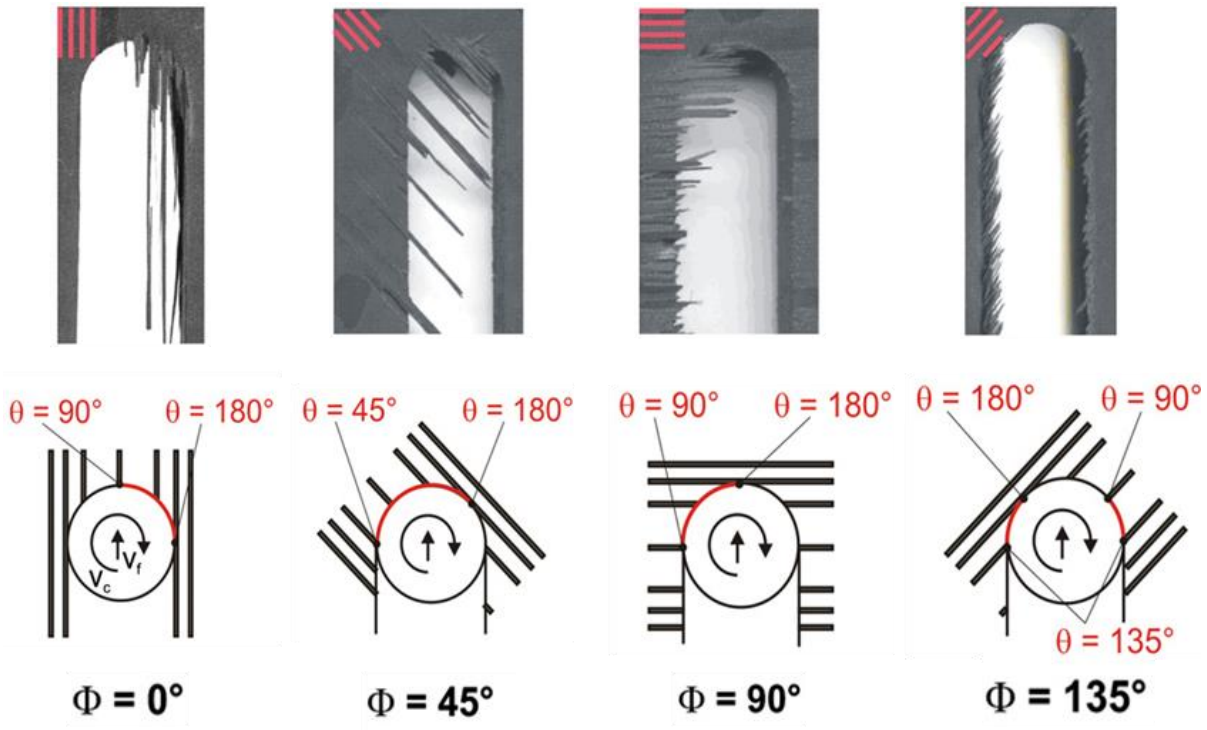

Figure 2.55: Fibre orientation angle and cutting angle [171]

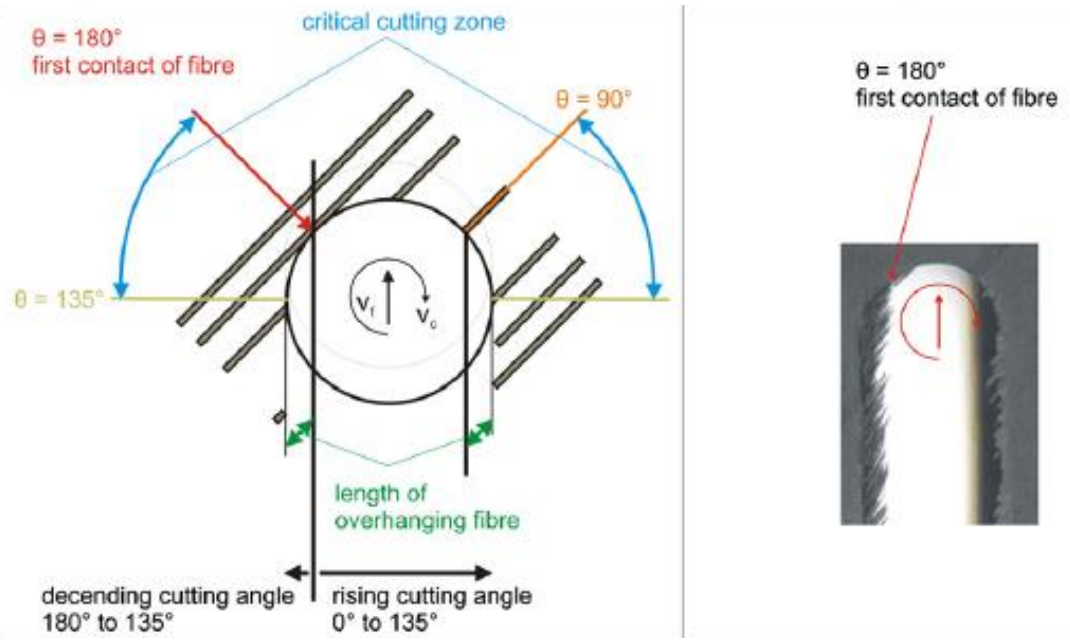

Figure 2.56: Delamination when slot milling at fibre orientation of 135° [171]

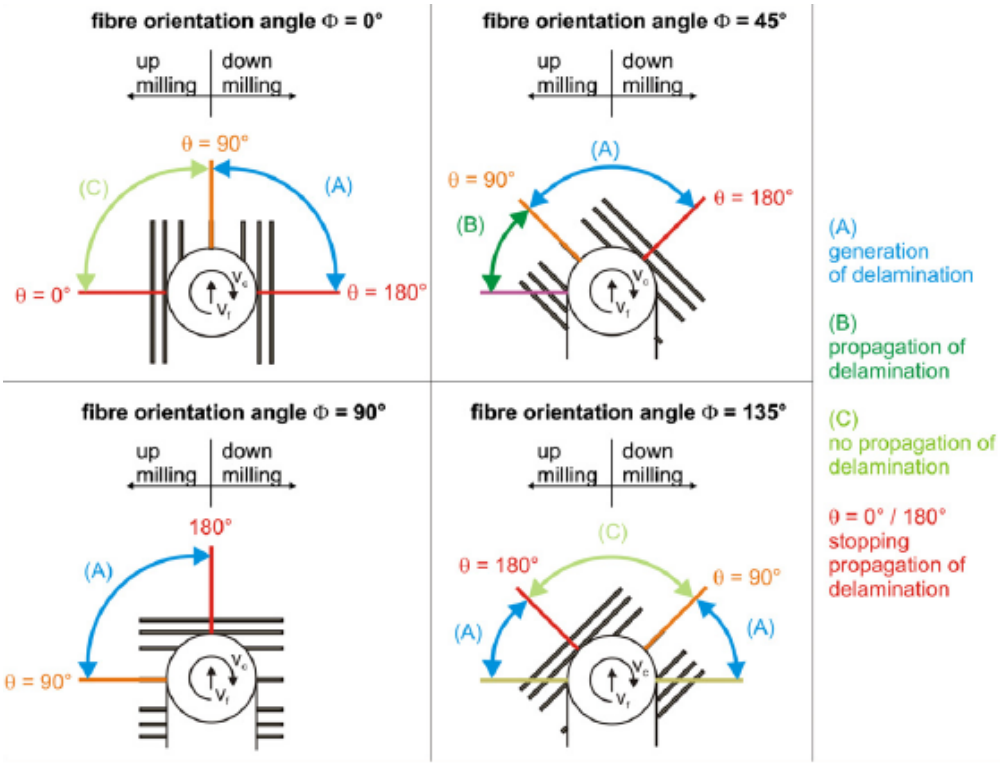

Figure 2.57: Delamination and propagation of delamination [171]

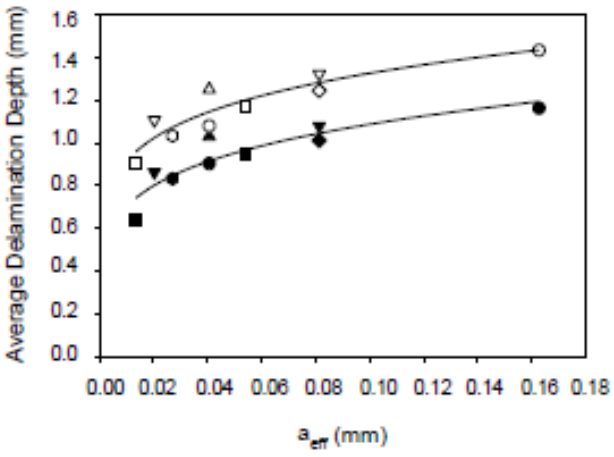

Figure 2.58 Effect of average chip thickness on delamination depth, dark symbols cutting 2.5 m. white symbols cutting 26 m [162]

Wang et al. [165] showed that delamination increased by increasing feed rate which in turn raised the cutting force. They noted that delamination was in the acceptable range as long as the cutting forces were below 200 N [169]. Delamination was dependent on tool geometry such that a 2 fluted tool was better than a 6 fluted tool as noted by Davim and Reis [160]. Additionally when helical milling Rahim et al. [170] found that tool geometry influenced damage.

2.3.11.2 Surface roughness

The surface roughness of a machined part affects friction, wear, light reflection, heat transmission, wetability with lubricants, and fatigue resistance [209]. Vibration of the machine tool, cutting speed, feed rate, depth of cut, material properties, fibre orientation, weave pattern, bond strength, and flank wear affect surface roughness [51, 52]. Surface roughness can be measured in the longitudinal and transverse direction but transverse measurement gives a better indication of surface quality [24].

The main roughness paramters used in respect of composite machining are average surface roughness Ra and peak-to-valley Rt [21, 23-25, 29]. Other roughness paramaters have been studied [23, 25] such as profile height probability, density of profile height, cumulative height distribution [24], and power spectra of the surface profile [26]. The average Ra has been shown to be as little as 1-2 µm with Rt 4-11 µm when orthogonal machining with PCD [26]. Here roughness was largley dependent on tool geometry such that increased rake angle was reported to result in finer chips due to the localised extent of fracture beyond the tool tip,

leaving a high quality machined surface. As previously detailed, fibre orientation has a significant influence on surface roughness and a critical value of 90˚ exists below which the roughness deteriorates, the surface being covered by a thin layer of matrix, and subsurface cracks [21, 29]. The nature of the milling makes cutting tools especially with small radii vulnerable to process dynamics and requires appropriate clamping otherwise wear resistance and quality of cut will be lower [156]. In milling the surface roughness is a function of the feed rate and the height of the profile H can be calculated using the feed rate f and cutter diameter D as shown in Figure 2.59.

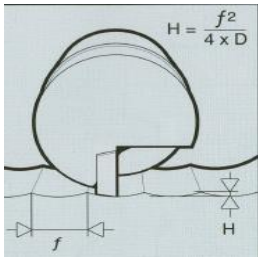

Figure 2.59: Surface roughness (profile height) as a function of the feed rate[19]

Richards et al. [142] noted a roughness requirement of 3 µm for Airbus A400M CFRP panels. Sandvik described a CFRP surface produced by routing with 1.25 µm Ra as a "good surface". In machining of unidirectional/multi-directional CFRP using PCD tools, Ramulu et al. [164] investigated the effectiveness of surface topography parameters in describing surface roughness. Using cumulative height distribution (CHD), power spectral density functions (PSDF), auto correlation function (ACF) techniques, and scanning electron microscopy (SEM), they found that the maximum peak-to-valley height (Rt) and ten-point height (Rz), are more accurate in describing the surface roughness than the arithmetic average roughness (Ra) and the root mean square height RMS (Rq). Differences in roughness in both longitudinal and lateral directions were also noticed. At smaller orientation angles fibres were exposed but matrix smearing was absent in the case of 0˚ fibres. Fibre pull out was attributed to 90˚ and 135˚ plies. Three-dimensional topography mapping/analysis is recommended for CFRP composites [164, 210].

An optimum speed of 50 m/min and 0.1 mm/tooth feed rate is recommended for best surface quality [139]. Matrix material type (thermoset or thermoplastic) effects surface roughness [176]. In machining carbon/peak (thermoplastic matrix) composite material, Rahman et al. [175] found that the average surface roughness Ra was in the range of 0.4-0.6

μm (1 μm normally in milling of metals). The Ra value was independent of cutting parameters. When increasing cutting speed from 25 m/min to 250 m/min the rise in temperature and consequently the softening of the material meant that the cutter left no distinguishable marks.

Feed rate has the most significant effect on surface roughness [177]. Cracks or feed marks which occur at high feed rates increase surface roughness especially when measured in the transverse direction [158, 160, 176]. Davim et al. [177] also found that the tolerance grade (IT) increased with material removal rate and decreased with cutting speed. In end milling of CFRP, Ucar and Wang [161] recommended a cutting speed of 18-25 mm/min, feed rate 0.019-0.04 mm/tooth, and 1 mm depth of cut in order to achieve a satisfactory surface. Higher feed rates are not recommended as they produce higher surface roughness and leave feed marks as shown in Figure 2.60 [158].

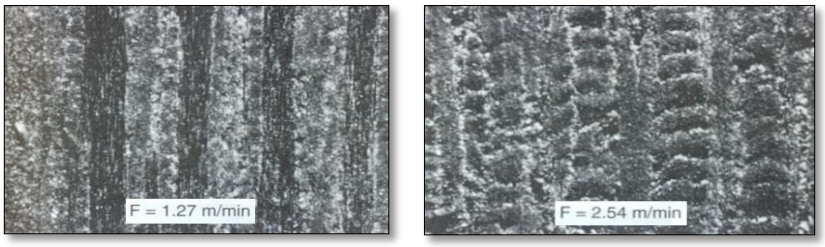

Figure 2.60: Effect of feed rate on quality in milling CFRP (cutter marks inclined by helix angle and spaced by approximately feed is visible on higher feeds [158].

Klocke and Wurtz [156] noted that workpiece surface roughness using PCD was better than WC and a 25% surface roughness improvement was achieved by using finer grained (2 μm) PCD tools compared with coarser grained PCD product (6-10 μm). This was attributed mainly to the smoothness of the cutter surface. Using burr tools in cutting CFRP composites, Prashanth et al. [162] reported surface roughness was lower at higher milling speeds and smaller feed rates. Fuzzing and fibre pull out were observed when using high effective chip thickness (a_{eff}). Generally, roughness measured in the transverse direction was higher compared to that in the longitudinal direction. The burr tools achieved maximum roughness values of 22 μm Rt in the longitudinal direction and 28 μm Rt in the transverse. Using burr tools produced surfaces with higher roughness than that obtained with abrasive tools.

When using diamond abrasive tools, Colligan and Ramulu [153] observed grooving on the cut surface although workpiece surface finish was not affected by feed rate, cutting mode or

cutter diameter. Surface roughness as fine as 2 µm was obtained by Richards et al. [142] using 60 grit diamond for roughing while diamond coated routers were used for finishing at 0.5 mm width of cut [142]. The work involved trimming lugs from the periphery of CFRP panels used in wing assemblies (for indexing or lifting) on Airbus A400M aircraft. This was similar to the high speed electric hand operated trimmers developed in the early 80's for edge finishing of plastics [211]. The diamond coated router bit did not wear during the process because forces were minimised. Grit sizes of 35, 50, 80 and 125 µm were evaluated by Colligan and Ramulu [153]. They found that each cutter had its own "irregular" signature see Figure 2.61. An empirical equation was established to predict surface finish which was not affected by feed rate, cutting mode or cutter diameter. Surface finish was inversely proportional to grit size such that:

$$\text{Surface finish} = 103.46\ (\text{Grit size})^{-1.31}$$

Recently, Soo et al. [197] achieved a surface roughness Ra (3-8 µm) using diamond and CBN grit tools. Gao et al. found that using ultrasonic assisted milling (4-5 µm amplitude and frequency of 20 kHz) could achieve a better surface but they did not clarify the improvement quantitatively [166].

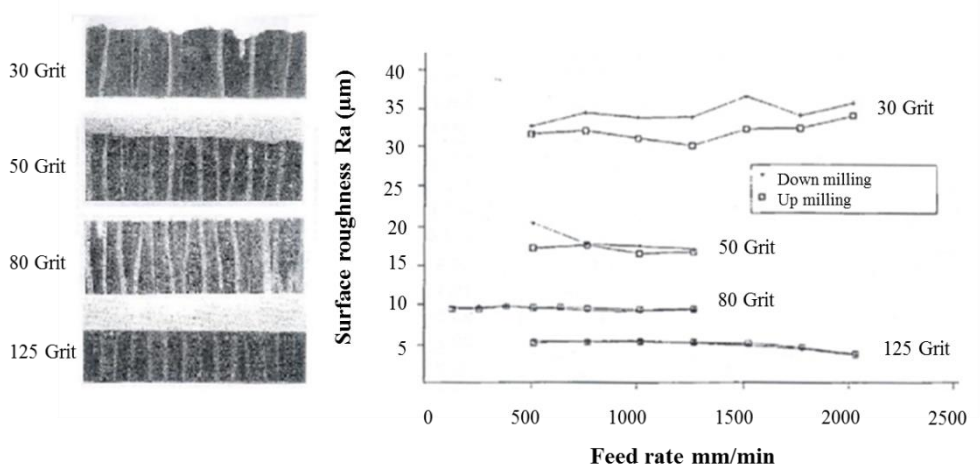

Figure 2.61: Fingerprint of different diamond grit sizes (left), effect of grit size and feed rate on Ra (right) [153]

2.3.12 Modelling and simulation of the milling process

Several research articles have included the modelling approach to predict the effect of different process parameters on responses such as tool wear, cutting forces, surface roughness or delamination factor [160, 169, 172-174, 176, 180, 181, 212]. For example, multiple regression analysis was used to generate a formula to predict resultant cutting force (Fm), surface finish (Rt), and delamination factor (FD) for each material as a function of cutting speed Vc (m/min) and feed rate *f* (mm/rev) [176]. Other equations exist for a different matrix material used with glass fibres.

$$Fm = 24.098 - 0.228\,V_c + 322.187\,f \quad \text{Equation 2.5}$$

$$Rt = 16.053 - 0.141\,V_c + 148\,f \quad \text{Equation 2.6}$$

$$DF = 0.986 + 4.66 * 10^{-4}\,V_c + 0.479\,f \quad \text{Equation 2.7}$$

Azmi et al. [180] presented a mathematical model to predict cutting force, tool life, and surface roughness. These responses were dependent on the rotational speed N (rpm), feed speed V_f (mm/min) and depth of cut (mm). However again, the equations were only suitable for GFRP composites.

$$Ra = 10^{0.293}\,N^{-0.323}{V_f}^{0.313}{a_p}^{0.025} \quad \text{Equation 2.8}$$

$$Tool\ life = 10^{11.398}\,N^{-0.911}{V_f}^{-1.922}{a_p}^{-0.201} \quad \text{Equation 2.9}$$

$$Fm = 10^{-1.214}\,N^{-0.156}{V_f}^{1.136}{a_p}^{1.048} \quad \text{Equation 2.10}$$

Equations related to milling of CFRP were presented by Wang et al. and they predicted the cutting force, delamination factor and surface roughness as follows:

$$F_c = 243.220{V_c}^{-0.661} f^{0.492}\,{a_e}^{1.09} \quad \text{Equation 2.11}$$

$$DF = 40.189 - 0.003V_c + 29.762f * 15417a_e \quad \text{Equation 2.12}$$

$$Ra = 0.942 - 55 * 10^{-6}V_c + 1.036f - 0.108\,a_e \quad \text{Equation 2.13}$$

In the modelling work done by Sheikh-Ahmad et al. [173], Sheikh-Ahmad and Yadav [174] and Kalla and Twomey [213], the authors used regression analysis to determine the specific cutting energy of CFRP composites for uni-directional and multi-directional fibre

orientations. An artificial neural network model was capable of predicting the cutting forces (without the oscillations accompanied with real cutting) in milling as a function of process parameters and fibre orientation. Force prediction equations for unidirectional and multidirectional orientations for FRP were presented [173, 174, 213]. Iliescu et al. [172] presented a model to predict tool wear as a function of feed which was helpful in optimising cutting conditions and tool diameter as shown in Figure 2.62 .

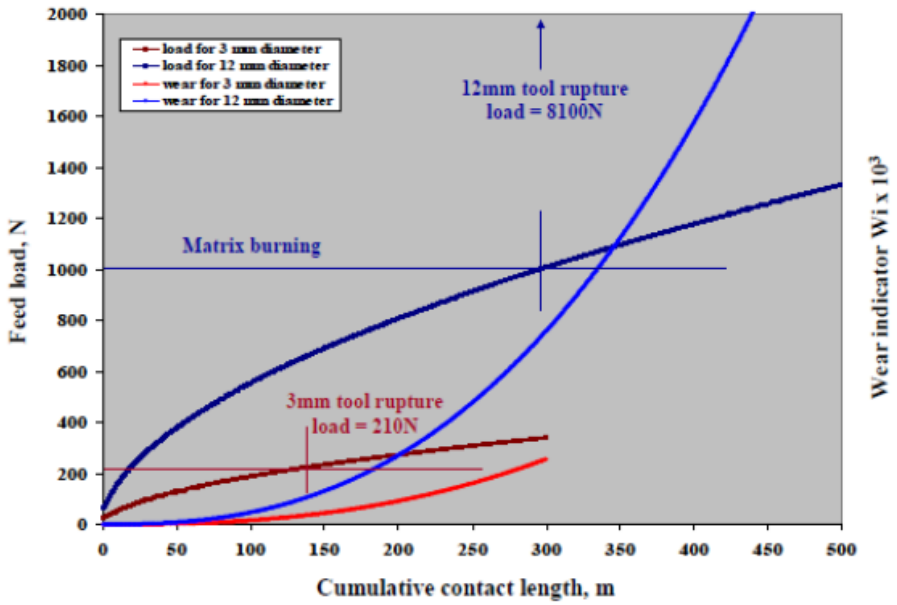

Figure 2.62: Wear indicator and feed load variation with contact length LC and tool diameter (V = 200 m/min, f = 0.05 mm/rev) [172]

Mechanistic modelling is a common method of modelling cutting forces and involves the analysis of chip area. In milling of FRP the instantaneous fibre orientation with respect to the cutting velocity vector is dependent on both laminate orientation and the instantaneous immersion angle [173]. Seikh-Ahmad et al. [173, 174] derived specific cutting pressures in the radial and tangential directions in order to predict cutting forces as a function of the fibre angle for unidirectional and multi-directional laminates. For the cutting of (n_p) plies with a thickness a_t, the total forces Fc and Ft was described in equations below where φ_i was the instantaneous immersion angle, a_c was the uncut chip thickness at laminate thickness, θ represented the fibre angle while Kc and Kt were the specific cutting energy in directions along and perpendicular to cutting speed (i.e. tangential and normal) respectively. The model was transferable to helical tools by slicing the tool into a number of discs [181].

$$\mathrm{Fc}\ (\emptyset_{\mathrm{i}}) = \Sigma_{j=1}^{n_p}\ [k_c\ (a_c, \theta_i), a_c(\emptyset_i).\, a_t]j \qquad \text{Equation 2.14}$$

$$\mathrm{Ft}\ (\emptyset_{\mathrm{i}}) = \Sigma_{j=1}^{n_p}\ [k_t\ (a_c, \theta_i), a_c(\emptyset_i).\, a_t]j \qquad \text{Equation 2.15}$$

Rusinek [212] correlated the chatter behaviour during milling of CFRP to the tool rotational speed and stated that there is a range of spindle speeds to be avoided during the cutting operation which result in large amplitude vibration (instability lobes), see Figure 2.63.

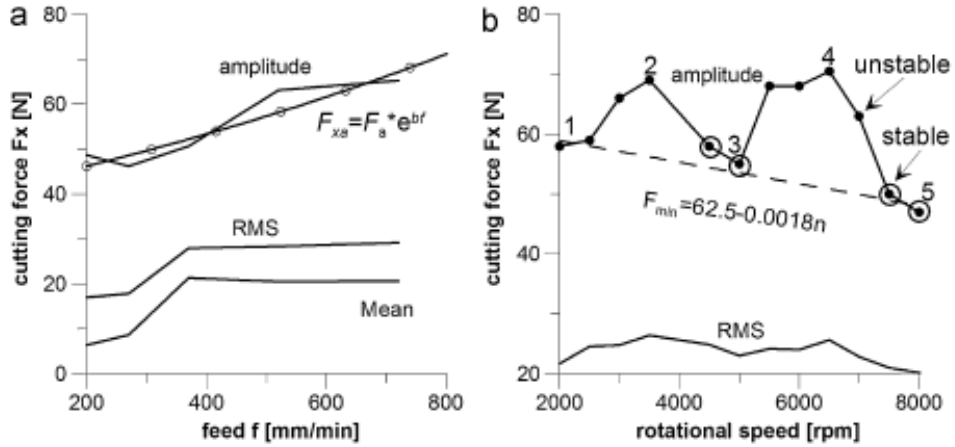

Figure 2.63: Effect of varying feed and rotational speed on cutting forces [212]

Finite element analysis (FEA) has also been used to model the machining of CFRP composites. Here there are two main challenges, the first is how to model the inhomogeneous material and the second the assumption of faliure criterion. It is possible in orthogonal cutting to model the material as an equivalent homogenous material (EHM) [32, 33]. There are many failure criteria such as maximum stress, maxium strain, Tsai-Hill, Tsai-Wu, and Azzi-Tsai Hill [214] but Tsai-Hill is most commonly used [34, 130].

Comparing macroscopic implicit to microscopic explicit FEA models (Figure 2.64), Rentsch et al. [215] found that the microscopic explicit modelling technique was capable of giving higher detail of the material removal process compared to macroscopic implicit modelling. However, the forces were lower compared to experimentation due to FEA element deletion, see Figure 2.65, which necessitates the experimental investigation.

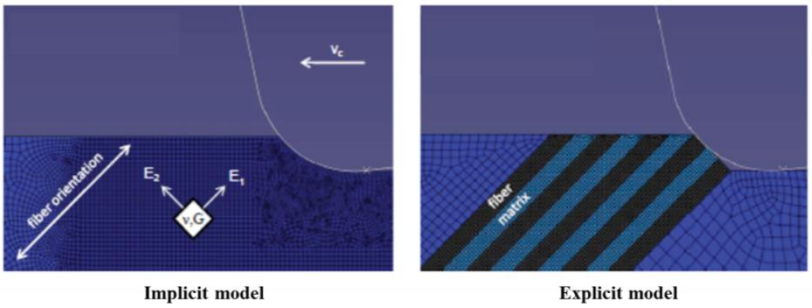

Figure 2.64: Implicit and explicit FEM model of CFRP [215]

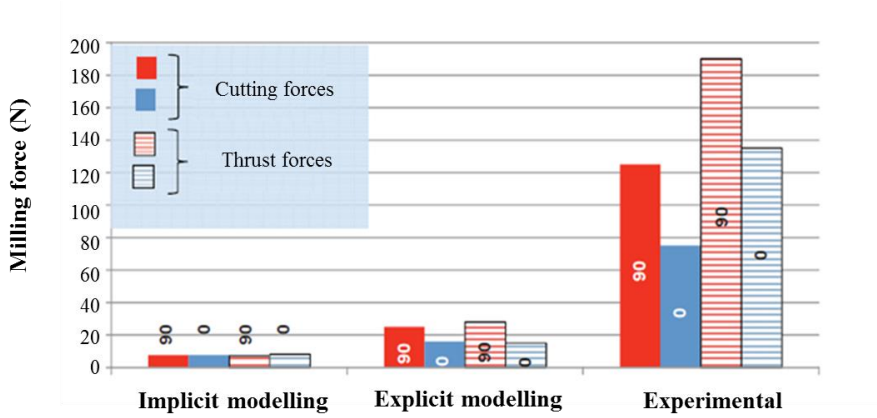

Figure 2.65: Calculated and measured cutting and thrust forces for 0° and 90° fibre orientation [215]

Using a variable helix cutter (three fluted tool with 3 different helix angles), Karpat et al. [216] found a sinusoidal relationship between cutting force and instantaneous fibre angle in slotting of unidirectional CFRP, see Figure 2.66. Consequently, tangential and radial forces showed variation with the rotation angle of the tool, see Figure 2.67 for 0° fibres example, the pattern of force varies with fibre orientation. They suggested that fibres at 45˚ and 135˚ were easier to cut than 0˚ and 90˚ fibres and preferred these to be top plies which conflicts with recommendations of Colligan and Ramulu mentioned earlier [152]. Cutting force coefficients were modelled as a function of the fibre angle [217].

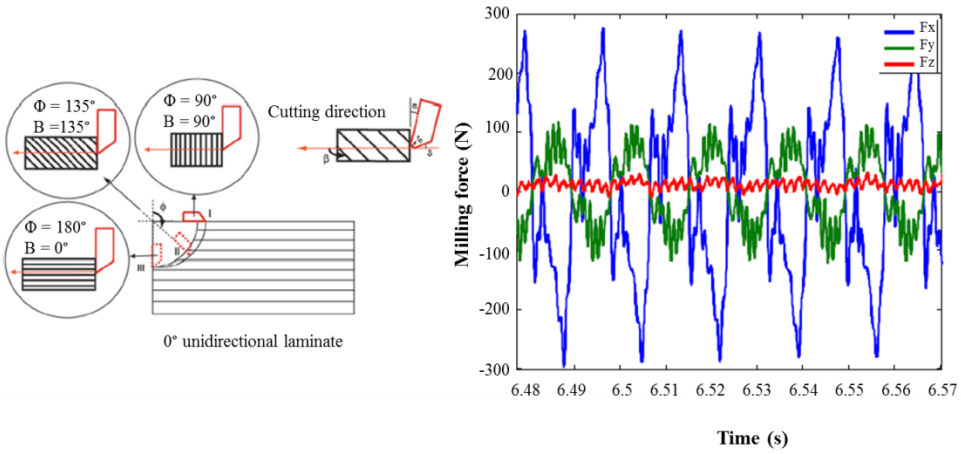

Figure 2.66: Instantaneous cutting angle (left) cutting force signal with sinusoidal response (right) [216]

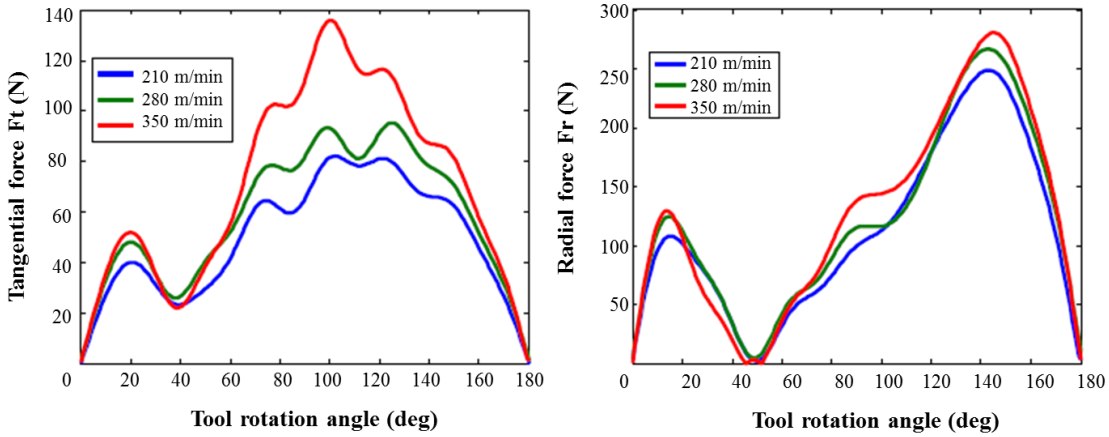

Figure 2.67: Variation of cutting forces within 1/2 rotation of the tool (for 0° fibres)

2.3.13 Cost analysis

The tool life is the time a newly sharpened tool cuts satisfactorily before it becomes necessary to regrind or replace. This time which is affected by the tool resistance to different types of wear has an impact on the total machining cost. Tool life is affected by cutting conditions, tool geometry, tool material, workpiece material, coolant and rigidity of the machine. Tool life criteria can be allowable tool wear, cut length, cutting forces, surface integrity/roughness or even noise.

For any process there are fixed and variable costs. Fixed costs may include the assets and the machines while variable costs vary depending on several factors such as production rate. Ideally, the total cost of a product should include all the cost elements to make it. This can be

raw material cost, machine cost (e.g. electricity, compressed air, gas, consumables, cutting fluids, lubricant oil, filters etc.), tooling cost (tools, regrinding), labour cost (wages). Some of the process by-products can be recycled and subtracted from the cost such as metal chips and scrap tools.

The cost of a single product C_{pr} reflects three main cost components which are machine cost C_m, tooling cost C_t and labour cost C_L and a total machining cost equation can be written as:

$$C_{pr} = C_m + C_t + C_l \qquad \text{Equation 2.16}$$

The machine cost is the running cost of the machine while the labour cost comes from time spent operating the machine during actual machining as well as replacing tools multiplied by the labour cost per hour. In this context the most important element is the tooling cost per product. The tooling cost C_T depends on the tool type whether disposable or regrindable. In the case of regrindable tools, the tool cost for a single tool is divided by the number of products it makes in the life time and the total tooling cost comes from the following equation:

$$C_T = \frac{(C_{new} - C_{scrap}) + n_s C_r}{n_s + 1} \qquad \text{Equation 2.17}$$

Where C_T is the total tooling cost for a single tool, C_{new} is the initial cost including grinding if applicable, C_{scrap} is the scrap cost, n_s is how many times the tool was sharpened and C_r is the tool sharpening cost. The tooling cost C_t can be calculated by dividing C_T by the number of products in a tool life time (z) which is:

$$C_t = \frac{C_T}{z} \qquad \text{Equation 2.18}$$

The total number of products in a life time z can be calculated from the following equation:

$$z = \frac{T}{t_m} \qquad \text{Equation 2.19}$$

Where T is the tool life time and t_m is the time required to machine a single product. Disposable tool cost is the cost of a new tool or prime cost minus the scrap cost if sold as scrap divided by the number of products made within the tool life time z.

In an interrupted process like milling, the tool life T is estimated based on the life of one edge, and in this case the tool life becomes the actual contact time between a single edge and workpiece. The Taylor model for tool life ($VT^n=C$) can be used to derive an equation to estimate the economic tool life (T_e) and the economic cutting speed (V_e) for minimum cost. It can also be used to formulate an equation for the tool life for maximum production rate (T_o) and the corresponding cutting speed (V_o) [218].

$$T_e = \left(\frac{1}{n}+1\right)\left[t_{ct} + \frac{C_T}{L(1+r)}\right] \quad \text{Equation 2.20}$$

$$V_e = \frac{C}{\langle\left(\frac{1}{n}+1\right)\left[t_{ct}+\frac{C_T}{L(1+r)}\right]\rangle^n} \quad \text{Equation 2.21}$$

$$T_o = \left(\frac{1}{n}+1\right)t_{ct} \quad \text{Equation 2.22}$$

$$V_o = = \frac{C}{[\left(\frac{1}{n}+1\right)t_{ct}]^n} \quad \text{Equation 2.23}$$

Here n is the Taylor exponent, C is Taylor constant, t_{ct} is the tool changing time, L is the labour wage per unit time and r is and overhead ratio.

Ideally, a detailed cost analysis should include fixed and variable costs such as interest, depreciation, wages, rents, energy costs, maintenance costs, and tool costs. Only few research articles have included a cost analysis in milling, see references [156, 159, 172]. The analysis conducted by Kocke and Wurtz [156] showed that the specific cost per cut meter (£/m) can be reduced by 9% through using tools capable of providing a longer tool life. Cost could also be reduced by increasing the cutting parameters by 18%. The cost using PCD was 18% less than that using WC tooling, see Figure 2.68.

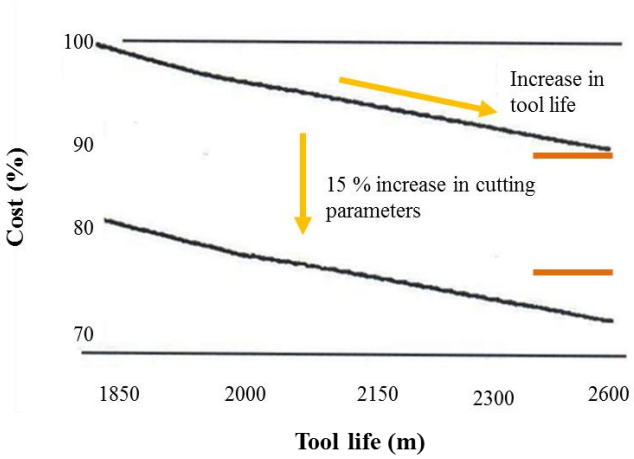

Figure 2.68: Cost reductions achieved by adjusting cutting parameters , specific cost £/m can be reduced by 9% by longer tool life, and 18% by proper selection of parameters (milling CFRP using an 8 mm PCD router at 800 m/min) [156]

Horman et al. [159] recently studied the tool wear/life associated with different tooling technologies. Veined PCD was a cost effective choice to cut 250 m CFRP despite its high unit cost as it allowed complex and more efficient router geometries, see Figure 2.69. In contrast, Lopez de lacalle et al. [150] recently concluded that the use of PCD is not economical in comparison with cheaper WC burr tools.

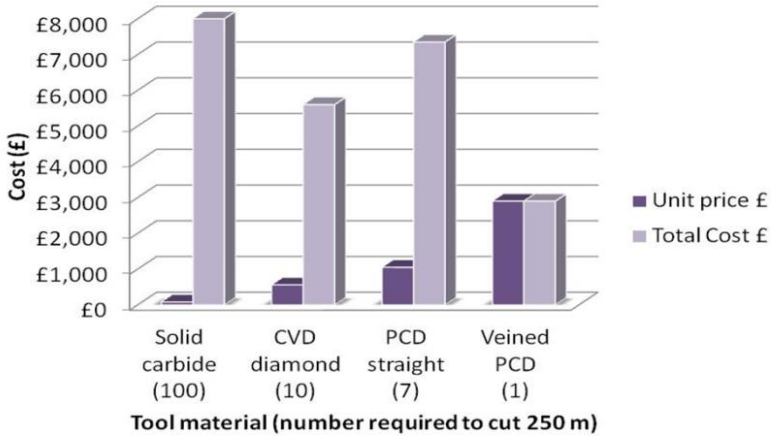

Figure 2.69: Different tool material cost analysis based on 250 m cut length at manufacturers recommended cutting speeds and feed rates [159].

2.4 Non-conventional machining

Non-conventional machining techniques have been used in cutting of FRP but each process has advantages and limitations. For example laser beam [219, 220], water jet [221], and abrasive water jet [222] have been used to cut CFRP. Water jet machining (WJM) is not

recommended for machining composites which can absorb water (hydrophilic) and cause separation, breakage, and hydrocracking. In the aerospace industry, abrasive water jet machining (AWJM) is used for rough routing of excess material, followed by milling for the final shape and dimensions. Traverse speed is inversely proportional to laminate thickness and in order to cut a 12.7 mm section of CFRP, the recommended traverse speed is 900 mm/min (at 345 MPa using 80 garnet mesh), which is slower than milling. Finishing can be performed using fine abrasive grains. AWJM is known to be better than plain WJM or laser beam machining (LBM) in terms of surface quality [222]. AWJM is environment friendly however it has drawbacks in that it can cause thermal damage at the exit side and damage due to high pressure water wedging as well as causing workpiece abrasive contamination [223].

Laser beam cutting is a non-contact ablation process in which the efficiency is determined by the thermal properties of the cut material. Difficulties are encountered if the plastic material cannot absorb the laser beam and this is why carbon black is added to plastics to facilitate light absorption. Laser cutting can also produce charred layers (where matrix is burned and fibres are bare) and beam divergence can affect workpiece geometry. The most common types of lasers used in industry are ND-YAG and CO_2 lasers. Lasers operate in two modes namely continuous wave (CW) and pulsed mode (PM) [224]. Pulsed mode is preferrable as it generates high power and allows cooling. ND-YAG laser can be used effectively in pulsed mode to cut CFRP by evaporating resin and fibres before matrix overheat. The main parameters governing laser operation are pulse duration, wave length, focal spot diameter, fluence, pulse energy, and scanning speed. With a 1500 W laser the maximum thickness that can be cut is 9.5 mm.

Electrical discharge machining (EDM) is capable of cutting conductive materials. In EDM the material is removed by high temperatures (8000 - 12,000°C) between two electrodes. A series of voltage pulses of about 20-120 V and frequency of ~5 kHz is applied between the two electrodes, which are separated by a small gap typically 0.01 to 0.5 mm, filled with a dielectric liquid [224]. Composites should have 1-3 ohm/m resistivity to allow for EDM. In cases where the matrix is nonconductive, copper can be added to facilitate operation. The process is more accurate than WJM and capable of producing holes down to 0.25 mm and is not affected by workpiece although. Conversely the process is slow. EDM can be used to produce cavities (die sinking/trimming mode) or contoured edges in wire cutting mode. Ultrasonic machining (USM) is not widely used for machining composites however,

ultrasonic vibrations can be employed to assist some conventional machining processes (turning, milling) as mentioned earlier.

2.5 Design of experiments

A set of experiments can be performed using either full factorial or fractional factorial designs. A full factorial design involves running all possible combinations. For example, three factors at two levels will require 8 experiments not counting replications. When the number of factors and levels increase, a factorial design will require a large amount of resources which in some cases is not realistic. However the full factorial design provides comprehensive assessment of results [225].

Taguchi fractional factorial designs or orthogonal arrays are normally used to reduce the amount of experiments. In Taguchi's method, the term 'signal S' represents the desirable value and 'noise N' represents the undesirable value. The S/N ratio indicates the degree of predictable performance of a product or process in the presence of noise factors. Process parameter settings with the highest S/N ratio always yield the best quality with minimum variance [53]. Analysis of variance (ANOVA) is a method of appointing variability into identifiable sources of variation and the associated Degrees of Freedom (DOFs) in an experiment. Here one of the methods to analyse the data is Pareto ANOVA. This is a quick and easy method to analyse the results of parameter design, which does not require an ANOVA table and, therefore, does not use F-tests [53]. In milling of composites authors such as Davim et al. [160, 177] reported that the use of ANOVA is beneficial in determining the contribution percentage of each factor and percentage of error. Azmi et al. [179] found that when using Taguchi and ANOVA in milling of UD-GFRP, that feed rate had the highest influence on the resultant force with 53.6% percentage contribution (PCR). For surface roughness the PCR was 66.3% and for tool life 85.2%. Main effects plots shown in Figure 2.70 are used to demonstrate the effect of varying factors on either the S/N ratio or means.

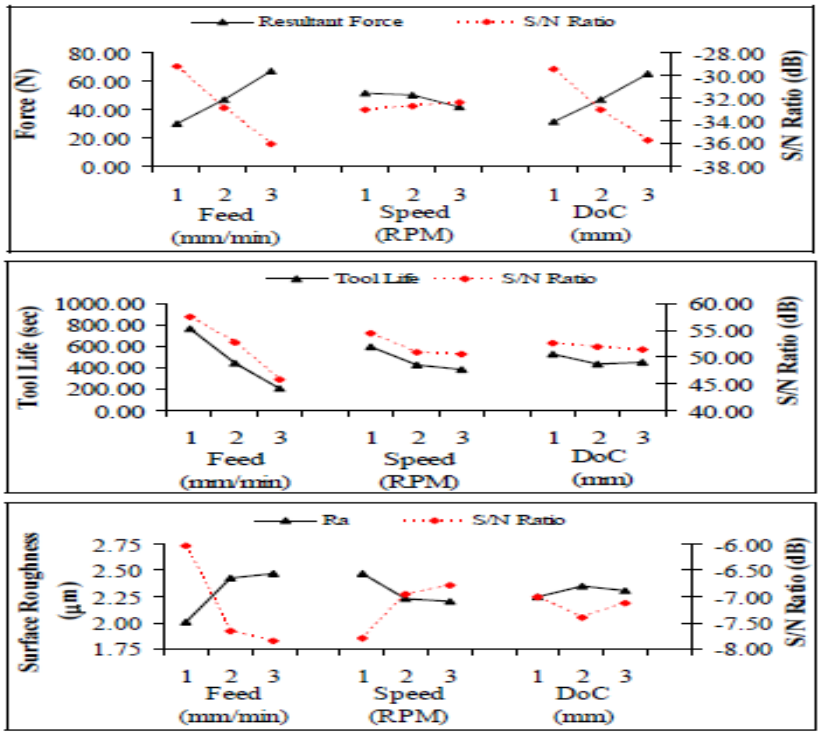

Figure 2.70: Main effects plot of process parameters

2.6 Summary of literature review

The literature review covered composite materials and their machinability. The material part presented the classification of composite materials and focused on fibre reinforced plastic (FRP) composites. The discussion around FRP composites covered the main constituents including the matrix and the fibre material. The most common fibre materials were then classified according to their physical and mechanical properties with emphasis on carbon fibres that were classified according to strength. The matrix material was discussed with more emphasis on polymeric types and their properties and applications.

The various forms of fibres and how they are normally used to make different composite architectures were mentioned. The laminated types, their anatomy and common codes were discussed in detail. Fabrication methods used to manufacture FRP composites were covered alongside the health and safety risks associated with such processes and the related regulations.

The machinability review covered the current trends in FRP machinability research. Starting from orthogonal cutting which was studied to understand the behaviour of fibre reinforced composites when they are machined. The key aspects studied were chip formation and the cutting mechanism of fibres at different orientations with respect to cutting tool

motion. Although these findings were useful, they could not be taken as indicative of results for the milling process which is different in nature and the values of the parameters used were inappropriate for adoption in a real production scenario. Turning of FRP composite was also reviewed with consideration of the fact that turning can be a continuous process whereas milling which is an interrupted one. There was no data relating to cutting temperature either in the orthogonal or other turning process research articles surveyed.

The most widely studied machining process of FRP composites was drilling. This was due to the extensive use of drilled holes in aircraft structures. The vast majority of the drilling research work was focused on how to assess delamination and how to minimise or avoid its formation using several techniques which help in reducing thrust force. The drilling of stacks is currently the challenge for researchers.

The milling of composites was thoroughly reviewed and the importance of the milling process in manufacturing FRP components was extensively highlighted. The different milling operations were detailed and the process requirements and related terminologies were explained. Previous machinability studies related to milling were categorised according to process variables and responses measured to evaluate the machinability and the related references were detailed. It was obvious that there was relatively few research articles compared to other processes especially drilling. There were few articles discussing the slotting operation the majority of research work involved the edge trimming process.

Although the cutting speeds and feed rates cited in the literature had a wide range of values, research concerning the use of high cutting speeds and feed rates especially where slotting was absent. End mill geometry and related research was divided into three main categories namely fluted, burr, and abrasive grit tools and the details of preferred geometry features from the literature were mentioned. However, there were no details on the effect of tool geometry neither on stability of cutting nor on the cutting temperature and their effects on surface integrity when slotting FRP composites.

In relation to carbide tool material aspects, cobalt content, grain size, and coatings were reviewed. The use of different PCD grades or different diamond coating in slotting of CFRP was lacking in the literature. Tool wear associated with different tool categories was detailed. There was no data covering tool temperature during slot milling nor on the use of vortex generated chilled air as a cutting environment. The effect of different chilled air flow rates on quality was not studied. In addition, delamination assessment using laser techniques was limited.

On the modelling side, the modelling approaches varied from mathematical to FEA modelling. The empirical formulas obtained to predict responses like such as, delamination, tool life, and surface integrity were however limited to process other than slot milling (i.e. edge trimming of CFRP) and other equations were limited to milling other materials such as glass fibre reinforced plastics GFRP.

Cost analysis with respect to tooling cost when slotting CFRP was not discussed. An up to date comparison between the cost per meter cut for slot milling and the most common non-conventional machining process used for roughing of CFRP panels was also missing. Different designs of experiments used in previous research were highlighted.

3 EXPERIMENTAL WORK

3.1 Workpiece material

Three different lay-up arrangements of CRFP workpiece material were employed for the research, which were denoted as Type-1, Type-2 and Type-3. Each type consisted of fibres at orientated at 0˚, 45˚, 90˚, and 135˚ but with different lay-up arrangements. Type-1 and Type-2 configurations are commonly used for wing skin panels while Type-3 are utilised for wing spars. Figure 3.1 shows a schematic of various wing structural parts currently made from CFRP. The composite materials are also generally described in the form of [A/B/C], with A, B, and C representing the percentage of fibres in the laminate aligned at 0˚, 45˚ or 135˚ and 90˚ directions respectively.

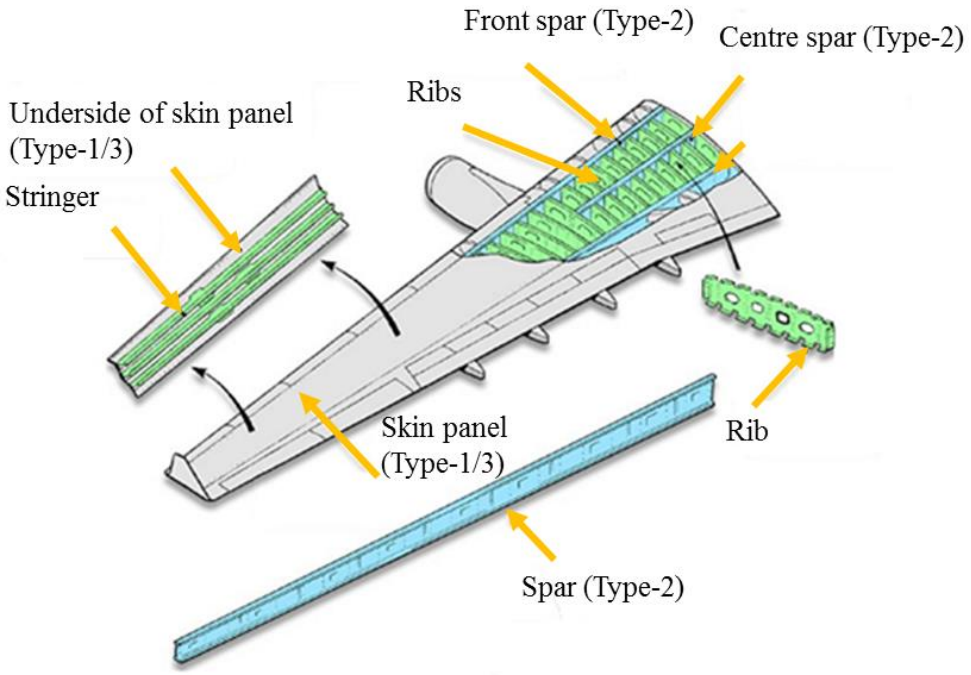

Figure 3.1: Wing structural part made of CFRP composites (courtesy of Airbus)

The CFRP laminates comprised unidirectional (UD) prepregs consisting of intermediate modulus (294 GPa) carbon fibres impregnated within an epoxy resin matrix (each 0.26 mm thick), which were manually laid up and subsequently autoclave cured for consolidation. The prepregs were manufactured by Toray Industries with a material designation of TORAY 3911/34%/UD268/T800SC-24K, which indicates the resin type, resin content by percentage weight, fibre areal weight (g/m^2), fibre type and tow size respectively. Figure 3.2 shows the

symmetric lay-up configurations of the 3 different laminates while details of the number of plies in a given fibre direction for each material type are detailed in Table 11.

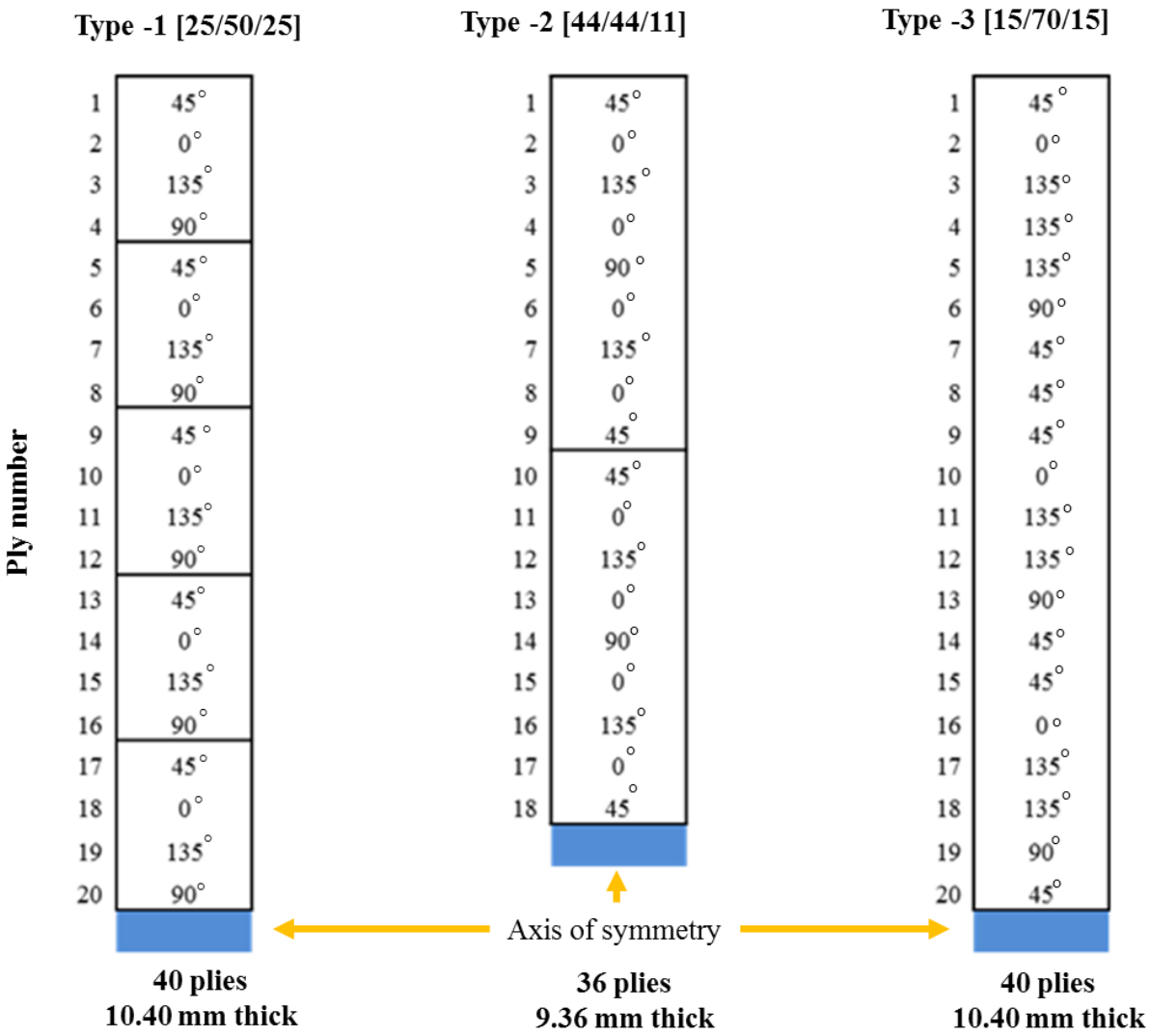

Figure 3.2: Schematic of Type-1, Type-2 and Type-3 lay-up configurations

Table 3.1: Number of different plies within the lay-up for Type-1, Type-2 and Type-3 material configurations

Fibre orientation angle	**Number of plies**		
	Type-1	Type-2	Type-3
45°	10	8	14
0°	10	16	6
135°	10	8	14
90°	10	4	6

Both Type-1 and Type-3 panels were each made up of 40 plies and stacked according to the sequence of $[45^{\circ}/0^{\circ}/135^{\circ}/90^{\circ}5]_{5S}$ and $[45^{\circ}/0^{\circ}/135^{\circ}/135^{\circ}/135^{\circ}/90^{\circ}/45^{\circ}/45^{\circ}/45^{\circ}/0^{\circ}/135^{\circ}/135^{\circ}/90^{\circ}/45^{\circ}/45^{\circ}/0^{\circ}/135^{\circ}/135^{\circ}/90^{\circ}/45^{\circ}]_{2S}$ respectively (total thickness of 10.4 mm), while Type-2 laminates involved 36 plies arranged in the order of $[45^{\circ}/0^{\circ}/135^{\circ}/0^{\circ}/90^{\circ}/0^{\circ}/135^{\circ}/0^{\circ}/45^{\circ}]_{4S,}$ with a post cure thickness of 9.36 mm.

All of the composite workpieces were prepared at Airbus in Filton with details of the manufacturing procedure, material safety datasheet and material properties of the carbon fibres shown in Appendix B, C and D respectively. The cured panels had dimensions of 600 × 550 mm, where the long edge facilitates identification of the 0° fibre direction. The panels were subsequently sectioned using a diamond abrasive disc saw rotating at ~ 4000 rpm under a water based emulsion environment (Figure 3.3), into workpiece specimens having dimensions of 260 × 240 mm and 100 × 100 mm for use in tool life and cutting force/surface integrity evaluation tests respectively, as shown in Figure 3.4.

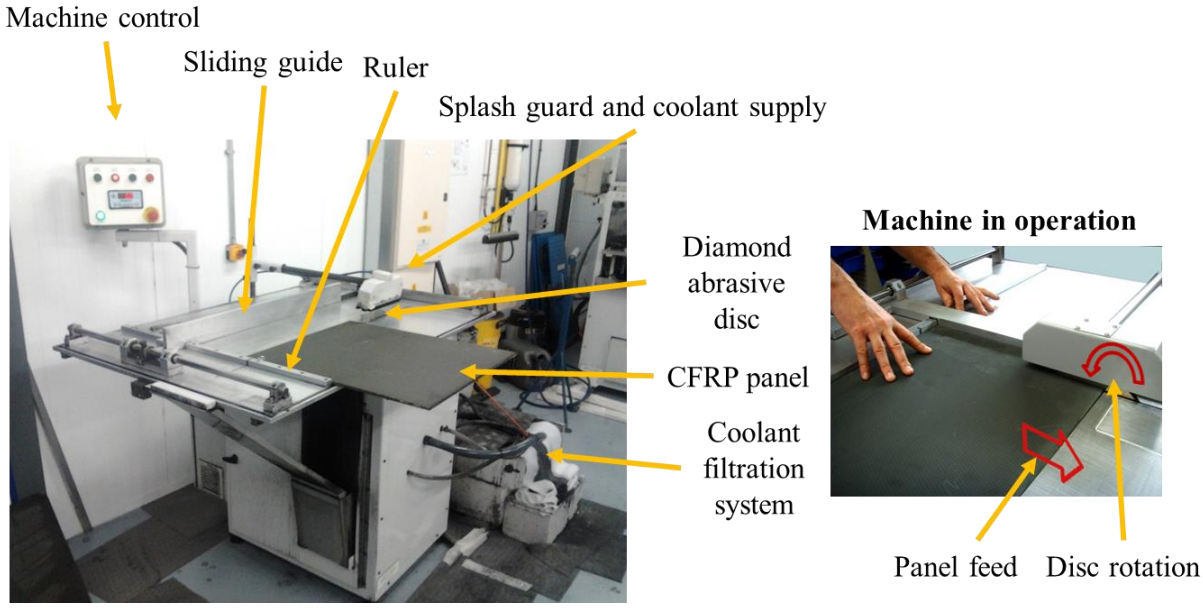

Figure 3.3: Diamond disc slitting saw and cutting operation

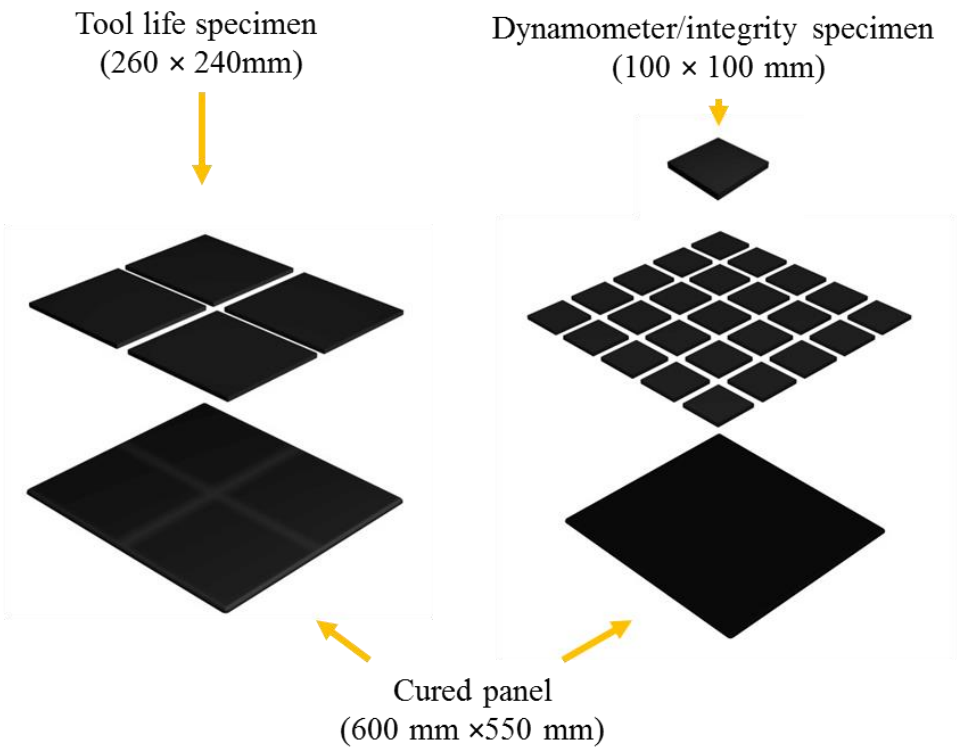

Figure 3.4 : Cutting of different specimen sizes from 600 × 550 mm cured panels

In addition, a further three panels were produced where all of the plies were oriented in one direction (0°/90°, 45° or 135°) and were used in Phase-2A experimental work. All 3 panels were cut into specimens with dimensions of 100 × 100 mm. Table 3.2 lists the CFRP materials used in the 3 main phases of experimental work (detailed in Section 3.5).

Table 3.2: CFRP materials used in the 3 main experimental work phases

	Phase-1	**Phase-2**	**Phase-3**
Prepreg material	TORAY 3911/34%/UD268/T800SC-24K		
Lay-up	Type-1 [25/50/25]	Single direction layup (0°, 45°, 90°,135°) Type-1 [25/50/25] Type-2 [44/44/11] Type-3 [15/70/15]	Type-1 [25/50/25]

3.2 Cutting tools routers/end mills

The cutting tools employed for testing included both uncoated and coated 2 fluted WC routers/end mills as well as various grades of brazed PCD tools. The performance of an uncoated and diamond coated burr type router was also evaluated. The majority of tooling was manufactured and supplied by Seco, with a small proportion of PCD routers provided by ITC and Exactaform for benchmarking trials. Details of the tools used are detailed in the following sections.

3.2.1 Tungsten carbide tools

3.2.1.1 Two-fluted routers

All of the two-fluted WC routers employed were 12 mm in diameter and had equivalent geometry of 0° helix, 0° rake, 12° primary relief and 22° secondary relief angles, as shown in Figure 3.5. These involved 3 variants, which included an uncoated as well as two having diamond based coatings (DLC and CVD diamond), with details of the carbide substrate material characteristics and mechanical/physical properties of the coatings outlined in Table 3.3 and Table 3.4 respectively.

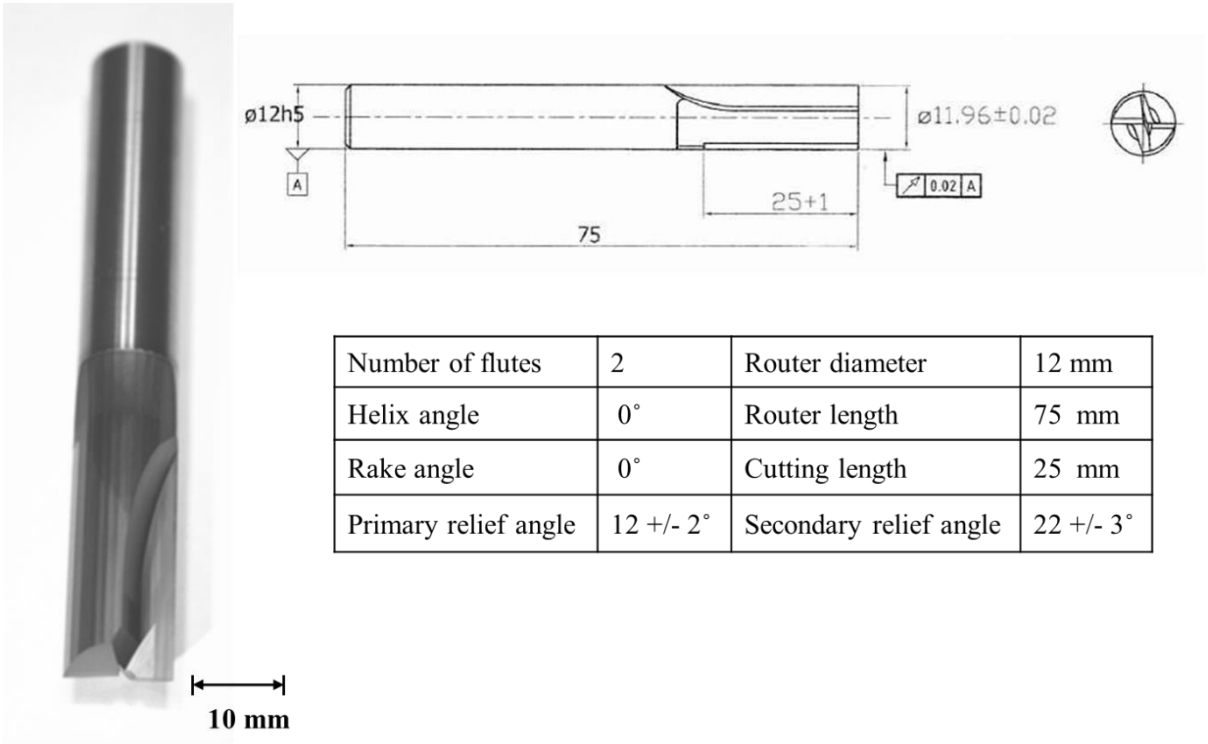

Number of flutes	2	Router diameter	12 mm
Helix angle	0˚	Router length	75 mm
Rake angle	0˚	Cutting length	25 mm
Primary relief angle	12 +/- 2˚	Secondary relief angle	22 +/- 3˚

Figure 3.5: Geometry of 2-fluted WC routers from Seco

Table 3.3: Properties of WC substrates (courtesy of Seco)

Substrate / Tool	Cobalt content Co %	Transverse rapture strength, TRS (MPa)	Vickers hardness (HV)	Modulus of elasticity E, (GPa)	Grain size (µm)
Uncoated (Seco Jabro 94120 d=12 87250 AMG)	10	3700	1680	580	0.5-0.8
DLC coated (Seco Jabro A033798-02696031)	6	3000	1830	640	0.8-1
CVD diamond coated (Seco 02692693)	6	3000	1830	640	0.8-1

Table 3.4: Properties of coating materials (courtesy of Seco)

Coating / Tool	Thickness (µm)	Deposition process	Composition / Structure	Vickers Hardness (HV)	Modulus of elasticity, E (GPa)	Edge radius, ER (µm)	3D average roughness, Sa (µm)
DLC coated	2-4	PVD	C-H free	5000	360	4-6	0.305
Diamond coated	6-8	CVD	C- sp3	10000	800	6-8	0.230

3.2.1.2 Burr type routers

The performance of uncoated (*Seco 871120.0 4486035-014*) and Dura coated (*Seco 871120.0 – Dura 4431601 - 011*) burr type routers were also evaluated. These cutters with pyramidal shaped cutting edges, are formed from two interlocking left and right hand helices, see Figure 3.6. The properties of the WC substrates and Dura coating were equivalent to those used for the 2-fluted routers. Geometry details of the burr-routers used are shown in Table 3.5.

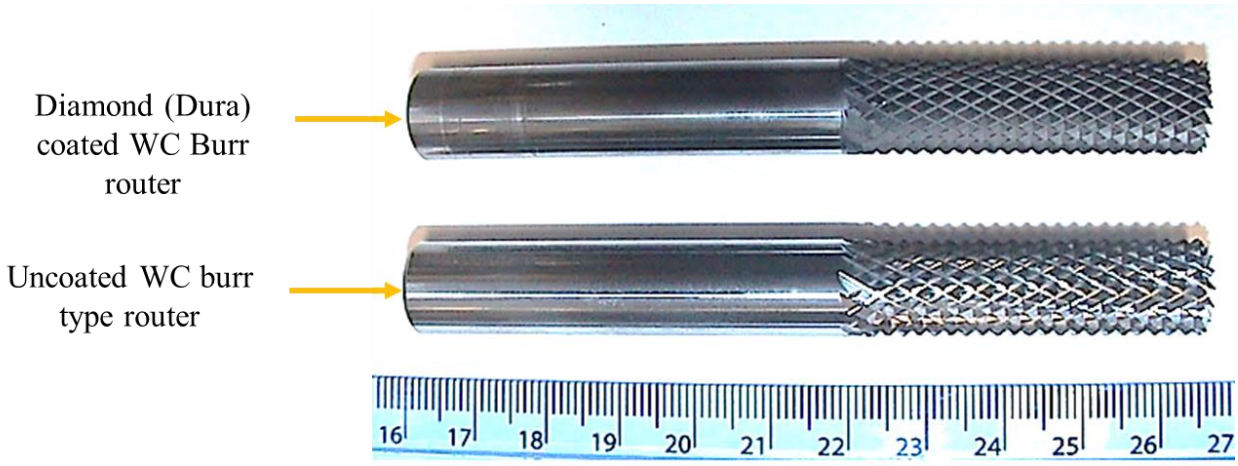

Figure 3.6: Uncoated and diamond coated (Dura) coated WC burr type routers

Table 3.5: Geometry details of burr type routers

Number of flutes	18	Cutting length	45 mm	Helix angle right	25°	Relief angle	18°
Router length	100 mm	Router diameter	12 mm	Helix angle left	27°	Rake angle	7°

3.2.2 Polycrystalline diamond (PCD) routers

Various PCD grades manufactured by Element 6 were evaluated in the mainstream testing. Limited comparative trials were also performed using routers with PCD grades produced by alternative manufacturers/tool fabricators.

3.2.2.1 Element 6 PCD grades

The routers were fabricated by Seco using PCD blanks supplied by Element 6 and brazed onto the cutter body. All of the cutters were 2-fluted 12 mm diameter with a corner chamfer together with rake and relief angles of 0° and 18° respectively. A detailed drawing of the tools is shown in Figure 3.7. Four commercially available PCD grades were tested based on recommendations from Element 6, which were CTM-302, CTB-010, CMX-850 and WPC-102 PCD, see Table 3.6 for brief descriptions of the tool characteristics. Further information regarding the structure and mechanical/physical properties of the different grades are detailed in Table 3.7.

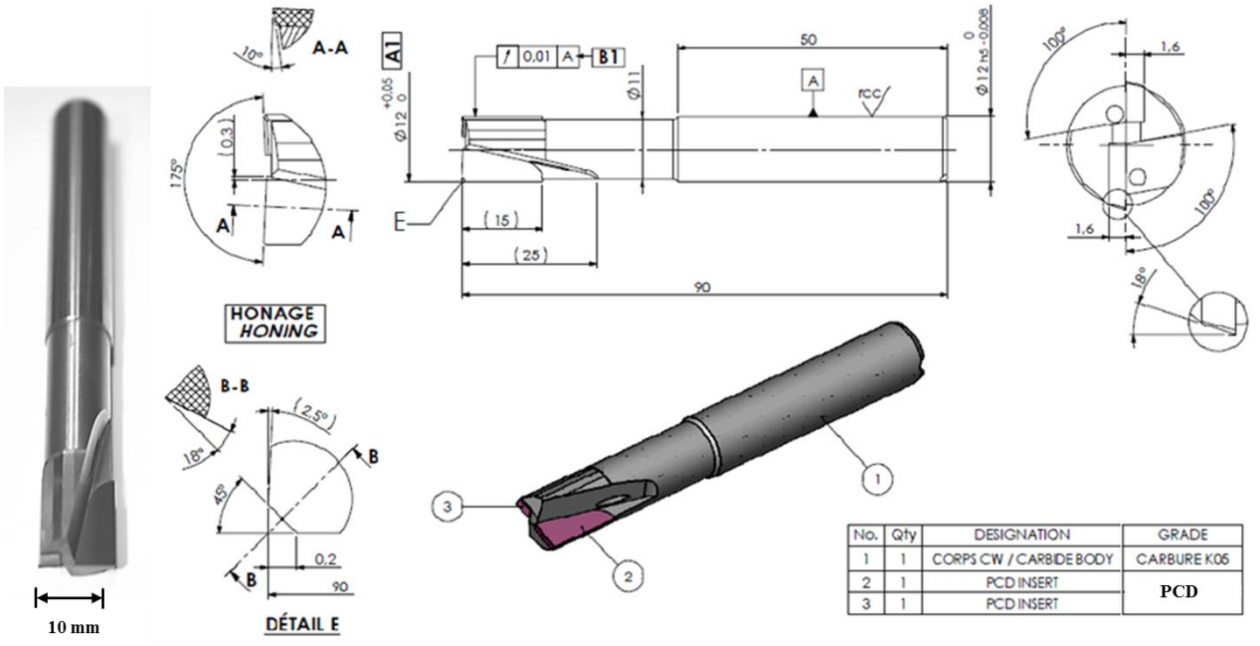

Figure 3.7: Geometry of PCD routers supplied by Seco

Table 3.6: Characteristics of Element 6 PCD grades

Element 6 PCD grade	Reference number	Description
CTM-302	Seco 28108-928	Grain sizes varying from 2-30µm. High abrasion resistance but relatively low chipping resistance
CTB-010	*Seco Reaming 28156-928** Seco BR28155 02692693 4361079 020/026**	Average grain size of ~ 6.7µm. Good balance of abrasion and chipping resistance
CMX-850	Seco 28155-928*** *Seco 890120E2s.0Z2A 8002081-0033 DC-12****	Grain size of 1.26µm, which enables fabrication of cutters with finer cutting edges and high resistance to milling forces
WPC-102	Seco 0269269	Developed for woodworking applications with multi-layered PCD structure consisting of functionally graded PCD with diamond to prevent chipping

* Mechanically ground edges (used in Phase-1)
** WEDM cut edges (used in Phase-2)
***18° primary relief
****10° primary relief and 18° secondary relief angles (used for benchmarking)

Table 3.7: Mechanical and physical properties of Element 6 PCD grades

Property	Units	PCD grade		
		CTM-302	CTB-010	CMX-850
Binder type	---	Co	Co	Co
Average grain size	μm	13.8	6.77	1.26
Grain size distribution	---	Multimodal*	Unimodal**	Unimodal
% Diamond	Area %	91.71	89.52	85.55
Fracture toughness	$MPa.m^{0.5}$	10.24	8.96	-
Thermal conductivity	$W.m^{-1}.K^{-1}$	560	459	212.16
Transverse rapture strength (TRS)	MPa	1131	1398	1595
Density	g/cm^3	3.99	4.08	4.37
Elastic modulus	GPa	883	1000	827
Thermal diffusivity	$mm^2.S^{-1}$	-	277	78.66
Coefficient of expansion	$10^6/^\circ C$	4.2	4.5	4.9
Specific heat	$J.kg^{-1}.K^{-1}$	0.471	0.468	0.458

* Contains grains with varying sizes
**All grains are approximately of same size

3.2.2.2 Alternative PCD routers

Three alternative PCD tools were tested, all of which were two-fluted and 12 mm in diameter. Each of the routers however had different cutting edge geometries, see following details:

- **Seco/Mega-Diamond PCD (Seco 890120E35.0Z2A/8002081-0018 DC-12):** The tools were fabricated with 10° primary relief, 18° secondary relief and 0° rake angles. Properties of the Mega-Diamond PCD grade were approximately equivalent to the CTB-010 outlined in Table 3.7.
- **ITC-PCD (ITC 2111-12.0-0.5 R):** Recommended for the milling of composites materials with rake and helix angles of 0°, a 15° relief angle and a 0.5 mm corner radius, see Figure 3.8(a).
- **Exactaform-PCD:** Three different variants were assessed involving 'Neutral' (EX 9703), 'Up-cut' (EX 8706) and 'Down-cut' (EX 8705) geometries. These tools have rake and relief angles of 0° and 18° respectively. The 'Up-cut' and 'Down-cut' tools however have helix angles of +3° (right hand) and -3 (left hand) respectively while the

'Neutral' cutter was straight fluted tool (0˚ helix), see Figure 3.8(b). The PCD grade used was similar to CTM-302.

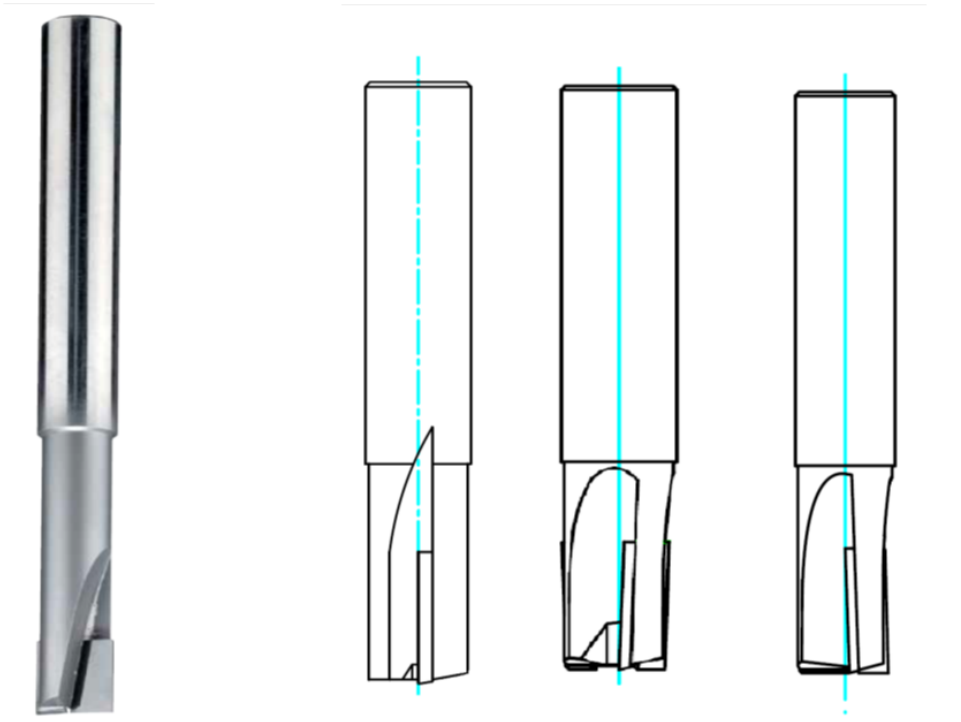

Figure 3.8 (a) ITC 2 fluted PCD router, (b) Schematic of Exactaform 3 fluted PCD routers (courtesy of Exactaform)

A summary of the routers employed in the different phases of experiments is shown in Table 3.8.

Table 3.8: Summary of cutting tools/routers used in the various experimental phases

Phase-1		**Phase-2**		**Phase-3**	
Phase 1A	ITC-PCD Exactaform-PCD	Phase-2A	ITC-PCD Exactaform-PCD	Phase-3A	ITC-PCD Exactaform-PCD
Phase-1B	DLC-coated WC CTM-320 PCD CTB-010 PCD CMX-850 PCD	Phase-2B	CTB-010 PCD	Phase-3B	CTB-010
Phase-1C	CTM-320 CMX-850 Mega-Diamond-PCD WPC-PCD CVD (Dura) coated WC	Phase-2C	CTB-010 PCD		
Phase-1D	Uncoated WC PVD (DLC) coated WC CVD (Dura) coated WC Uncoated WC Burr router Dura coated WC Burr router				

3.3 Test and analysis equipment

3.3.1 Machine tool

All tests were performed on a Matsuura FX-5 high-speed machining centre, shown in Figure 3.9 (a), with a spindle rotational speed of 200 to 20000rpm, a maximum feed rate of 15m/min and a power rating of 15kW, The machine was fitted with a Renishaw TS27R contact tool setting probe while a vacuum extraction system (Filtermist), shown in Figure 3.9 (b), capable of removing airborne particles down to 0.3 µm was installed to extract CFRP dust from the cutting zone. Face masks were used all the times during the tests to provide additional protection from any airborne dust.

Figure 3.9: (a) Matsuura FX-5 vertical CNC machine, (b) Filtermist extraction system

3.3.2 Tool holding

All of the routers/cutters were held using a BT-40 taper tool holder with a 12 mm diameter collet except those used in the temperature measurement experiments, which were held in a special HSK-63 tool holder fitted with a wireless transmitter and connected to a HSK BT-40 adapter to allow mounting on the FX-5 machine. Figure 3.10 shows the tool holders used.

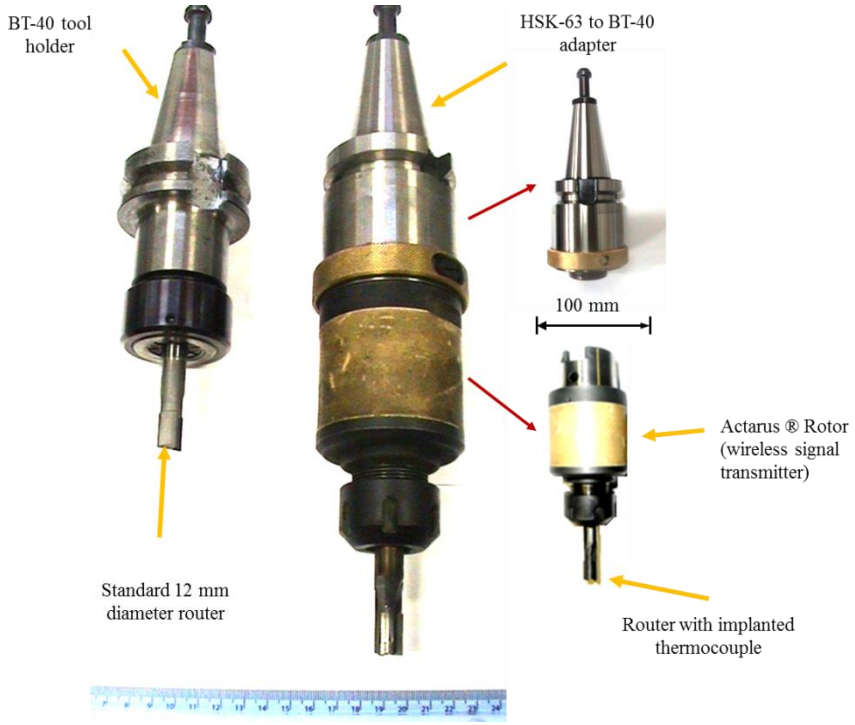

Figure 3.10: Various tool holders used in the experiments

3.3.3 Work holding

The large CFRP workpiece samples (260 × 240 mm) primarily used for tool life testing were held using a VacMagic VM 300 vacuum pallet unit with a universal top plate, see Figure 3.11(a). A safety valve interlock system was installed to stop the machine in the event of a sudden loss of vacuum. The dimensions of the top plate were 365 × 325 mm with an array of pre-drilled holes to fit guide pins for precise location of the workpiece. A further 6 clamps were also added for additional rigidity. Conversely, the smaller workpiece coupons (100 × 100 mm) for cutting force/surface integrity analysis were mounted on a 3-component force dynamometer by means of a bespoke fixture as shown in Figure 3.12.

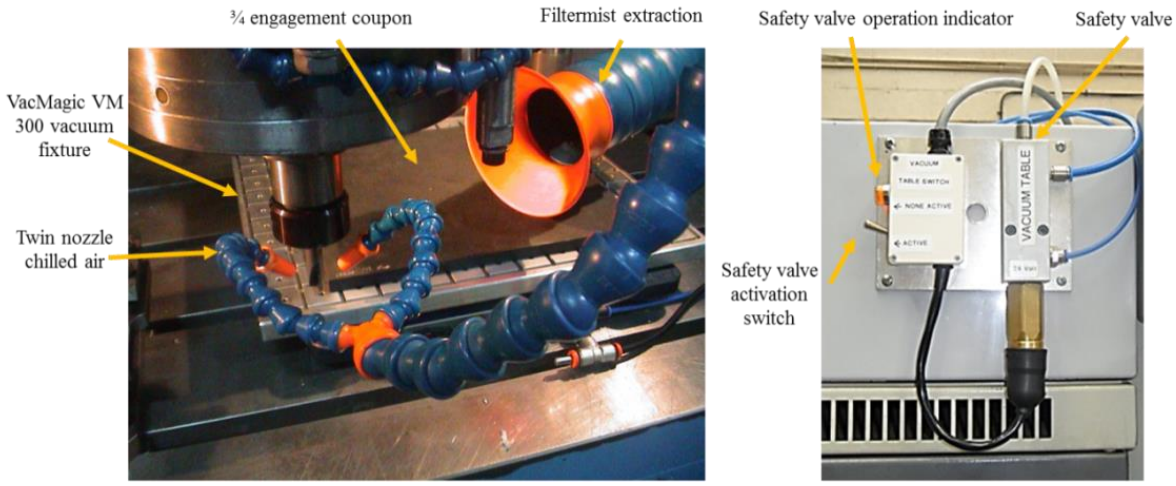

Figure 3.11: (a) VacMagic VM 300 vacuum pallet unit (b) safety valve

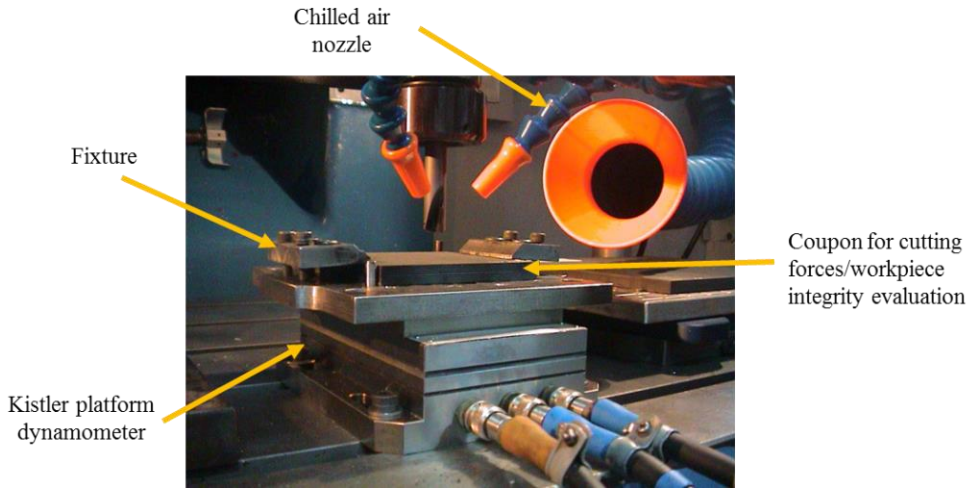

Figure 3.12: Cutting force /surface integrity coupon clamped on dynamometer

3.3.4 Cutting environment

Typically, water soluble coolant is recommended for cutting composites whereas air cooling and strong extraction is preferred for hydrophilic composites [15]. The application of liquid based cutting fluid leads to the absorption of moisture by the resin phase [5], which deteriorates part dimensional accuracy and mechanical properties in addition to the formation of sludge [226]. In the present work, the CFRP was machined either dry or under chilled air conditions. The latter was generated using a NexFlow Frigid-X 57030FD vortex tube, which was attached to side of the machine spindle as shown in Figure 3.13 (a). Compressed air injected into the unit separates into flows of hot and cold air due to the vortex tube phenomenon, which is illustrated by the schematic shown in Figure 3.13 (b).

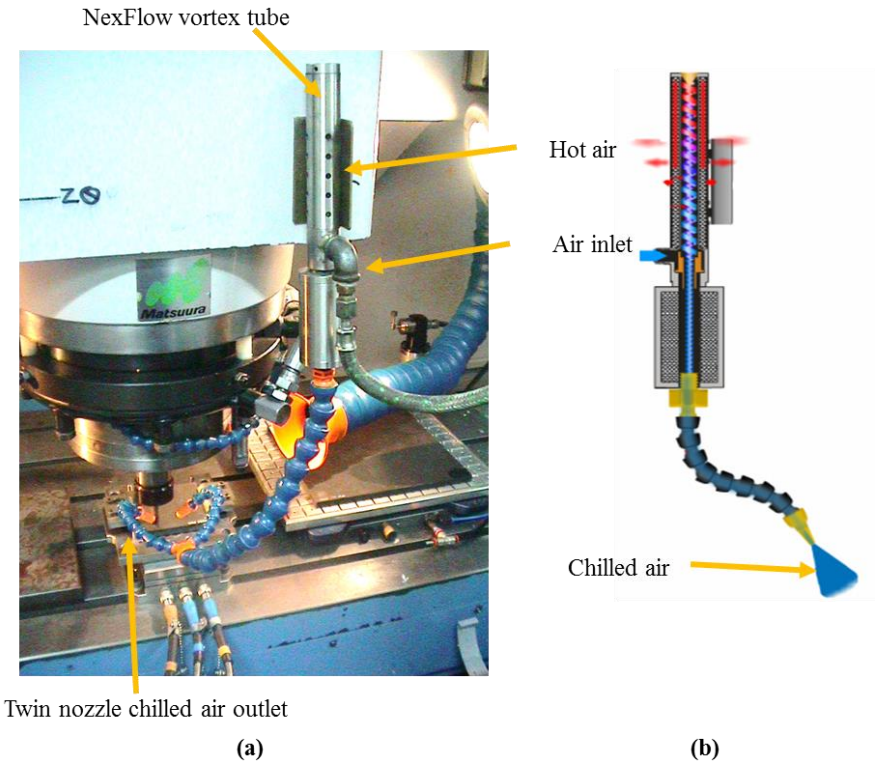

Figure 3.13: (a) NexFlow vortex tube twin nozzle chilled air outlet, (b) vortex tube working principle

The chilled air (CA) was directed to the cutting zone through adjustable hoses, either in a twin-nozzle or single-nozzle mode. The temperature of the chilled air delivered at different parameters was measured using a thermometer placed directly after and at ~10 mm from the nozzle exit, with results detailed in Table 3.9.

Table 3.9: Chilled air conditions in single and twin-nozzle arrangements

Chilled air mode	**Air speed* (m/s)**	**Air temperature** (°C)**		**Output pressure (bar)**
		At 10 mm from nozzle edge	At nozzle edge	
Single-nozzle	29	2	-3	0.72
Twin-nozzle	17	5	0	0.40

*Measured using an Extech AN200 anemometer at 10 mm distance from nozzle
**Measured using a thermometer

3.3.4 Force measurement

Cutting forces (maximum and average) were measured using a Kistler platform dynamometer (Type 9257A) connected to three single-channel charge amplifiers (Kistler Type 5011A). Force signals were recorded and manipulated using Kistler Dynoware software in the majority of the experiments with the exception of temperature measurement trials where corresponding force data was acquired at a rate of 10000 samples/second and analysed using a Nicolet Sigma 60 4-channel oscilloscope (detailed further in the next section).

3.3.5 Temperature measurement

Cutting temperature measurement was carried out using a wireless telemetry system from Actarus (on loan from Airbus), which involved a K-type thermocouple implanted on the back face of a PCD router; see Figure 3.14. Cutting temperature (in form of voltage signals) was measured by the thermocouple system and displayed on a Microtel K-1 digital readout unit. The data was subsequently relayed to and recorded (simultaneously with cutting force traces) using a Nicolet Sigma 60 oscilloscope, see Figure 3.15. The thermocouple was calibrated to 0.01V for every 1˚C prior to the start of testing.

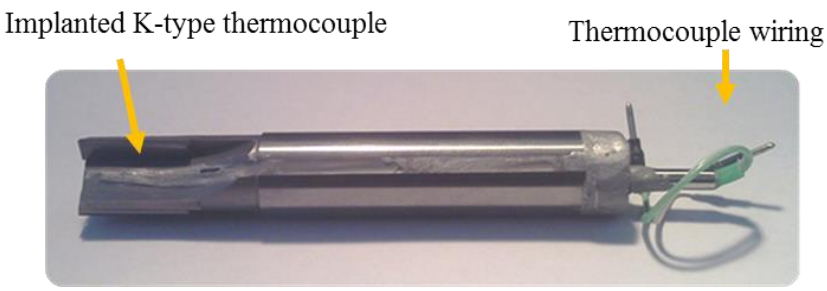

Figure 3.14: Implanted thermocouple in Exactaform router

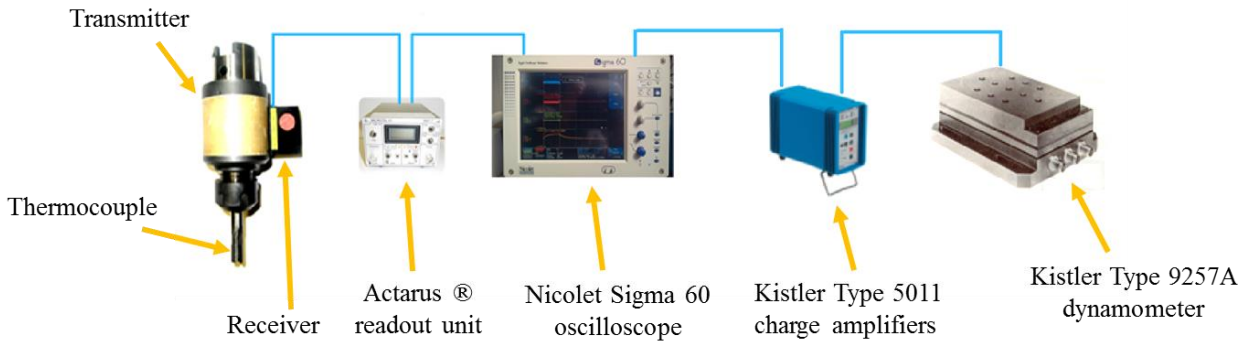

Figure 3.15: Arrangement for simultaneous force and temperature signal capture using Sigma 60 oscilloscope

3.3.6 Tool wear/life evaluation

New and worn routers were photographed using a Canon EOS400D digital camera mounted on a Wild M3z toolmakers microscope equipped with a digital micrometre stage (resolution of 1µm) and bespoke fixture for flank wear measurement as shown in Figure 3.16. Tool flank wear was measured over the entire tool-workpiece engagement length (5mm) at appropriate intervals of 100, 200, 300, 900, 2000, 4100, 8200, 12300, 16400, 20500, 24600 and 28000 mm cut length.

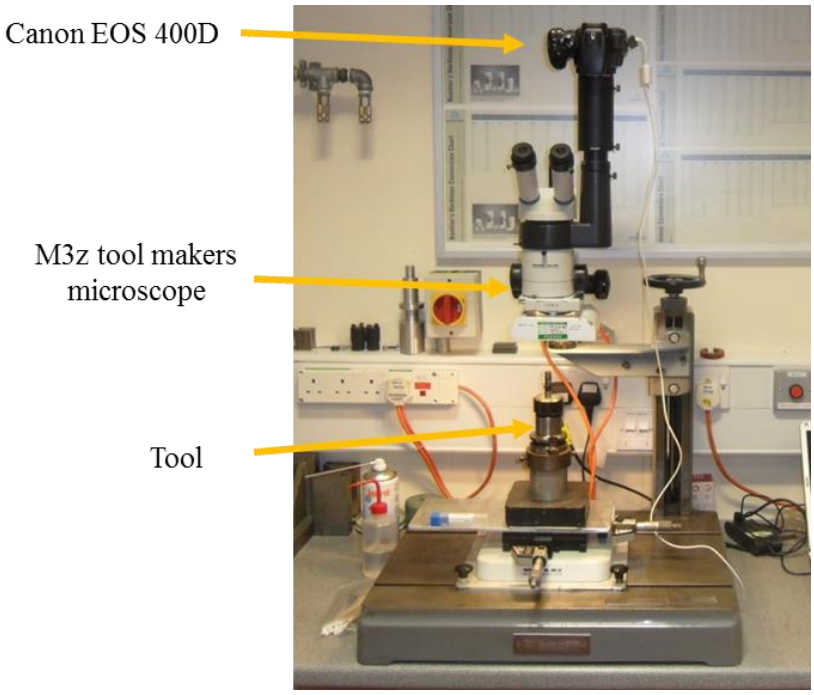

Figure 3.16: Wild M3z toolmaker microscope fitted with Canon EOS 400D

Higher resolution wear micrographs were also obtained using a JEOL 6060 scanning electron microscope (SEM) at the University of Birmingham as well as a LEO ULTRA 55 FEG-SEM at Seco Tools in Sweden, while limited 3D surface scans of worn cutting edges were taken using an Alicona optical measurement system at Element 6.

3.3.7 Workpiece surface/slot quality

The condition/quality of the machined surfaces including characterisation of workpiece damage/defects and dimensional accuracy were assessed using various techniques, which are described in the following sections.

3.3.7.1 Laser scanning

3D digital images of the machined slots were generated using an Impact coordinate measuring machine (CMM) retrofitted with a Kreon Zephyr KZ-25 laser head (10µm accuracy and 500 × 1000 mm scanned part size) mounted on a Renishaw PH 10M indexing head as illustrated in Figure 3.17. The head was manually traversed over the machined workpiece surface with the indexing unit in different orientations, which guaranteed a comprehensive point cloud file of the slot edges and walls.

The point cloud data was subsequently converted to an STL file (example shown in Figure 3.18) using Polygonia software with dimensional/damage analysis performed using Geomagic-Studio package. Features measured include length of uncut fibres (fuzzing), width of damage/delamination and width/depth of slot while the delamination factor (DF) was calculated using Equation 3.1:

$$DF = \frac{W_{max}}{W} \qquad \text{Equation 3.1}$$

Where W_{max} is the maximum width of damage and W is the nominal width of slot as shown previously in Figure 2.53 [176].

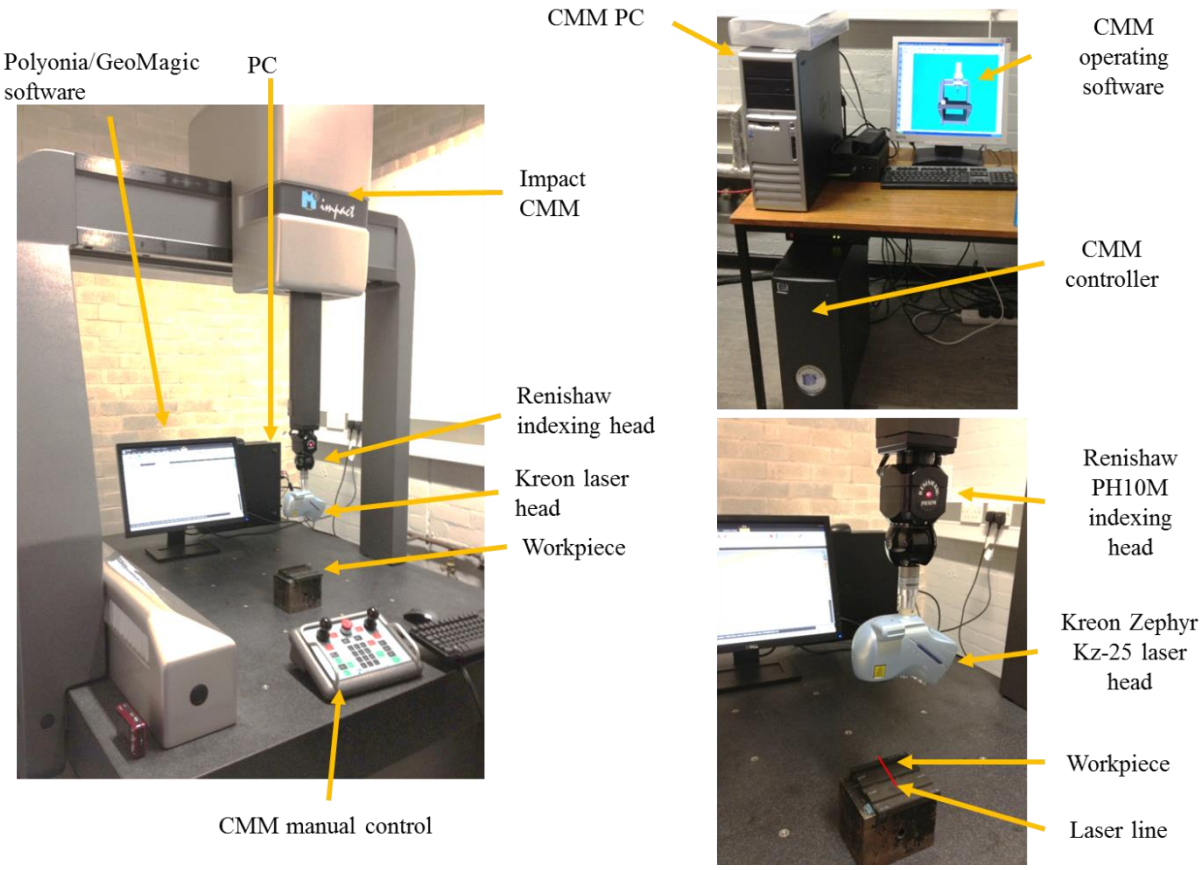

Figure 3.17: Impact CMM with 3D laser scanner for slot quality/damage evaluation

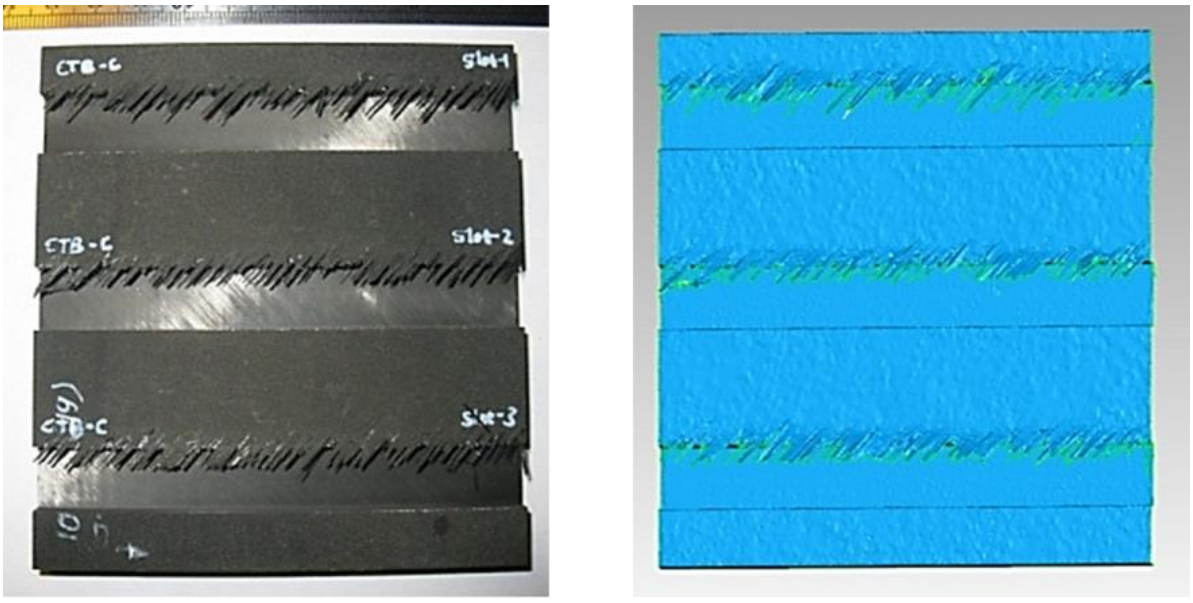

Figure 3.18: Machined workpiece sample and corresponding STL scan

3.3.7.2 Optical microscopy imaging

Optical micrographs of the machined surfaces were captured using the digital camera and toolmakers microscope setup described previously for tool wear measurement (Section 3.3.7) while images of selected samples were also taken using the Alicona optical measurement system. The machined slots were sectioned (following dimensional analysis) using a diamond disc along the length as shown in Figure 3.19 in order to analyse slot wall quality. In addition only the surfaces produced by the down milling cutter direction was assessed as this was representative of the machining operation (end routing/trimming) to be utilised in production. Figure 3.20 shows a schematic of the approximate positions on the workpiece samples that were examined.

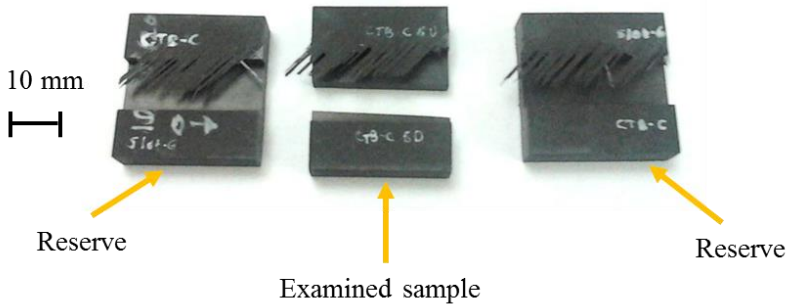

Figure 3.19: Sectioning of workpiece coupons for slot wall analysis

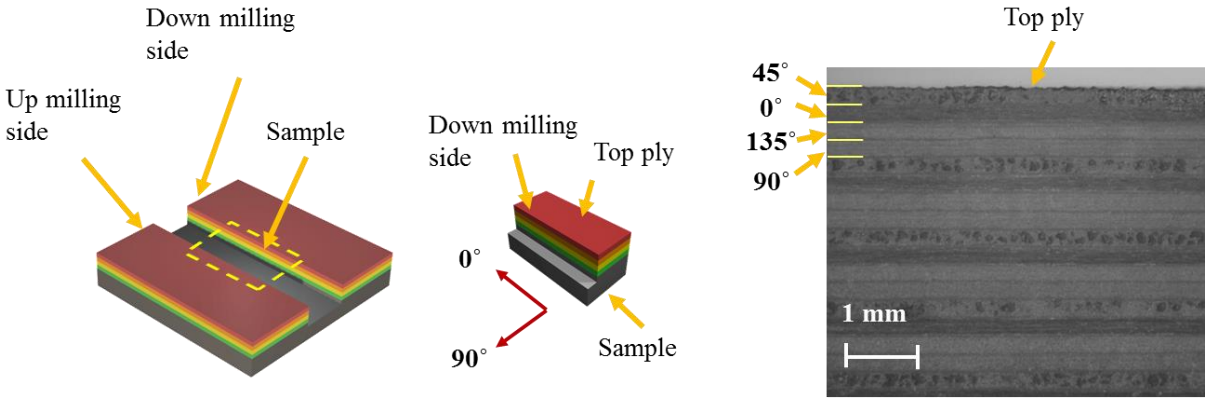

Figure 3.20: Position in sample for optical microscopy imaging

3.3.7.3 Scanning electron microscope (SEM) imaging

High resolution micrographs of the machined surfaces were obtained using a JEOL 6060 scanning electron microscope (SEM). Samples were mounted on aluminium stubs (35 mm diameter × 10 mm thickness) by using carbon adhesive tabs (25 mm diameter) and were gold

(Au) sputtered (several nanometres thick) to increase the electrical conductivity of the workpiece to avoid 'charging' (blurring of the image) during analysis. Images were taken at 90 to 950X magnifications. Figure 3.21 shows the JEOL 6060 SEM unit together with an example of a mounted/sputtered specimen.

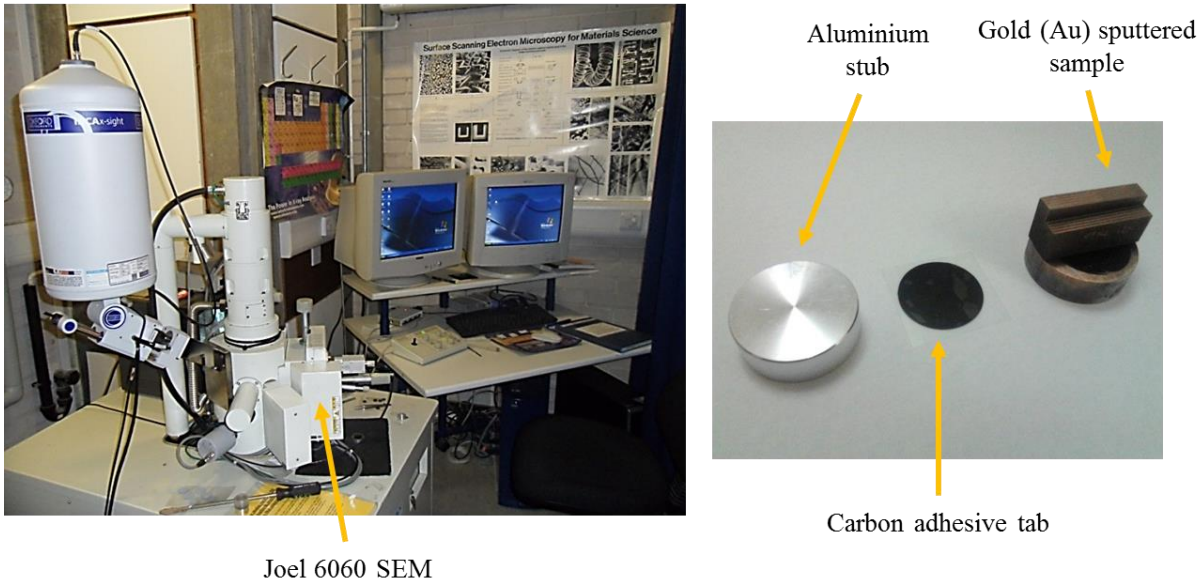

Figure 3.21: JEOL 6060 scanning electron microscope (SEM) and sample mounting

3.3.7.4 Surface roughness evaluation

Surface roughness of the slot walls on the down milling side were measured perpendicular to the cutting direction (transverse direction) using a Taylor Hobson Talysurf 120L contact stylus tester (2.5 µm stylus tip radius) as shown in Figure 3.22. Three 2D readings (Ra and Rt) were taken for each surface over an evaluation length of 2.4 mm (0.8mm cut-off) such that one reading was in the middle of the sample with the other two ~10 mm on either side and subsequently averaged. In contrast, 3D surface topography plots (Sa and St) were assessed over an area of 2.4 x 1.5 mm with one measurement recorded after the first (new tool) and last pass (worn tool) in the middle of the sample. Stylus measurements did allow more for an evaluation length greater than 2.4mm due to slot depth. In addition, 3D topography plots were also obtained using the Alicona optical measurement system (shown in Figure 3.23), which were assessed over an area of 2.5 x 1.5 mm at 10X magnification.

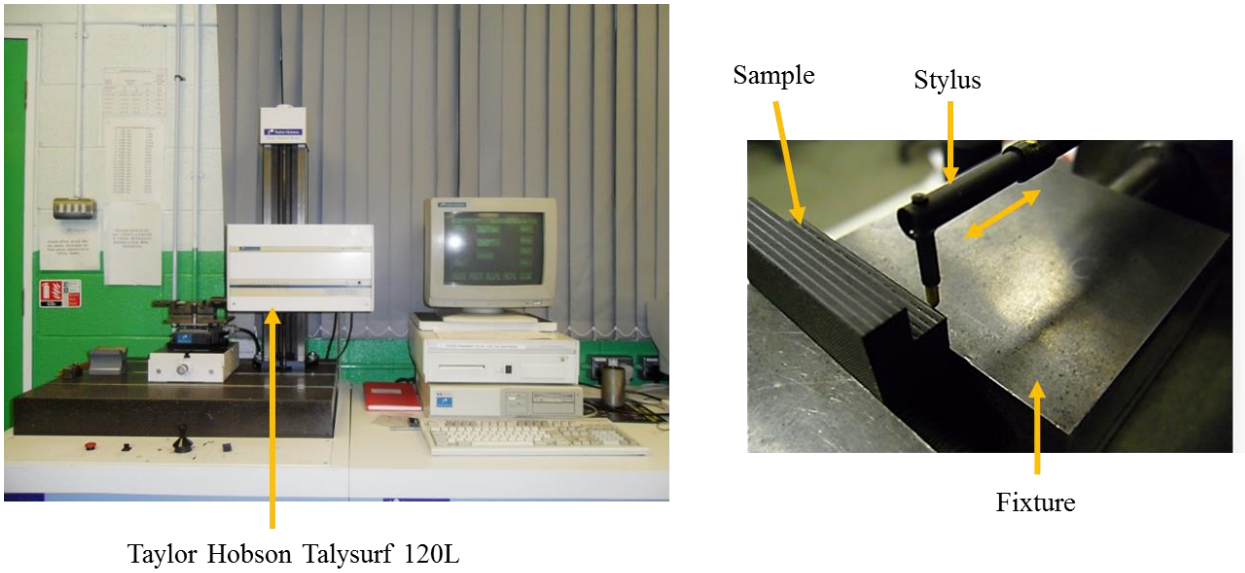

Figure 3.22: Surface roughness tester and sample position during surface roughness measurement

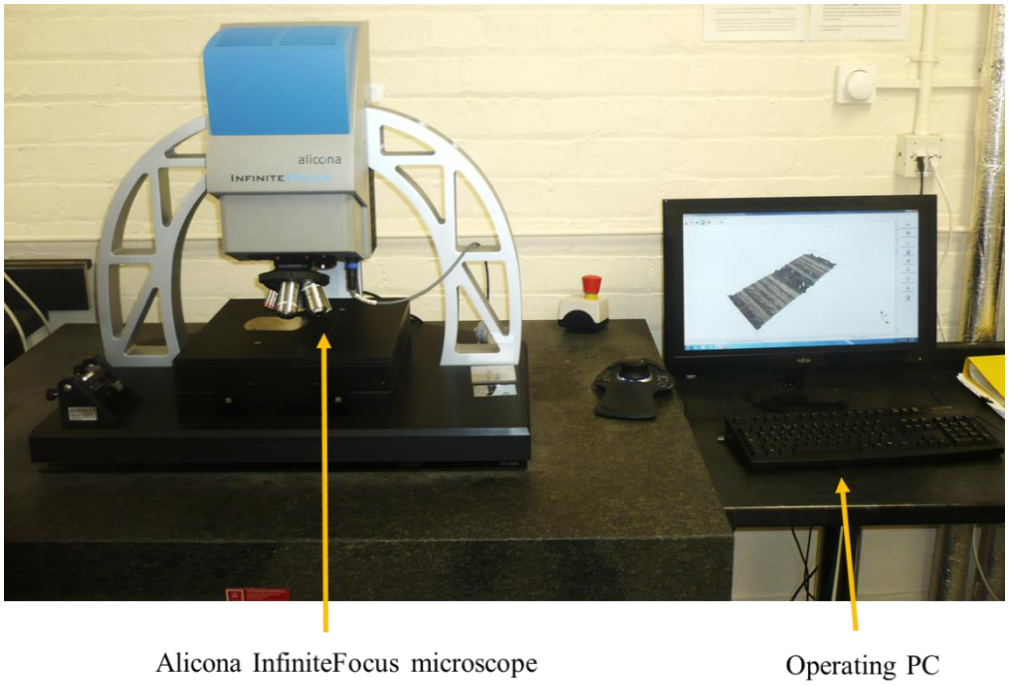

Figure 3.23: Alicona optical measurement system

3.3.7.5 Calibration of Alicona optical system

Alicona Infinite-Focus optically scans the surface by slicing the scanned area (box shaped) into a stack of images and stitches them together to make a 3D surface. This method is a non-contact method and capable of scanning down to 20nm resolution. For example, using 10X magnification and 159 nm 3.91 µm vertical and lateral resolutions respectively,

scanning the surface of standard samples with an area of 1.5 mm X 5 mm, the surface roughness parameters obtained were very close to the standard values as shown in Table 3.10.

Table 3.10: Comparison between standard samples and Alicona measurements

Standard samples	Alicona measurements
Ra 3.2 µm	Ra 2.94 µm Sa 2.92 µm
Ra 6.3 µm	Ra 6.69 µm Sa 6.71 µm
Ra 12.5 µm	Ra 12.7 µm Sa 13.66 µm

3.4 Experimental design, test procedure and test arrays

3.4.1 Phase-1: Effect of operating conditions, tool materials and cutter design

The overall aim of this phase of work was to investigate the effect of different process variables such as cutting speed, feed rate, cutting environment and tool material when routing/slotting CFRP composites. The experimental work undertaken was divided into four sub-phases.

3.4.1.1 Phase-1A: Preliminary work

Following some initial setup verification cuts, a series of pilot trials were performed using commercial 'off the shelf' PCD routers in order to assess the influence of different operating parameters on cutting forces, temperature and surface integrity. All trials involved Type-1 CFRP material with depth of cut fixed at 5 mm under a chilled air environment. Only one slot was machined for each set of parameters. Table 3.11 and Table 3.12 detail the test array for experiments to evaluate the influence of varying cutting speed and feed rate on cutting forces and workpiece surface integrity respectively. The PCD router employed was supplied by ITC.

Table 3.11: Test array to evaluate the effect of cutting speed on forces and slot quality

Test	Cutting speed (m/min)	Tool	Feed rate (mm/tooth)	Cutting environment	WP configuration
1	200	ITC-PCD	0.03	Twin nozzle chilled air	Type-1
2	350				
3	500				
4	650				

Table 3.12: Test array to evaluate the effect of feed rate on cutting forces and slot quality

Test	Cutting speed (m/min)	Tools	Feed rate (mm/tooth)	Cutting environment	WP configuration
1	200 (5308 rpm)	ITC-PCD	0.03	Twin-nozzle chilled air	Type-1
2			0.05		
3			0.07		
4			0.09		

Trials to evaluate the effect of varying depth of cut on cutting forces and temperature at a constant cutting speed and feed rate were carried out using 2 different Exactaform PCD routers, see Table 3.13. Similarly, the tools were utilised to investigate the effect of varying cutting speed and feed rate on cutting temperature, with the lower cutting speed and feed rate levels chosen to avoid PCD chipping as detailed in Table 3.14.

Table 3.13: Test array to evaluate the effect of varying slot depth on cutting temperature

Test	Cutting speed (m/min)	Tool material	Feed rate (mm/tooth)	Cutting environment	WP configuration	Depth of slot (mm)
1	200 (5308 rpm)	Exactaform Neutral	0.03	Twin-nozzle Chilled air	Type-1	1
2						2
3						3
4		Exactaform Up-cut				1
5						2
6						3

Table 3.14: Test array to evaluate the effect of cutting speed and feed on temperature

Test	Cutting speed (m/min)	Tool material	Feed rate (mm/tooth)	Cutting environment	WP configuration
1	200 (5308 rpm)	Exactaform Down-cut	0.03	Twin-nozzle chilled air	Type-1
2			0.06		
3		Exactaform Neutral	0.03		
4			0.06		
5	350 (9289 rpm)	Exactaform Down-cut	0.03		
6			0.06		
7		Exactaform Neutral	0.03		
8			0.06		

3.4.1.2 Phase-1B: Influence of operating conditions and tool materials

Following on from Phase-1A, mainstream experiments were undertaken to evaluate the influence of operating parameters (cutting speed and feed rate), tool materials and cutting environment on cutting forces, tool wear/life and surface roughness. The fixed factors are shown in Table 3.15 while the variable parameters are detailed in Table 3.16.

Table 3.15: Fixed factors for Phase-1B experiments

Parameter	**Units**	**Levels**
Depth of slot	mm	5
Tool diameter Dc	mm	12
Number of tool flutes Z	---	2
WP material (prepreg)	---	TORAY 3911/34%/UD134/T800SC-24K
WP configuration	---	Type-1 [25/50/25]

Table 3.16: Variable parameters and levels in Phase-1B experiments

Parameter / **Level**	**Cutting speed (m/min)**	**Feed rate (mm/tooth)**	**Tool material**	**Cutting environment**
1	200	0.03	DLC-coated WC	Dry
2	350	0.06	CTM-PCD	Twin-nozzle chilled air
3	500	0.10	CTB-PCD	
4	650	0.15	CMX-PCD	

A Taguchi fractional factorial experimental design involving 16 tests was specified consisting of 3 factors at 4 levels (tool material, cutting speed and feed rate) and 1 factor at 2 levels (cutting environment). This was selected as opposed to a full factorial (4^3*2^1 = 128 tests) in order to reduce the number of tests, but which would still allow statistically significant factors to be identified to a high level of confidence. Due to the relatively high number of factors and corresponding levels evaluated, a modified L16 orthogonal array (OA) had to be employed rather than the standard L16 OA shown in Table 3.17.

Table 3.17: Standard L16 orthogonal array [227]

	1	2	3	4	5	6	7	8	9	10	11	12	13	14	15
Run	**A**	**B**	**AB**	**C**	**AC**	**BC**	**ABC**	**D**	**AD**	**BD**	**ABD**	**CD**	**ACD**	**BCD**	**ABCD**
1	-1	-1	1	-1	1	1	-1	-1	1	1	-1	1	-1	-1	1
2	1	-1	-1	-1	-1	1	1	-1	-1	1	1	1	1	-1	-1
3	-1	1	-1	-1	1	-1	1	-1	1	-1	1	1	-1	1	-1
4	1	1	1	-1	-1	-1	-1	-1	-1	-1	-1	1	1	1	1
5	-1	-1	1	1	-1	-1	1	-1	1	1	-1	-1	1	1	-1
6	1	-1	-1	1	1	-1	-1	-1	-1	1	1	-1	-1	1	1
7	-1	1	-1	1	-1	1	-1	-1	1	-1	1	-1	1	-1	1
8	1	1	1	1	1	1	1	-1	-1	-1	-1	-1	-1	-1	-1
9	-1	-1	1	-1	1	1	-1	1	-1	-1	1	-1	1	1	-1
10	1	-1	-1	-1	-1	1	1	1	1	-1	-1	-1	-1	1	1
11	-1	1	-1	-1	1	-1	1	1	-1	1	-1	-1	1	-1	1
12	1	1	1	-1	-1	-1	-1	1	1	1	1	-1	-1	-1	-1
13	-1	-1	1	1	-1	-1	1	1	-1	-1	1	1	-1	-1	1
14	1	-1	-1	1	1	-1	-1	1	1	-1	-1	1	1	-1	-1
15	-1	1	-1	1	-1	1	-1	1	-1	1	-1	1	-1	1	-1
16	1	1	1	1	1	1	1	1	1	1	1	1	1	1	1

To statistically accommodate a four-level factor within a two level OA, three mutually interactive, two-level columns (for example columns 1, 2 and 3 in Table 3.17) were replaced with one four-level column, which provide the same information potential and maintained the orthogonality of the final modified orthogonal array [227], see Table 3.18. The merging of mutually interactive columns for the 4 factors meant that interactions between experiment factors could not be assessed. The final test array indicating the parameter levels for each experiment is shown in Table 3.19.

Table 3.18: Modified Taguchi L16 orthogonal array

	Cutting speed			Tool material			Feed rate			Cutting environment	
Run	A	B	Level	C	D	Level	AC	BD	Level	BC	Level
1	-1	-1	1*	-1	-1	1	1	1	4	1	2
2	1	-1	2	-1	-1	1	-1	1	3	1	2
3	-1	1	3	-1	-1	1	1	-1	2	-1	1
4	1	1	4	-1	-1	1	-1	-1	1	-1	1
5	-1	-1	1	1	-1	2	-1	1	3	-1	1
6	1	-1	2	1	-1	2	1	1	4	-1	1
7	-1	1	3	1	-1	2	-1	-1	1	1	2
8	1	1	4	1	-1	2	1	-1	2	1	2
9	-1	-1	1	-1	1	3	1	-1	2	1	2
10	1	-1	2	-1	1	3	-1	-1	1	1	2
11	-1	1	3	-1	1	3	1	1	4	-1	1
12	1	1	4	-1	1	3	-1	1	3	-1	1
13	-1	-1	1	1	1	4	-1	-1	1	-1	1
14	1	-1	2	1	1	4	1	-1	2	-1	1
15	-1	1	3	1	1	4	-1	1	3	1	2
16	1	1	4	1	1	4	1	1	4	1	2

* For factors levels: (-1 × -1 = 1), (1 × -1 = 2), (-1×1 =3) and (1×1 = 4)

Table 3.19: Fractional factorial test array for Phase-1B experiments

Test	Cutting speed (m/min)	Tool material	Feed rate (mm/tooth)	Cutting environment
1	200	DLC-coated WC	0.15	Twin nozzle chilled air
2	350	DLC-coated WC	0.10	Twin nozzle chilled air
3	500	DLC-coated WC	0.06	Dry
4	650	DLC-coated WC	0.03	Dry
5	200	CTM-302 PCD	0.10	Dry
6	350	CTM-302 PCD	0.15	Dry
7	500	CTM-302 PCD	0.03	Twin nozzle chilled air
8	650	CTM-302 PCD	0.06	Twin nozzle chilled air
9	200	CTB-010 PCD	0.06	Twin nozzle chilled air
10	350	CTB-010 PCD	0.03	Twin nozzle chilled air
11	500	CTB-010 PCD	0.15	Dry
12	650	CTB-010 PCD	0.10	Dry
13	200	CMX-850 PCD	0.03	Dry
14	350	CMX-850 PCD	0.06	Dry
15	500	CMX-850 PCD	0.10	Twin nozzle chilled air
16	650	CMX-850 PCD	0.15	Twin nozzle chilled air

Analysis of variance (ANOVA) was performed to identify significant factors affecting cutting forces, tool life and surface roughness (Ra, Rt, Sa) together with corresponding main effects plots produced using Minitab 15 software with the response values normalised at a flank wear of 0.1 mm. The percentage contribution ratio (PCR) of each factor was also calculated. A confirmation test was carried out using the preferred operating parameter levels based on the ANOVA results as shown in Table 3.20.

Table 3.20: Confirmation test parameters for Phase-1B

Test	Cutting speed (m/min)	Tool material	Feed rate (mm/tooth)	Cutting environment	WP Configuration
Confirmation	500	CTB-010 PCD	0.15	Twin nozzle Chilled air	Type-1

3.4.1.3 Phase-1C: Benchmarking of Element 6 PCD grades at preferred operating parameters

Using the preferred combination of cutting parameters identified based on results from Phase-1B, benchmarking trials were performed to evaluate the performance of alternative Element 6 PCD grades. Experiments were carried out at a fixed cutting speed and feed rate of 500 m/min and 0.15 mm/tooth respectively, under a chilled air environment as detailed in the experimental array shown in Table 3.21. Output measures included tool wear/life, cutting forces, surface roughness and workpiece delamination. The end of test criterion was a 0.3 mm flank wear or a 28,000 mm cut length.

Table 3.21: Test array to evaluate the performance of Element 6 PCD grades

Test	Cutting speed (m/min)	Tool material	Feed rate (mm/tooth)	Cutting environment	WP configuration
1	500	CTM-302 PCD	0.15	Twin-nozzle chilled air	Type-1
2		CMX-850 PCD			
3		WPC-102 PCD			

3.4.1.4 Phase-1D: Benchmarking of carbide tooling products

Based on results of the DLC coated WC routers in Phase-1B, trials were undertaken to benchmark the performance of DLC coated WC tools against uncoated and CVD diamond

(Dura) coated 2 fluted and burr type WC routers at a cutting speed of 200 m/min and feed rate of 0.03 mm/tooth, see Table 3.22. Tests aimed to identify wear types resulting from the slotting operation of CFRP composites. Response measures included tool wear/life, cutting forces and workpiece surface roughness. A tool life criterion of 0.3 mm flank wear or occurrence of fuzzing on down milling side were specified for the 2-fluted tools while a 0.3 mm flank wear or 28,000 mm cut length was selected in the case of burr type routers.

Table 3.22: Test array to evaluate the performance of different WC routers

Test	Cutting speed (m/min)	Tool material/configuration	Feed rate (mm/tooth)	Cutting environment	WP configuration
1	200	2-fluted DLC coated WC router	0.03	Twin nozzle chilled air	Type-1
2		2-fluted Dura coated WC router			
3		2-fluted Uncoated WC router			
4		Uncoated WC burr type router			
5		Dura coated WC burr type router			

3.4.2 Phase-2 Effect of workpiece material lay-up configuration

The overall aim of Phase-2 experiments was to determine the effect of varying workpiece configuration on the machinability of CFRP. More specifically, the objectives of the work relate to investigating the influence of laminate/ply orientation on machined surface quality (surface roughness, delamination etc.), cutting forces and tool life/wear, tool temperature and to determine best parameters for each laminate configuration/orientation tested.

3.4.2.1 Phase-2A: Preliminary testing and temperature measurement

A series of tests were carried out to evaluate the effect of fibre orientation at 0°, 45°, 90° and 135° (all plies in single direction) as well as the three workpiece material configurations; Type-1, Type-2, and Type-3. A single slot was machined for each experiment with the cutting forces and surface roughness recorded. The trials were performed using a partially worn 2-

fluted ITC-PCD router (flank wear less than 0.1 mm). Similarly, the effect of workpiece configuration on cutting forces and temperature were also investigated using semi-worn (flank wear of ~ 0.1 mm) 3-fluted Exactaform PCD routers (Up-cut, Neutral and Down-cut). The test array is detailed in Table 3.23.

Table 3.23: Test array to evaluate the effect of workpiece configuration

Test	Cutting speed (m/min)	Tool material	Feed rate (mm/tooth)	Cutting environment	WP configuration
1	200	ITC-PCD Exactaform Up-cut Exactaform Neutral Exactaform Down-cut	0.03	Twin-nozzle chilled air	0˚
2					45˚
3					90˚
4					135˚
5					Type-1
6					Type-2
7					Type-3

The influence of cutting environment (single-nozzle and twin-nozzle chilled air as well as dry) on cutting temperature was assessed using Exactaform Neutral and Down-Cut PCD routers when machining Type-3 CFRP workpieces. Initial trials involved a slotting operation over a distance of 100 mm; see Table 3.24, while a further 3 tests were undertaken under an edge routing configuration over 5000 mm at 3/4 engagement of the tool, see Table 3.24.

Table 3.24: Test matrix to evaluate the effect of cutting environment on cutting temperature during slotting operation

Test	Cutting speed (m/min)	Tool material	Feed rate (mm/tooth)	Cutting environment	WP configuration
1	200	Exactaform Neutral	0.03	Dry	Type-3
2				Single-nozzle chilled air	
3				Twin-nozzle chilled air	
4		Exactaform Down cut		Dry	
5				Single-nozzle chilled air	
6				Twin-nozzle chilled air	

Table 3.25: Test matrix to evaluate the effect of cutting environment on cutting temperature during a continuous edge routing operation

Test	Cutting speed (m/min)	Tool material	Feed rate (mm/tooth)	Cutting environment	WP configuration
1	200	Exactaform Neutral	0.03	Dry	Type-3
2				Single-nozzle chilled air	
3				Twin-nozzle chilled air	

3.4.2.2 Phase-2B: Effect of workpiece material lay-up configuration

Phase-2B involved mainstream testing to evaluate the effect of CFRP lay-up configuration with variable operating parameters and tool material selected based on results from Phase-1B. All tests were performed under a chilled air environment delivered through a single-nozzle based on results from Phase-2A. Table 3.26 and Table 3.27 details the fixed factors and variable parameters utilised respectively. A full factorial design was employed involving 12 tests (see Table 3.28), which resulted from the combination of 2 factors at 2 levels (cutting speed and feed rate) and one factor at 3 levels (workpiece material).

Table 3.26: Fixed factors for Phase-2B experiments

Parameter	Units	Levels
Depth of slot/cut per pass	mm	5
Tool material	---	CTB-010 PCD
Tool diameter, Dc	mm	12
Number of flutes, Z	---	2
Cutting environment	---	Single-nozzle chilled air
WP material (prepreg)	---	TORAY 3911/34%/UD134/T800SC-24K

Table 3.27: Variable parameters and levels for Phase-2B experiments

Parameter / Level	Cutting speed (m/min)	Feed rate (mm/tooth)	WP configuration
1	350	0.10	Type-1
2	500	0.15	Type-2
3			Type-3

Table 3.28: Full factorial test matrix for Phase-2B experiments

Test	Cutting peed (m/min)	Feed rates (mm/tooth)	Material configuration
1	350	0.1	Type-1
2	350	0.1	Type-2
3	350	0.1	Type-3
4	350	0.15	Type-1
5	350	0.15	Type-2
6	350	0.15	Type-3
7	500	0.1	Type-1
8	500	0.1	Type-2
9	500	0.1	Type-3
10	500	0.15	Type-1
11	500	0.15	Type-2
12	500	0.15	Type-3

3.4.2.3 Phase-2C Effect of cutting environment

Results from Test 11 and confirmation trial in Phase-1B as well as Test 10 in Phase-2B were compared in order to investigate the influence of cutting environment. All three tests involved the CTB-010 PCD router, which were performed using Type-1 CFRP material configuration. Response measures included cutting forces, tool wear/life, surface roughness, and delamination factor. A summary of the test parameters used are detailed in Table 3.29.

Table 3.29: Test matrix to evaluate effect of cutting environment

Test	Cutting speed (m/min)	Tool material	Feed rate (mm/tooth)	Cutting environment	WP configuration
1*	500	CTB-010 PCD	0.15	Dry	Type-1
2**				Twin-nozzle chilled air	
3***				Single-nozzle chilled air	

*Phase-1B: Test-11
**Phase-1B: Confirmation test
***Phase-2B: Test-10

3.4.3 Phase-3: Effect of varying tool geometry

The overall aim of Phase-3 experiments was to determine the effect of varying tool geometry on the machinability of CFRP, with all tests undertaken using PCD routers. Variables assessed included the influence of different helix and secondary relief angles on machined surface quality (surface roughness, delamination), cutting forces, temperature and tool life/wear when slotting CFRP workpieces having Type-1 lay-up configuration.

3.4.3.1 Phase-3A: Influence of router helix angle

The effect of tool helix angle on cutting temperature was investigated using Exactaform Up-Cut, Neutral and Down-Cut PCD routers when machining CFRP at a cutting speed and feed rate of 200 m/min and 0.03 mm/tooth respectively. A tool life criteria of 28,000 mm cut length or 0.1 mm maximum flank wear was employed with the test matrix detailed in Table 3.30.

Table 3.30: Effect of helix angle on cutting temperature

Test	Cutting speed (m/min)	Tool helix angle	Feed rate (mm/tooth)	Cutting environment	WP configuration
1	200	Exactaform Up-cut (+ 3°)	0.03	Twin nozzle chilled air	Type-1
2		Exactaform Neutral (0°)			
3		Exactaform Down-cut (- 3°)			

3.4.3.2 Phase-3B: Effect of secondary relief angle

The influence of a secondary clearance angle on tool life, cutting forces and surface quality/roughness when slotting CFRP was evaluated. The Mega Diamond (similar to CTB-010) and CMX-850 PCD grades were employed, with results compared against those from trials in Phase-1B and Phase-1C respectively. The tests were performed at fixed operating parameters of 500 m/min cutting speed and 0.15 mm/tooth feed rate under a twin-nozzle chilled air environment based on results from Phase-1B. The end of test criterion was a flank wear of 0.3 mm or 28,000 mm cut length. Details of the tools and test parameters used are detailed in Table 3.31.

Table 3.31: Test matrix to evaluate the effect of secondary relief angle

Test	**Cutting speed (m/min)**	**Tool material (PCD)**	**Relief angle**		**Feed rate (mm/tooth)**	**Cutting environment**	**WP**
			Primary	**Secondary**			
1*	200	CTB-010	18˚	-	0.15	Twin nozzle chilled air	Type-1
2		Mega-diamond	10˚	18˚			
3**		CMX-850	18˚	-			
4		CMX-850	10˚	18˚			

*Used in Phase-1B: Confirmation test
** Used in Phase-1C: Benchmarking test

3.5 Cutting strategy

Two different machining strategies were employed during the experiments involving slotting or edge routing at ¾ engagement of the tool diameter. The latter was generally performed during tool life testing in a raster operation (alternating between up and down milling) in order to conserve workpiece material. The use of 3/4 engagement was preferred over the full-engagement in order to make the available test panels sufficient for the planned tests. In addition, compared to ½ engagements, it also allowed a closer machining scenario to slotting operation. A schematic illustrating the slotting and ¾ engagement cutting strategy is shown in Figure 3.24. The CNC code for both the full (slotting) and ¾ engagement is found in Appendix D together with the modified CNC code to enable continuous machining. In addition, tool run-out was measured using a dial gauge prior to the start of each test and did not exceed 10µm.

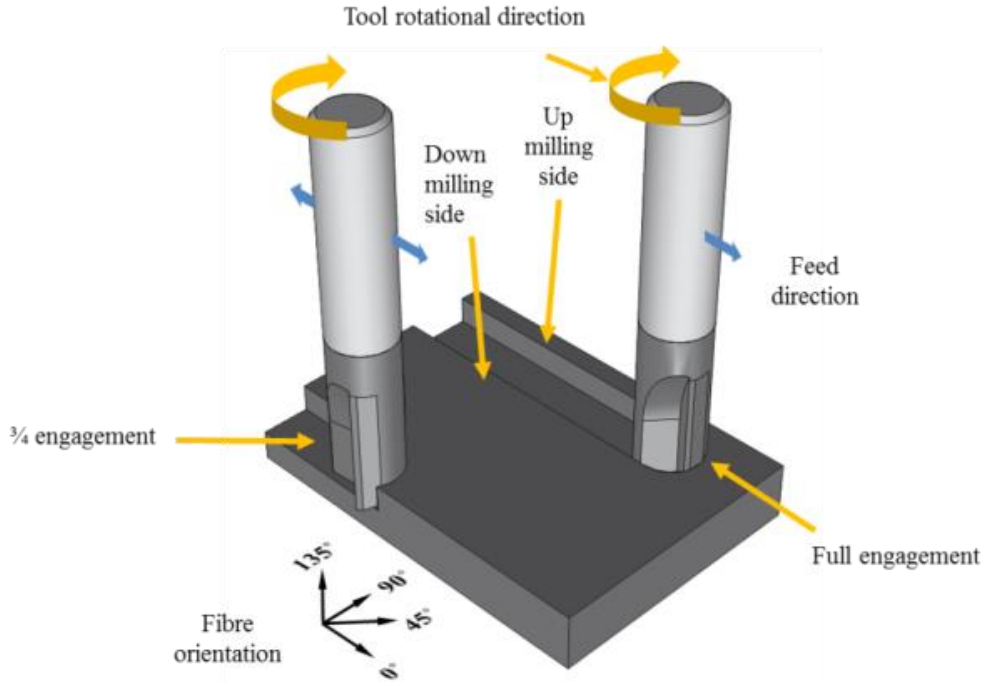

Figure 3.24: Full and ¾ engagement of router

3.6 Summary of experimental work

This chapter presented the details of workpiece material used in the experimental work and how it was fabricated. It also covered the three main workpiece lay-up configurations used by Airbus for the wing applications that are under investigation in terms of machinability. Cutting tools from SECO (WC and PCD grades) and grades from other manufacturers were detailed and assigned to different phases of experiments. The experimental tests were divided into three main phases and related sub-phases. Test arrays including Taguchi's orthogonal arrays in Phase-1 and full factorial experiments were detailed showing the parameters used in every individual test and the anticipated output responses were also listed. All test equipment and measuring instruments during and after machining were discussed and illustrated and finally a procedure for running the experiments was detailed.

4.1 Phase-1A: Preliminary work

When machining using the ITC PCD router at the lowest cutting speed and feed rate combination of 200 m/min and 0.03 mm/tooth respectively, flank wear was minimal (~0.038 mm) even after 1860 mm cut length, see Figure 4.1, with negligible fuzzing on the workpiece. Matrix residue marks however were visible on the tool rake face, due to the accumulation of melted CFRP resin, as a result of temperatures generated during machining. No signs of crater wear were detected, which is generally rare when milling CFRP as flank wear is usually the dominant form [148, 175].

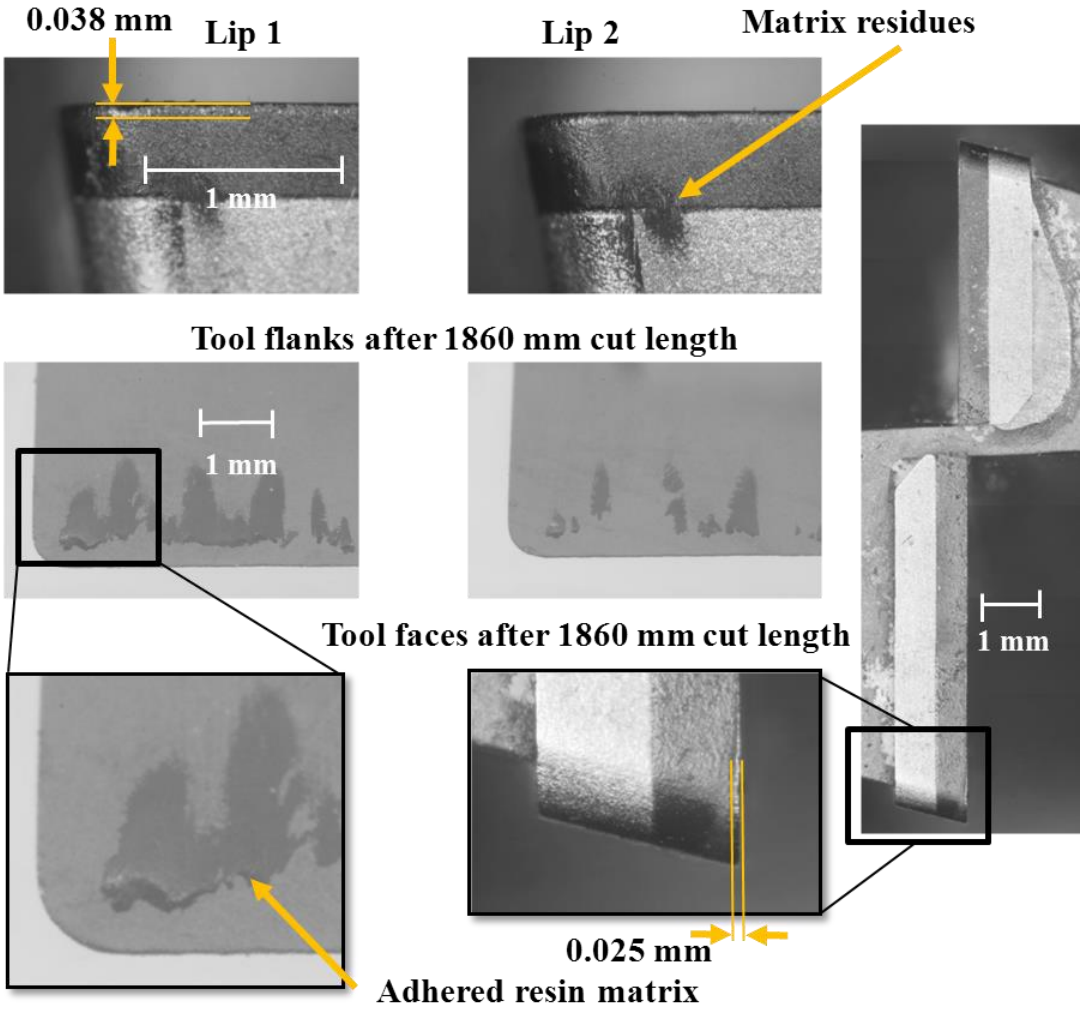

Figure 4.1: Tool wear and matrix residues on ITC-PCD router

All three force components were observed to increase with cutting speed and feed rate, with mean values for the cutting and feed forces in the region of 300 N, see Figure 4.2. This was higher by a factor of 10 compared to results on edge-trimming of CFRP reported by Ucar and Wang [161]. The results can be attributed to the smaller radial depth of cut/stepover employed for edge-trimming (9% of tool diameter) compared to slotting (100% of tool diameter).

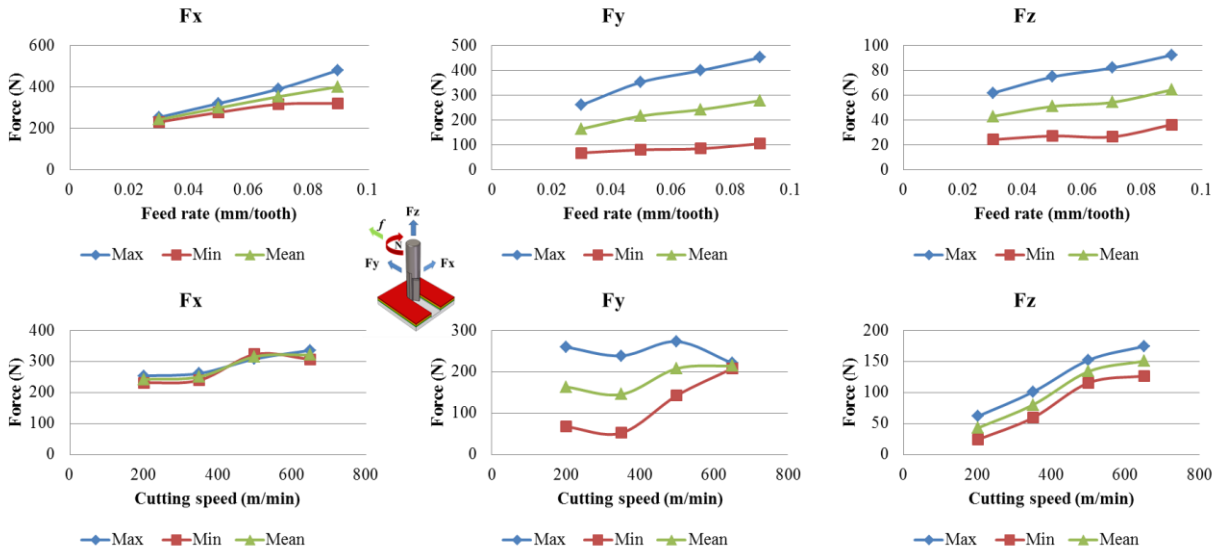

Figure 4.2: The effect of feed rate and cutting speed on force components (Fx, Fy, Fz)

The machined surfaces produced at different test conditions are shown in Figure 4.3. The area surface roughness parameter (Sa) generally varied between 6-10 µm over the range of operating parameters employed. The 3D surface topography of the surfaces generated with respect to variation in cutting speed and feed rate are shown in Figure 4.4 and Figure 4.5 respectively. Damage was most severe on the 45° direction ply with signs of material pull out irrespective of cutting speed or feed rate. Figure 4.6(a) shows that the surface roughness parameter Sa initially increased with cutting speed but subsequently reduced at higher cutting speeds (> 350 m/min), possibly due to melting of the resin matrix. In contrast, surface roughness was found to decrease as feed rate increased from 0.03 to 0.06 mm/tooth but y increased subsequently at elevated feed rate levels, see Figure 4.6(b), which was likely due to greater damage on the workpiece surface.

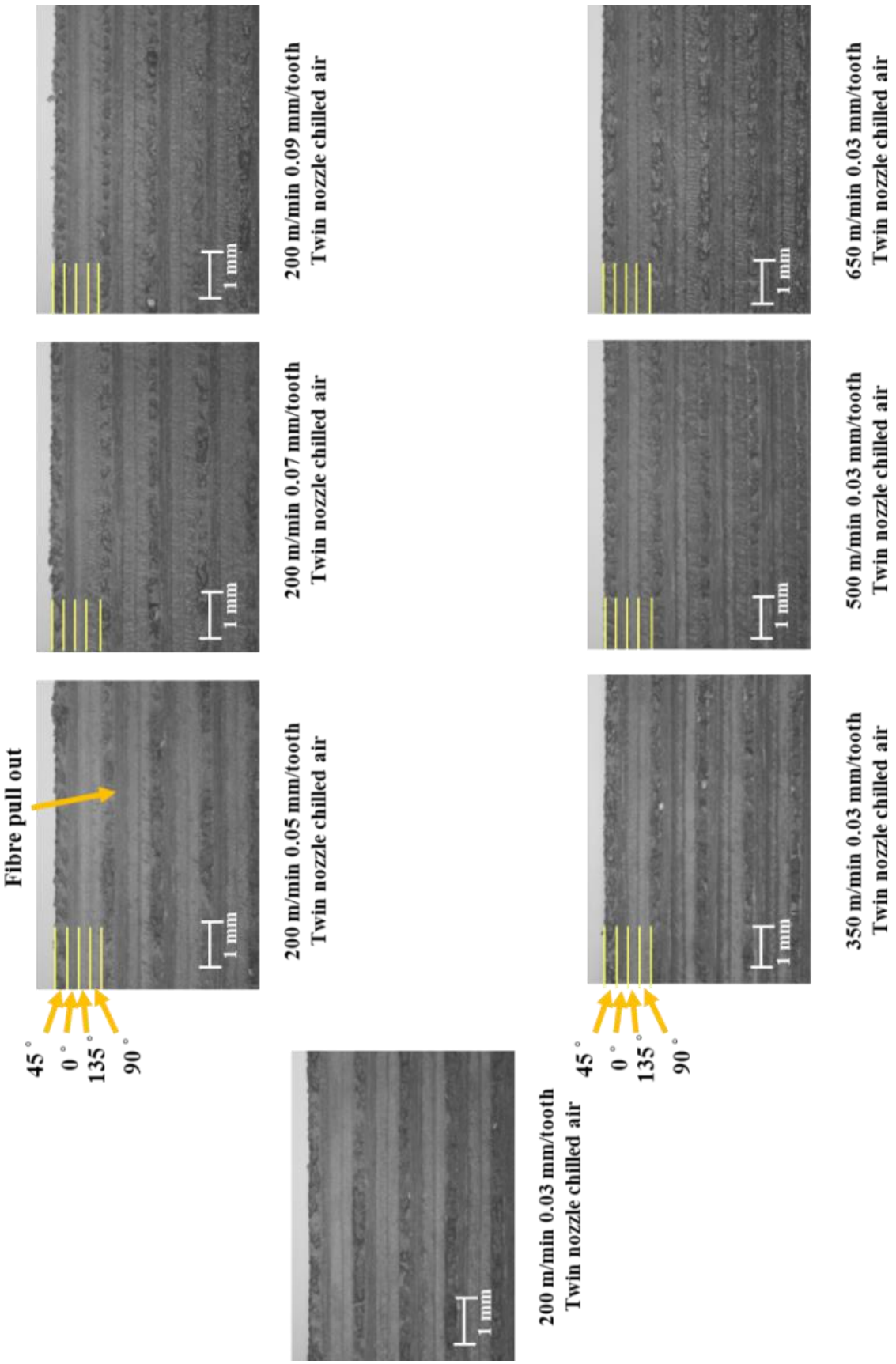

Figure 4.3: Machined CFRP surface at different cutting parameters

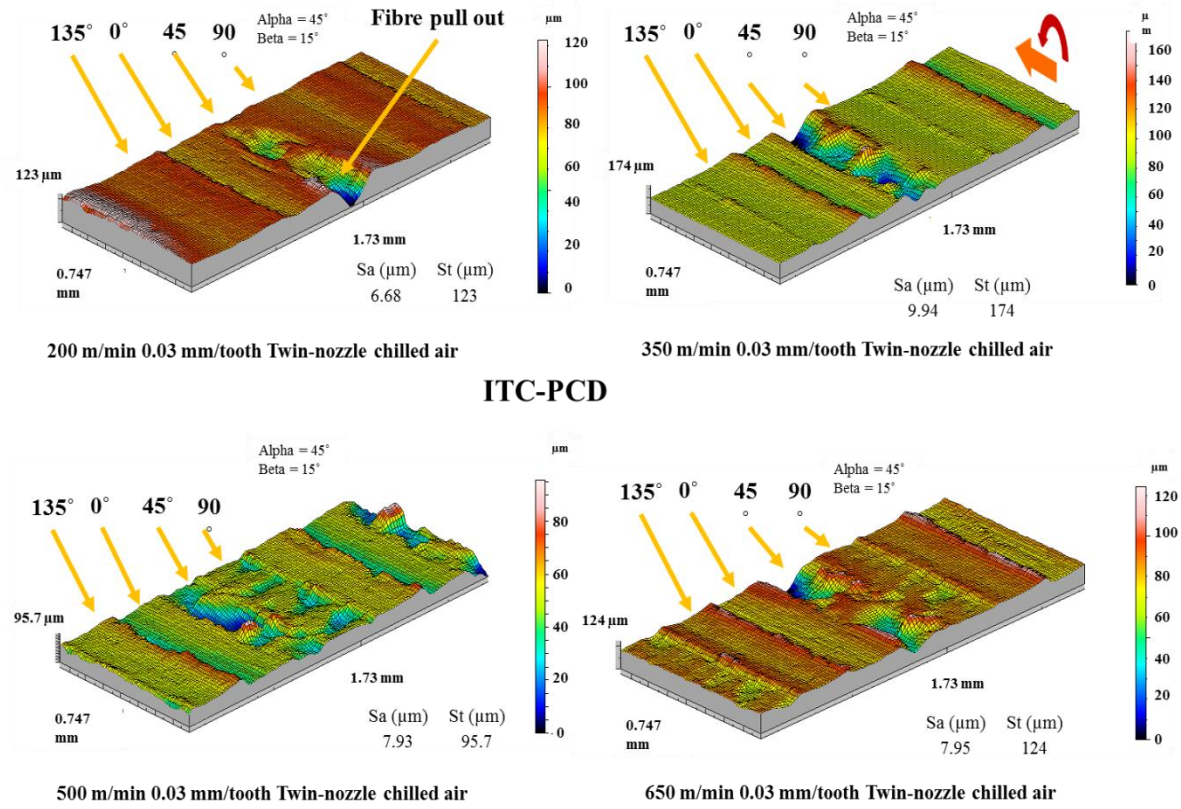

Figure 4.4: 3D surface topography and roughness parameters using different cutting speeds

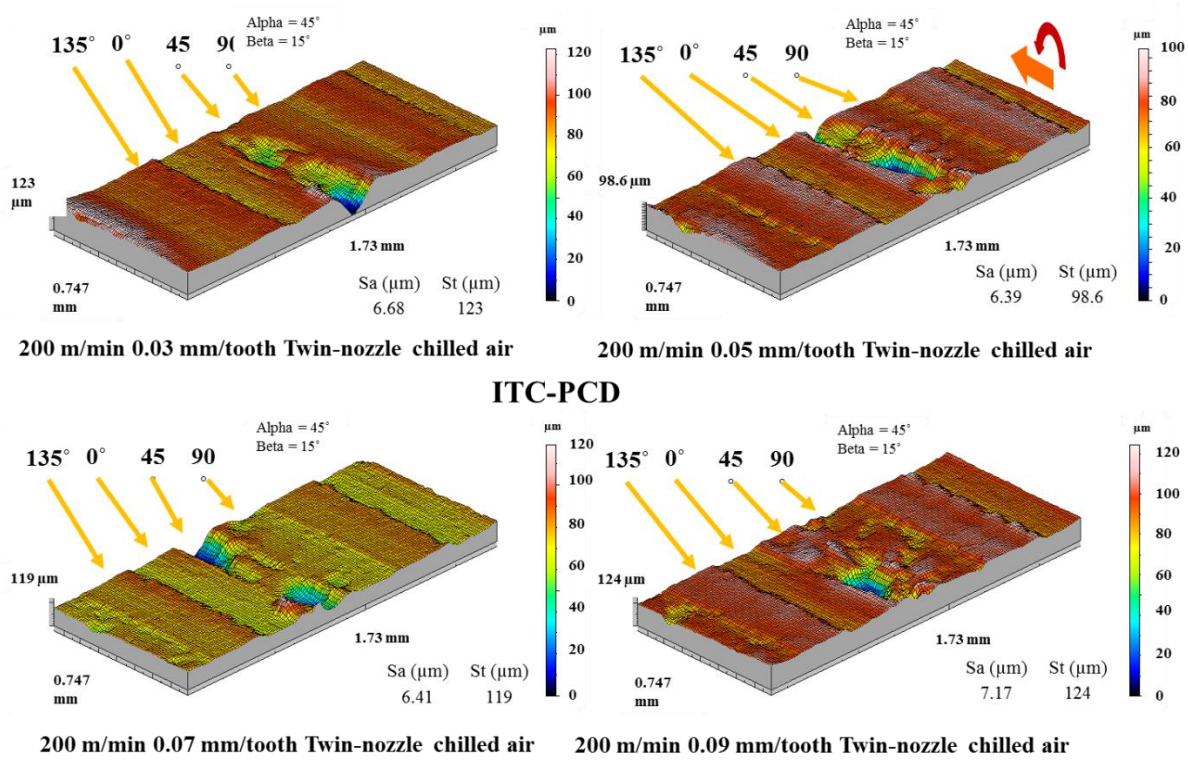

Figure 4.5: 3D surface topography and roughness parameters using different feed rates

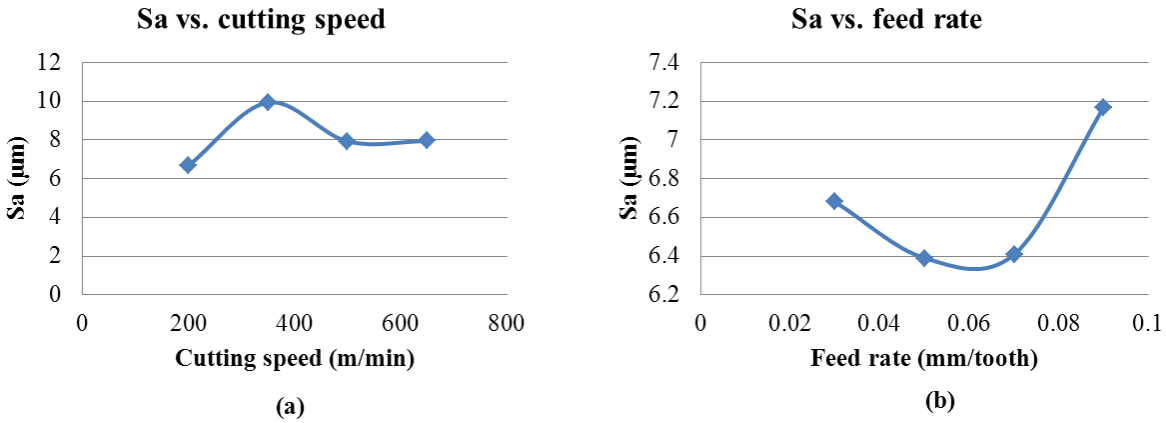

Figure 4.6: 3D surface roughness parameter Sa (µm) vs. cutting speed and feed rate

Figure 4.7 details the influence of cutting speed and feed rate on temperature when machining with the Exactaform routers (Neutral and Down-cut geometries). In general, temperature increased with cutting speed but decreased at higher feed rates due to the reduced tool-workpiece contact time. Similarly, larger slot depths (axial depth of cut) resulted in an approximately linear increase in cutting temperatures from ~ 70°C (at 1 mm depth of cut) to 170°C (at 3 mm depth of cut) due to the greater area of tool-workpiece contact.

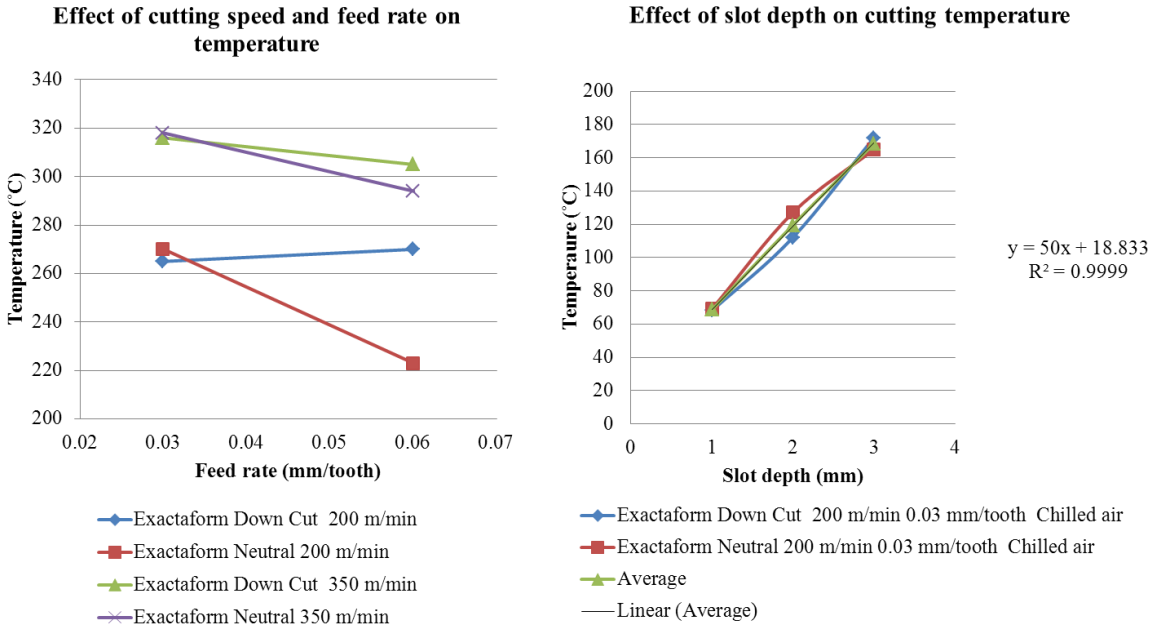

Figure 4.7: Cutting temperature at different cutting parameters.

4.2 Phase-1B: Influence of operating conditions and tool materials

4.2.1 Tool life (cut length)

The tool wear progression against cut length for each test is shown in Figure 4.8. Typically, the abrasive carbon fibres cause 'shedding' of the tool particles resulting in attrition wear [47, 48]. The tool life of the PCD routers were significantly higher in comparison to WC, which was also reported by Klocke and Wurtz [156]. The cut lengths obtained at 0.1 mm flank wear for all tests are shown in Figure 4.9.

The main effects plot for tool life is shown in Figure 4.10. None of the factors was statistically significant with respect to cut length. The trends indicated that mean tool life decreased at the lowest and highest cutting speed level (200 and 650 m/min), which was likely due to the larger uncut chip thickness which is equal to feed/tooth (causing chipping of the CTM-302 PCD tool) and increased abrasion of the cutting edge respectively.

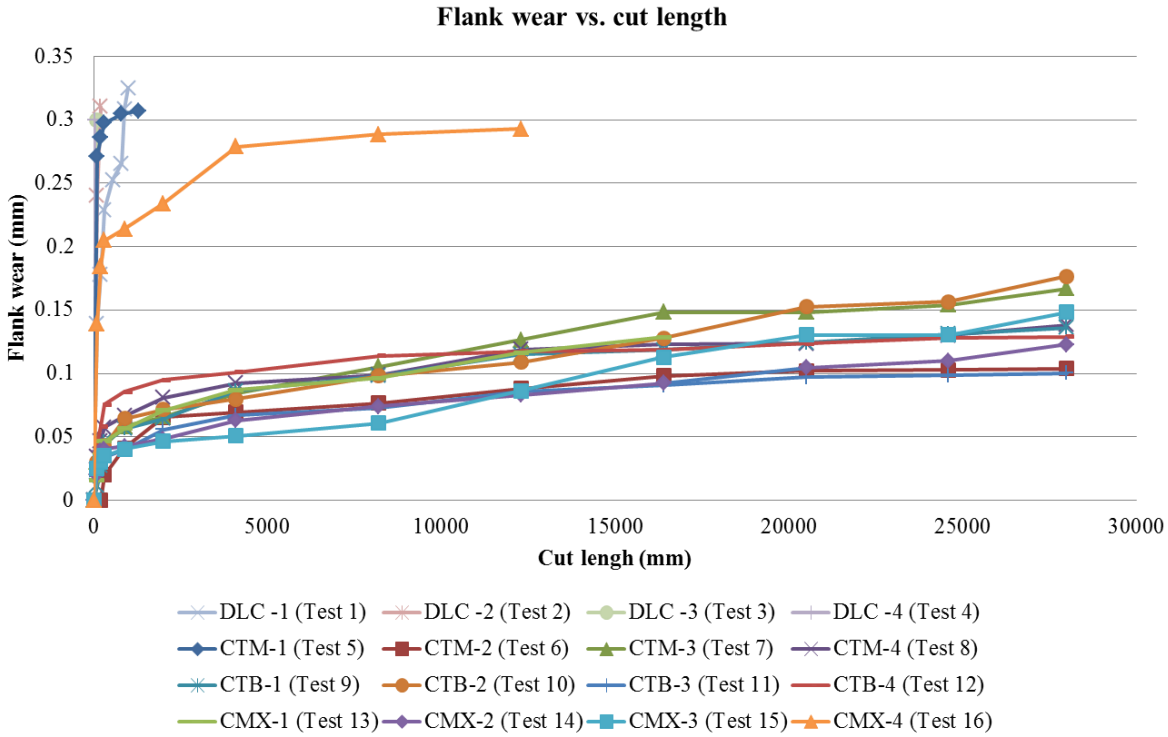

Figure 4.8: Tool wear vs. cut length (all tests)

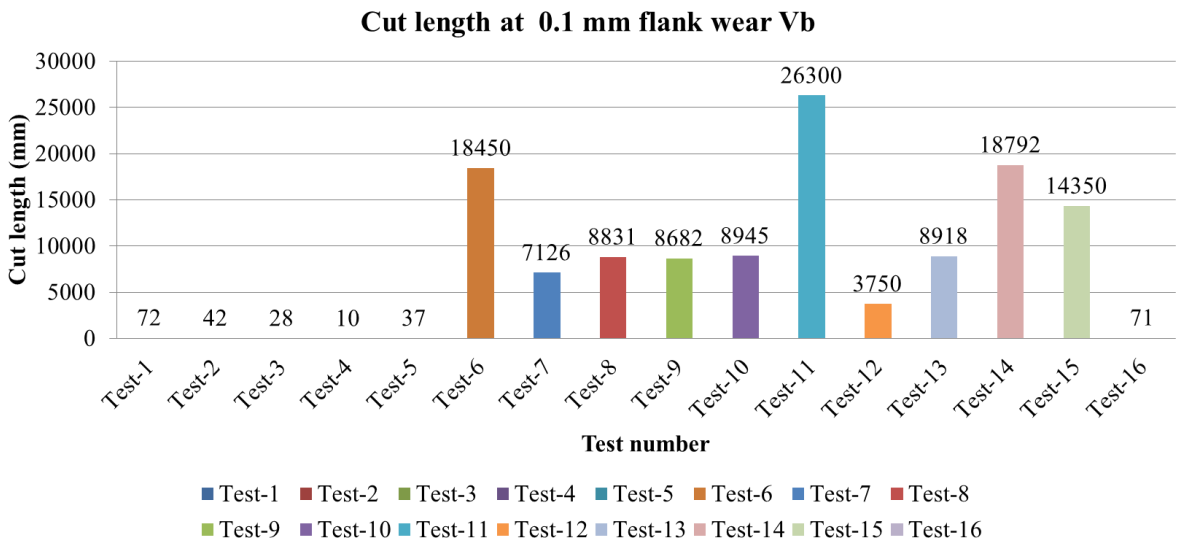

Figure 4.9: Cut length at 0.1 mm flank wear

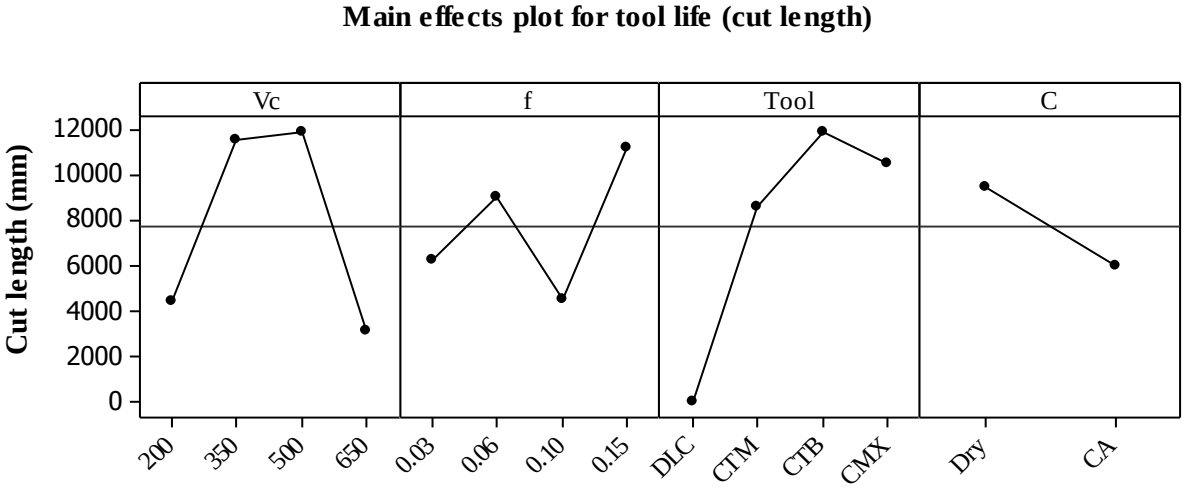

Figure 4.10: Main effects plot for tool life

The ANOVA calculations and percentage contribution ratio of the different factors are shown in Table 4.1. An error level of 70% was observed, which was possibly due to interactions between the factors that was not considered due to the limitations of the fractional factorial experimental design employed. Such high error percentage suggests that the modified orthogonal array used (with no interactions) was not the optimal and that a different experimental design should be employed (full factorial for example) which considers a more comprehensive number of factors and levels.

Table 4.1: ANOVA table for tool life

Source	DOF	Seq SS	Adj MS	F calc.	F tab.	P	PCR (%)
Vc	3	256797325	85599108	1.72	5.41	0.277	10.76
f	3	105456085	35152028	0.71	5.41	0.588	0
Tool	3	341381533	113793844	2.29	5.41	0.196	19.20
C	1	49574815	49574815	1	6.61	0.364	0
Residual error	5	248440946	49688189				70.08
Total	15	1001650705					

Tool wear doubled when cutting speed increased in Test-2 compared to Test-1 from 0.12 mm to 0.24 mm VB possibly due to the higher cutting speed which had larger effect (higher PCR) on tool wear despite the decrease in feed rate from 0.15 mm/tooth to 0.1 mm/tooth.

Regardless of the cutting conditions, DLC coated WC generally suffered from severe wear in the form of coating loss and exposed substrate, while the tool was serrated due to the varying fibre orientation. At high tool feed rates, signs of plastic deformation was prominent. The amount of tool wear was highest at the point of maximum axial depth of cut or corners. Using WC tools some signs of plastic deformation possibly due to high forces resulting from high feed rate were also visible, (see Figure 4.11) where the effect of high cutting speed in Test-4 was prominent. Coating was removed by abrasion which indicates enhanced adhesion. An EDX analysis of the worn surface also showed that the carbon layer was completely removed from the worn area. Using CMX-850 PCD, the high cutting speed and feed rate (Test-16) caused fracture of the router at 0.290 mm flank wear and 12300 mm cut length.

The severe tool wear associated with DLC-coated WC tools resulted in the extremely short tool life of no more than 900 mm cut length at 0.308 mm flank wear in Test-2. Tools suffered from abrasion tracks and serrated cutting edges due to the different ply orientation. Similar serration in edge were noted by Davim [228].

The CTM-302 grade showed the least resistance to chipping especially at high feed rate (Test-5) possibly due to the large grain structure and high mechanical load although it has the highest abrasion resistance, see Figure 4.12. Large chunks of cutting edge were fractured at equi-spaced points of the type CH1 mode according to ISO standard [145] which looked like the serrated tool in DLC-coated tool despite the different wear mechanism. Tool life was dictated by chipping which reached the tool life criteria of 0.3 mm (~900 mm cut length)

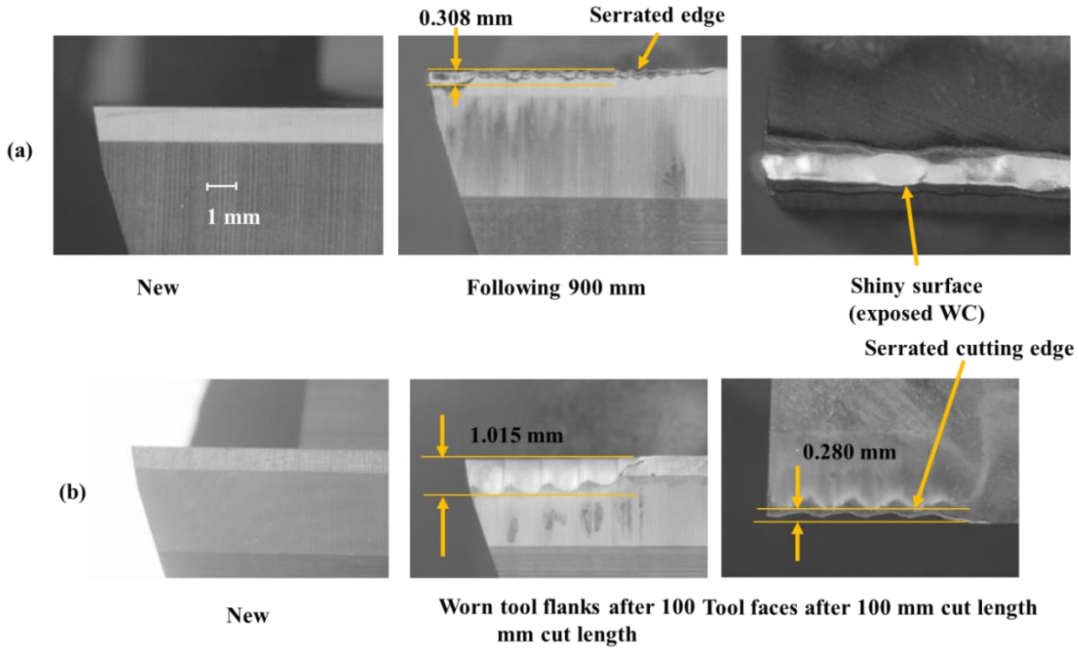

Figure 4.11: (a) worn edge Test-1 (b) worn edge Test-4

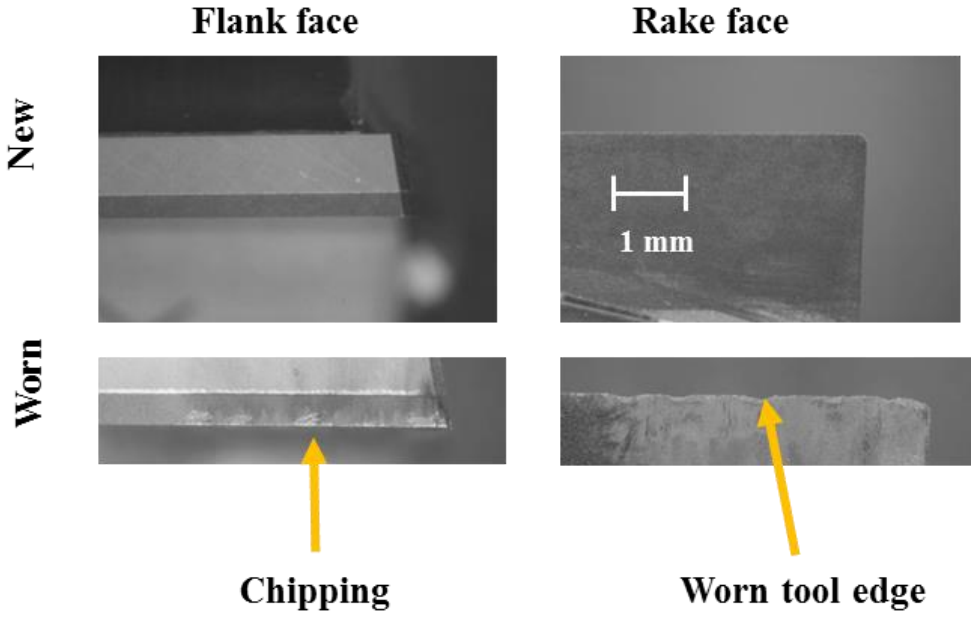

Figure 4.12: Chipping in CTM-302 PCD (Test-5)

Tool material had the highest PCR (19.2%). Significant improvement, using PCD compared to DLC-coated WC (up to 95 times), was achieved. CTB-010 PCD achieved the best tool life, on average, possibly due to the balanced mechanical/thermal properties. Despite the good properties of the CMX-850 PCD it comes second due to the relatively low abrasion

resistance of the small grain size PCD. The thermal cycling and fatigue could be a reason that the tool life was slightly lower as noted by Rahman et al. [203].

The CTB-010 in general was capable of cutting without fuzzing on down milling side at high cutting speed/feed rate combination with only the signs of abrasion wear and the least amount of tool wear was achieved using cutting speed 500 m/min, feed rate of 0.15 mm/tooth and in dry conditions (Test-11), see Figure 4.13. The performance may improve if chilled air is used. The CTB grade had a good balance of physical/mechanical properties (i.e. compared to the rest of the grades used) such that having medium (cobalt content, diamond area, transverse rapture strength (TRS), fracture toughness) and the highest elastic modulus which made it a better choice for applications where the tool is subjected to cyclic loading. It had also better thermal properties than the CMX-850 PCD grade. The CMX-850 grade was also suitable for the process at high cutting speed and high feed rate (Test-15) but it came second after CTB-010. At extreme condition (650 m/min cutting speed and 0.15 mm/tooth feed rate) the tool fractured (Test-16).

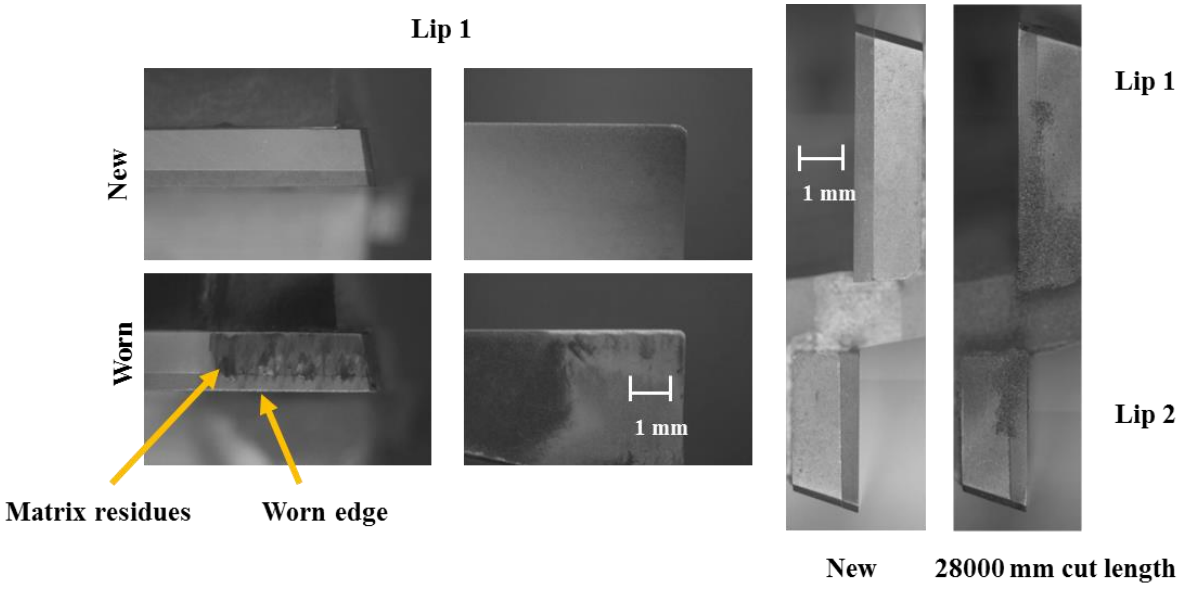

Figure 4.13: Worn CTB-010 following 28,000 mm cut length (Test-11)

Although statistically insignificant, the use of chilled air was found to be crucial for chip evacuation and preventing rubbing against CFRP dust like chips. The CFRP dust caused severe a rise in temperature which in turn accelerated tool wear and promoted burning. The burning of dust lead to matrix degradation and surface deterioration and was a potential health/fire hazard.

4.2.1 Cutting forces

The maximum cutting force Fx was in the range of 150.76 N using CMX-850 PCD at low cutting speed and low feed rate (Test-13) to 1032 N (Fx) using DLC-coated WC at high cutting speed and low feed rate (Test-3) due to tool wear. Figure 4.14 shows an example of the increase in the cutting forces with the length of cut. The cutting forces Fx and Fy at 0.1 mm flank wear are shown in Figure 4.15.

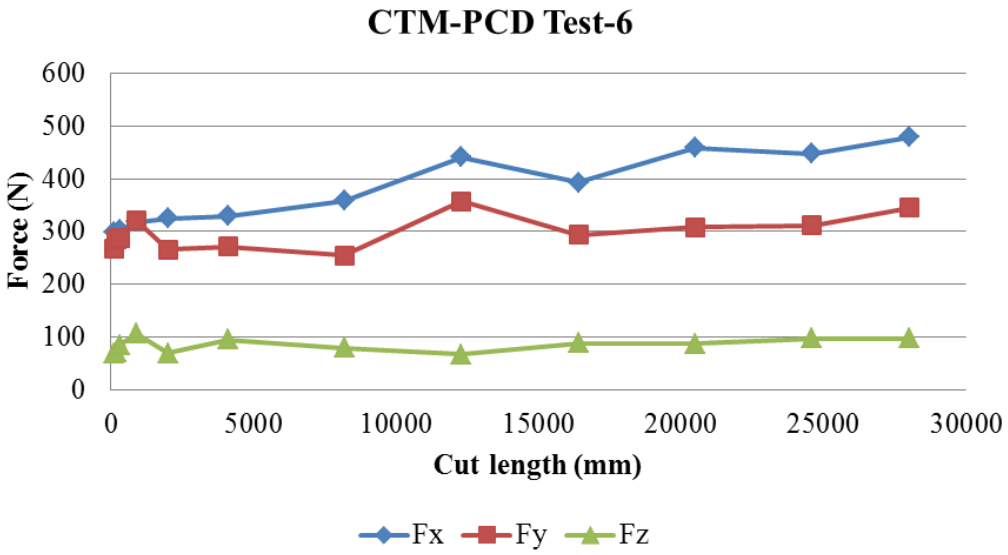

Figure 4.14: Cutting force components against cut length (Test-6)

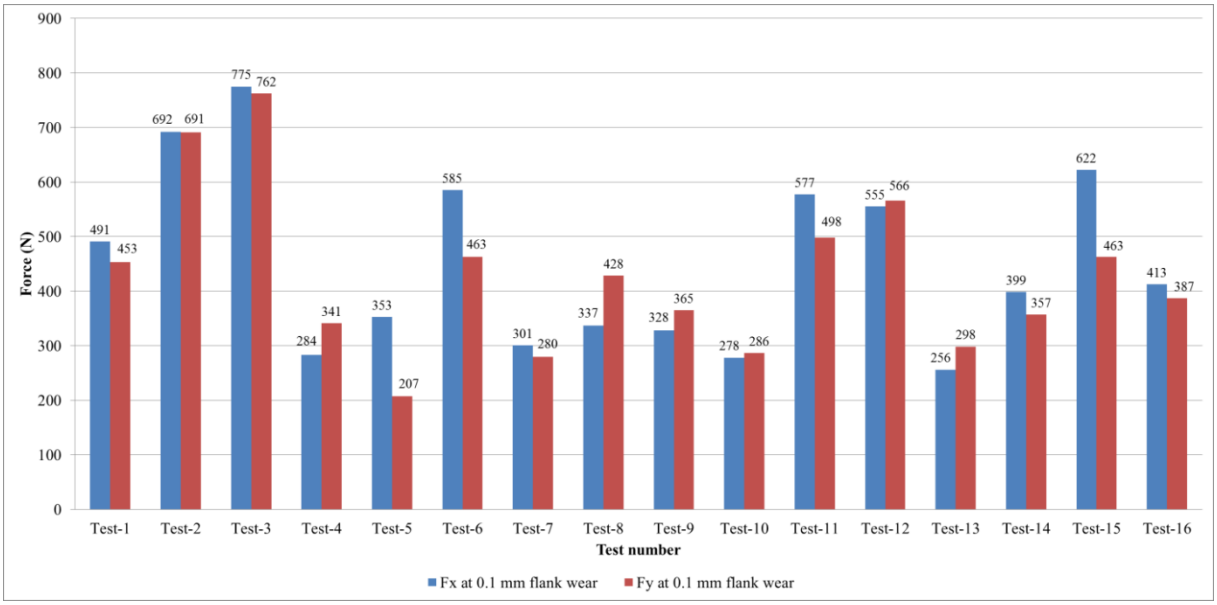

Figure 4.15: Cutting forces at 0.1 mm flank wear

The maximum cutting force Fx represents the actual cutting force at the point of maximum chip thickness. The main effects plot for the cutting force component (Fx) is shown in Figure 4.16. The cutting forces increased with cutting speed up to a critical point where the thermal softening of matrix took place which might have contributed to lowering the cutting force as noted by Wang et al. [88]. The low mean force at high speed can be explained by the early premature failure of tool at such high cutting speed (due to high abrasion and high temperature). Feed rate caused some increase in the mean cutting forces. Similarly, when cutting under the extreme condition (highest feed rate), the mean forces were lower due to the effect of feed rate on tool life (i.e. premature chipping).

DLC-coated WC tools were obviously responsible for the highest cutting forces due to the severe rounding of the cutting edge and loss of its sharpness (twice as large compared to PCD tools). Low cutting forces using CTM-PCD could be attributed to the high abrasion resistance of the large grained PCD.

The low mean forces also can be related to chipping of the cutting edge at low speed/high combination as in (Test-5). The relatively high wear resistance and hence the extended tool life of CTB-PCD and CMX-850 PCD raised the mean forces over the forces obtained by CTM-302 PCD tools. The CMX-850 PCD was lower in forces (Fx) compared to CTB-PCD possibly due to the sharper cutting edge and inherent smooth surface of the fine grained PCD which reduced the coefficient of friction.

The percentage of different factors affecting the cutting force (Fx) shown in ANOVA analysis for cutting force Fx are shown in Table 4.2. Feed rate was the most significant factor affecting Fx. This is because of the fact that in slotting operation, the maximum chip thickness is equal to the feed rate per tooth in such a case. Percentage contributions were 38 % for feed rate, 20.92 % for cutting speed while the tool was responsible for 10 %. This agrees with findings of Hocheng et al. [139].

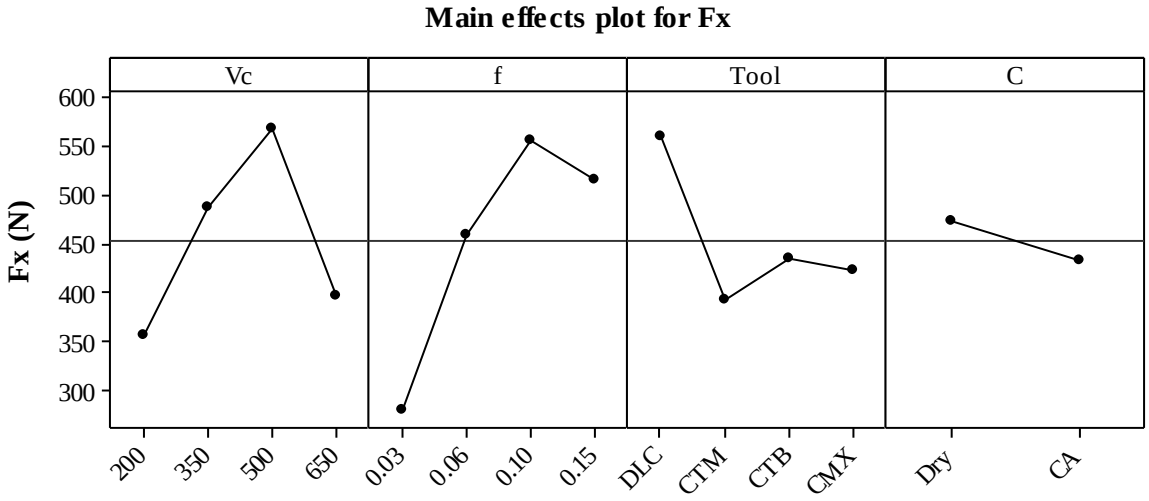

Figure 4.16: Main effects plot for cutting force (Fx)

Table 4.2: ANOVA analysis for cutting force Fx

Source	DOF	Seq SS	Adj MS	F calc.	F tab.	P	PCR (%)
Vc	3	108031	36010	4.41	5.41	0.072	20.92
f	3	178673	59558	7.3	5.41	0.028	38.62*
Tool	3	65233	21744	2.66	5.41	0.159	10.20
C	1	6494	6494	0.8	6.61	0.413	0.00
Residual error	5	40820	8164				30.25
Total	15	399250					

*significant at the 5% level

In case of the feed force Fy, none of the factors was significant. It can be seen that increasing cutting speed resulted in increased tool wear. Further increase in cutting speed reduced the feed force possibly because of either temperature effect (softening of matrix) or premature tool wear at such high speeds. The effect of feed rate was quite similar, the lowest feed rate force was using CTM-302 PCD because of its low chipping resistance promoting early chipping which reduced the mean forces for such tool. The low wear resistance and the severe tool wear exhibited by the DLC coated WC contributed to the high feed force as shown in the main effects plot. CTB-010 PCD was in general around the average. Although there is no difference in abrasion resistance between CTB-010 and CMX-850 PCD grades, the sharp and smooth CMX-850 resulted in lower feed forces. The percentage contribution of tool material was the highest (19.75% PCR) while negligible contribution was made by the chilled air environment at a high error percentage due to many factors discussed earlier, see Table 4.3.

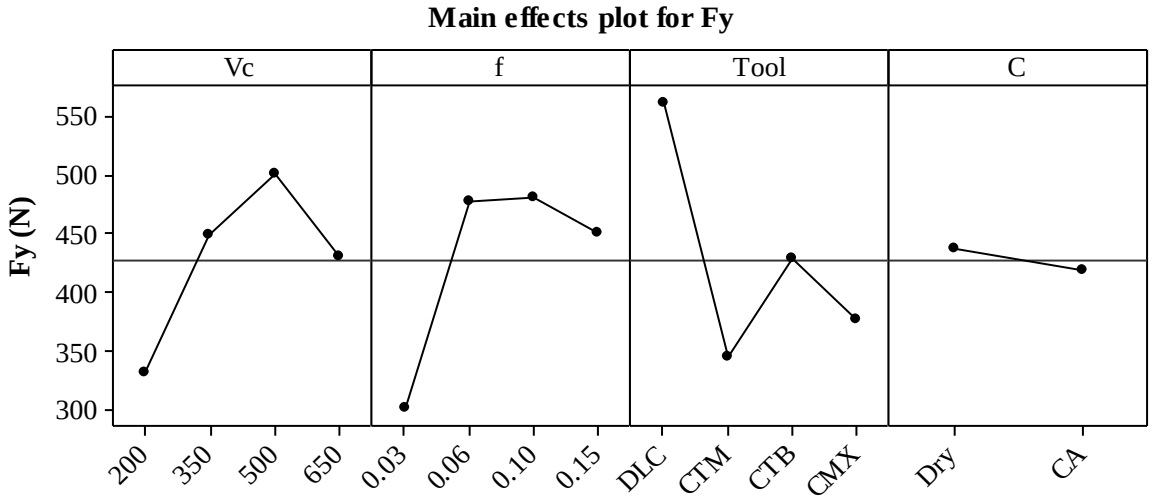

Figure 4.17: Main Effects plot for Fy

Table 4.3: ANOVA analysis for cutting force Fy

Source	DOF	Seq SS	Adj MS	F calc.	F tab.	P	PCR (%)
Vc	3	60863	20288	1.37	5.41	0.352	4.96
f	3	87699	29233	1.98	5.41	0.235	13.00
Tool	3	110233	36744	2.49	5.41	0.175	19.75
C	1	1208	1208	0.08	6.61	0.786	0.00
Residual error	5	73817	14763				62.28
Total	15	333820					

The feed force (Fy) increased with feed rate and was also between 130.33 N (Test-13) using PCD and 1301.88N using DLC-coated WC (Test-4). Using DLC-coated at high cutting speed and low feed rate resulted in feed force 10 times higher than PCD owing to the severe rounding of the cutting edge. The cutting forces increased with cut length obviously because of tool wear. Within a single revolution the forces varied because of the altering of fibre orientation with respect to the instantaneous cutting edge direction.

The axial force Fz was not a deterministic factor in the process this is why it was excluded from the statistical study. The resultant force, calculated by the formula using Fx and Fy, was in the region of 206.286 N (Test-13) to 1560 N (Test-3, 4) and increased as a result of tool wear. The calculated resultant angle was between ~ 32˚ when tool was new (Test-13) to ~ 57 ˚ (Test-4) when tool was worn. This angle generally increased by increasing the cut length or tool wear (due to increased feed force). The smaller the resultant force angle, the cleaner and the better quality is the cut and vice versa. Similarly, the calculated specific cutting resistance was 550-5712 N/mm^2 and was increasing with cut length and tool wear. The specific cutting

resistance of steel is 2000-2200 N/mm^2 [150] which suggested the great contribution of the cutting forces to the tool wear process.

4.2.2 Surface integrity/roughness

The defects at slot entry in all tests were less compared to slot exit. This was in form of fibres pulled out by the tool or frayed uncut fibres. Such uncut fibres were not supported at the end of the slot which suggests the use of a backup material or a pre-cut as detailed by Puw and Hocheng [157]. Fuzzing/delamination significantly affected up milling side especially at the top ply oriented at 45° because the flexible fibres at such orientation escape from the cutting edge. It was noted that a cutting edge radius should remain less than or equal the fibre diameter to obtain a clean cut [228]. Fuzzing on the down milling side occurred when tool flank wear was ~ 0.1 – 0.13 mm.

The use of chilled air prevented the carbon fibre from accumulating and agglomerating within slot or sticking to the workpiece surface. The blown away dust was loose as a result of the little temperature effect which means that the cutting was mostly achieved by crushing of composites by brittle fracture. Conversely, the absence of chilled air promoted the rise in cutting temperature which resulted in fumes and burning within slots as shown in Figure 4.18. These were signs that it had exceeded the glass temperature Tg (180 °C) had been exceeded and the test was stopped, on examination of the tool was found to have an excessive amount of matrix residues. The burning dust can be a fire hazard and such parameters (high cutting speed and low feed rate) are not recommended for slotting. There was also visible fuzz on both up and down milling sides. The extraction system used was capable of removing airborne dust but it was unable to suck the heavy agglomerated dust. A stronger extraction system would have been better especially in such dry conditions to avoid fire hazard.

The transverse roughness measurement were recommended as it gave more accurate representation of the surface since longitudinal measurements (parallel to cutting direction) might represent one layer only depending on stylus path and tend to be more periodic [24, 164]. Surface roughness parameters Ra and Rt increased with cut length. For example in Test-13 surface roughness increased from 3.6 µm to 21 µm Ra when the tool was worn because of mechanical and thermal damage. However, the trend (Figure 4.19) was not increasing uniformly possibly due to the inhomogeneous nature of carbon fibre unlike metals. This short traverse length of the stylus may contribute to those fluctuations but the limited traverse

length was imposed by the slot depth. Surface roughness parameters Ra and Rt at 0.1 mm flank wear are shown in Figure 4.20 and Figure 4.21 respectively.

Figure 4.18: Burning of dust within slot Test-3

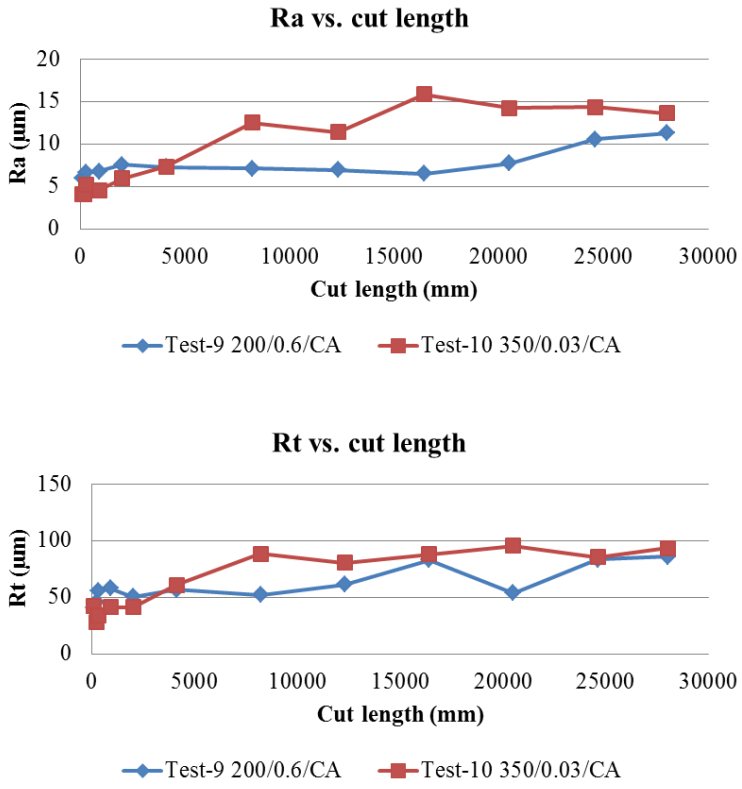

Figure 4.19: 2D surface roughness parameters (Ra, Rt) vs. cut length

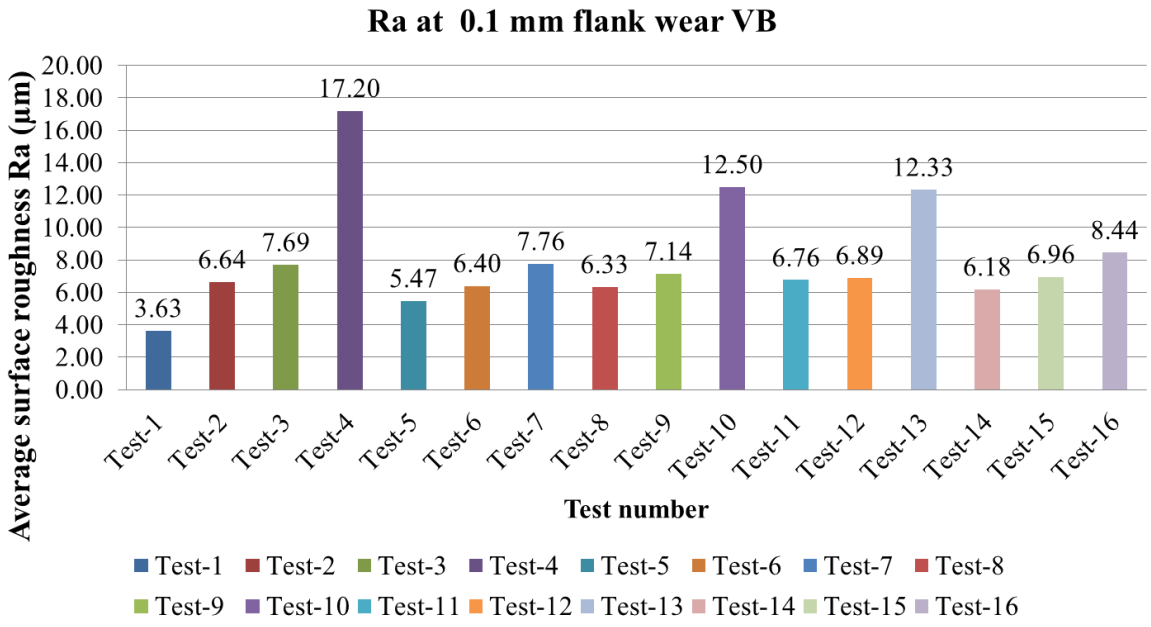

Figure 4.20: Average surface roughness Ra (µm) at 0.1 mm VB flank wear

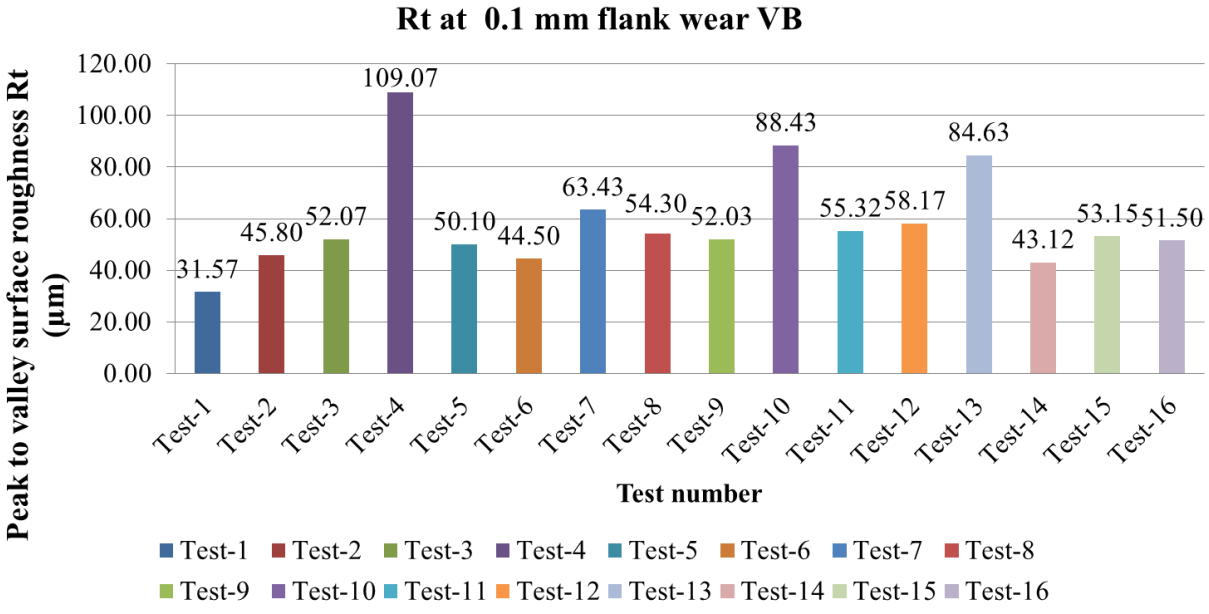

Figure 4.21: Peak to valley roughness Rt (µm) at 0.1 mm VB flank wear

The main effects plot of surface roughness is shown in Figure 4.22. Surprisingly, the surface roughness increased at higher cutting speed and decreased at high feed rate, unlike commonly observed in metal cutting and unlike findings of others in machining of composites by operations other than slotting as found by Sheikh-Ahmad and Sridhar [158]. The statistical

trend complies with the explanations provided earlier. The highest surface roughness, generally, resulted from the use of DLC-coated tools. The use of CTM-302 PCD resulted in surfaces with 5.6 µm Ra on average which suggests the use of CTM-302 PCD for finishing purposes. Chilled air contributed to a slight reduction in surface roughness possibly because of the flushing action of chilled air which reduced the frictional heat.

Higher cutting speed may improve surface roughness in case of thermoplastic composites because of matrix softening [175]. While high cutting speeds and low feed rates are recommended for edge trimming CFRP, the situation is somewhat different in slot milling where the low thermal conductivity of the resin matrix tends to retain the heat within the cutting zone. This leads to softening, degradation and burning of the matrix material that binds fibres together [210]. The softened matrix allows flexible fibres to 'escape' from the cutting edge and spread over a wider area, especially those in the 90˚ and 135˚ direction. This was observed in trials at low levels of feed rate and cutting speed (Test 13) where disintegration of the matrix also resulted in the loss of fibres particularly in the 0˚ direction. This is because of the accumulation of heat and the poor thermal conductivity of the resin [139]. The best surface roughness produced using PCD end mills was with the CMX-850 grade where an Ra/Sa of 3.60µm/3.65µm was obtained with a new tool (Test-13), although this test had to be stopped after 16,400mm cut length (flank wear ~0.13mm) due to burning of the workpiece. This was similar to the 3.2µm Ra typically required for aerospace applications [142].

Operating without chilled air was thought to be a further contributory factor as burning of the workpiece generated an acrid odour, suggesting that the glass transition temperature of the resin (180°C) was exceeded. Increasing cutting speed and feed rate in Test 15 with chilled air led to significantly improved surfaces, due to the absence of thermal damage. The main effects plot showed that low cutting speed with high feed rate was the best combination for minimum surface roughness, as this most likely reduced cutting temperatures as well as the total contact time between the tool and the work piece.

In terms of ANOVA results, feed rate was the only statistically significant variable affecting surface roughness with a 57.5% contribution. While the use of chilled air improved the removal of dust particles from the slot and helped reducing the incidence of matrix burning/sticking, the corresponding ANOVA showed that cutting environment was not statistically significant with respect to the workpiece surface roughness together with a negligible PCR. The percentages of different factors affecting the surface roughness Ra are

shown in Table 4.4. In case of Rt, the most significant factor was the feed rate with 67% PCR and the error level was 30% as shown in Table 4.5.

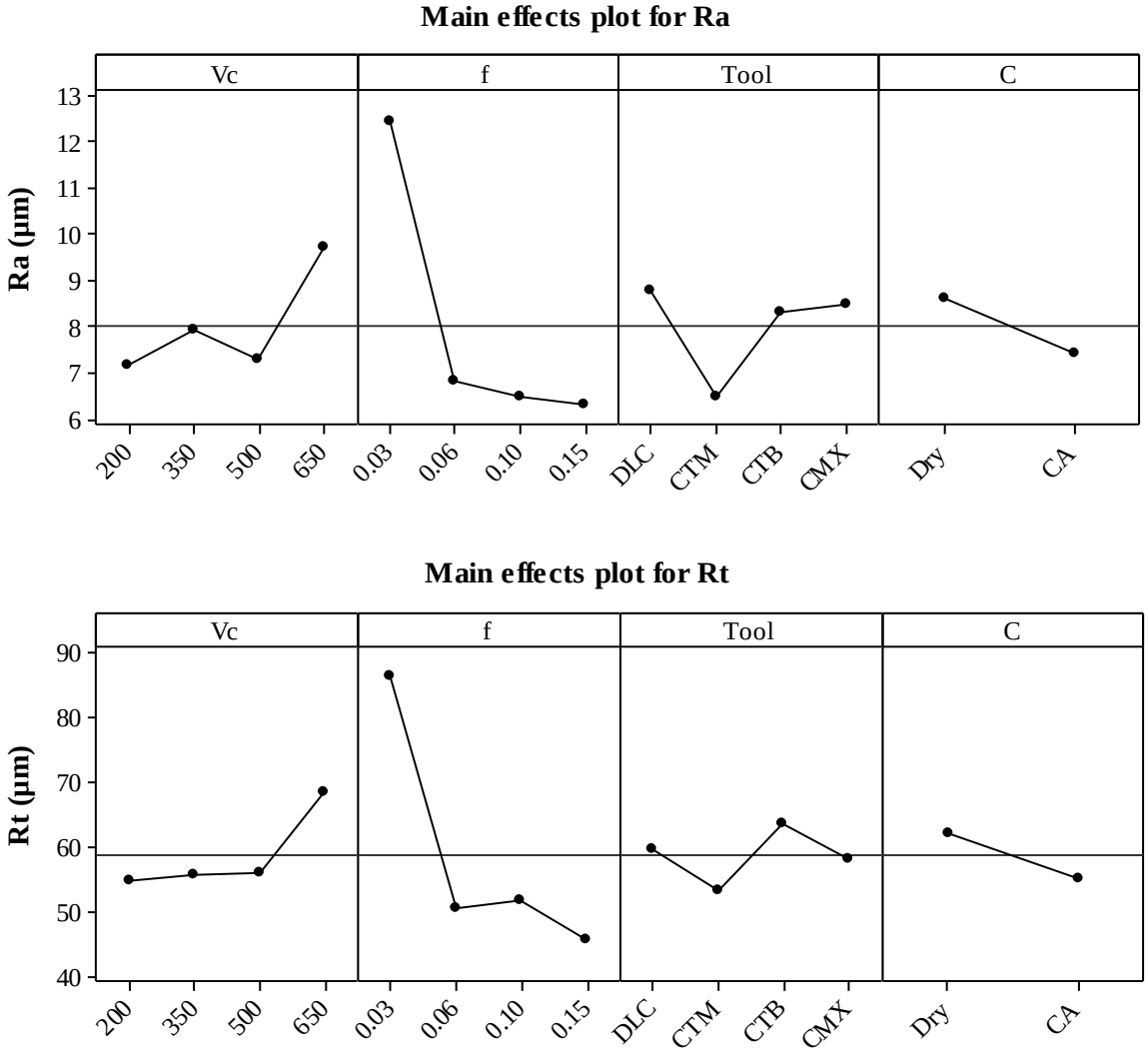

Figure 4.22: Main Effects plot for surface roughness Ra, Rt

Table 4.4: ANOVA analysis for surface roughness parameter Ra

Source	DOF	Seq SS	Adj MS	F calc.	F tab.	P	PCR (%)
Vc	3	18.446	6.149	1.51	5.41	0.321	3.46
f	3	115.132	38.377	9.4	5.41	0.017	57.47*
Tool	3	22	7.333	1.8	5.41	0.264	5.45
C	1	3.031	3.031	0.74	6.61	0.428	0.00
Residual error	5	20.416	4.083				33.62
Total	15	179.024					

*significant at the 5% level

Table 4.5: ANOVA analysis for surface roughness parameter Rt

Source	DOF	Seq SS	Adj MS	F calc.	F tab.	P	PCR (%)
Vc	3	504.2	168.8	1.51	5.41	0.412	2.48
f	3	4208	1402.68	7.27	5.41	0.028	67.02*
Tool	3	222.5	74.16	0.89	5.41	0.505	0.00
C	1	201.3	201.29	1.18	6.61	0.327	0.00
Residual error	5	602.7	120.55				30.49
Total	15	5738.8					

*significant at the 5% level

The three dimensional surface roughness measurement was recommended for better understanding of machined surface of composites [164]. The 3D surface topography plots revealed some feed marks on the machined surface which were visible also by naked eye. Similar feed marks were observed by Sheikh-Ahmad and Sridhar [158] and were explained as a result of high feed rate [158]. The lowest surface roughness obtained in this test matrix was 2.6 Sa µm and 49.1 µm St obtained using DLC-coated in chilled air environment at 200 m/min cutting speed and 0.15 mm/tooth feed rate (when tool was new). Regardless of the tool performance in terms of wear/life, the slotting operation of CFRP seems to prefer low cutting speed with higher feed rate which promoted the removal of chips by brittle fracture without softening of the matrix. The 3D roughness parameters Sa and St for all tests for a tool (first pass) are shown in Figure 4.23 and Figure 4.24 respectively while the main effects plot for the 3D surface roughness parameter Sa is shown in Figure 4.25. Generally, for non-bearing surfaces of wing panels and wing spars, where there is no mechanical requirement for a fine surface finish, the surface roughness should be 3.2 µ Ra or Sa or less. The lower the peak to valley surface roughness (Rt or St) the better as this indicates a smaller the depth of damage left by the milling process. In this test, the peak-to-valley values were ~ 10 to 25 times larger than the average surface roughness, however, this was mainly due to test parameters and the type of surface is related to the parameters selected.

The high average surface roughness value (17.9 µm Sa) in Test-4 was a result of the severe wear associated with the use of coated WC at high cutting speed and low feed rate in a dry environment (thermal damage). On the other hand, the higher tool wear in Test-2 compared to Test-1 was due to a rise in cutting speed from 200 to 350 m/min which caused a combined mechanical and thermal effect which resulted in high surface roughness 11.8 and 200 µm Sa and St respectively. The dry environment and the consequent matrix melting and smearing caused a reduction in the St Value in Test-4 (170 µm) compared to (200 µm) Test-2.

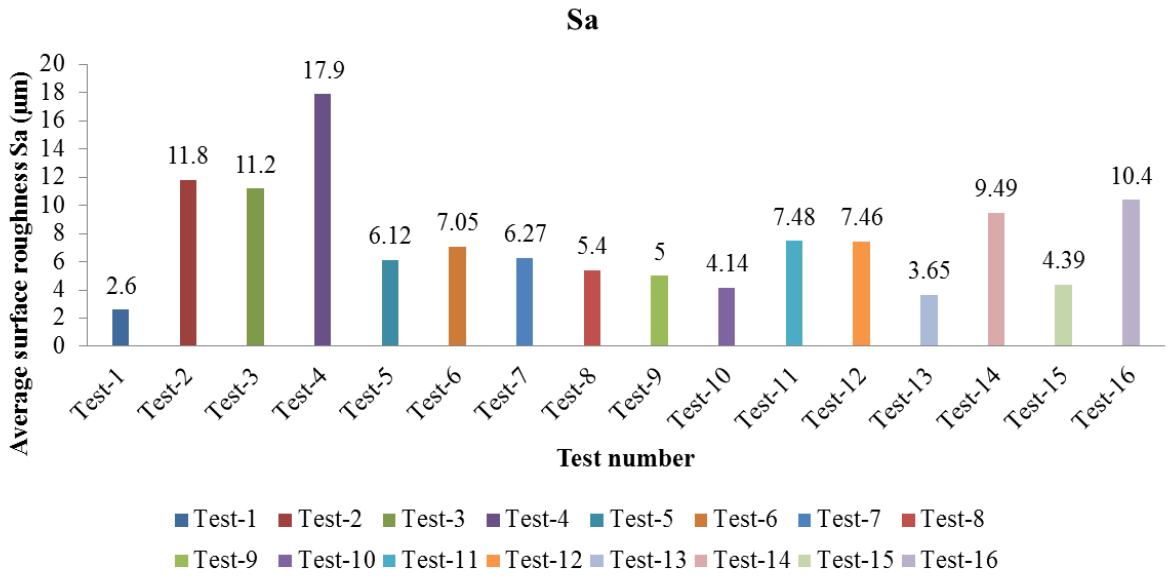

Figure 4.23: 3D surface roughness parameters Sa for all tests

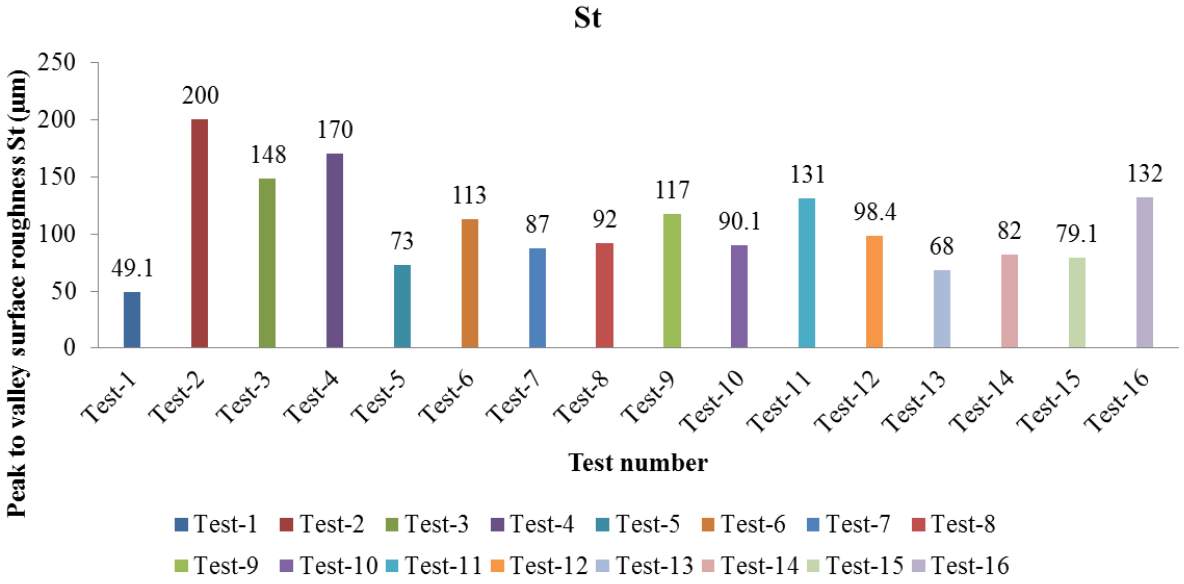

Figure 4.24: 3D surface roughness parameters St for all tests

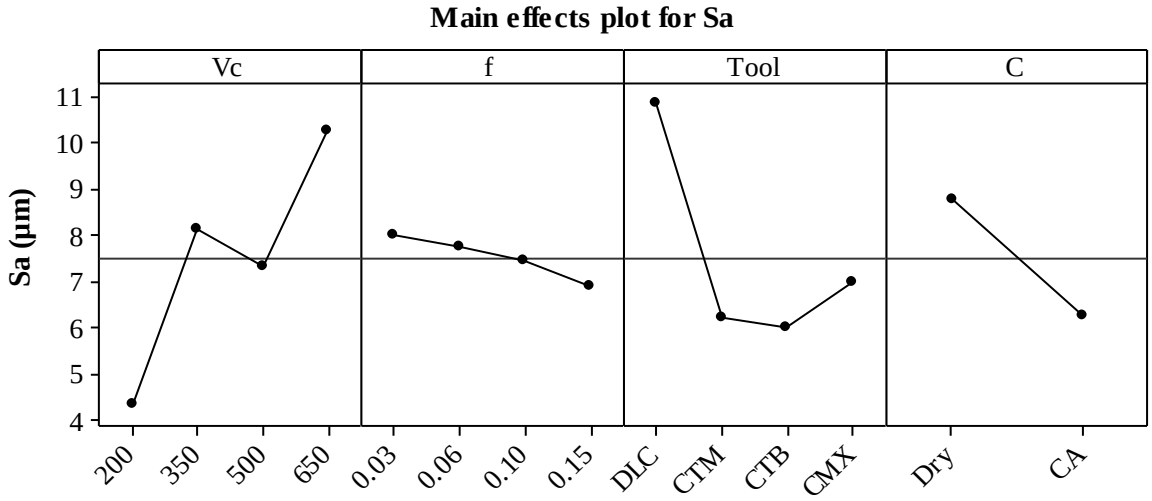

Figure 4.25: Main Effects plot for surface roughness Sa

Figure 4.26 shows SEM micrographs of the slot wall (down milling side) machined using DLC coated WC routers. The 45° oriented plies typically exhibited 'wavy' surfaces which were especially evident in trials at lower cutting speed (200 and 350 m/min) involving chilled air. When operating dry at higher cutting speeds however, matrix cracking, material pull out was evident, most likely due to the increased temperature. In contrast, the 135° plies were generally characterised by loose fibres, particularly when machining dry as a result of matrix burn. 3D surface topography using DLC coated WC tools (Figure 4.27) shows that low cutting speed along with higher feed rate (Test-1) result in relatively good surface (2.6 µm Sa) possibly because of low heat input and low wear rate of the tool compared to poor surfaces (17.9 µm Sa) in Test-4 due to matrix burning.

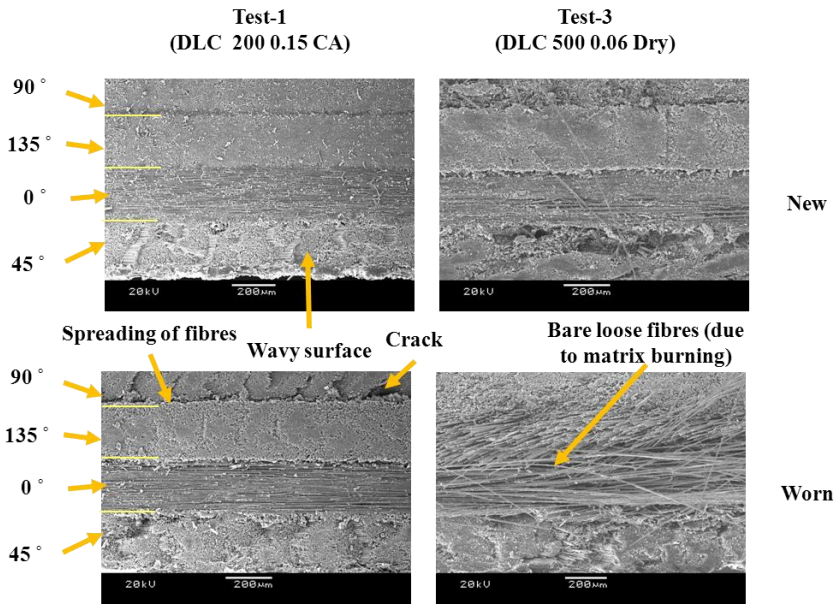

Figure 4.26: SEM micrographs of machined surfaces produced using DLC coated WC

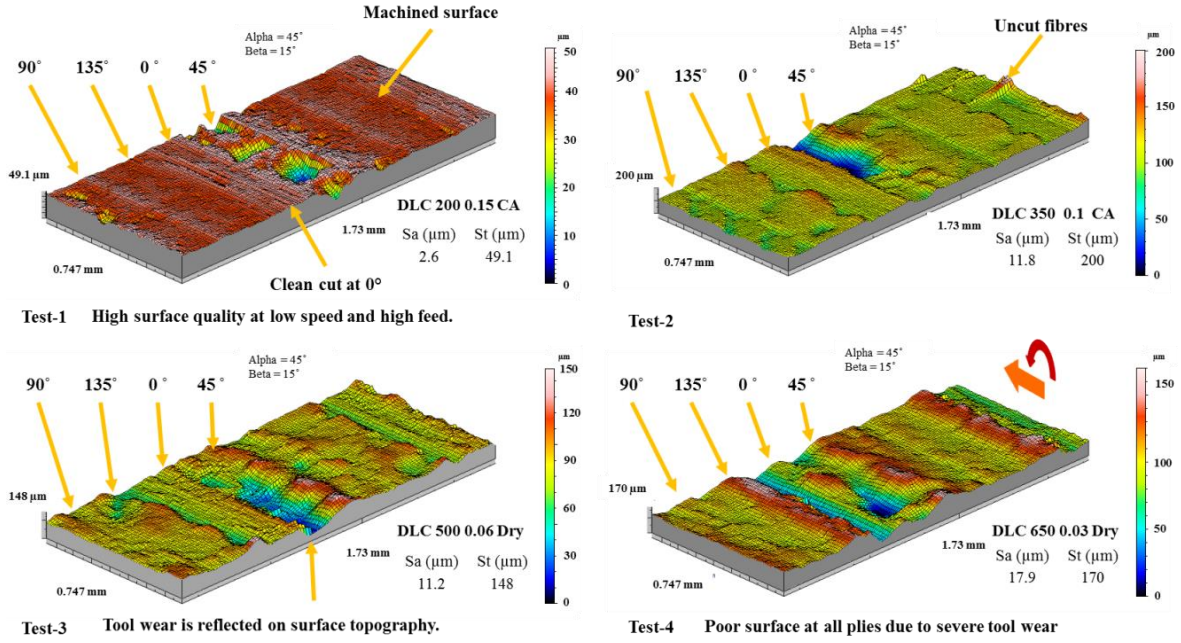

Figure 4.27: 3D surface topography using DLC-coated WC

Despite the localised chipping on the CTM-302 PCD tool used in Test-5 the machined surface exhibited minimum amount of damage. This contradicts with high cutting speed and low feed rate being the key to smooth surface as reported by Davim et al. [160, 176, 177] possibly because they were not measuring roughness of the slot walls or other researchers may have come to such conclusion that high speed and low feed is better due to difference in process, i.e. edge-trimming as reported by Ucar and Wang [161] and Prashanth et al. [162].

Feed marks on the machined surface were similar to those associated with milling of metallic materials. These marks occurred due to either mill deflection and vibration [229] or could be formed by the softened matrix as explained by Bissacco et al. [230], alternatively, they could also be due to self-excited chatter caused by the straight fluted tool. The marks were more prominent when tool was new but disappeared when the tool was worn especially when using PCD routers only as can be seen in Tests 6, 14, 15 and 16. The higher cutting forces (especially in Test-6) caused by high feed rate resulted in grooves especially in fibres at 90° orientation as shown in Figure 4.28.

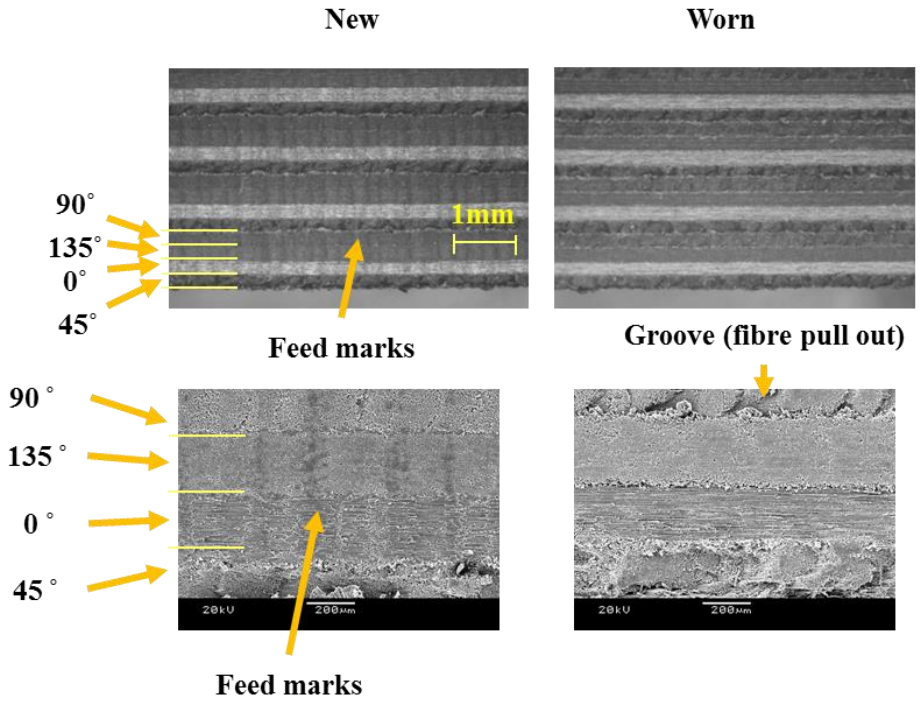

Figure 4.28: Optical microscope and SEM images of surfaces produced using CTM-302 PCD showing Test-6 feed marks on surface

In Test-7 and Test-8, the melting of resin matrix and loose fibres were evident in 0° layers due to high temperature while fibres at 45° direction were bent. In contrast, fibres oriented at 135° were spread over a wider area 'brooming' which were more severe in Test-7. Cracks normally occur in matrix since the matrix is weaker than fibres [157] normally associated with fibres at 90° [21] and this is also evident in Test-8 for example, see Figure 4.29.

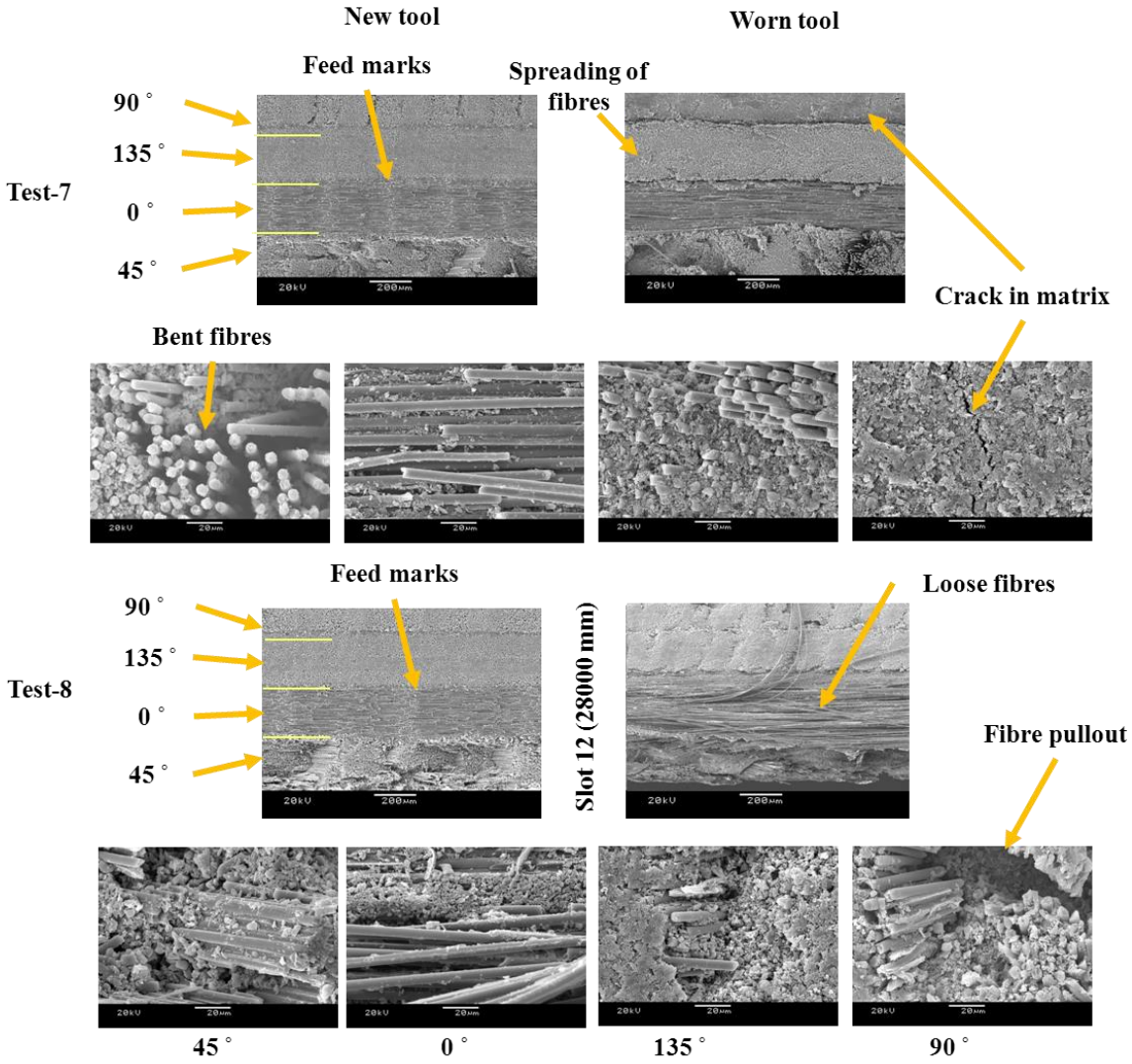

Figure 4.29: SEM micrographs of surfaces obtained in Test-7 and Test-8 showing the common surface defects associated with slotting of CFRP

Generally large grain PCD has the advantage of high abrasion as noted by Klocke and Wurtz [156]. The use of CTM-302 PCD routers was relatively better in terms of quality. Regardless of the cutting conditions, the CTM-302 produced surfaces 5-7 µm Sa and 70-113 µm St when tool was new as shown in Figure 4.30. The chipping associated with CTM-302 may have left some marks on the surface at chipping locations since every tool leaves its own signature on the surface as reported by Colligan and Ramulu [153].

Chilled air showed a great effect in lowering the surface roughness. Using CTB-010 the surface roughness was 4.14 -5 µm Sa, 90-117 µm St compared to 7.5 µm Sa and 98-131 µm St in case of dry cutting. The use of chilled air results in more flat surface while a wavy

surface with feed marks were attributed to dry cutting possibly because of the response of the soft matrix as shown Figure 4.31.

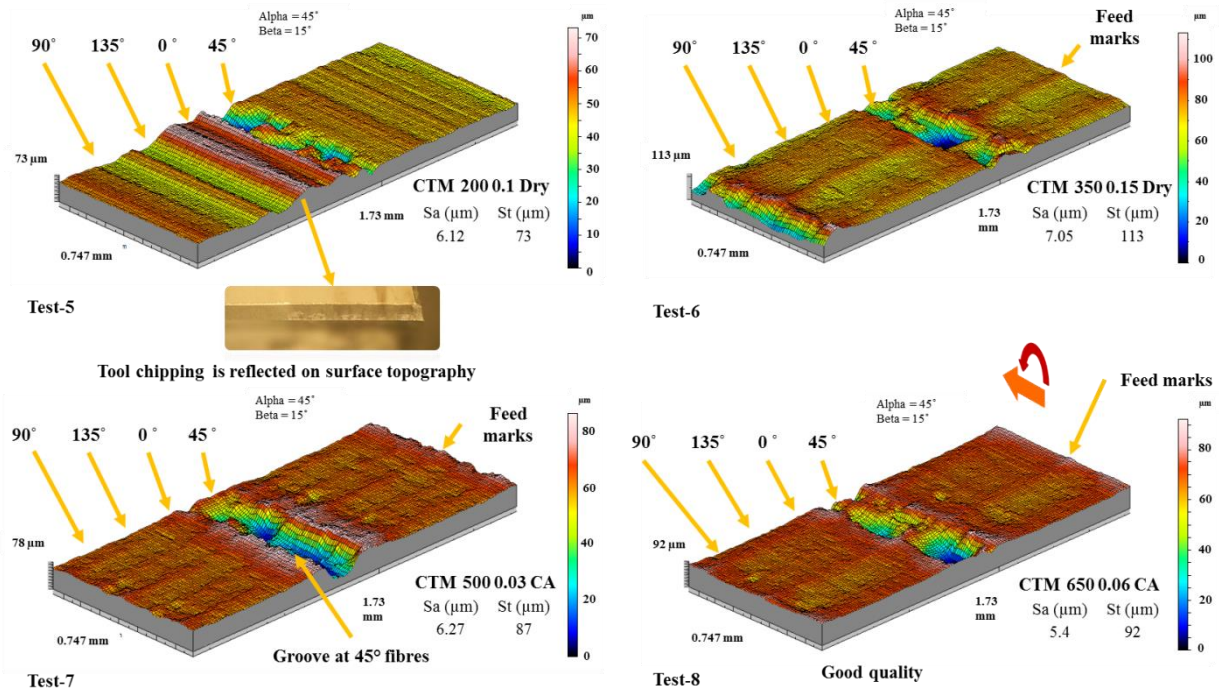

Figure 4.30: 3D Surfaces obtained using CTM-302 PCD

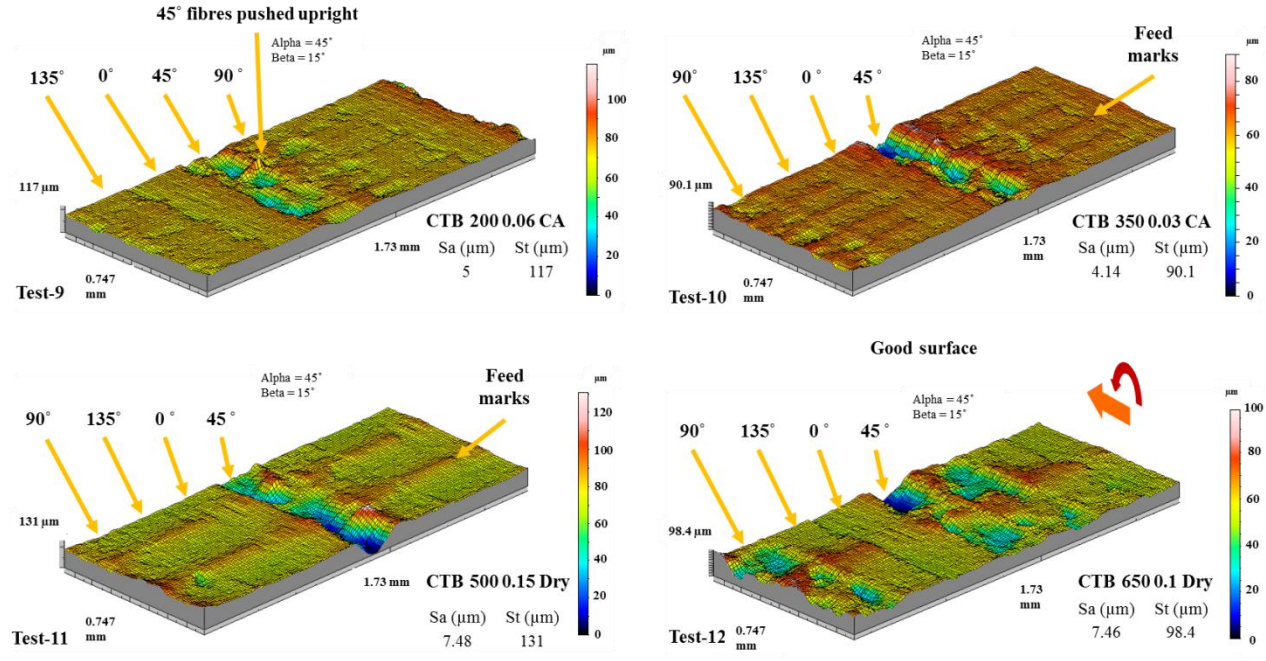

Figure 4.31: 3D surface topography using CTB-010 PCD

Thermal effects also increase with higher cutting speeds. When the cutting is done utilising higher feed rates, the mechanical effects become dominant as in Test-11 and Test-12. This can be seen in samples cut by using CMX-850 PCD which can be explained by altering the cutting mechanism to brittle fracture in case of chilled air. The use of CMX-850 PCD at very low feed rate in dry condition (Test-13) resulted in smooth surface when the tool was new with 3.65 µm Sa, 68 µm St when tool was new which can be further improved using chilled air, see Figure 4.33. Accumulation and burning of dust caused poor surface.

The use of CMX-850 PCD at very low feed rate in dry condition (Test-13) resulted in smooth surface when the tool was new but accumulation and burning of dust caused poor surface as shown in Figure 4.33. Increasing feed rate (Test-14) helped in reducing the thermal damage slightly. Some signs of feed marks were visible on the surface. High cutting speed/feed rate combination in chilled air produced a very smooth surface as in (Test-15) but some cracks and fibre pull-out were visible when the tool lost its sharpness. At extreme conditions (Test-16) both mechanical and thermal effects on surface were prominent. Such surface finish may result from the superior cutter surface of the fine grained PCD as noted by Klocke and Wurtz [156].

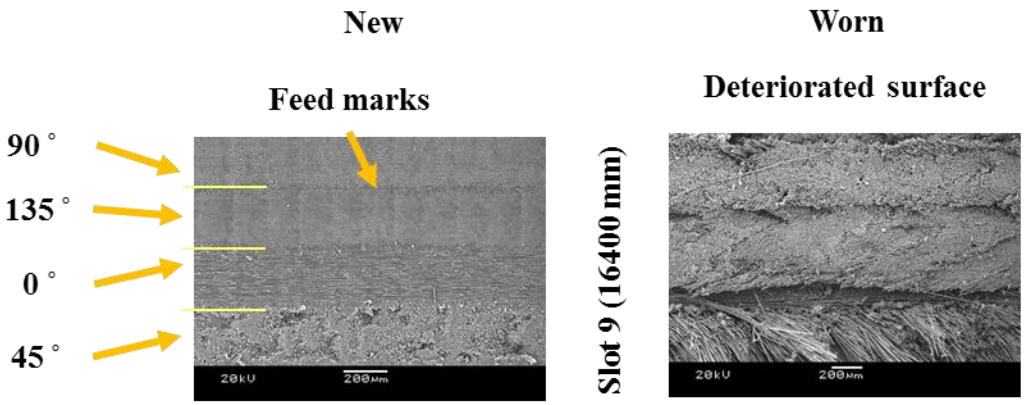

Figure 4.32: Deterioration of surface in absence of chilled air in Test-13

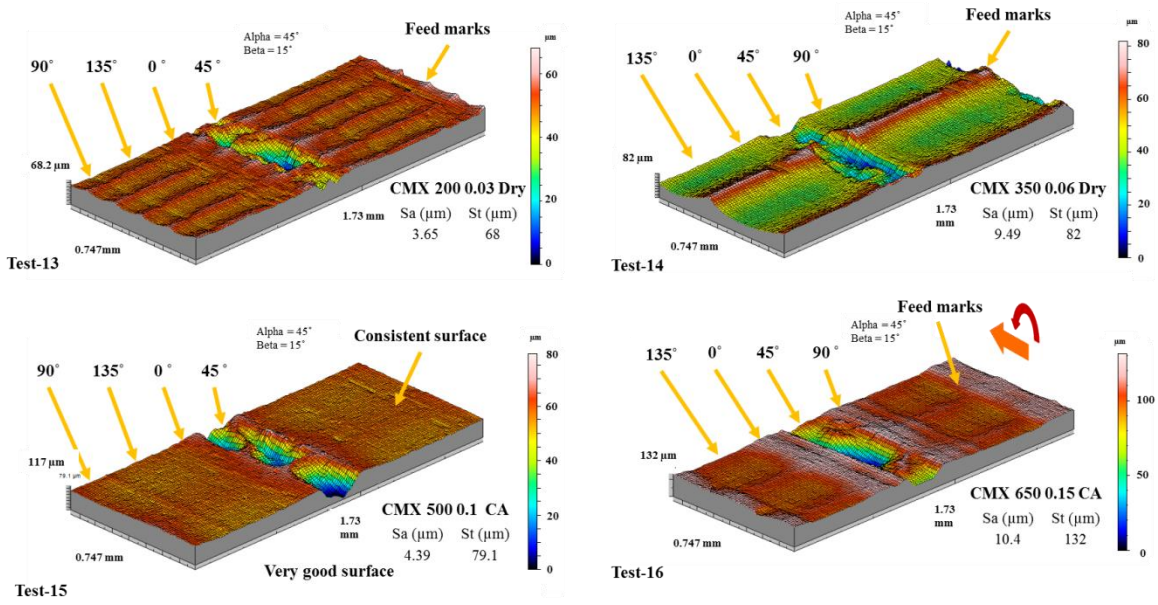

Figure 4.33: 3D surfaces using CMX-850 PCD

Plies oriented at 45˚ sustained severe damage where fibres were generally bent and 'lifted-up' as the cutting edge advanced, which can subsequently cause splitting/interfacial failure of fibre bundles and the matrix. Some of these fibres then proceeded to fracture/were pulled out while others were merely flexed, thereby producing a wavy surface. High cutting forces (worn tool) and matrix softening can also result in reorientation of 45˚ fibres, and surface delamination of the unsupported top ply.

Surfaces with fibres at 0˚ generally showed the least damage with fibres removed cleanly as a result of fracture by buckling [140]. All other layers exhibited matrix smearing except 0˚ layers which was noted also by Colligan and Ramulu [152]. Matrix smearing normally reduce surface roughness [23]. The 0˚ layers however were responsible for high cutting forces as they became orientated at 90˚ with respect to the cutting edge at the point of maximum chip thickness (middle of slot), which causeed loose fibres to form. Fibre pull out was observed in 90˚ and 135˚ plies leading to empty holes or large grooves as fibres tended to break at locations beneath the machined surface/depth of cut [157]. Matrix cracking as a result of elevated forces at high feed rates also occurred.

In summary, CTB-010 PCD tools showed the lowest flank wear rate compared to the other PCD grades and DLC coated cutters tested. The high cutting forces (~500N) encountered when operating at high feed rate (0.15 mm/tooth) led to chipping of the CTM-

302 PCD. Flank wear on the CMX-850 tool (Test 15) was ~0.15mm after 28m cut length which was ~50% greater than the CTB-010 router at similar parameters. The relatively high magnitude of cutting force experienced by the CTB-010 PCD did not appear to have a detrimental effect on tool life under certain conditions. For example, at 500 m/min cutting speed and 0.15 mm/tooth feed rate combination (Test 11), the flank wear after 28m cut length was approximately 0.10mm, despite Fx force level of ~600N. The CTB-010 grade did not suffer any chipping at high feed rates as uniform flank wear was dominant. No sign of fuzzing or delamination was detected on the down milling side of the slot after 28m cut length (0.10mm flank wear), despite machining dry with CTB-010 at 500 m/min cutting speed and 0.15 mm/tooth feed rate (Test-11). Conversely, severe fuzzing was observed when using the CMX-850 grade even at low operating parameters (Test 13).

Since cutting speeds of 350 m/min and 500 m/min were shown to give the highest tool life and feed rates of 0.10 and 0.15mm/tooth were selected for Phase-2 experiments (section 4.6: Phase-2B). The selection was made in order to achieve workpiece quality/surface roughness and productivity requirements. Chilled air is recommended to prevent burning of dust particles. A tool life criterion of 0.10 mm flank wear was recommended for future trials as the majority of PCD grades tested achieved a 28 m cut length with a corresponding flank wear level ranging between 0.10 and 0.18 mm. Additionally, it was observed that the probability for fuzzing and delamination increased as tool flank wear exceeded 0.10 mm.

4.2.3 CTB-010 PCD confirmation test

The CTB-010 PCD grade was selected because of the relatively extended tool life over the other tool materials. This tool surprisingly suffered from chipping and signs of cracks were evident. The difference between this tool and the tool used in Phase 1 (Tests-9 to 11) was mainly due to the manufacturing method. This tool was shaped to the cutting angles by wire electro-discharge machining (WEDM) compared to mechanical grinding as in Phase-1. The mechanical grinding is known to lower heat effect on tools as WEDM may leave residual stresses which result in cracks [188]. The different edges are shown in Figure 4.34. Such cracks can be promoted by the use of chilled air. Using laser to obtain the cutting edge angles is still under investigation by Dold et al. preliminary testing show that it gives equal results to ground PCD [189].

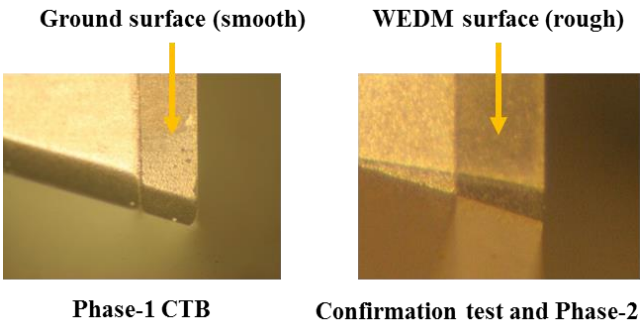

Figure 4.34: Tool surface of WEDM versus mechanical grinding

This CTB-010 tool was capable of cutting 28000 mm length without fuzz on the down milling side at only 0.072 mm flank wear (uniform abrasion) without taking into account the chipping. The flank wear in the chip area reached and exceeded 0.5 mm wear into substrate. However, the quality of the top ply was not affected i.e. no fuzzing, see Figure 4.35.

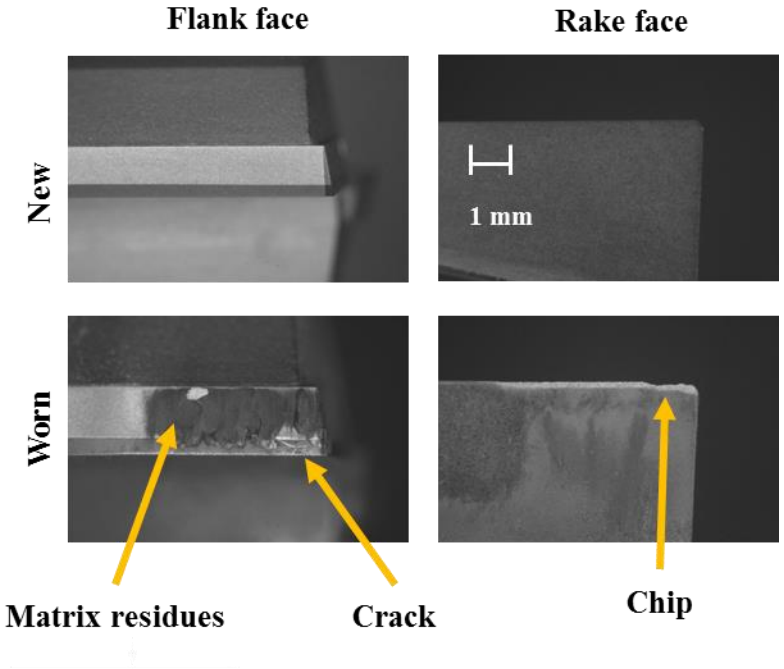

Figure 4.35: Worn CTB-010 PCD tool (confirmation test)

4.3 Phase-1C: Benchmarking of Element 6 PCD grades at preferred operating parameters

4.3.1 CTM-302 PCD

The CTM-302 PCD lacked chipping resistance especially at higher tool loads associated with higher parameters and suffered from drastic tool edge chipping following only 100 mm cut length as shown in Figure 4.36. Although the cut was free of fuzzing on the down milling side with 8.75 Sa and 116 St surface roughness parameters, the wear performance does not recommend CTM-302 PCD grade from being used in high feed rate cutting. The cutting forces (maximum) were higher compared to other PCD grades due to loss of cutting edge (661 N Fx and 518 N Fy).

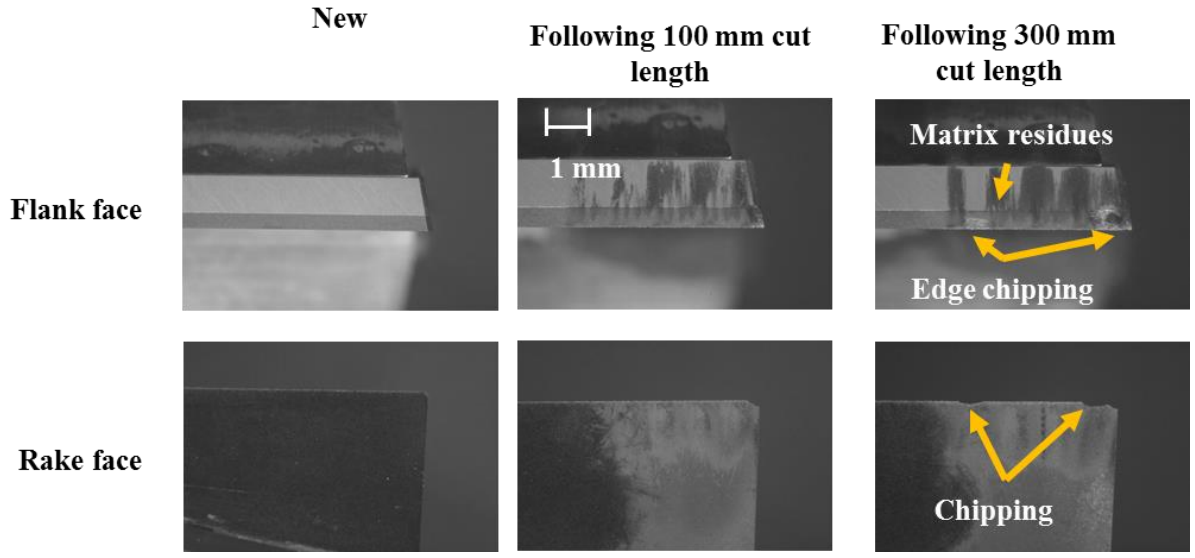

Figure 4.36: Worn CTM-302 PCD router at 500 m/min cutting speed and 0.15 mm/tooth feed rate in chilled air environment

4.3.2 CMX-850 PCD

The CMX-850 PCD router obtained was not properly sharpened and the blunt edge resulted in early fuzzing on down milling side. Besides, the cutting forces were very high compared to other PCDs even the surface roughness was not as usually obtained by CMX-850 PCD tools which were greater than 8 µm Sa. The router was reground to ~ 11.590 mm diameter and the test was repeated. After tool re-sharpening, the tool lasted for only 850 mm cut length where it suddenly fractured in the middle of the slot as shown in Figure 4.37. The last reported force peaks were 185 N Fx, 246 N Fy, and a very high peak Fz of 1400 N. A replacement tool was ordered and another bench marking test was performed from scratch.

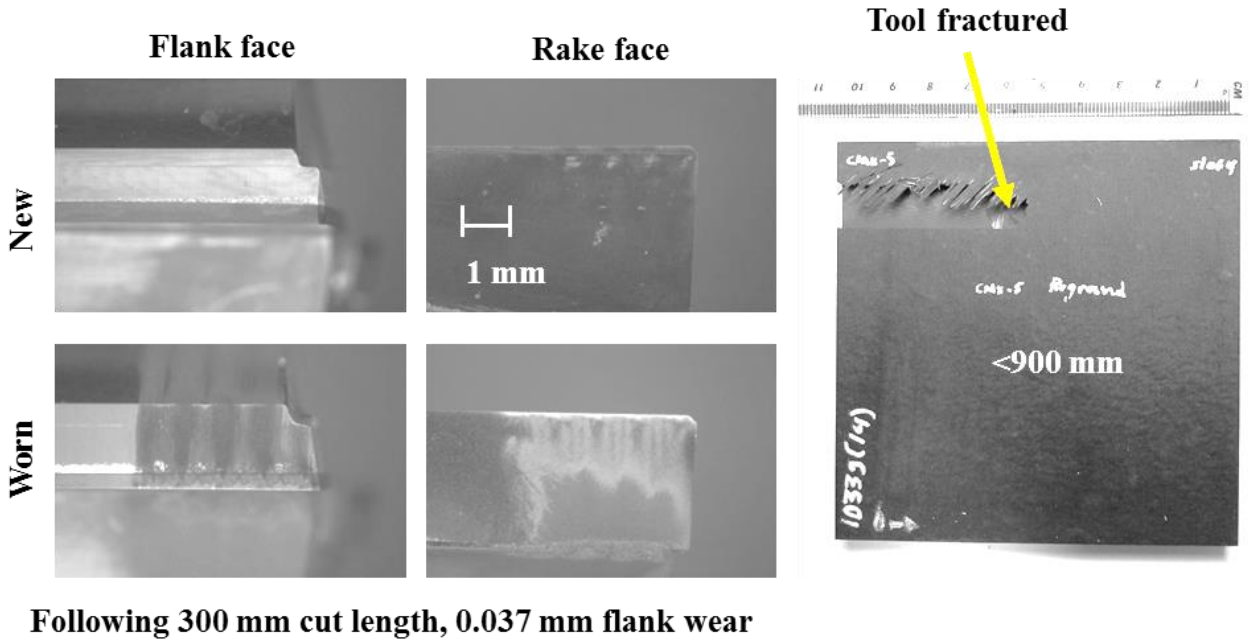

Figure 4.37: Un-completed slot due to tool fracture

4.3.3 WPC-102 PCD

The WPC-102 PCD router had 18^{o} primary relief and consequently it suffered from chipping which may be spalling of one of the top layer of the functionally graded material. The tool was capable of cutting 28000 mm cut length with no fuzz in down milling side at flank wear VB reaching ~ 0.197 mm, see Figure 4.38.

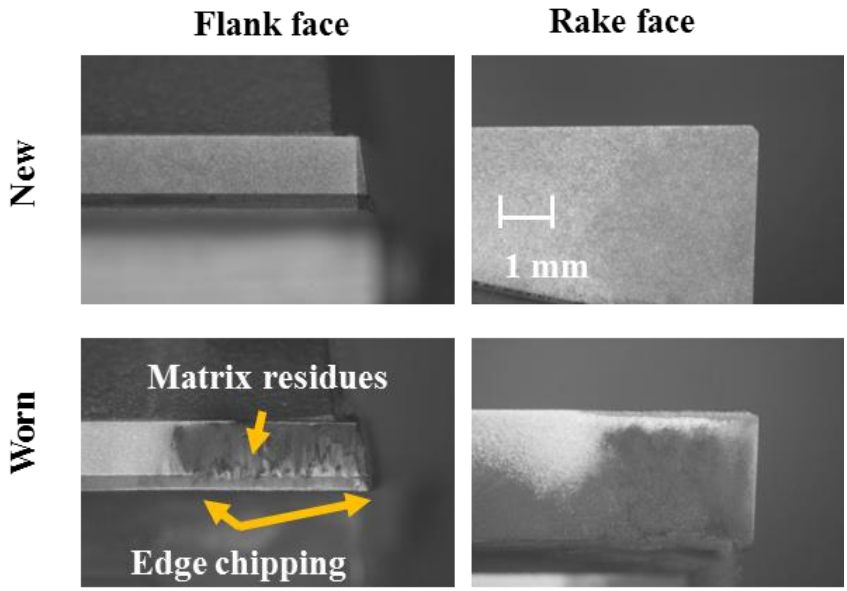

Figure 4.38: Worn WPC-102 PCD tool following 28000 mm cut length

4.3.4 Tool wear summary

Without taking into account the chipping which occurred to the tool used in the confirmation test, the results conform to the outcomes of Phase-1. The chilled air used improved the performance in terms of flank wear which reached 0.072 mm compared to 0.101 mm in dry environment (Phase-1 Test-11) which means ~ 30 % improvement in tool life. The WPC-102 PCD exhibited higher amount of wear compared to CTB-010 (> 2 times CTB-010 wear), see Figure 4.39 for tool wear against cut length.

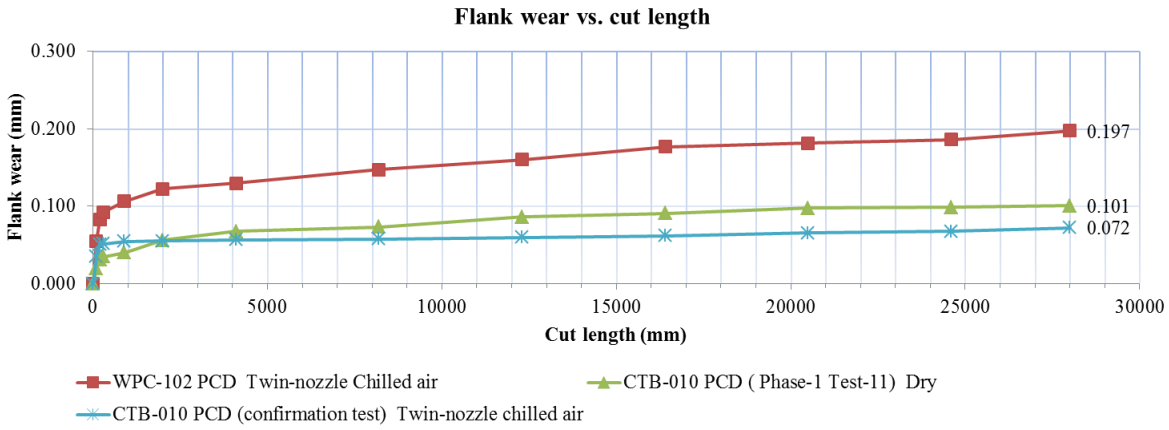

Figure 4.39: Tool wear versus cut length for different PCD blades

4.3.5 Cutting forces

The average cutting forces Fx of CMX-850 and WPC-102 PCD grades were the highest in both new and worn conditions, possibly due to high wear rate, see Figure 4.40. The CTB-010 PCD had the lowest rate of increase in cutting force from new to worn state due to the steady wear rate. The use of chilled air also helped in reducing forces in both cases of new and worn conditions (356.9 N dry, 323.4 N CA) when the tool was new, (408 N dry, 396 N CA) when the tool was worn. Comparing Fx when using CTB-010 PCD in Test-11 (dry) and the confirmation test, the chilled air environment slightly reduced the forces.

The WPC-102 PCD was responsible for the highest average feed force (Fy) most likely due to the tool wear as mentioned before. CTB-010 confirmation test resulted in higher average feed force compared to Test-11 may be due to the lowered friction between tool and workpiece by the softened resin matrix in the dry condition in Test-11 which lowered the force, see Figure 4.41. Figure 4.42 illustrates the recorded force signals for the different tools which are similar to a great extent to the force profile obtained by Zaghbani et al. [231] and they show how the tool wear contributed in minimising or eliminating the initial dynamic

forces associated with the milling process. The consequences of such dynamic forces will be detailed in the surface integrity section.

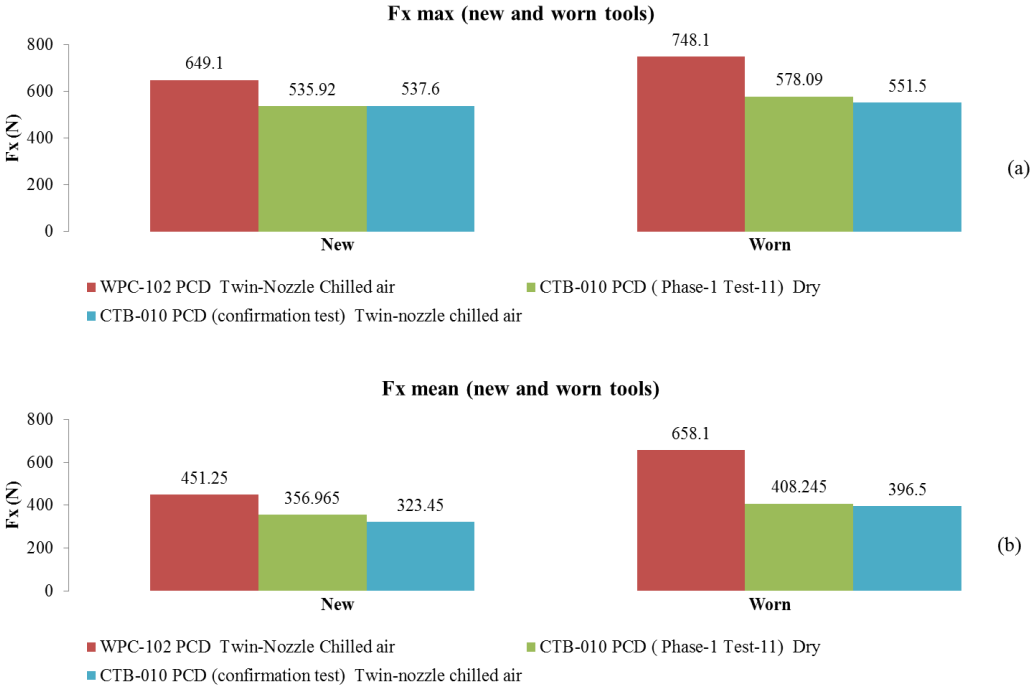

Figure 4.40: Cutting forces Fx for benchmarked tools a) max b) mean

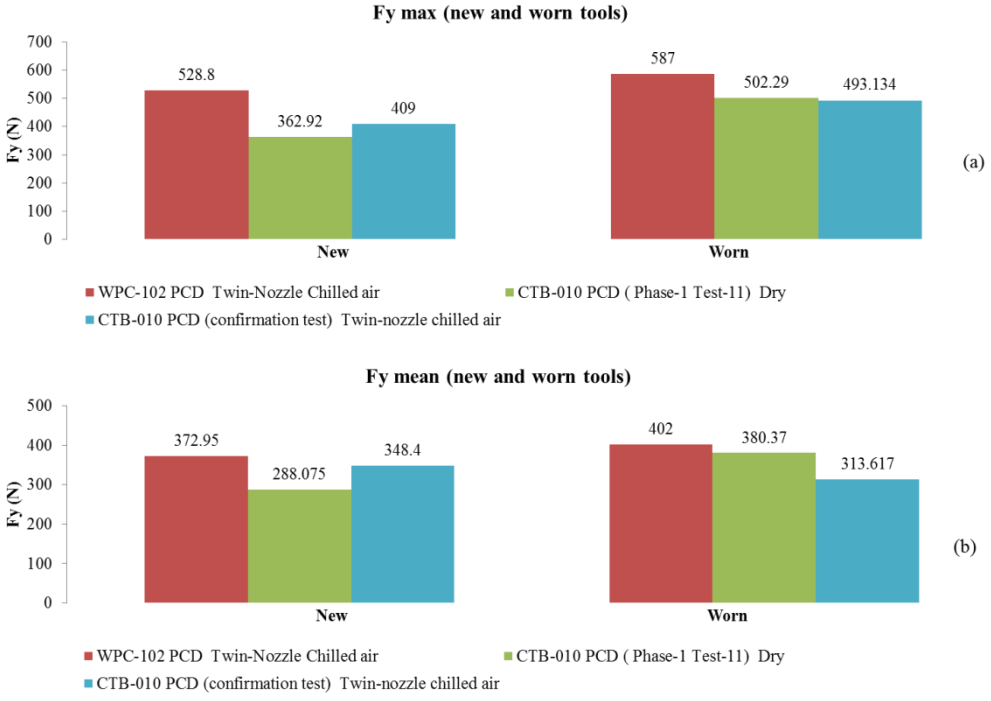

Figure 4.41: Cutting forces Fy for bench marked tools a) maximum b) mean

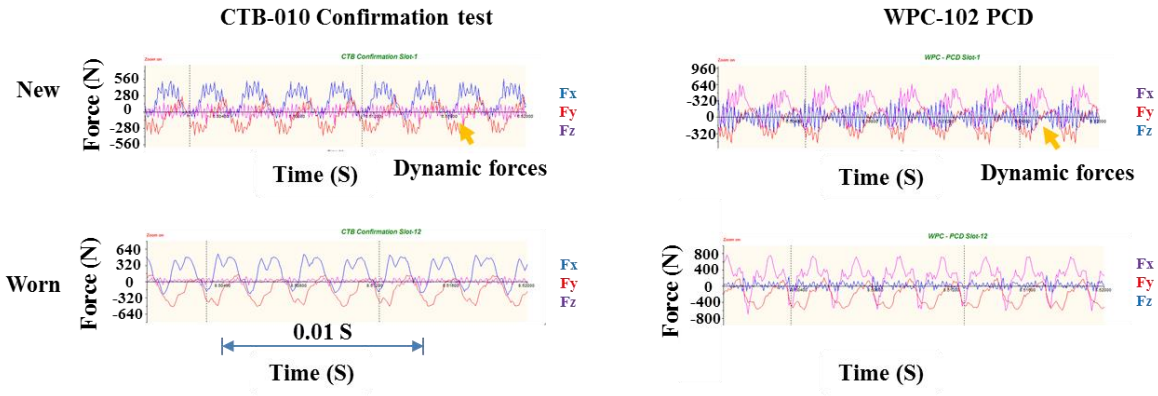

Figure 4.42: Force signals for different cutting tools

4.3.6 Surface integrity/roughness

The optical microscope images of benchmarking test samples show that the feed marks were visible at start using WPC-102 and CTB-010 PCD tools when tools were new. No fuzzing on the down milling side but it occurred mostly on the up-milling side. The optical microscope images did not show enough details and from the images shown in Figure 4.43 the surface obtained using the worn tools appeared almost the same. The SEM graphs (Figure 4.44) show that using either router, when tools were new there was no significant difference in quality. However the relatively superior wear resistance of the CTB-010 produced a better surface when the tool was worn.

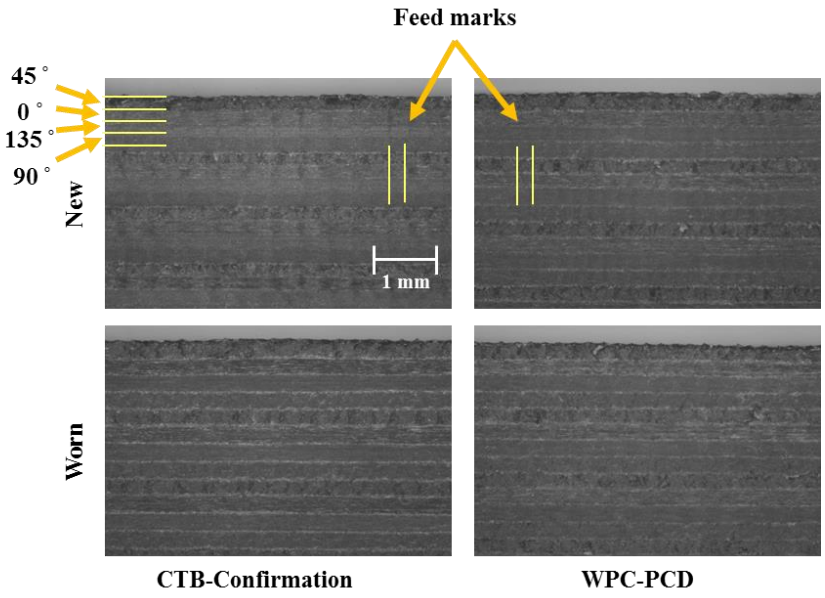

Figure 4.43: Machined surface under toolmakers microscope

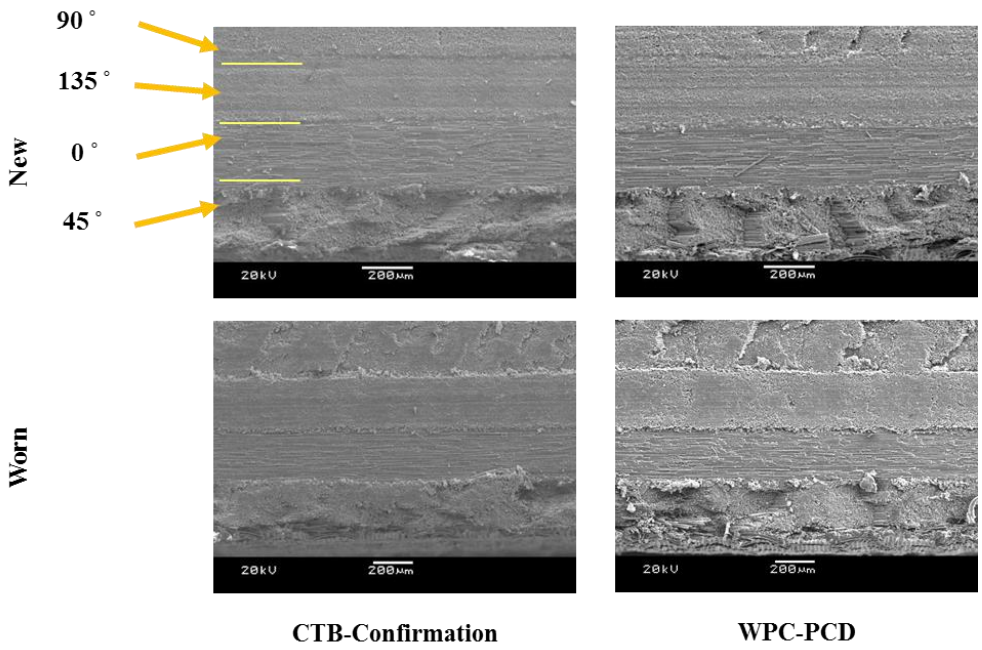

Figure 4.44: SEM images of surfaces obtained using new and worn tools

Surface topography and surface roughness parameters are shown in Figure 4.45 and Figure 4.46 respectively. In the confirmation test using CTB-010 PCD, prominent feed marks were observed at the beginning of the test (new tool) however they diminished by the end of the test. As a result, the surface roughness using the worn tool was better than that of the new tool (6.2 µm Sa compared to 14.3 µm Sa) due to the contribution of the feed marks attributed to new tools. When tools were new and sharp, the cutting was done mostly by shear producing feed marks which were mostly visible at the higher feed rate. Such phenomena bring to mind the possibility that the tool edge encounters flank regrinding by the fibre as noted by Klocke and Wurtz [156] which may provide the tool with a new edge geometry. The damage in 45° layers was the highest as usual and some fibres were pulled out distorting the common wavy pattern of those layers. When the tool was worn the damage was extended to the adjacent layer (90°). The 135° layer was easily compressible, which was the reason that fibres here were observed to spread over the neighbouring plies.

Using WPC-102 PCD, there were some elevated regions on the surface which correspond to the minor chipping the WPC-102 PCD tool encountered at the beginning despite being covered later by subsequent uniform abrasion wear. The surface roughness obtained using WPC-102 PCD was relatively high in new and worn conditions because of the relatively higher tool wear attributed to this tool which in turn resulted in higher cutting and feed forces all those factors contributed to the surface roughness. Fibres at 45° were not cut evenly and

some of them were reoriented and pushed back. Fibres at 90° showed some deep marks on the surface (cracks) which possibly resulted from the high cutting forces (649 N Fx , 528 N Fy) when the tool was new. The forces were higher compared to CTB-010 PCD used in confirmation test (537.6 N Fx and 409 N Fy).

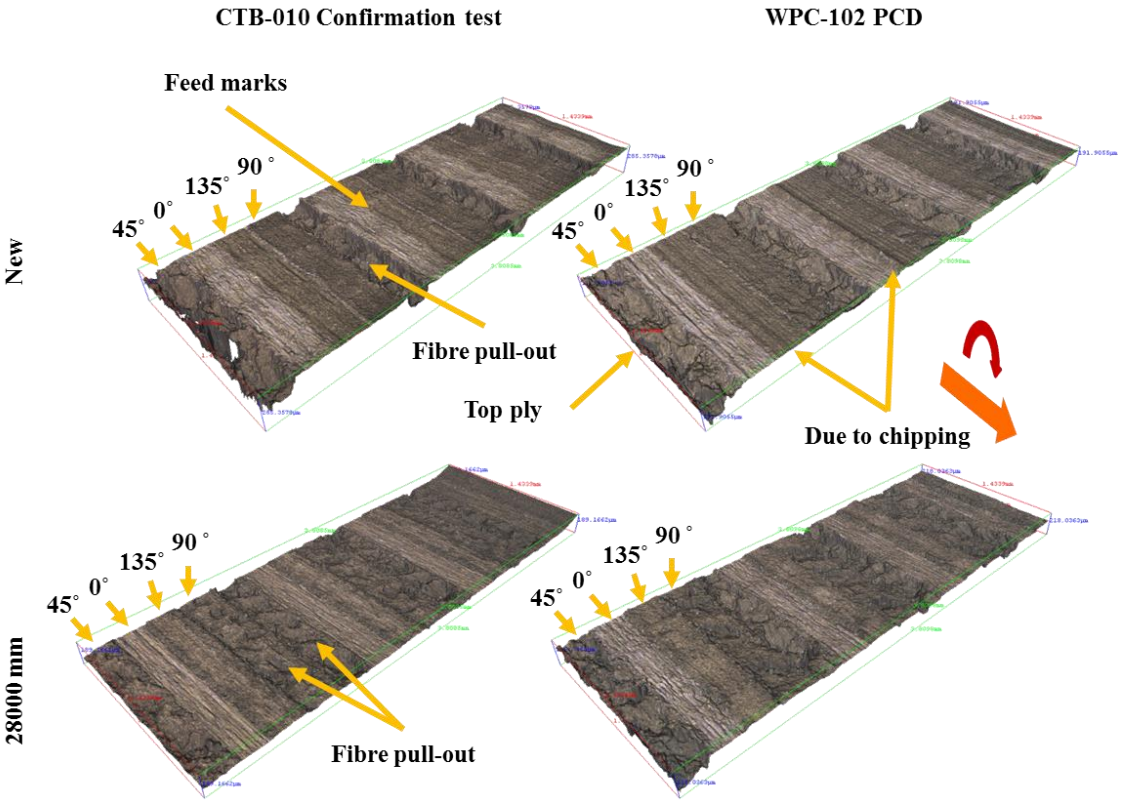

Figure 4.45: Alicona 3-D scans of slot wall machined by different tools

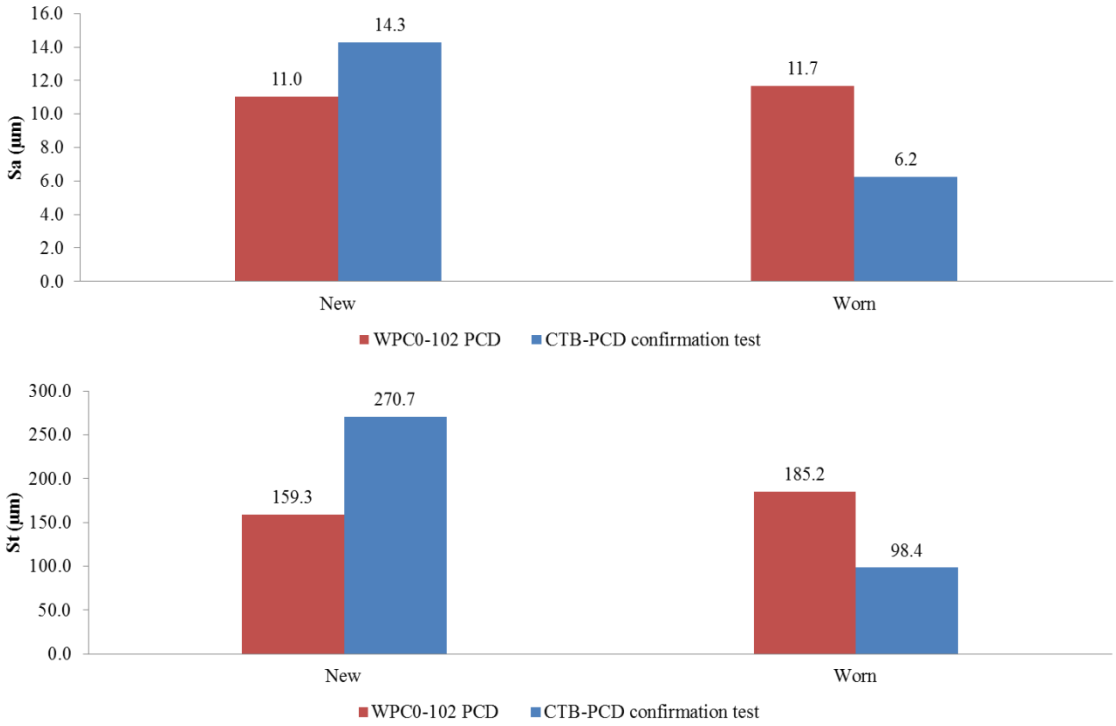

Figure 4.46: 3D surface roughness parameters using different tools

4.3.7 Fuzz (uncut fibre) and delamination factor

The most observed delamination mode was Type-II as described by Colligan and Ramulu [151], which occurred mainly on up milling side in the 45° top ply although they said Type-I was the most dominant for the 45° top ply may be because the fibres used in this test are very flexible and did not break easily or due to the coolant type they used. The amount of uncut fibre generally increased with the increase in cut length because of the tool wear as the tool became blunt and rounded, the condition, which allowed the flexible fibres to escape from the cutting edge. This, in turn, caused subsurface delamination the extent of which was measurable using laser scanning. Measuring the length of uncut fibre on the up-milling side, the tools performed similarly, see Figure 4.47.

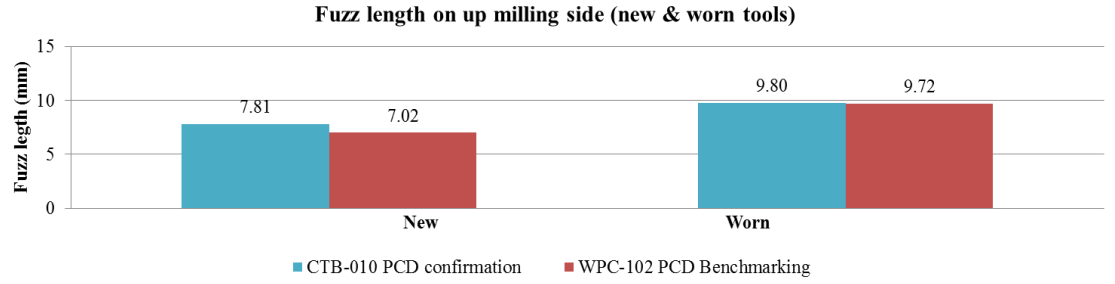

Figure 4.47: Fuzz length for different tools

Despite the lower cutting forces using CTB-010 PCD, the delamination factor using the worn CTB-010 PCD was higher compared to the WPC-102 PCD, see Figure 4.48. This may be due to cutting temperature using the WPC-102 PCD being lower, however this needs to be further investigated. The use of laser scanning during milling to measure fuzzing and delamination factor can be used as an indirect method to evaluate tool wear. Delamination factor and fuzz length measurements are found in Appendix-G.

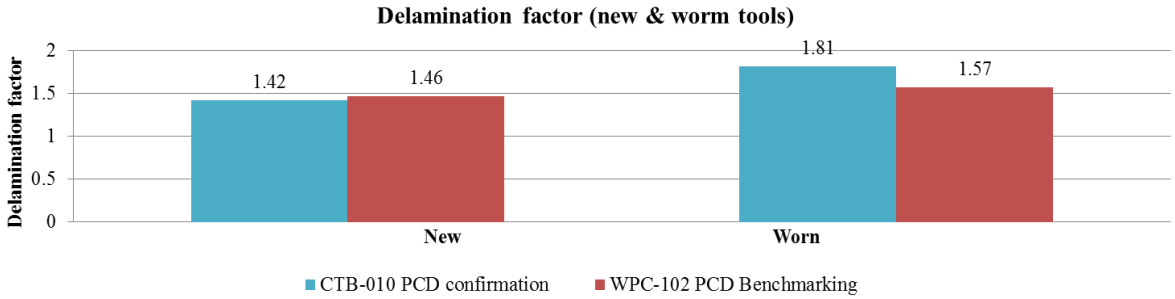

Figure 4.48: Delamination factor for different tools

To summarise the selection of which tool is best, the radar graph in Figure 4.49 sorts the tools on a scale of 1 to 2 (higher is better) based on their responses when these tools were new. The fabrication of the CTB-010 to such geometry may result in better performance provided that the edge is ground rather than wire cut. Poor slotting performance of WPC-102 PCD in most of the aspects exclude it from being used in slotting of CFRP composites.

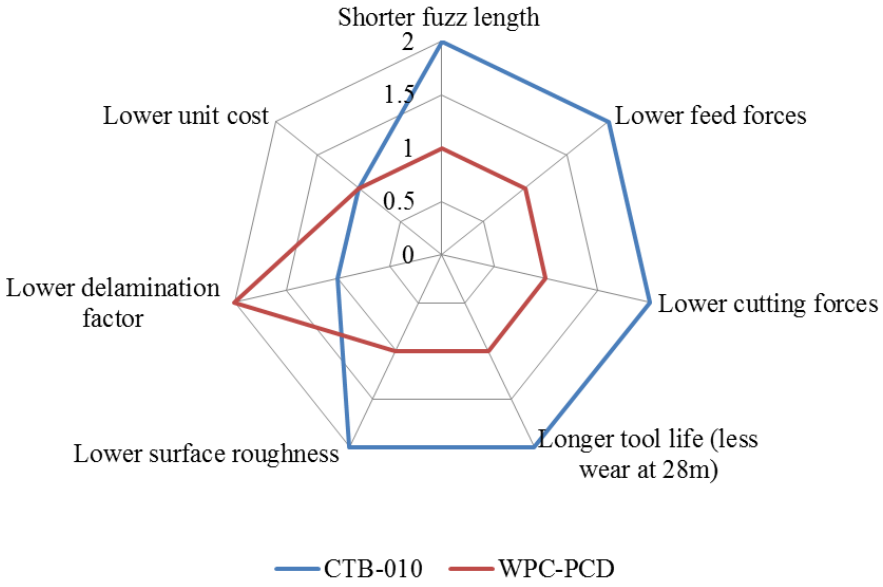

Figure 4.49: Performance of benchmarked tools in slotting

4.4 Phase-1D: Benchmarking of carbide tooling products

4.4.1 Two-fluted routers

Diamond-coated carbides can be better than polycrystalline diamond (PCD) being 30% lower in cost and easier to manufacture to complex geometries [41]. Dura coated WC was tested at 500 m/min cutting speed and 0.15 mm/tooth feed rate in chilled air environment and sustained severe tool wear in the form of breakage, spalling of Dura coat, and subsequent wear in the substrate which was also observed by Sheikh-Ahmad and Sridhar [158] in fluted tools and also by Lopez et al. [150] in burr tools. The Dura coated tool suffered from chipping of the brittle coating and chunks of coating removed by spalling and flacking of coating leaving an exposed substrate with wear beyond the tool life criteria (0.57 mm VB) as shown in Figure 4.50. Cutting forces were considerably high from first pass mainly due to excessive tool wear (1020 N Fx 1090 Fy) compared to only 600 N when the CTB-010 PCD router was worn (Test-11).

The breakage may be a result of the dynamic forces associated with the process caused by material inhomogeneity [22]. Intermittent cutting process with such fluctuating forces accelerates fatigue induced flaking of cutting tool coating [186]. Images of worn tools show severe wear where coating was removed by brittle fracture as a result of the high cutting forces measured under such high cutting speeds and feed rates.

There was no fuzz on the down milling side and although the tool sustained severe wear from first pass, the surface quality of the down milling side was not bad compared to PCD grades used in Phase-1 see Figure 4.51. A smooth surface with reasonable surface roughness 5.74 µm Sa 99.4 µm St was obtained possibly because of cutting characteristics of the CVD diamond. However the DURA coated tool can perform in a better way if lower cutting speed/ feed rate combination was used. The produced surface, for the unit tool cost, suggests that CVD diamond is the option for finishing. This test will be discussed again later in the following section.

From results of this test and also the results previously obtained in Phase-1, it was suggested to test different WC tools at low machining parameters combination (i.e 200 m/min cutting speed and 0.03 mm/tooth feed rate) in chilled air environment. Because of the tool performance exhibited at high cutting speeds or high feed rates depending on the costing type, the test entailed DLC coated, Dura-coated and uncoated WC. In such a case, the test was stopped at the point of initiation of major fuzz (~ 3 mm long uncut fibres on down milling side).

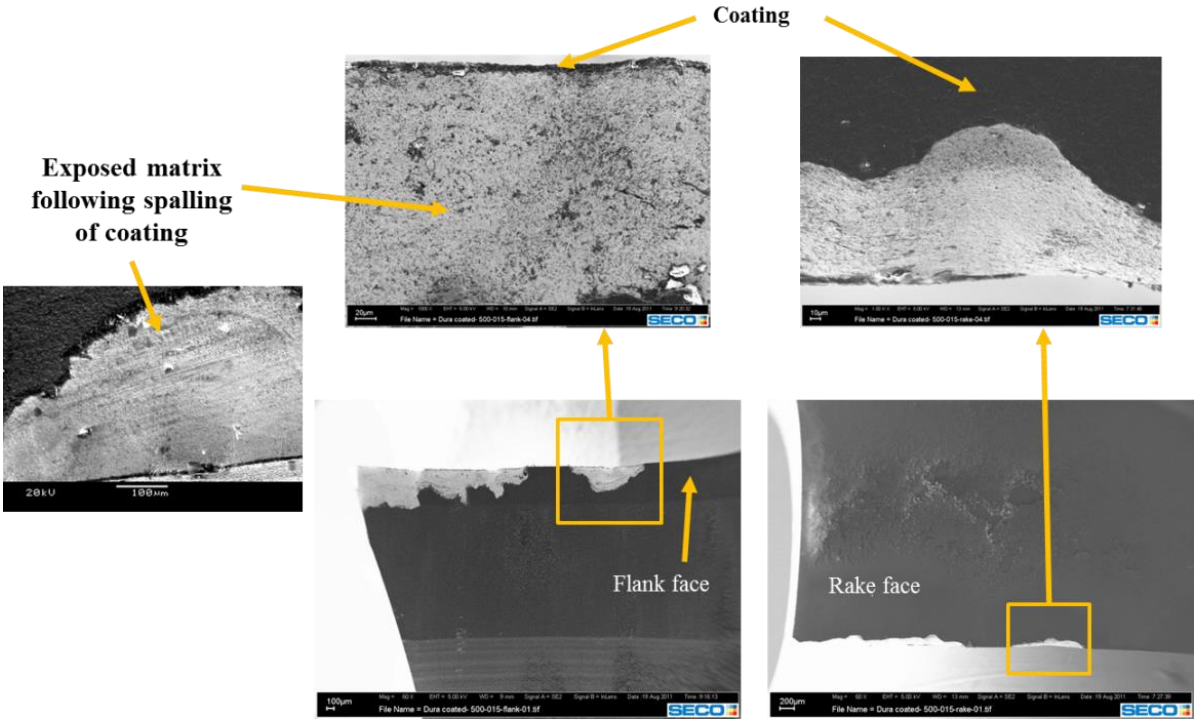

Figure 4.50: Severely worn Dura coated WC tools at 500 m/min, 0.15 mm/tooth, and chilled air after 100 mm cut length

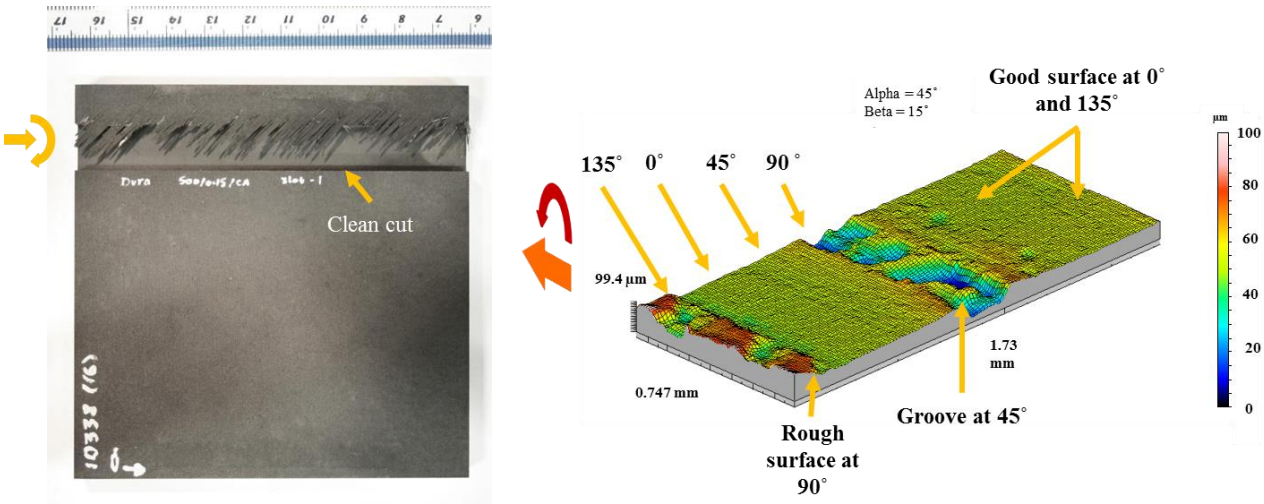

Figure 4.51: Surface quality following 100 mm cut length using Dura-coated WC at 500 m/min, 0.15 mm/tooth

4.4.1.1 Tool wear

The tool flank wear reached 0.1mm after a cut length < 100 mm (~ 90 mm). Abrasion wear was the dominant wear pattern in this case, see Figure 4.52 for the worn DLC coated tool.

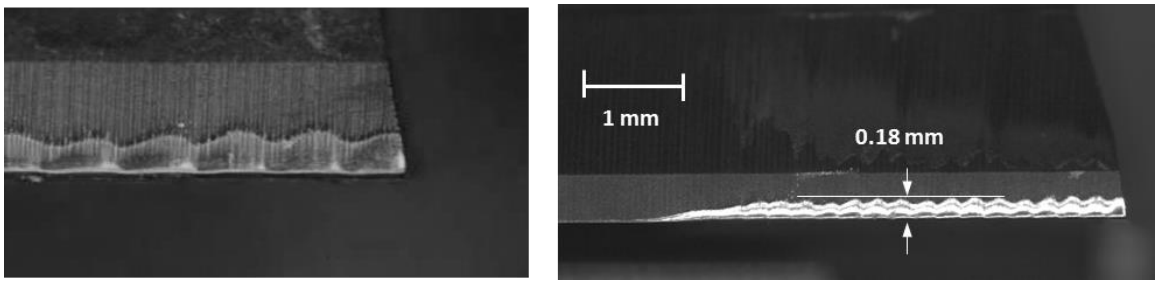

Figure 4.52: Edge of a worn DLC-coated tool following 300 cut length

The tool edge suffered from coating spalling and subsequent abrasion wear on substrate (0.22 mm VB following 8200 mm cut length) which may be due to abrasive carbon fibres brushing action plus being reacting with cobalt during machining which promoted shedding of the WC particles as explained by Masuda et al. [47], see Figure 4.53.

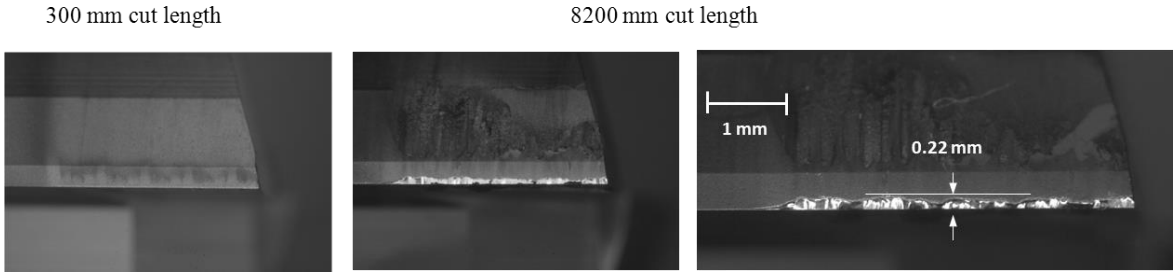

Figure 4.53: Worn Dura-coated WC tool edge following 300 mm cut length and 8200 mm cut length

The polycrystalline structure of the CVD diamond makes it tougher than the monocrystalline diamond (~5.5 compared to 3.4 MPa/m^2) [193]. The hardness of the CVD diamond (described as pure PCD) was even better than PCD because the later contains cobalt and porosity [194]. This may be the reason behind the extended tool life of the diamond coated tool although being used in harsh slotting operation.

When the uncoated WC tool was used, fuzzing started to occur on the up milling side after ~ 50 mm cut length. The cutting edge was worn quickly due to the absence of protective coating and exhibited serrations with equally spaced ridges (spaces equal to the ply thickness). The serrated edge valleys occurred due to the brushing action of the abrasive

carbon fibres while the peaks were located at ply/ply interface. Here the concentration of the fibres was less compared to the matrix [164] which made it the weakest point and prone to separation during cutting. The tool reached ~ 0.1 mm flank wear at ~ 270 mm cut length, see Figure 4.54.

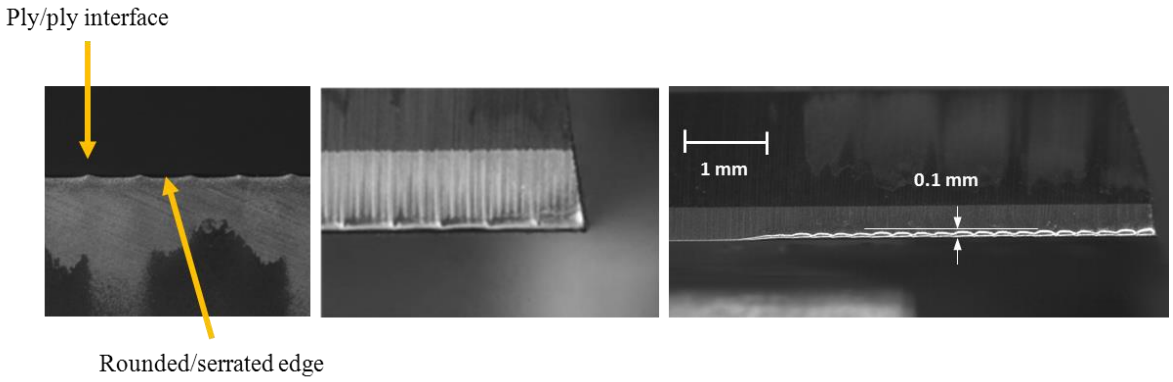

Figure 4.54: Worn uncoated WC tool following 300 mm cut length

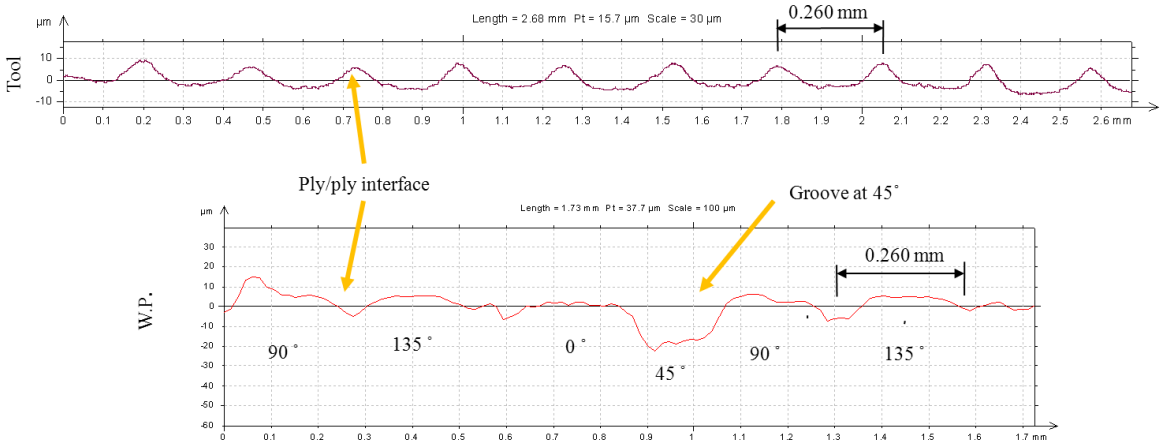

Figure 4.55: Profile of machined surface and worn/serrated edge of the uncoated tool

It should not be misunderstood from tool wear in Figure 4.53 that Dura sustained the highest wear as it performed 48 times better than DLC, and 16 times better than the uncoated (based on 0.1 mm flank wear criterion). Tool wear was plotted against cut length as shown in Figure 4.56. The tool wear rate of the diamond coated WC (Dura-coated) was the slowest but increased considerably following 4000 mm cut length which was the turning point where the tool started to lose coating rapidly and as a result of wear that started to make fuzz. The DLC-coated tool showed the lowest wear resistance because of wear occurring in both substrate and coating that made the worn part look larger.

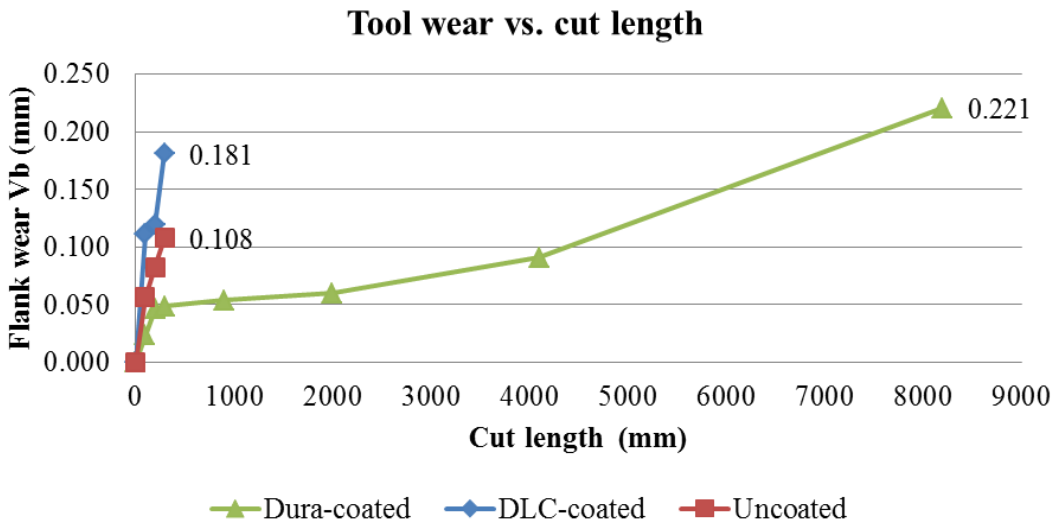

Figure 4.56: Tool wear vs. cut length for different WC tools, tool wear

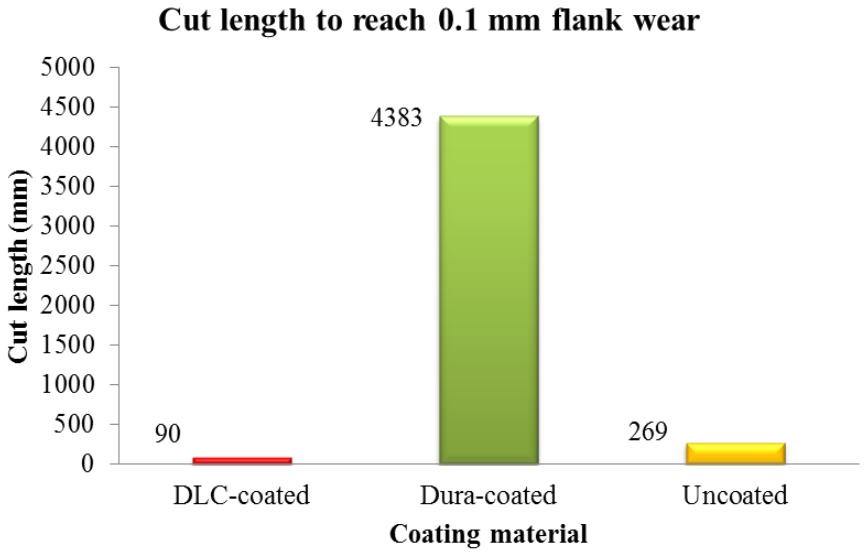

Figure 4.57: Tool wear vs. cut length for different WC tools, tool wear

SEM micrographs also revealed that the DLC-coated and the uncoated WC tools suffered from uniform abrasion wear with no signs of chipping. The uncoated tool was more serrated than the DLC-coated due to the lack of coating and also due to the sharp edge. Good adhesion (the ability of coating to remain attached to substrate under operating conditions) is vital [192].There was a transition zone between the substrate and coating in DLC which indicated that coating was removed by abrasion thus giving a good adhesion sign. Such transition zone

was also noted by Sheikh-Ahmad and Sridhar [158]. Generally, the substrate surface requires treatment because diamond prefers surface defects, humps (which etching will produce) as these provide anchoring sites on surface. Good adhesion permits predictable uniform abrasive wear [190, 191]. High CVD process temperature and mismatch of thermal expansion coefficients of CVD diamond coating and WC substrate (3.85 and 5.6 10^{-6}/°C) may cause the spalling of the coating [4, 191, 192]. In case of Dura-coated, the worn edge resembled a "bite in an ice-cream sandwich" where the brittle abrasion resistant coating was removed and subsequent brushing action from the fibres abraded the substrate leaving a concave surface with some marks from ply/ply interface as shown in Figure 4.58. Brushing marks and the concave surface may be an indicator of good abrasion resistance of the diamond coating.

A hand sketch of the worn edge showing the convex and concave surfaces generated by different wear patterns is shown in Figure 4.59. The tools' worn edges were also scanned using Alicona and the scan results conform to the expectations that Dura coated worn edge was concave while the others were convex. Horman et al. [159] compared between WC, CVD diamond, and PCD in edge trimming process. Accordingly, the tool life ratio was 1:10:15 respectively while the cost ratio was 1:7:13, which indicate the cost effectiveness of the CVD diamond. In this case the tool life and cost ratios were 1:6:104 and 1:2.3:4.2 for Un-coated WC, Dura-coated and PCD respectively based on 28000 mm cut length target despite the expectation that Dura coated would have performed better in edge trimming process rather than slotting with full engagement. The superior wear resistance of the CVD diamond may be caused by the crystalline tetrahedral sp3 covalent bond structure. DLC on the other hand contains less sp3 and a mixture of sp2/sp number within the structure which makes the structure amorphous [192]. Containing higher number of sp3 within structure may be the reason CVD diamond is better than the amorphous DLC coating in terms of abrasion resistance.

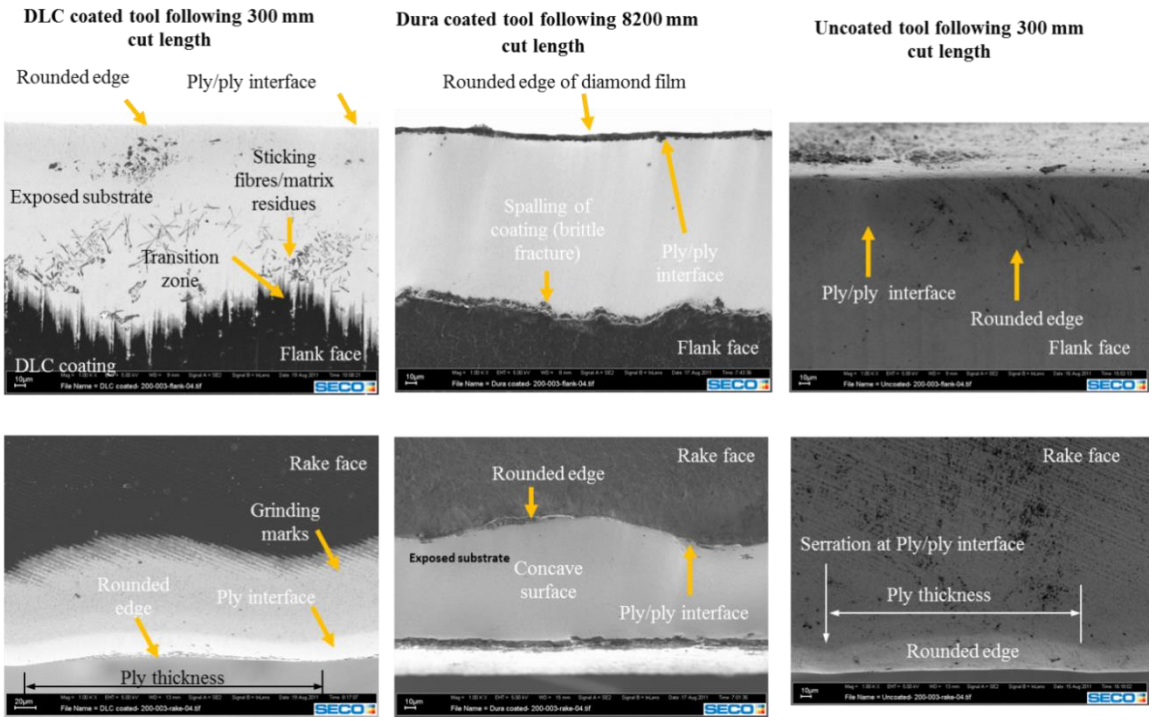

Figure 4.58: SEM micrographs of worn edges

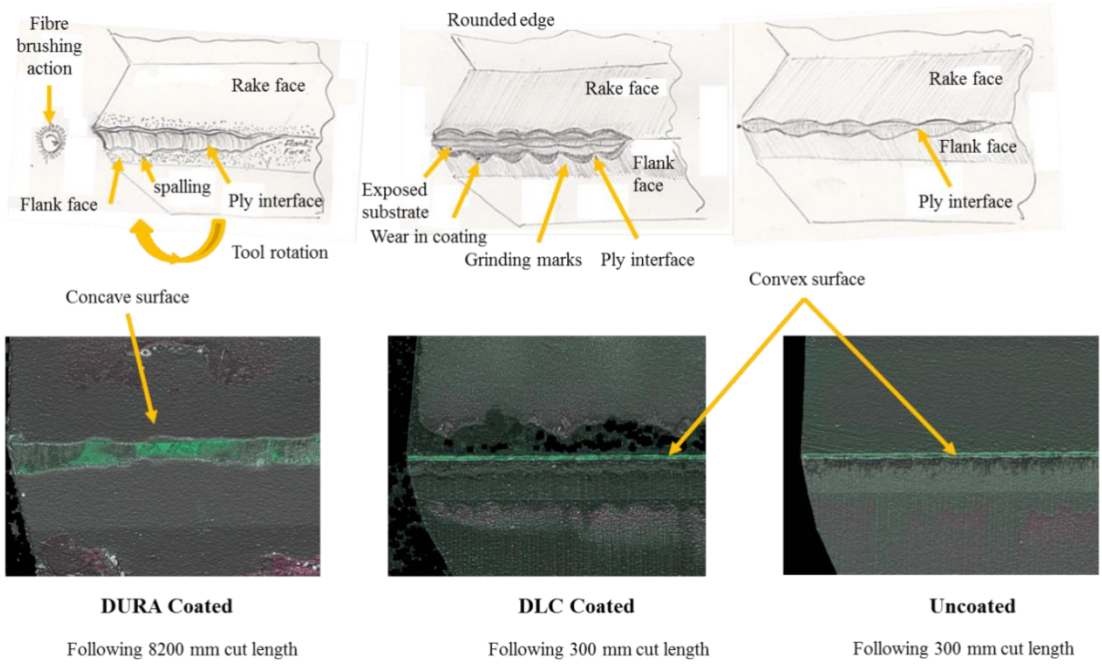

Figure 4.59: Alicona 3D surface vs. a hand sketch depicting different wear patterns

4.4.1.2 Cutting forces

Using DLC-coated tools, the cutting forces reached 310 N Fx and 320 N Fy when the tool finished only 300 mm cut length. The cutting forces using Dura-coated were the lowest. Additionally, the cutting forces using uncoated WC were the highest in comparison while the tool wear was lower than DLC-coated but serration and lack of coating may have contributed. In case of the Dura-coated, the cutting force trend was similar to the tool wear (increased gradually with cut length) as can be seen in Figure 4.60. The variation of the cutting forces may not only be because of the different cutting tool material or coating. The coating fabrication process itself may play a role in adding to the friction between the tool and workpiece. The cutting forces observed using the DLC coated may be because the diamond like carbon used was hydrogen free and removing hydrogen from the DLC coating was normally performed to increase tetrahedral Sp3 carbon structure [192]. The hydrogen free tetrahedral amorphous carbon (ta-C) was said to be better in terms of wear resistance than a-C:H but lowering hydrogen resulted in higher coefficient of friction [232] . Also the surface of the DLC coated tool appeared rougher and would be better if it was treated following the coating process to remove the droplets [187]. SEM micrographs of DLC and Dura coatings are shown in Figure 4.61 while surface topography of the different tools are shown in Figure 4.62. Added to the wear resistance of the diamond it has a low coefficient of friction from 0.05 to 0.1 [159].

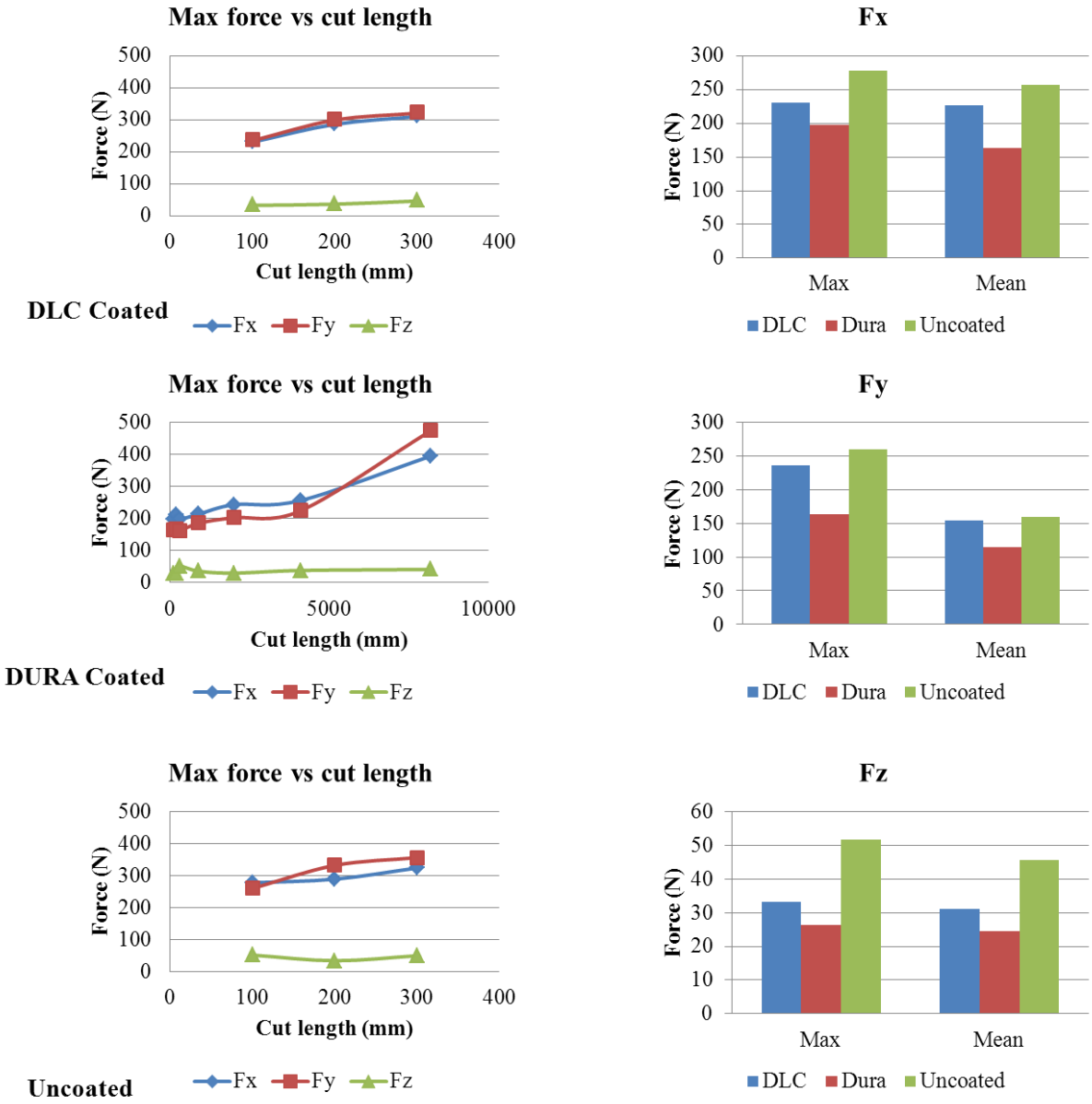

Figure 4.60: Cutting forces for different tools

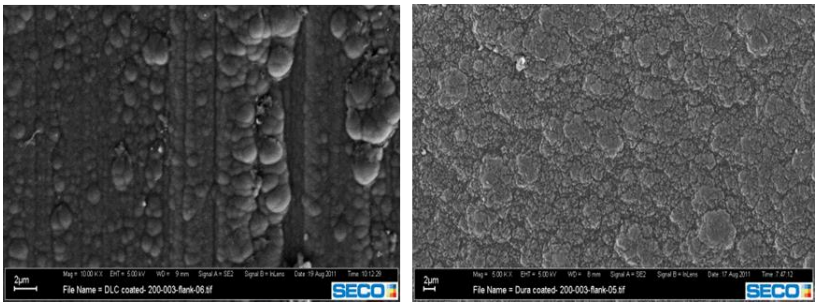

Figure 4.61: SEM micrographs of coating surfaces of DLC coating and Dura coating

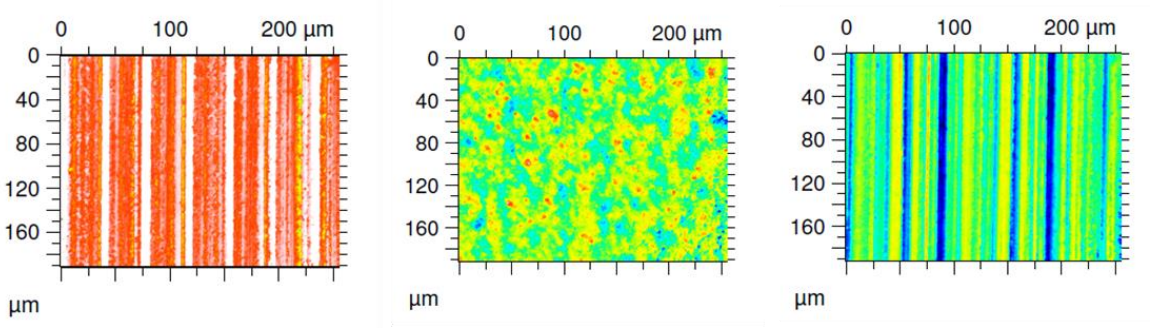

Figure 4.62: Surface topography and 3D roughness values for different WC tools

4.4.1.3 Surface integrity/roughness

The DLC-coated tools succeeded in cutting without fuzz in either sides of the slot for only 100 mm beyond which fuzz started to appear due to the rounding of the cutting edge as a result of tool wear. Following 200 mm cut length, fuzz started to appear in the down milling side (see Figure 4.63).

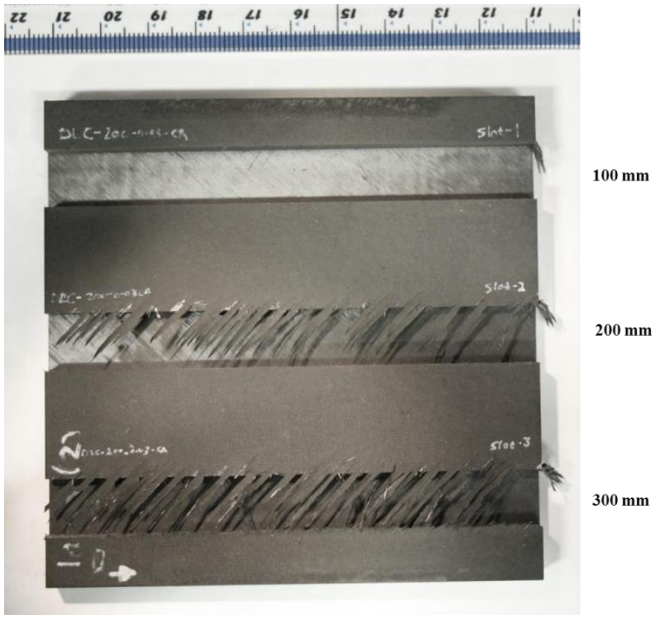

Figure 4.63: Slot quality using DLC-coated tool

Dura coated router, on the other hand, produced fuzz free slots until reaching a cut length of 4100 mm (0.09 mm VB) when fuzz occurred. Fuzz on down milling side occurred following 4400 mm (0.1 mm VB) but increased to become major fuzzing following ~ 8000 mm at the point where the test was stopped, see Figure 4.64.

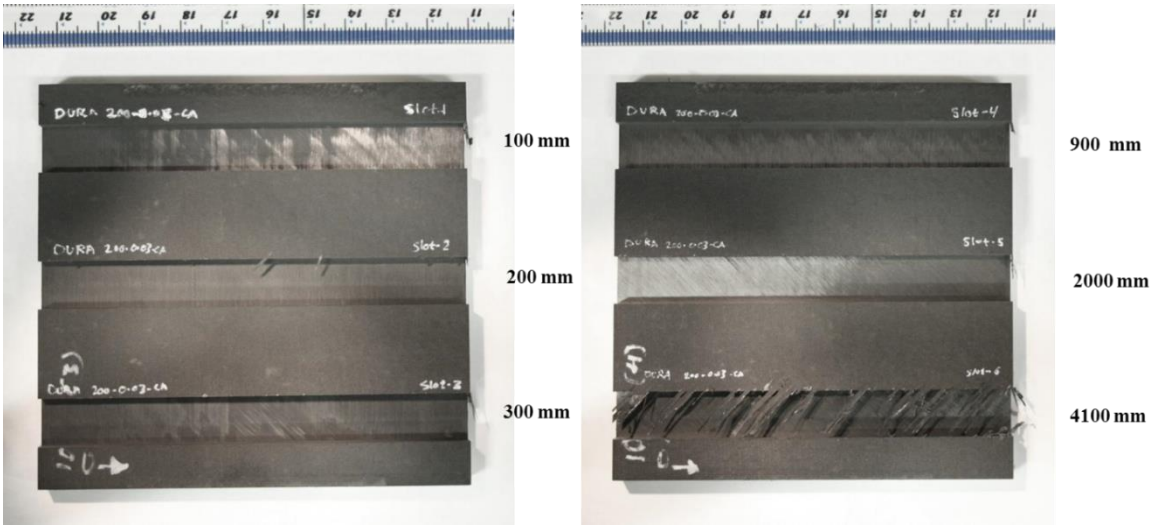

Figure 4.64: Slot quality using Dura-coated WC

Using the uncoated WC, significant fuzz in down milling side was produced during third pass (slot) because of edge rounding, test was then stopped, see Figure 4.65. As shown previously in Figure 4.55, the serration in the tool edge resembled the profile of the machined surface traversed.

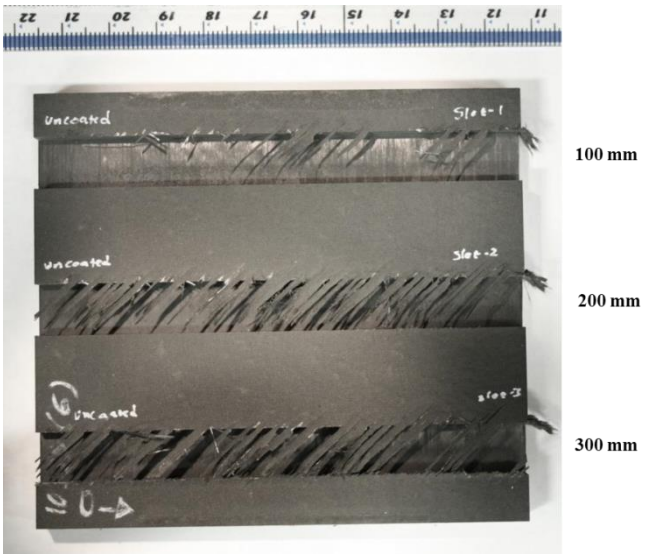

Figure 4.65: Slot quality using uncoated WC tool

Comparing the surface roughness of down milling side slot wall produced by the different WC tools, it was found that the uncoated tool produced the roughest surface followed by the DLC coated tool while the Dura coated produced the smoothest surface. The Dura coated benefited from the high abrasion resistance of the diamond coat which is actually a "pure

PCD" [4] i.e. diamond crystals with no binding cobalt which weakens the structure (and promote attrition wear Figure 4.66 shows the 3D surface topography and the values of Sa and St roughness parameters.

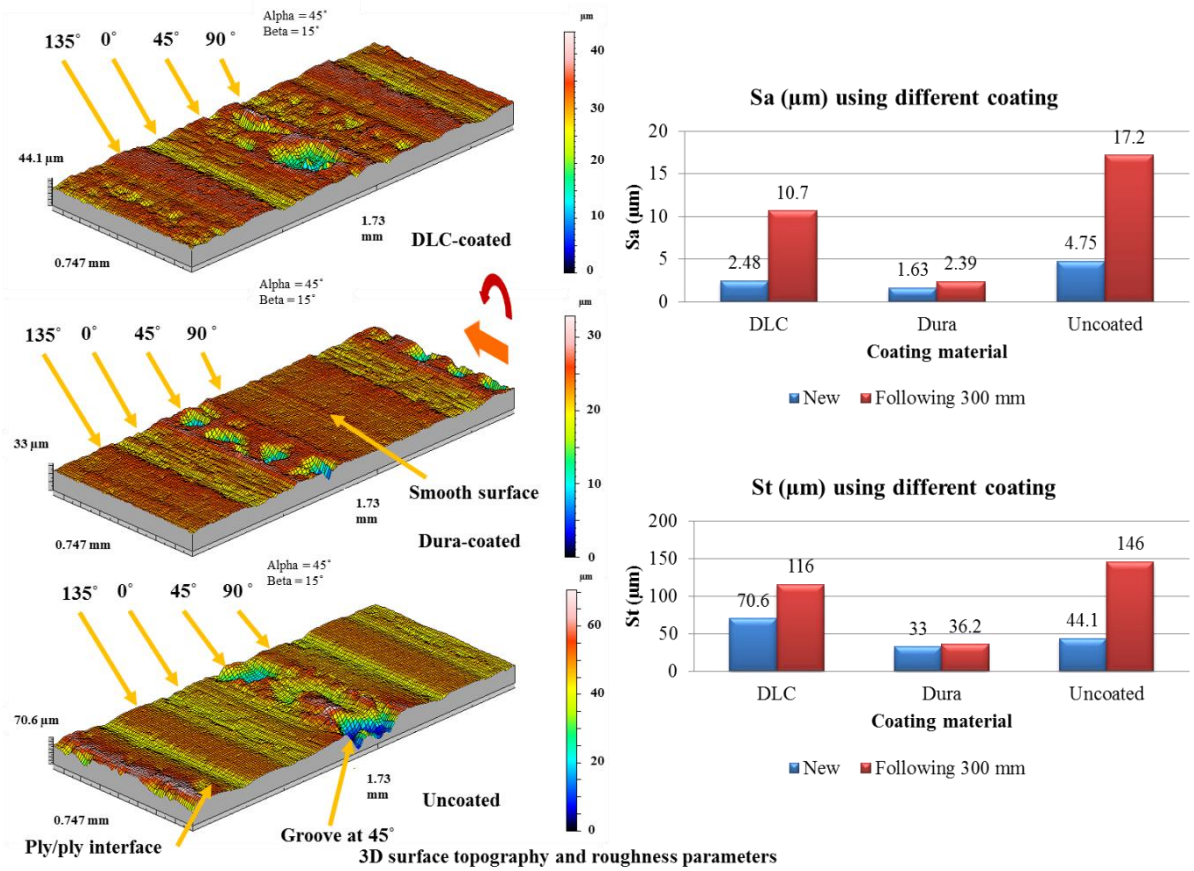

3D surface topography and roughness parameters

Figure 4.66: 3D surface topography and roughness parameters using Talysurf

The enhanced surface quality obtained using the CVD diamond and their wear pattern promoted by the high cutting forces in slotting operation suggested that the CVD coated tool was an ideal choice for finishing, at small radial depth of cut where the tool performed better in such condition. This agrees with the findings of Sheikh-Ahmad and Sridhar [158] who also concluded that CVD diamond was suitable for finishing.

Figure 4.67 shows the surface quality for the new tool compared to worn tool following only 300 mm cut length. Smooth surface using CVD diamond coated tool in comparison to rough and deteriorated surface in case of DLC coated and uncoated WC.

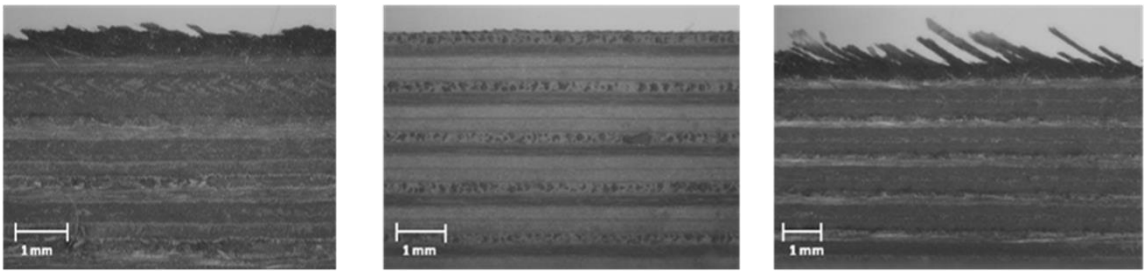

Figure 4.67: Optical microscope images of down milling side slot wall when tool was new and following 300mm cut length

Higher magnification SEM micrographs of the down milling side revealed high amount of damage in case of uncoated tool followed by DLC coated while best surface integrity was attributed to Dura coated tool, see Figure 4.68.

In case of DLC-coated tool, the cut at 0˚ and 135˚ was clean with visible ply interface between them and some matrix smeared on 135˚ layer. Some deep grooves were noticed at 45˚ ply as a result of the cutting mechanism of those fibres. Cracks and fibre pull out were seen on 90˚ as a result of high cutting forces. Signs of matrix smearing may be the reason behind the low surface roughness obtained. Using Dura-coated WC, the cut surface was clean and the difference between 90˚ and 135˚ was barely noticeable. Repetitive shallow pockets or grooves were left behind the tool when cutting 45˚, the pitch correspond to the feed per tooth, this was caused by the breakage of these fibre bands while flexed back by the retreating cutting edge. The Dura coated tool was capable of shearing the fibres without causing any pressure, this explains the relatively low cutting forces obtained.

On the other hand, the relatively high cutting forces using uncoated WC caused damage in 45˚ in the form of pushed back fibres, made grooves by fibre breakage and pull out and this is evidenced by the poor surface at these plies. Cracks in 90˚ plies were caused by the high pressure of the cutting edge on the plies which cause splitting and cracks within the matrix. Small pores were seen in this layer because of fibre pull out. The ply to ply interface which caused less wear on tool and resulted in serrated form of edge looks deeper than the slot wall surface. Bare fibres were seen at 0˚ plies.

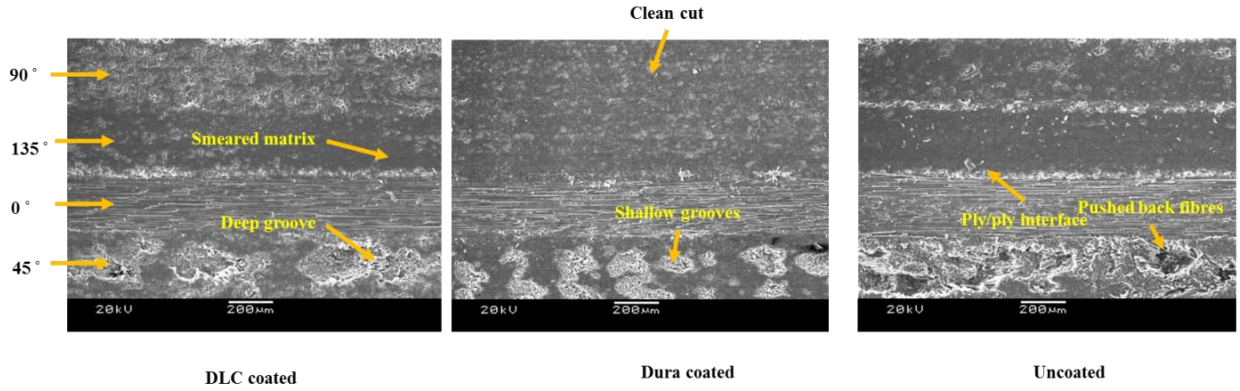

Figure 4.68: SEM micrographs of machined surface

The fabrication method, coating structure, and deposition method defined the tool surface smoothness. Comparing the surface roughness of the different versions of the WC tools, it was found that the uncoated tool surface had marks of abrasion tracks from the grinding process. The addition of coating layer did not mean that the surface was going to be smoother than the ground substrate. For example, the surface roughness of the DLC coated tool increased after coating as a result of the spattered PVD diamond like carbon coating droplets as shown earlier in Figure 4.61. In case of the CVD coating, the grown diamond crystals lower the surface roughness from ground substrate by ~ 22 % from 0.294 µm Sa to 0.230 µm Sa which may have contributed to the surface roughness and cutting forces.

Despite the higher roughness of the DLC coated tool, it produced better surface quality possibly due to enhanced tribological effect of the tool surface by the added coating layer compared to a bare WC with grinding marks. The DLC coating may have prevented the serration of the cutting edge compared to the uncoated tool. Alicona 3D scanned images of the down milling slot wall machined surface also reveal a lot about the quality characteristics of the surface, see Figure 4.69. Alicona 3D scans also revealed that the surface obtained using Dura coated possessed superior surface finish which was nearly twice as good as the recommended surface roughness by the manufacturer which was 3.2 µm Ra [142]. Generally, the surface roughness obtained using Alicona was up to 6 times higher than the Talysurf results especially in St peak-to valley roughness values possibly because Alicona uses non-contact optical technology which can measure narrow areas the stylus cannot reach. 3D surface topography of machined surface as well as surface roughness parameters obtained using different two fluted are shown in Figure 4.69.

Based on the observations described above a radar graph (Figure 4.70) can combine the results of the three router materials and compare them in order to facilitate the selection process for the application.

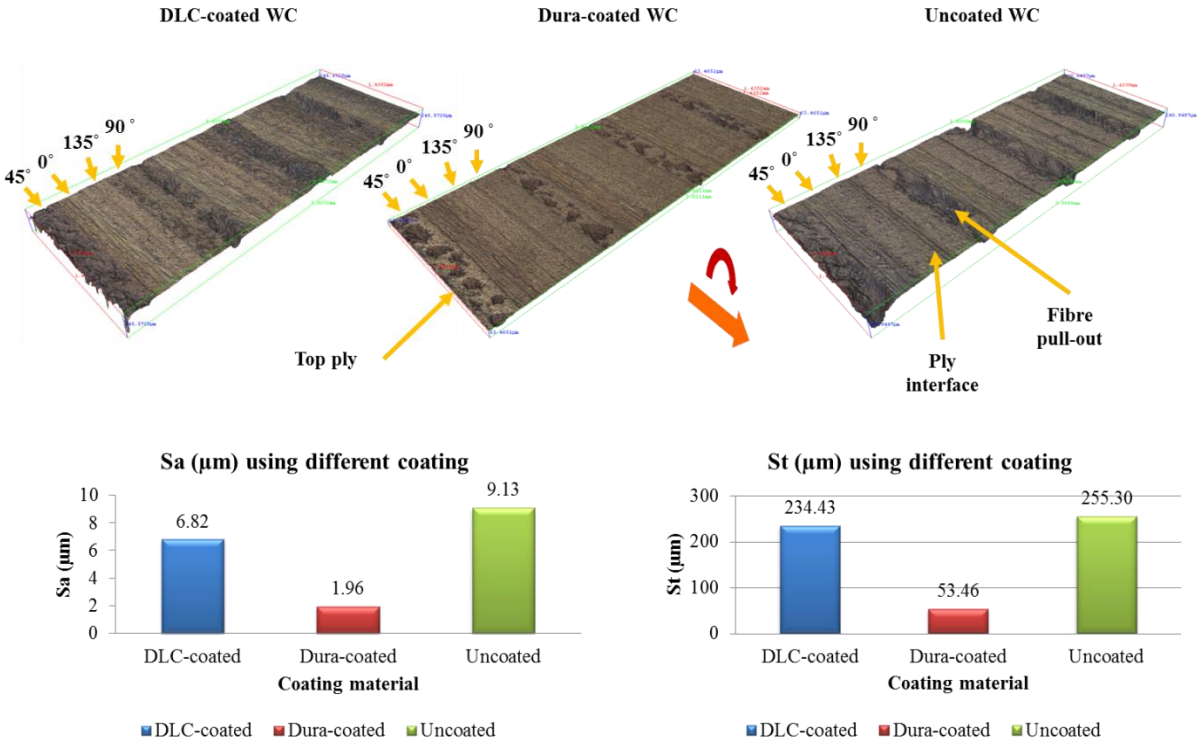

Figure 4.69: Alicona 3D scans of machined surface

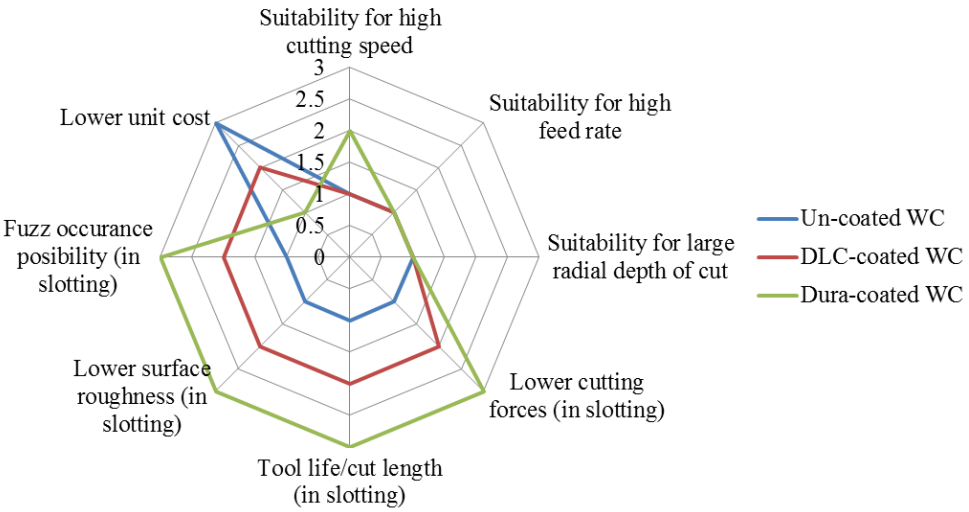

Figure 4.70: Router performance and suitability for the DLC-coated, Dura-coated and uncoated WC.

4.4.2 Burr routers

A variant of the WC tools namely Burr router was tested (uncoated and Dura coated) because of their reputation in cutting composites especially glass fibre but recently (Lacalle) noted their performance in cutting CFRP. The use of this 16 flute tool permitted an 8 times increase in productivity in terms of machining time at the same feed per tooth compared to the 2 flute version.

4.4.2.1 Tool wear

The uncoated tool sustained some marks of edge rounding; also the edge was serrated as shown in (Figure 4.71). The tool end was severely worn however such wear was not considered because of the application was mainly intended for separation of the excess material rather than actual slotting.

On the other hand, the coated Burr router sustained higher amount of tool wear in the form of breakage and spalling of the thick and brittle coating. The uncoated one was capable of cutting 28000 mm while the diamond coated one reached the criteria following only one pass, i.e. 100 mm cut length. In this case, the use of lower feed rate could be better for extended tool life. A WC carbide tool with up to 10% cobalt and with micro-grain fulfil the requirements for machining of CFRP composites [4]. However, the use of lower cobalt content may be advantageous [178].

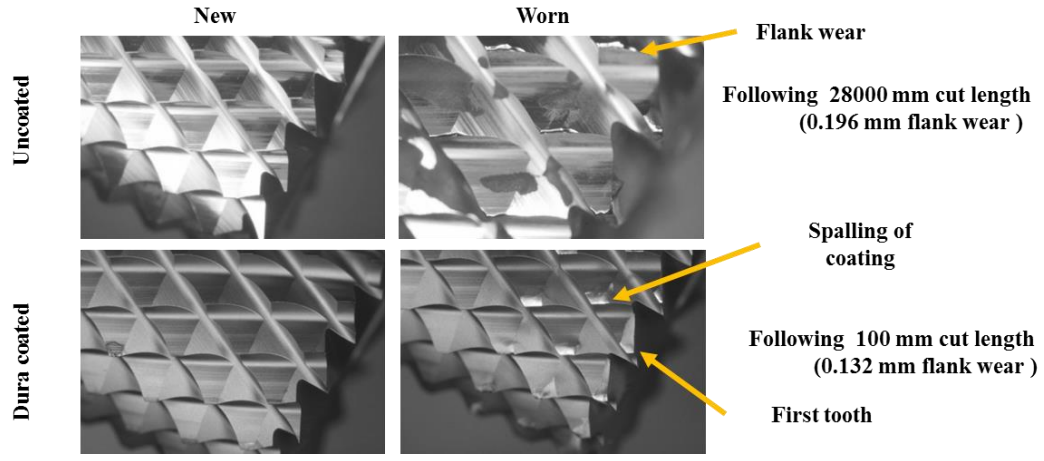

Figure 4.71: worn WC Burr tool

4.4.2.2 Cutting forces

The cutting process was accompanied with a whistle like noise. The tool geometry (helix) allowed cutting of the CFRP downwards. The axial force Fz was relatively high (~830-890N) compared to straight flutes in region of ~ 40N. The fluctuation in the axial force could be reduced if a full axial immersion was used instead of slotting. Cutting forces using 16 flute burr routers were higher than that of the 2 fluted tools because of the feed speed, see Figure 4.72 for first slot forces. Accordingly, it can be seen that the coated burr tool resulted in higher cutting force.

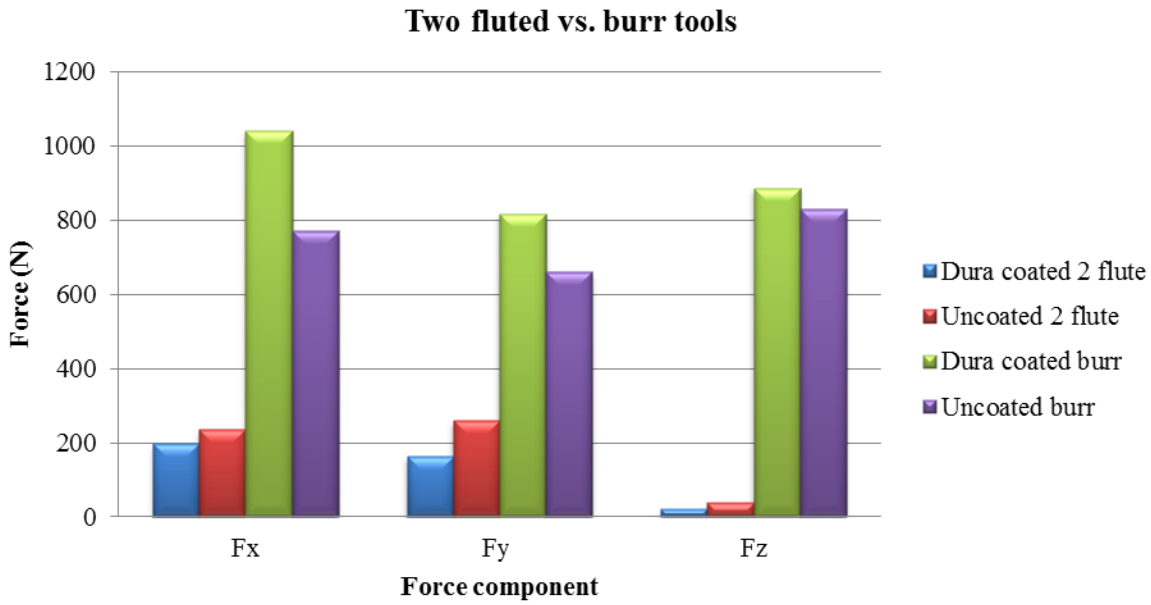

Figure 4.72: Cutting forces (2 fluted vs. burr routers)

4.4.2.3 Surface integrity/roughness

The uncoated burr router was capable of producing slots with no uncut fibre on neither up nor down milling side which makes the burr router flexible for use in any direction (up or down milling). The downward cutting action may have contributed to a clean cut without fuzz possibly due to tool leaving no chance for fibres to bend upwards and escape the cutting, see Figure 4.73.

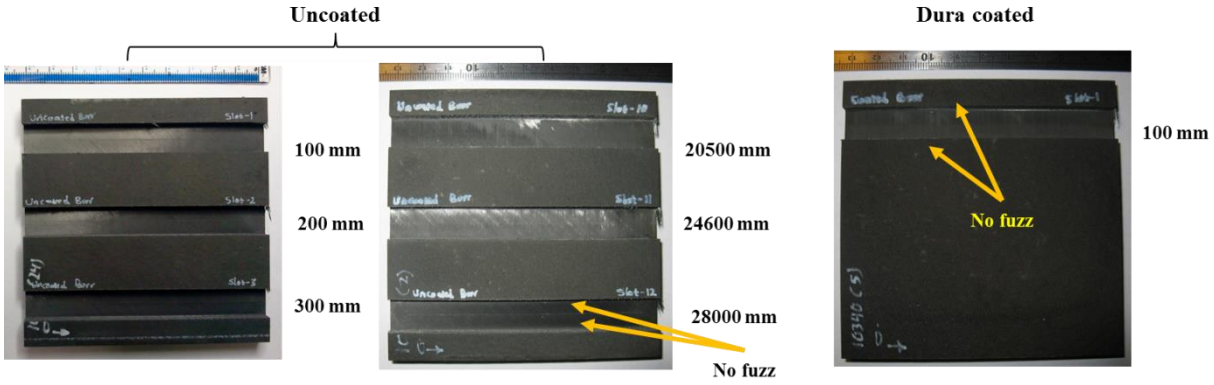

Figure 4.73: Slot quality for uncoated and coated burr type tools

The machined surface (i.e. slot wall) was very rough and it was difficult to identify the different layers. The quality of the surface obtained using coated was better than that of the uncoated as shown in Figure 4.74 which depicts the SEM micrograph and Figure 4.75 for the 3D surface scans. The surface scans show the saw like marks on the machined surface using the new uncoated tool where it is difficult to identify different layers. The worn burr router resulted in a surface with fibres pushed back where less shearing was taking place.. The high surface roughness of (24.3 µm Sa and 300.25 µm St when tool was new), and (22.62 µm Sa and 288.00 µm St when tool was worn) in case of uncoated tool with little variation in roughness parameters from new to worn condition suggest that the burr router is an ideal choice for roughing while a finishing pass at 0.3- 0.5 mm radial depth of cut using a 2 fluted Dura coated tool will be necessary to remove the wavy layer and to obtain reasonable surface quality which agrees with the recommended depth of cut by Richards et al. [142] for similar finishing pass for Airbus application. The surface obtained using the diamond coated burr router on the other hand exhibited. Using Dura coated burr type router, the surface was relatively better (14.2889 µm Sa and 168.6455 µm St), however the tool cost compared to the uncoated version did not justify the use of coated router for slotting added to the fact that a coated tool is relatively blunt compared to the uncoated [140]. A comparison between the two burr routers is shown in Figure 4.76.

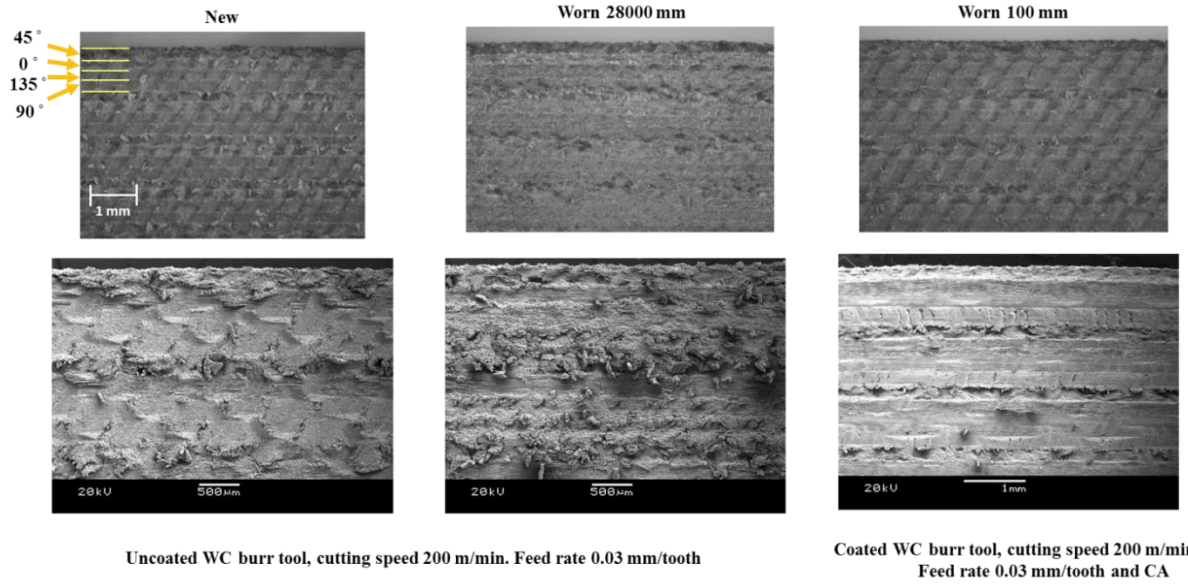

Figure 4.74: Optical tool maker's microscope images (up) and SEM images (down)

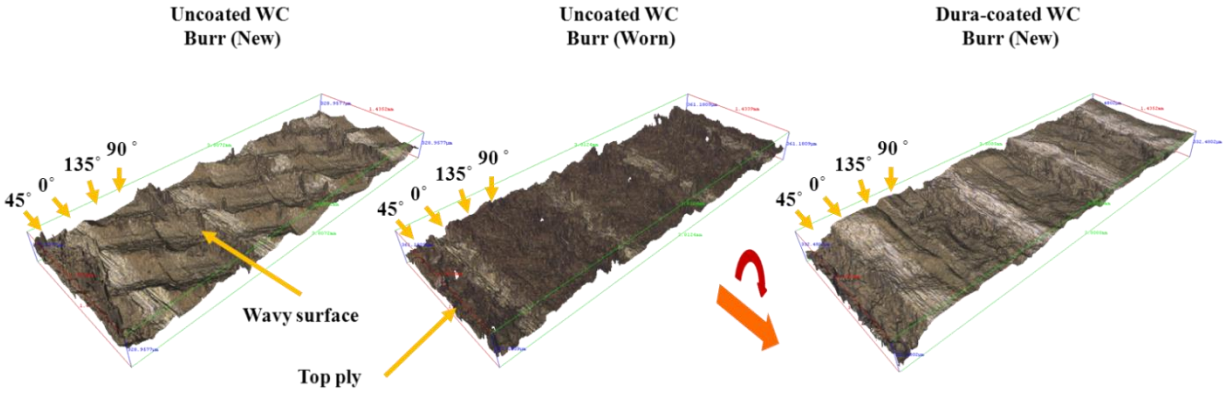

Figure 4.75: 3D surface scans using uncoated and Dura coated WC burr routers

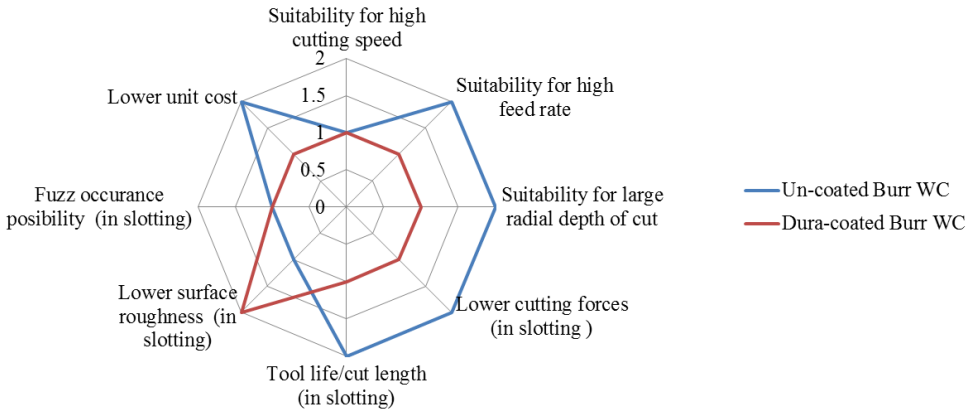

Figure 4.76: Router performance and suitability for the uncoated and Dura-coated WC Burr routers

4.5 Phase-2A: Preliminary testing and temperature measurement

4.5.1 Effect of workpiece lay-up on cutting force/surface integrity

4.5.1.1 Cutting forces

Although it is commonly known that 0° fibres are the easiest to cut, the cutting force component Fx in this case was the highest because the maximum cutting force is dependent on the orientation of the fibres at the point of maximum chip thickness (i.e. the middle of the slot) which in this case is 90°. In different cutting scenarios or different operations such as edge trimming the cutting forces may be lower because of the smaller radial depth of cut utilised. Feed force Fy was smaller in comparison such that it was nearly half of the Fx component, see Figure 4.77. The variation of forces with fibre angle showed a cyclic pattern similar to that described in orthogonal cutting by Bhatnagar et al. [22].

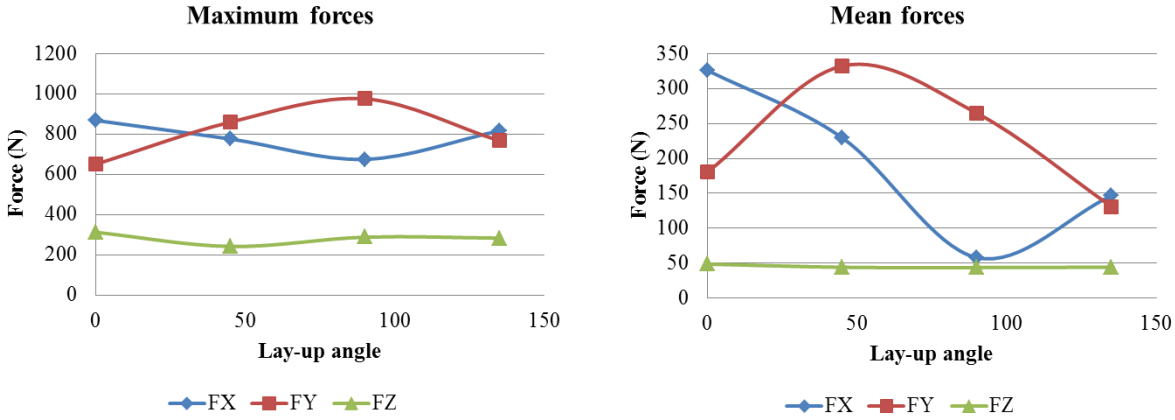

Figure 4.77: Cutting forces when slotting unidirectional laminates 500 m/min cutting speed, 0.15 mm/tooth feed rate, and using chilled air environment

Conversely, fibres at 90° orientation angle resulted in the lowest Fx force component despite the high feed force Fy . Similarly, this can be explained by the orientation at the middle with respect to the tool cutting direction which turns to be 0° which is easier to cut (due to the cutting mechanism) so it produced lower cutting forces but on the other side produced higher feed force Fy. The highest feed forces were recorded when slotting fibres at 45° orientation because the cutting direction was against the fibre orientation causing more compression and pressure on the tool. Lowest feed force Fy was attributed to 135° fibres, while Fz showed a decrease with the fibre, see Figure 4.78. The cutting force per ply was calculated using the maximum and mean forces assuming that a 5 mm slot included a number of 20 plies. These forces were used for force prediction discussed later.

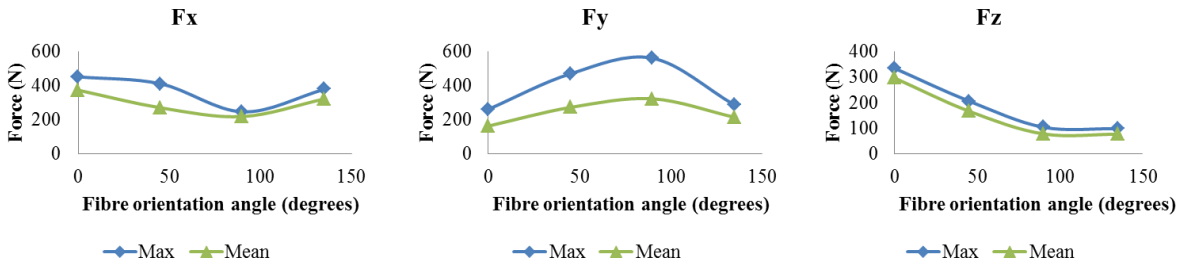

Figure 4.78: Forces when slotting different unidirectional laminates (200m/min, 0.03 mm/tooth) using ITC two fluted router

The cutting force Fx when cutting unidirectional laminates showed a similar trend to using 2 flutes tool (at same feed per tooth) but the feed force magnitude which was higher because of the higher feed speed in case of the 3 flutes tools. The relatively high cutting forces during slotting of 0° workpiece caused fracture of Exactaform Up-cut router. For example, at 90° the 2 fluted tools resulted in 500 N compared to 650 N in case of using neutral tools. The main cutting force Fx remained almost the same. Results shown in Figure 4.79 do not include the Up-cut router which was severely damaged during cutting of the 0° unidirectional laminate at Fx, Fy 554 and 348 N. Added to these high forces, the implanted thermocouple may have weakened the tool.

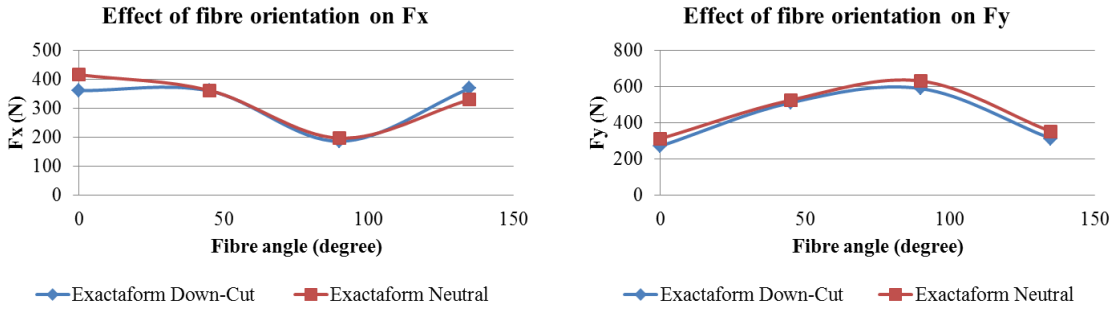

Figure 4.79: Fx and Fy when slotting unidirectional laminates using Exactaform Neutral and Down-cut.

4.5.1.2 Surface integrity

Slotting of the unidirectional laminates at 0° resulted in no fuzz either up or down milling sides. The fibres at 0° were easily removed by buckling resulting in no damage or delamination. On the other hand, fibres at 45° exhibited uncut fibres on up milling side because fibres in top plies of this orientation flexes away from cutting edge and escape the cutting and due to the tool being partially worn and rounded which increased the tendency to

such phenomenon. Fibres at 90° suffered from fuzz on both sides while fibres at 135° showed some fuzz on down milling side, see Figure 4.80. The results agree well with results obtained by Hintze et al. [171].

Surfaces generated (down milling only) using different unidirectional laminates are shown in Figure 4.81. The 0° exhibited the best surface with some bare fibres and some areas had sticking debris which were the ply/ply interface having higher concentration of resin. Wavy surface was generated in 45° fibres. Cracks and fibre pull-out were prominent in 90° fibres while 135° showed some signs of fibre pull-out.

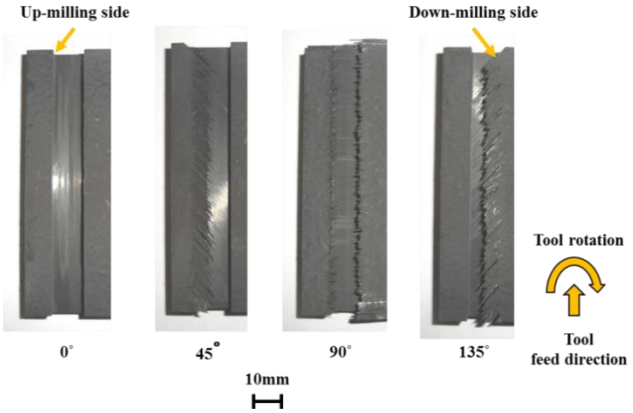

Figure 4.80: Slot quality when cutting slots in unidirectional laminates

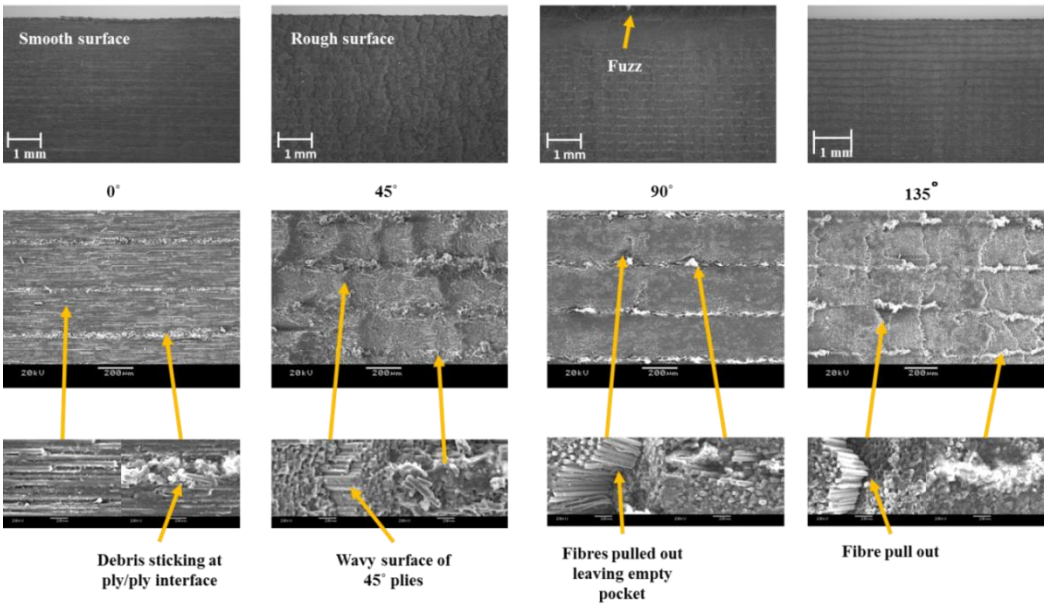

Figure 4.81: Machined surfaces obtained in different unidirectional laminates (down milling side) using ITC-PCD at 500 m/min cutting speed, 0.15 mm/tooth feed rate and CA (twin nozzle)

The 3D micrographs of the surfaces are shown in Figure 4.82. Surface roughness corresponded to a great extent with results of optical and SEM microscopy where 0° exhibited the lowest surface roughness with 1.59 µm Sa and 17.6 µm St, 45° fibres exhibited wavy surface and the highest surface roughness Sa 14.1 µm and St 91.1 µm. Fibres at 90° had a surface with 7.36 µm Sa and 75.7 µm St due to fibre pull out while the 135° with 3.79 µm Sa and 57.4 µm St. The surface roughness values (Sa) are plotted in Figure 4.83. The results are similar to results reported by Wang and Zhang [29].

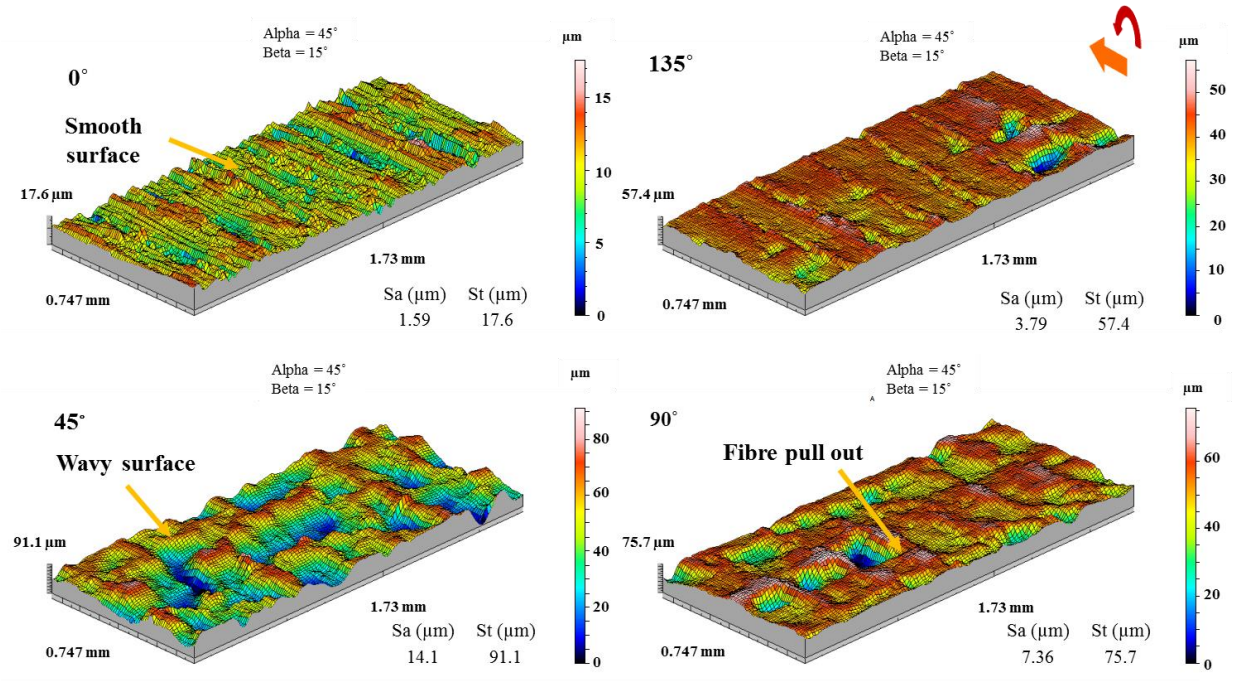

Figure 4.82: 3D surface topography obtained using ITC-PCD at 500 m/min cutting speed, 0.15 mm/tooth feed rate and twin-nozzle chilled air

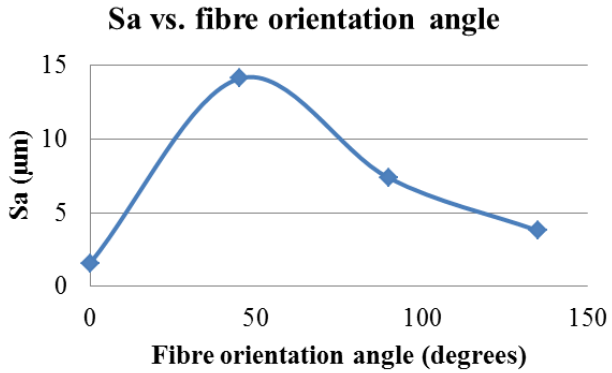

Figure 4.83: Values of surface roughness parameter Sa for different unidirectional layups

4.5.2 Effect of workpiece lay-up on temperature

4.5.2.1 Cutting forces

The main cutting forces Fx was the highest during cutting of Type-2 material which was obviously because the Type-2 lay-up contained larger number of 0° oriented plies in the layup (~ 8 layers) and obviously along the slot depth. Type-1 had the lowest Fx component be because the lay-up was balanced, See Table 4.6. The number was approximated assuming the ply thickness was 0.250 mm instead of 0.260 mm to simplify the calculations. Type-3 gave the second highest force Fx because it had 7 layers oriented at 135°.

Table 4.6: Number of plies in 5 mm slot

	Number of plies in 5 mm depth		
Ply angle	**Type-1**	**Type-2**	**Type-3**
0°	5	8	5
45°	5	5	5
90°	5	3	3
135°	5	4	7

The highest feed force Fy when slotting Type-1 can be explained by that Type-1 contained the highest number of 90° layers. Type-2 exhibited the lowest feed force because it had the largest number of 0° fibres in the lay-up. The force component Fz showed a response trend similar to Fx.

In cutting force modelling approach by Sheikh Ahmad et al they managed to predict cutting forces by summation of forces at different fibre orientations [173, 174, 181] and it was also noted by Wang et al [24] that forces in orthogonal cutting of multi-directional laminates was nearly the summation of forces from individual ply forces. Similarly but on experimental basis in slotting, it was possible to calculate the mean cutting force Fxmean when slotting different types of material using the force per ply and the number of different plies within the slot depth. The results of the calculated and the experimentally measured mean forces are shown in Table 4.7. Calculation of the maximum force was done by adding the (Max-mean) force per ply to the calculated mean force.

Table 4.7: Experimental vs. calculated forces (using ITC at 200m/min, 0.03 mm/tooth, CA)

		Type-1	Type-2	Type-3
Ply angle	**(Fx_{max}-Fx_{mean})/ply**	**Fx_{max} calculated (N)**		
0°	17.02	272.28	292.30	280.48
45°	15.37	**Experimental Fx_{max} (N)**		
90°	8.98	252	285	249
135°	13.08	**% variation**		
		8.04	2.56	12.64

4.5.2.2 Surface integrity/roughness

Despite that the ITC-PCD tool was partially worn, the top ply did not exhibit any fuzzing when slotting the three lay-up configurations on either up milling or down milling sides. Only minor fuzzing at tool entry and exit which was normal to the slotting process. See Figure 4.84.

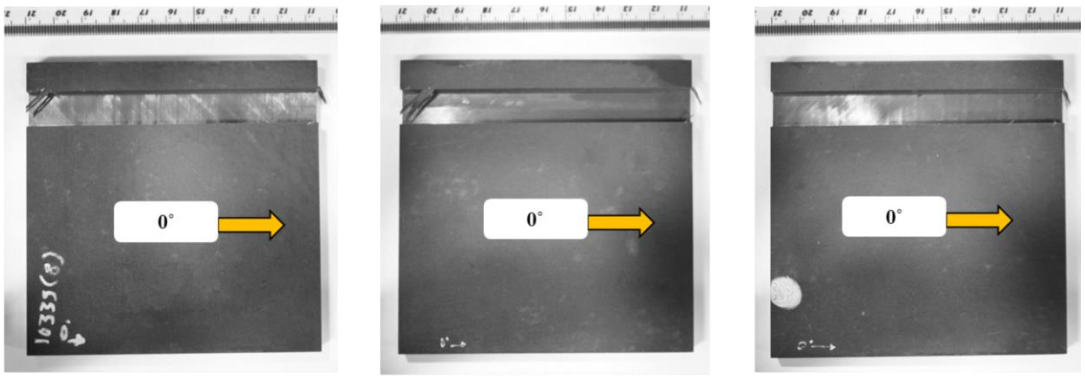

Figure 4.84: Slot quality when slotting Type-1, Type-2 and Type-3 laminates

The machined surface (down milling side) showed that the damage is concentrated in the 45° plies in form of grooves from pulled out fibres. Some fibres were also bent over (Type-3). Matrix smearing was evident in 135° and 90 plies and loose fibres were observed in 0° fibres as shown in Figure 4.85.

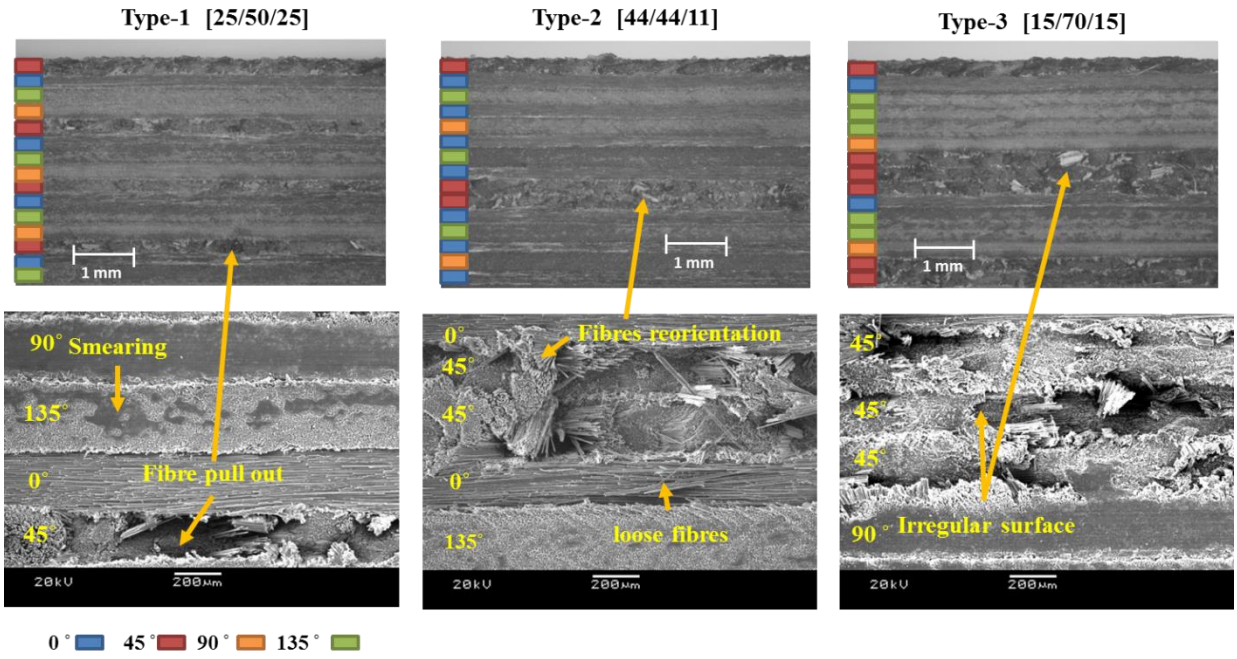

Figure 4.85: Machined surface (down milling side) Type-1, Type-2, and Type-3 (ITC-PCD 200 m/min 0.03 mm/tooth CA)

It was noted by that surface profile is dependent on fibre orientation and periodic damage zones in multilayer laminates [24, 164]. The surface roughness was also dependent on the number of plies and also on the different ply orientation traversed by the stylus during the surface roughness measurement. The lowest surface roughness was attributed to Type-2 (Sa 2.4 µm) because it had larger number of 0° layers in the lay-up as well as in the traversed area. Type-3 was the highest in surface roughness because it had higher concentration of 45° and few of them were adjacent to each other making a wider area of damage and wavy surface. See Figure 4.86 for the 3D surface topography.

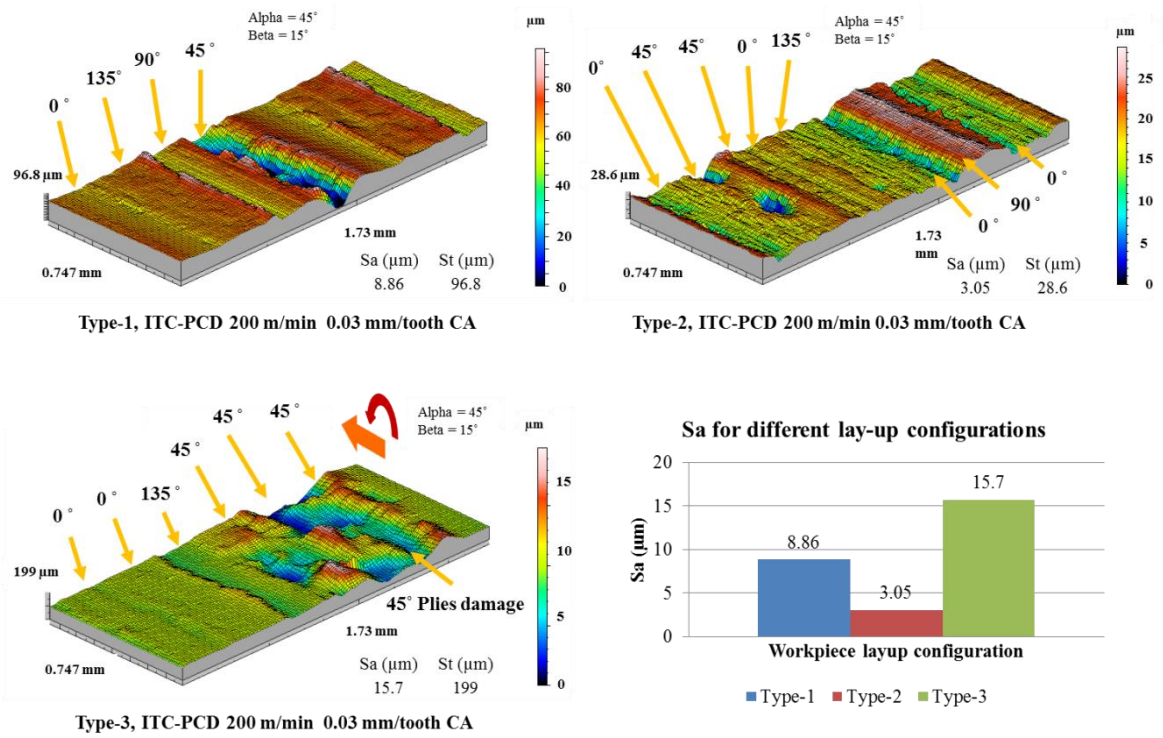

Figure 4.86: 3D surface topography of the down milling side of slots in Type-1, Type-2 and Type-3 (Talysurf)

Comparing the results obtained from the Talysurf with the results obtained using Alicona (for the same surfaces), the Alicona roughness were higher than Talysurf due to the high accuracy of the variable focus optical system which was capable of scanning deep and narrow areas the stylus could not traverse. The results show that the surfaces on the up milling side were better than the down milling possibly due to the low cutting edge temperature at the tool entry (within one complete revolution of the tool) such that there was reduction in Sa values by ~ 70% in Type-1, 73% in Type-2 and 75% in Type-3, see Figure 4.87. In edge trimming operation, Prashanth et al. [162] and Konig et al. [233] observed better surface roughness on up milling side but the observation of the present study does not agree that up milling side possesses better delamination/fuzz response than down milling. This suggested that up milling should be adopted for any finishing pass for better quality. There were no feed marks on the surface possibly because a worn tool stabilised and reduced vibration in cutting as if a virtual primary relief was created by abrasion.

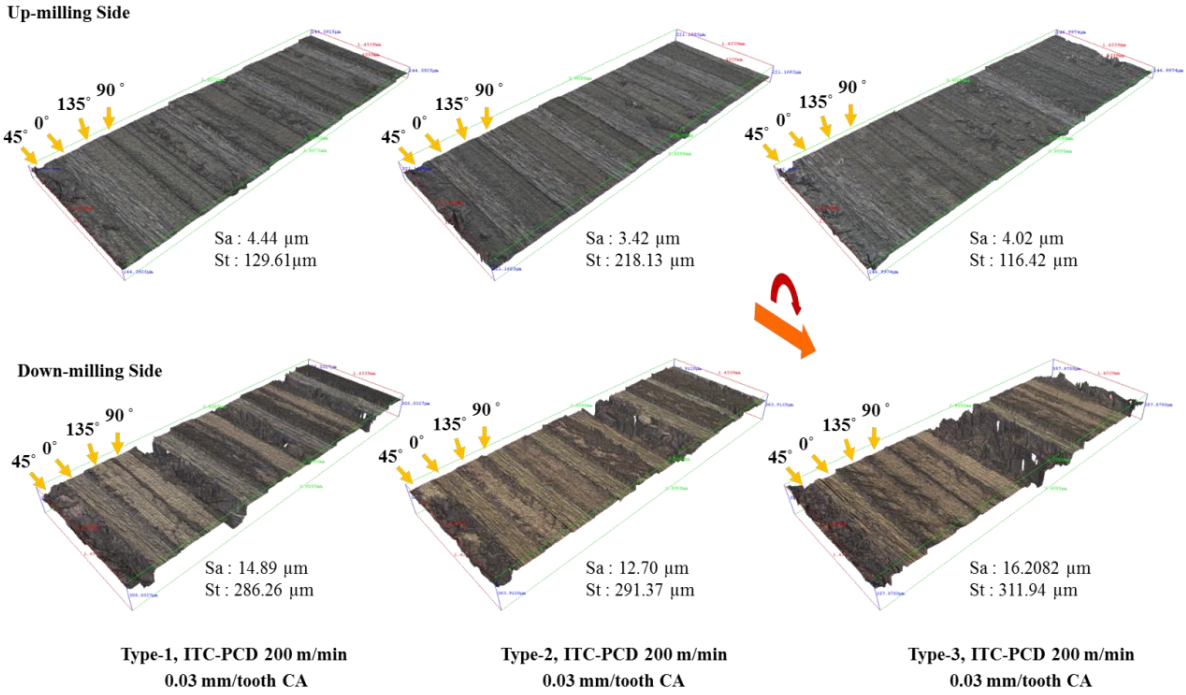

Figure 4.87: 3D surface of the up and down milling side of slots in Type-1, Type-2 and Type-3 (Alicona)

4.5.2.3 Cutting temperature

Temperature measurements (Figure 4.88) show that temperature when cutting 135° fibres was the lowest followed by 0° laminates. This could be due to the friction between tool and those layers were lower. The highest temperature was attributed to the 45° fibres followed by 90°.This implies that 45° is the most difficult layer to cut in terms of both forces and temperature and this explains the severity of the damage of those layers. The use of emulsion coolant was reported by Mondelin et al. [131] to reduce the coefficient of friction between diamond and CFRP from 0.06 to 0.02. However, for this aerospace applications the use of liquid coolant should be avoided for the absorption concerns.

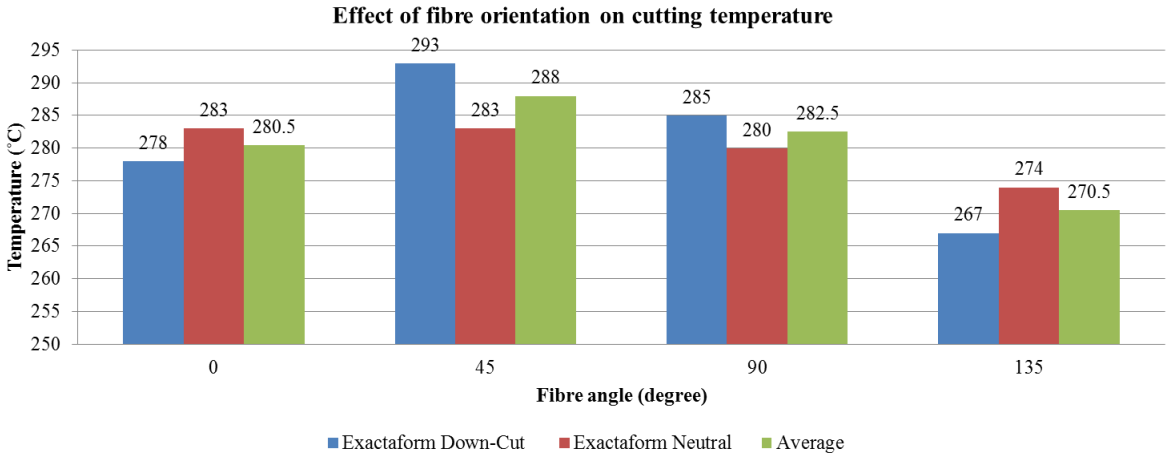

Figure 4.88: Temperature measured when slotting unidirectional laminates (200 m/min cutting speed, 0.03 mm/tooth and Twin-Nozzle CA)

Comparing cutting temperature when slotting laminates of Type-1, Type-2 and Type-3 materials, using the Neutral tool, the temperature when cutting Type-1 was the lowest ~ 242 °C. The cutting temperature when slotting Type-2 material was the highest (271°C) while Type-3 temperature was slightly below Type-2. However, on average, Type-3 produced the highest temperature followed by Type-2 and the lowest was Type-1. In case of a tool with helix the cutting temperature was lower because of the longer edge and lower heat per unit length as explained by Sasahara et al [182]. The reduction was from ~5 % (Type-3) to 8 % (Type-1and 2) in case of using Exactaform Down-cut and (from 2.5 % (Type-3 to 4 % (Type-1 and 2) in case of Exactaform Up-cut. Down-cut generally produced lower temperature while neutral produced 270°C, see Figure 4.89.

On average, the cutting temperature can be ranked as Type-1 (253 °C), Type-2 (261 °C) and Type-3 (263 °C) from low to high. This was also the same order obtained by the Up-cut and Down-Cut routers. In milling of CFRP, the temperature lies in the middle between tempreature normally generated in cutting Titanium ~ 600 °C and cutting Aluminum ~150 °C. These temperature values for Al and Ti were obtained by Coz et al [205] in drilling of stacks using a similar measuring system.

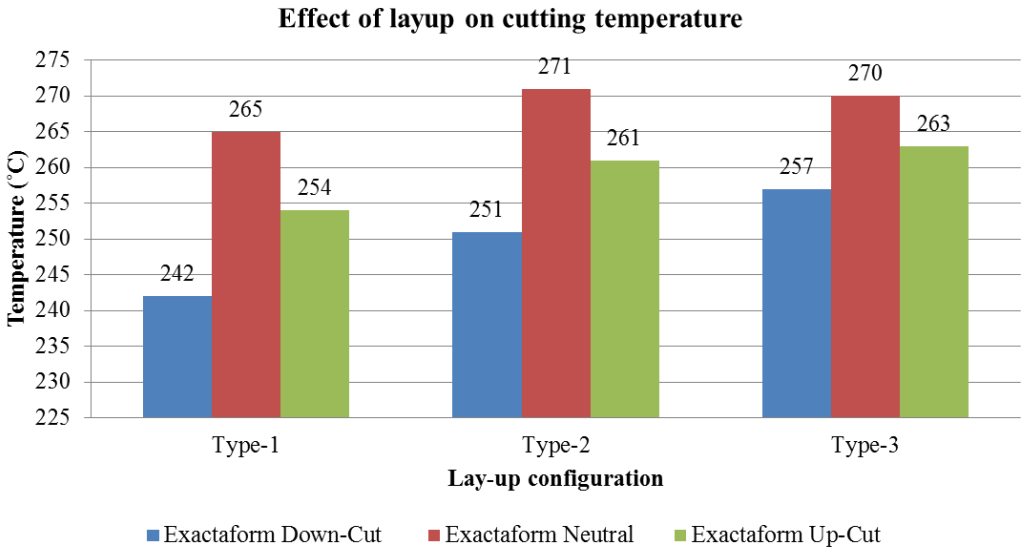

Figure 4.89: Temperature measured when slotting Type-1, Type-2 and Type-3 laminates (200 m/min 0.03 mm/tooth, Twin-Nozzle CA)

Dry environment was ~100 °C higher than chilled air while the heating and cooling rate varied, see Figure 4.90 and Figure 4.91. It was necessary to carry out a continuous cut of 5000 mm using tool life coupon to mimic the real production process, see temperature profile Figure 4.92. It was found that the single nozzle chilled air outperformed the twin nozzle. The worst case was the dry cutting environment which caused burning of dust and melting of the thermocouple braze. It was observed that the temperature increased rapidly in the beginning of the cut then remained almost the same level with very slow growth. Cutting temperature when machining ¾ coupons was found 85% of the temperature of the slotting. This means the temperature in real continuous slotting would definitely be higher when cutting was continuous. It was observed that during the up milling pass the peak temperature was lower than that of the down milling pass, which was also reported by Sato et al. [234].

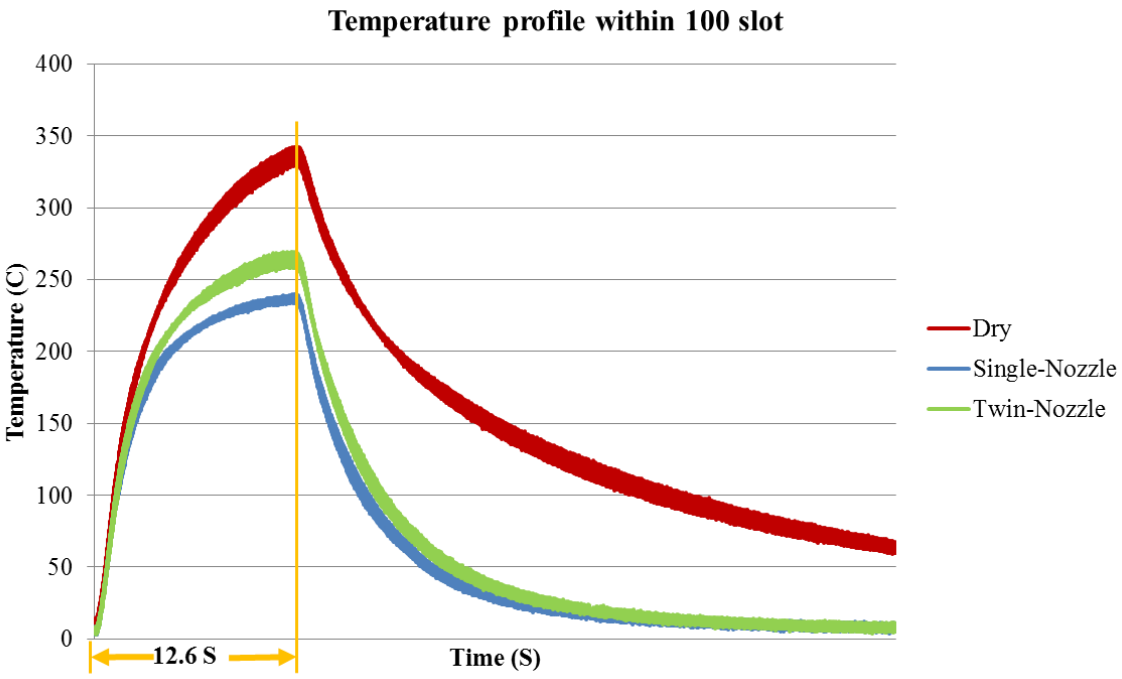

Figure 4.90: Temperature profile when slotting a 100mm slot (12.6 S) at 200 m/min cutting speed, 0.03 mm/tooth feed rate using Exactaform 3-fluted PCD router

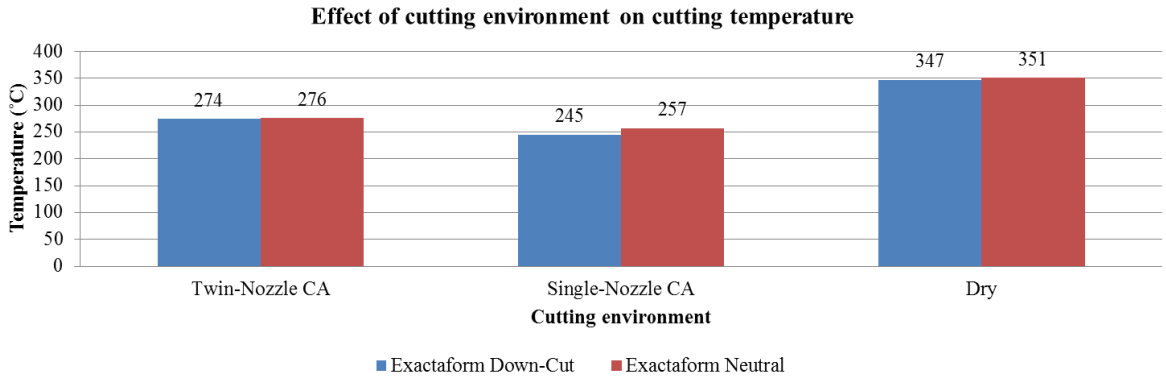

Figure 4.91: Slotting temperature when using single nozzle, twin nozzle, and dry environment (200 m/min, 0.03 mm/tooth)

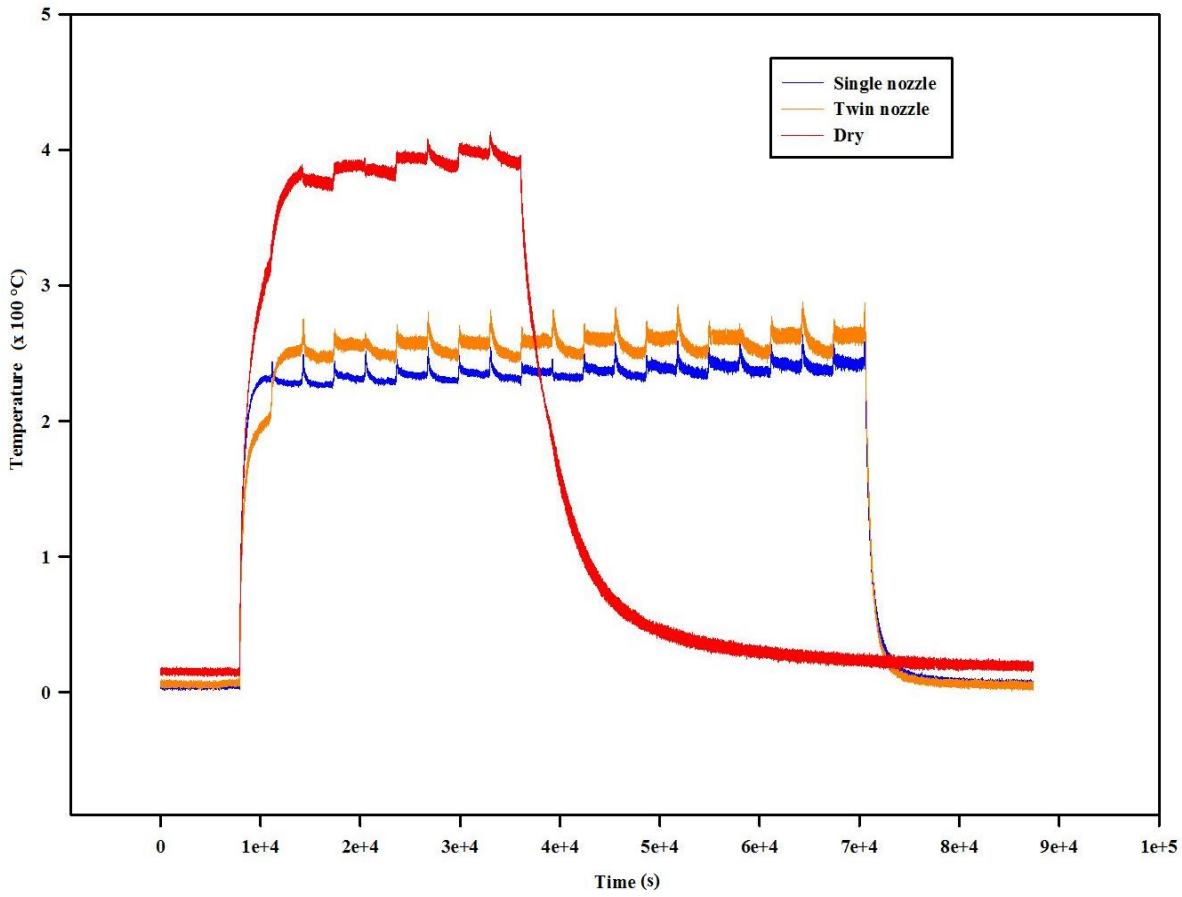

Figure 4.92: Temperature profile using Dry, Single-Nozzle CA and Twin-Nozzle in a continuous cut (200 m/min cutting speed, 0.03 mm/tooth feed rate in Type-3 material configuration.

The single nozzle chilled air resulted in lower cutting temperature (20°C) because the air temperature in this case was ~ 2°C compared to ~ 5°C in case of double nozzle. The flow rate and air speed also played a role in cooling efficiency such that the air speed using single nozzle was almost twice the speed of the double nozzle (~ 29 m/s and ~17 m/s respectively). The higher flow rate enables the quicker evacuation of the dust from the cutting zone. Since single nozzle was lower in temperature it was decided to perform mainstream Phase-2 testing using single nozzle chilled air.

4.6 Phase-2B: Effect of workpiece material lay-up configuration

4.6.1 Tool life/cut length

The cut length results obtained using different combinations are shown in Figure 4.93. Although tools were able to cut longer the tool life was limited by the chipping such that the statistical analysis was carried out taking chipping into consideration as an end of life criteria.

Main effects plot (Figure 4.94) shows that cutting speed and feed rate have almost the same effect on tool life. Increasing the cutting speed at the same feed rate did not cause a great variation in the abrasion wear such that tool sustained 0.09 mm flank wear in Test-1 compared to 0.088 mm flank wear in Test-7 following 28000 mm cut length with a light reduction. The feed rate had a higher contribution ratio compared to cutting speed (8% compared to 0.6%) due to effect of feed rate on chipping of the cutting edge. For example increasing the cutting speed in Test-7 also caused chipping at 900 mm cut length due to the increase in feed speed. On the other hand when the feed rate was increased, the amount of chipping on the cutting edge increased due to the increase in the cutting forces, see Figure 4.95. Percentage contribution (PCR) and ANOVA are shown in Table 4.8.

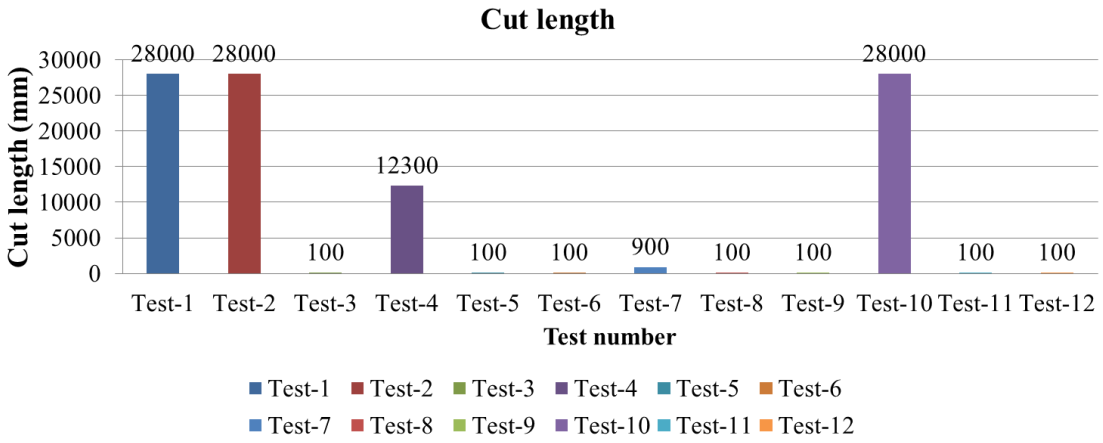

Figure 4.93: Cut length achieved in all tests

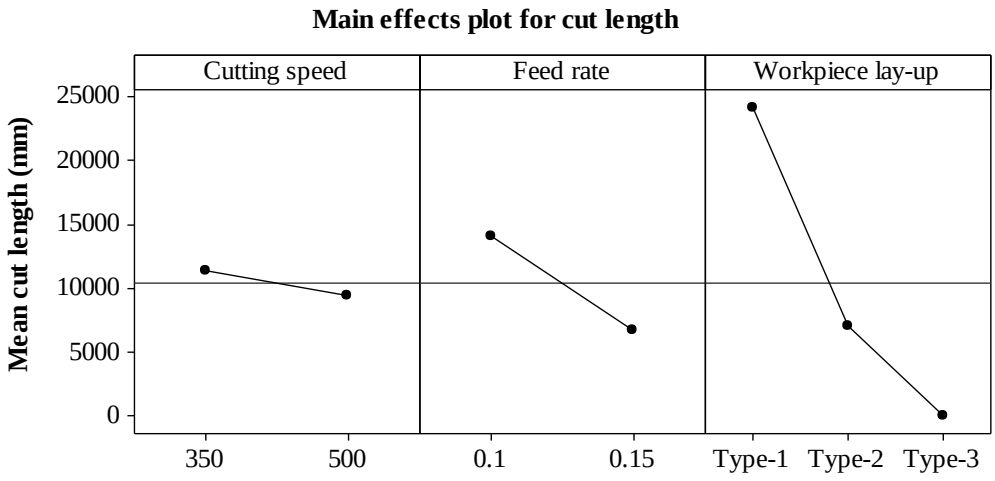

Figure 4.94: Main effects plot for tool life

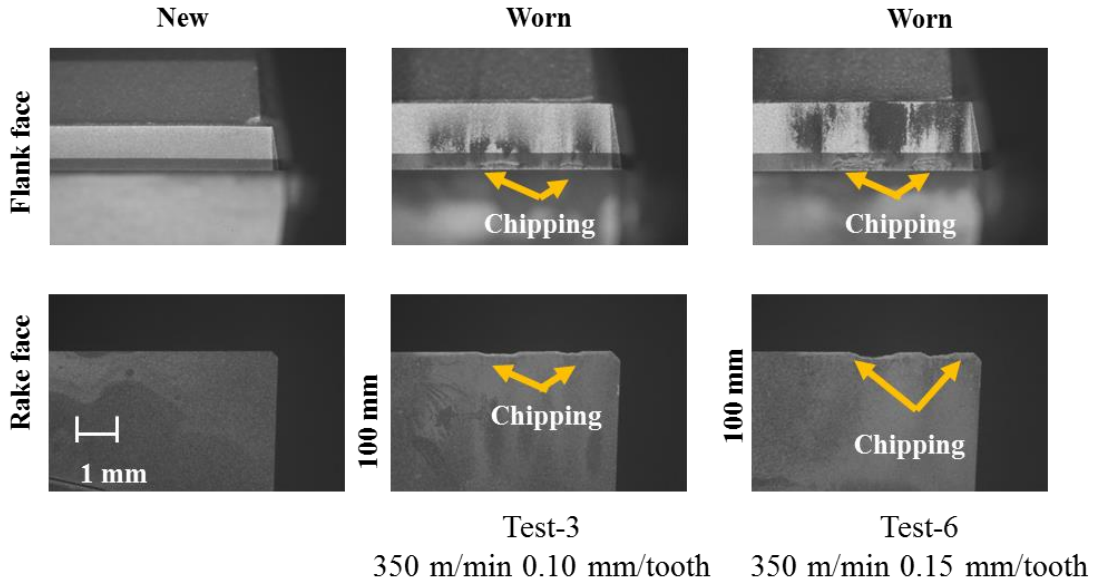

Figure 4.95: Severe chipping associated with Type-3 layup configuration, increasing with feed rate

Table 4.8: ANOVA for tool life

Source	DOF	Seq SS	Adj MS	F calc.	F tab.	P	PCR (%)
V	1	12403333	12403333	0.11	5.59	0.714	0.6
f	1	158413333	158413333	0.23	5.59	0.215	8.0
Lay-up	2	1216601667	608300833	3.19	4.74	0.021	61.3*
Error	7	597858333	85408333				30.1
Total	11	1985276667					

*significant at the 5% level

The most significant factor influencing the tool life was the workpiece layup configuration (61.3 % PCR). Based on the cut length results, Type-1 material was the easiest to cut while Type-3 was the most difficult, see Figure 4.96. In Type-3 layup, the chipping occurred at two locations on the cutting edge corresponding to layers with 45° layers and was prominent following one pass of 100 m accompanied with a high cutting force Fx spike of 676 N which. Generally, when using PCD tools, mechanical shock at tool entry should be avoided [187], hence, it is recommended to use slow feed rate with Type-3 especially at initial contact, a gradual increase in feed rate may also reduce the impact spikes and resulting chipping.

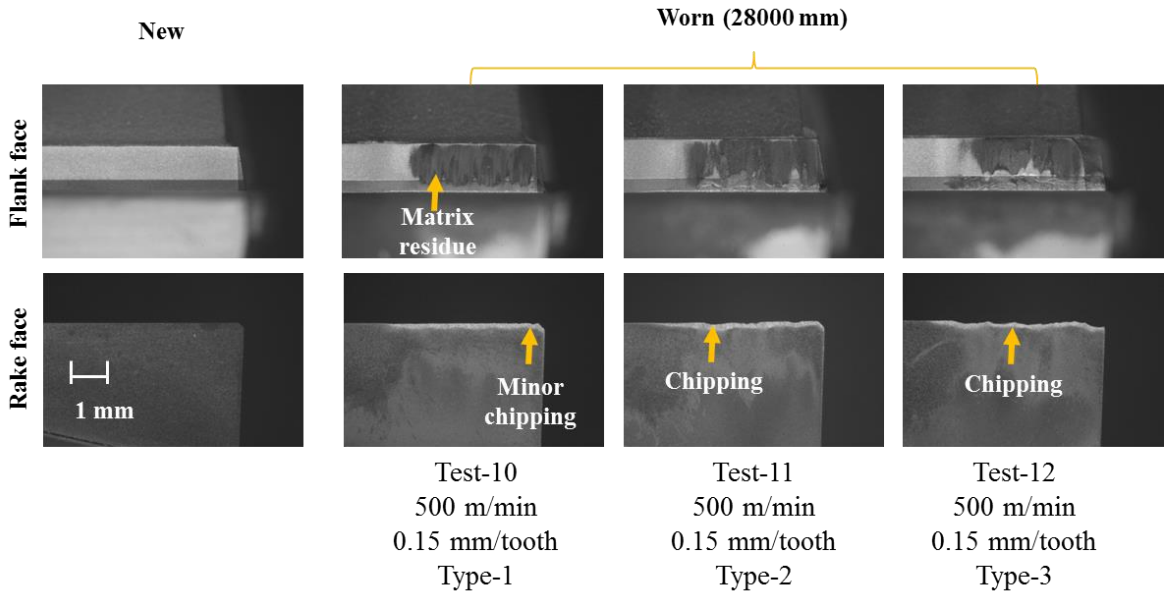

Figure 4.96: Effect of material layup configuration on edge wear

4.6.2 Cutting forces

Cutting force results agreed with preliminary testing results apart from the difference in force magnitudes (Fx range 418-690 N at 500m/min and 0.15 mm/tooth instead of 249-285N Fx at 200 m/min and 0.03 mm/tooth) obviously due to the higher parameters used. Type-1 was again the lowest Fx followed by Type-3 while the highest Fx cutting forces were attributed to Type-2 as explained earlier.

The force trace within one revolution of the cutting showed that the cutting force varied with tool rotation such that peaks and valleys corresponded to the changing of the ply angle with respect to the tool during its rotation. See Figure 4.97 for example force traces from slotting of different material lay-up.

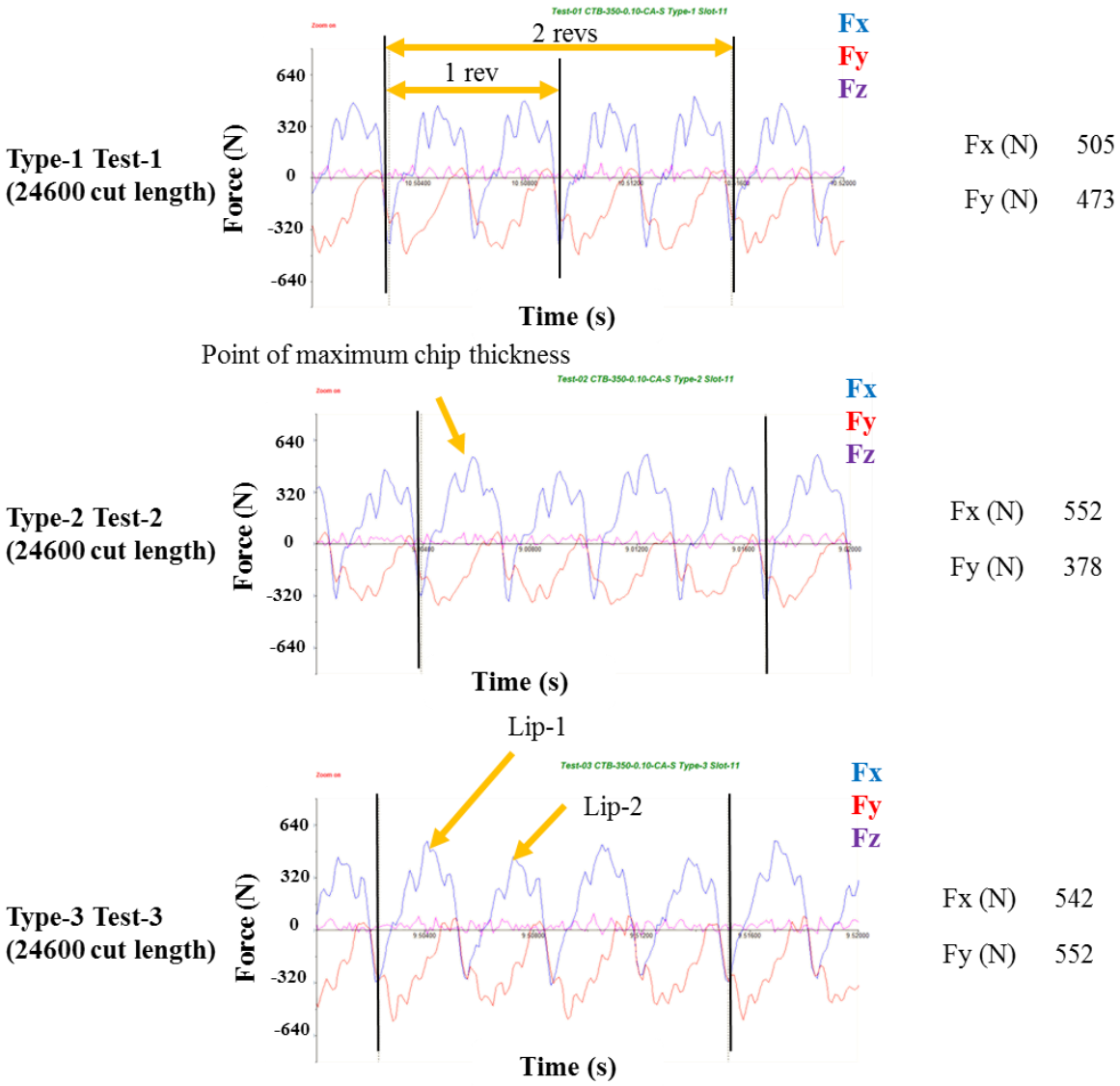

Figure 4.97: Force traces during slotting different material lay-up

The maximum cutting forces Fx when the tool was new (shown in Figure 4.98) were used in the analysis to obtain the main effects plot for the cutting force shown in Figure 4.99. Cutting force (Fx) was increasing with cutting speed because of its indirect effect on feed speed. Feed rate was the most significant factor affecting cutting force because of the chip thickness which agreed with Phase-1 results. Type-2 was the most difficult to cut in terms of Fx owing to its zero degree fibre content. ANOVA table is shown in Table 4.9 where none of the factors is significant.

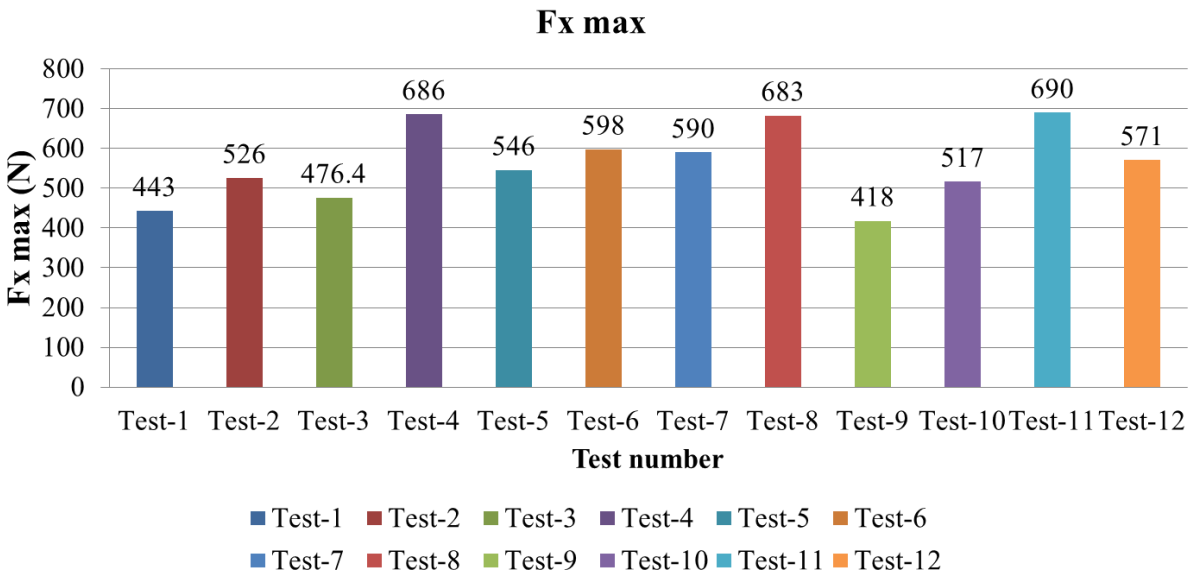

Figure 4.98: Cutting force Fx for all tests

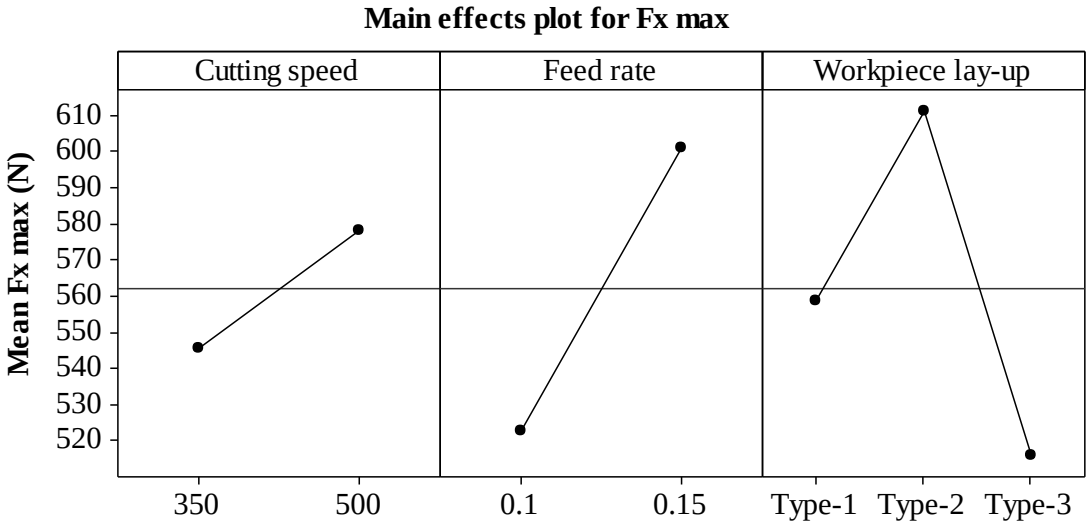

Figure 4.99: Main effects plot for Fx (max)

Table 4.9: ANOVA for cutting force Fx

Source	DOF	Seq SS	Adj MS	F calc.	F tab.	P	PCR (%)
V	1	3123	3123	0.4	5.59	0.546	3.3
f	1	18534	18534	2.38	5.59	0.167	19.6
Lay-up	2	18258	9129	1.17	4.74	0.363	19.3
Error	7	54449	7778				57.7
Total	11	94363					

It was also possible to use the (Fx max-Fx mean)/ply obtained using the ITC-PCD and to compare the calculated results with the results obtained from Phase-2 (Test-10, Test-11 and Test-12). The results obtained were quite similar but the percentage variation may be high possibly due to the variation in the cooling environment (i.e. preliminary test used Twin-Nozzle chilled air compared to Single-Nozzle chilled air in Phase-2 tests added to the difference in tool material, see Table 4.10.

Table 4.10: Calculated and experimental forces at 500 m/min cutting speed, 0.15 mm/tooth feed rate

		Type-1	**Type-2**	**Type-3**
Ply angle	**(Fx_{max}-Fx_{mean})/ply**	**Fx_{max} calculated (N)**		
0°	27.15	532.68	542.69	559.10
45°	27.38	**Experimental Fx_{max} (N)**		
90°	19.41	517	690	571
135°	32.61	**% variation**		
		3.03	21.34	2.08

4.6.3 Feed force

The maximum feed force Fy is shown in Figure 4.100. The most significant factor affecting feed force was the feed rate and very small contribution come from cutting speed. Type-2 lay-up caused the lowest cutting force for the same reason mention in Fx. Main effects plot for feed force Fy is shown in Figure 4.101. ANOVA showed that the most significant factor affecting feed force was the feed rate with 49.4 % PCR as shown in Table 4.11.

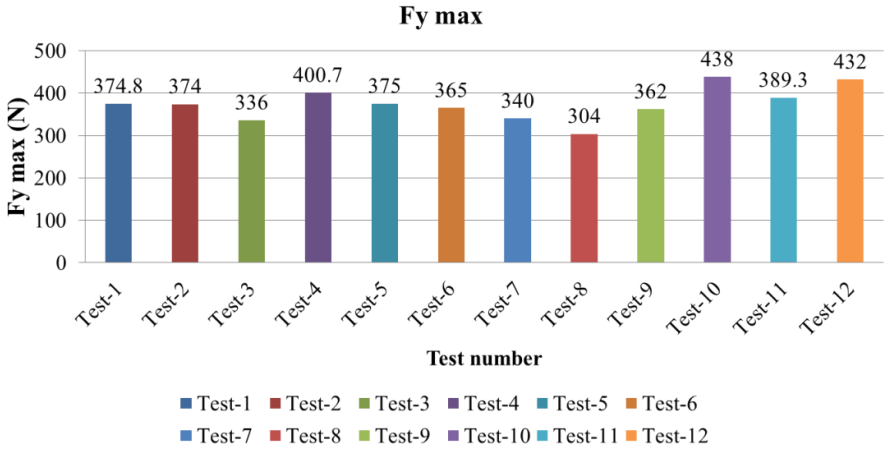

Figure 4.100: Feed force Fx for all tests

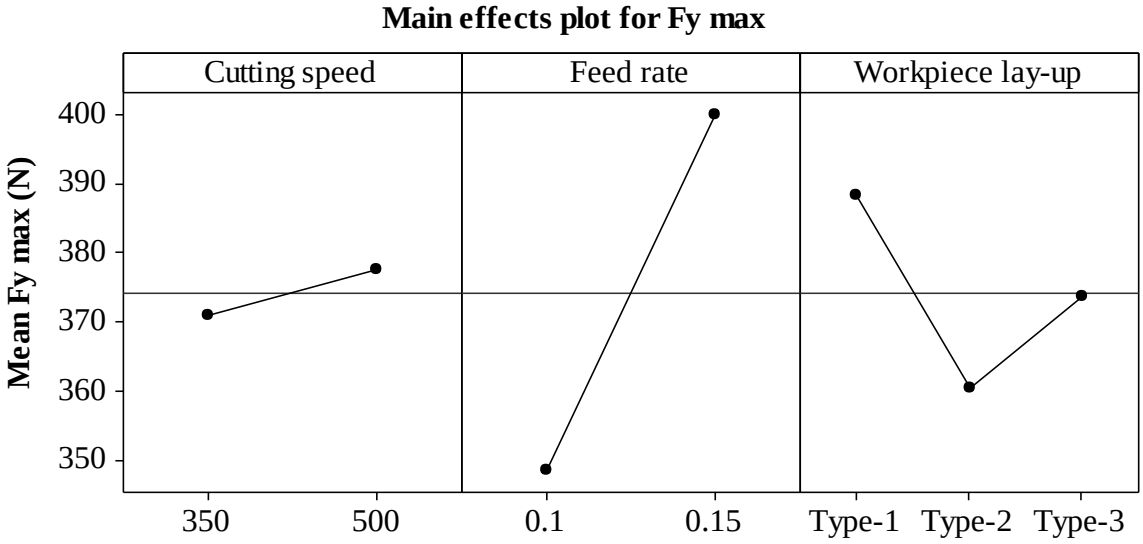

Figure 4.101: Main effects plot for Fy

Table 4.11: ANOVA for Fy

Source	DOF	Seq SS	Adj MS	F calc.	F tab.	P	PCR (%)
V	1	132	132	0.14	5.59	0.717	0.8
f	1	7967.1	7969.1	8.6	5.59	0.022	49.4*
Lay-up	2	1547.1	773.5	0.83	4.74	0.473	9.6
Error	7	6486.8	926.7				40.2
Total	11	16133					

*significant at the 5% level

4.6.4 Surface roughness

The use of 3D surface topography with real surface appearance obtained using the optical imaging system (Alicona) was sufficient enough to describe the surface details. The values of the roughness parameters are shown in Figure 4.102 and Figure 4.103. Similar to preliminary testing Type-2 exhibited the smoothest surface followed by Type-1 and the lowest quality surface was of that of Type-3. Looking at the first three tests, the Type-1 lay-up had a high surface roughness Sa as in Test-1 due to the wavy surface caused by vibration and this also occurred in most of the subsequent tests. Although Type-3 had several 45° in the lay-up, their effect on average suarface roughness Sa was lower compared to the waviness associated with Type-1 lay-up especially when the tool was new. However, Test-3 was an exception possibly due to premature tool failure due to chipping which may have caused further damage and fibre pull-out. This can be seen evident in the 3D scans obtained using Alicona for the first

slot of the 12 tests which are shown in Figure 4.106 where severe damage in 45° layers in particular is prominent.

Surface roughness parameters (Sa and St) were extracted from the scans following waviness removal. Since the surface roughness was measured for all tests when tool was new, there was little variation in the surface roughness values. In case of Sa there was a slight decrease in surface roughness with increase in cutting speed from 350 to 500 m/min may be because of the temperature effect. The increase in feed rate from 0.1 to 0.15 mm/tooth did not result in any improvement. The vibration associated with milling Type-1 material made Type-1 material look the poorest quality but may improve when tools are worn. The main effects plot for Sa is shown in Figure 4.104 while ANOVA is in Table 4.12. The lay-up was the most significant factor affecting Sa with 63% PCR.

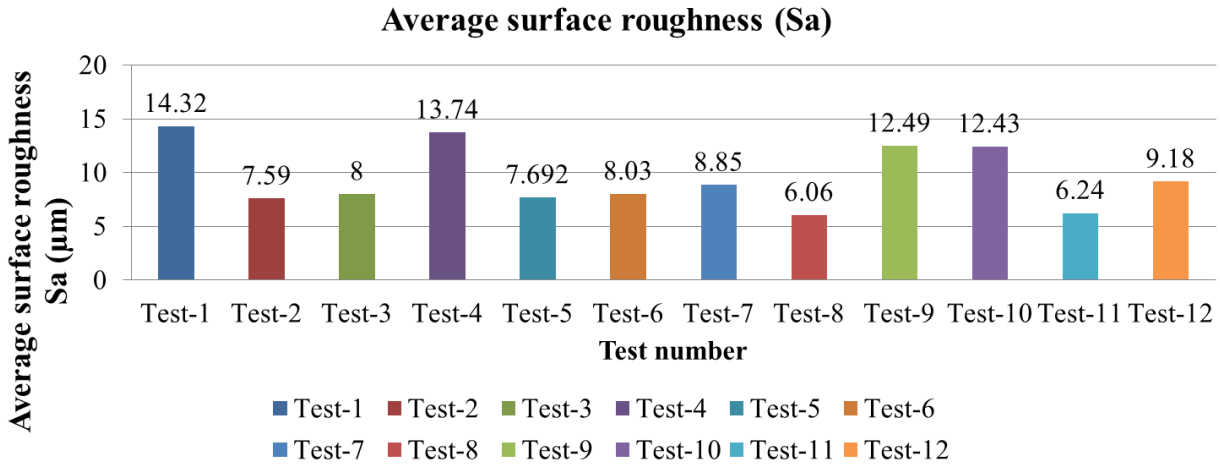

Figure 4.102: Average surface roughness Sa

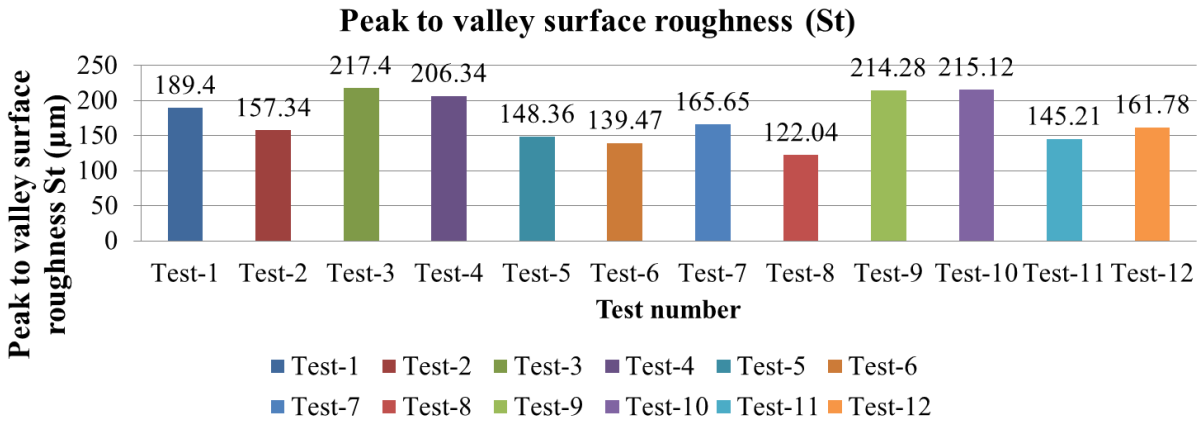

Figure 4.103: Peak to valley surface roughness St

Apart from average surface roughness, some researchers considered only Peak-to-Valley roughness such as Davim and Reis [176]. In case of St, the feed rate showed smaller effect which can be explained by shortened contact time between edge and workpiece surface. The main effects plot of St is shown in Figure 4.105 and ANOVA is in Table 4.13.

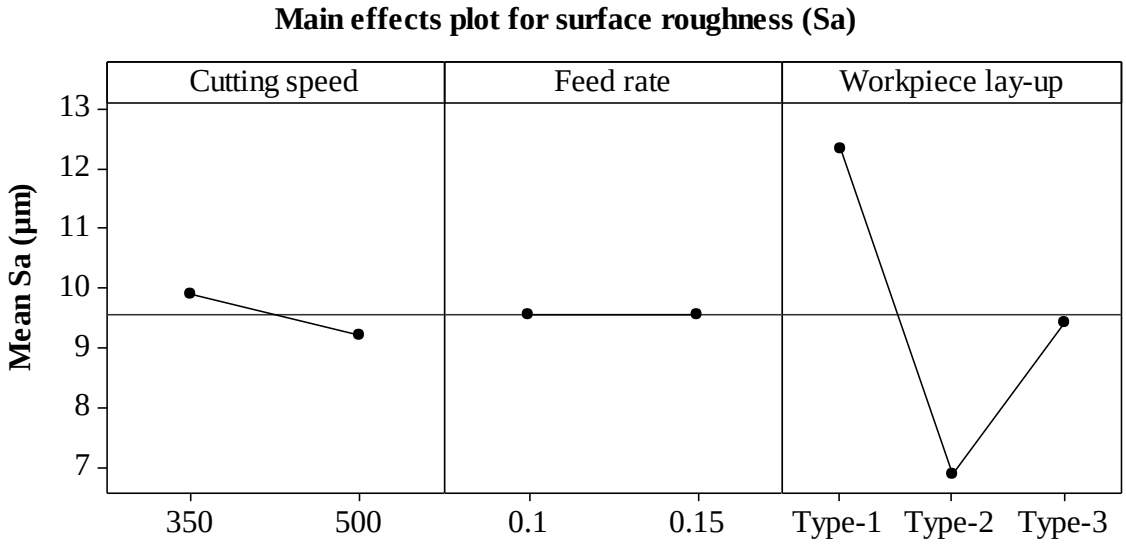

Figure 4.104: Main effects plot for 3D surface roughness parameter Sa (µm) for new tools

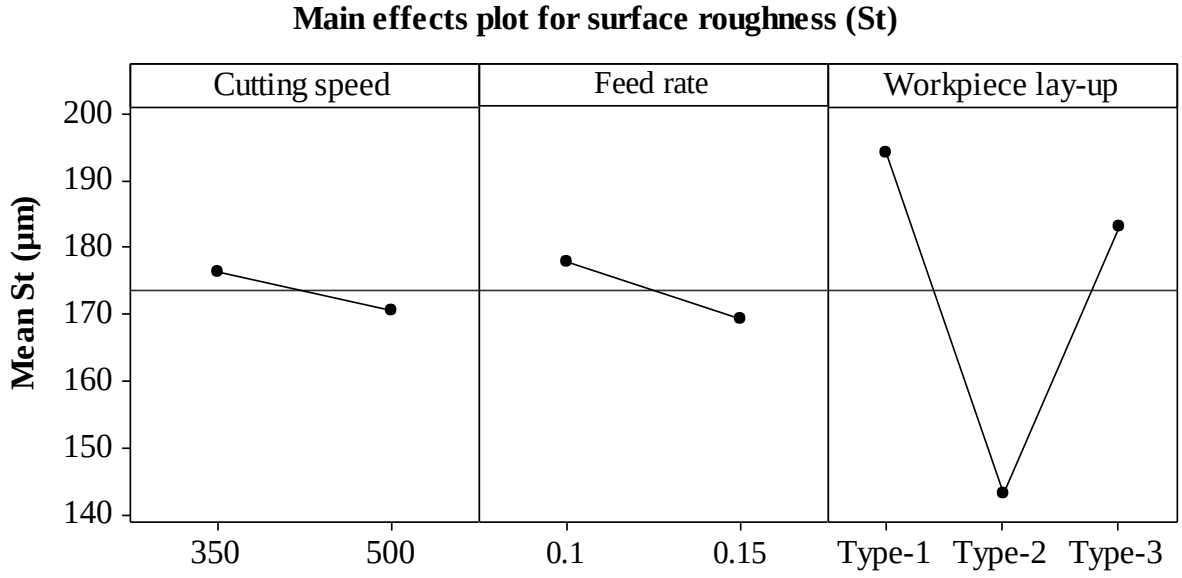

Figure 4.105: Main effects plot for 3D surface roughness parameter St (µm) for new tools

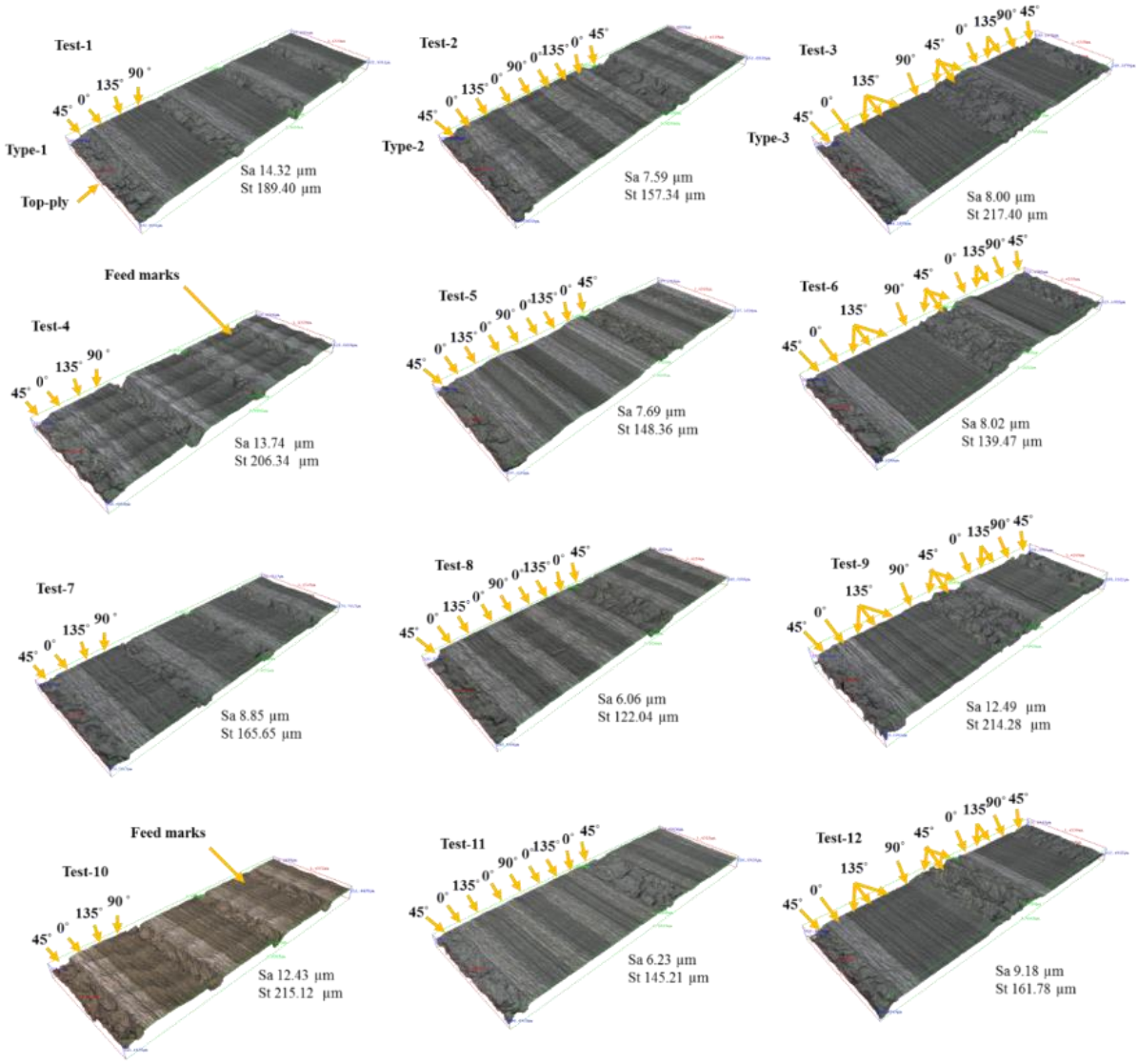

Figure 4.106: 3D scans of first slot down milling side (new tool)

Table 4.12: ANOVA table for Sa

Source	DOF	Seq SS	Adj MS	F calc.	F tab.	P	PCR (%)
V	1	1.414	1.414	0.31	5.59	0.597	1.5
f	1	0	0	0	5.59	0.999	0.0
Lay-up	2	59.255	29.627	6.42	4.74	0.026	63.7*
Error	7	32.324	4.618				34.8
Total	11	92.993					

*significant at the 5% level

Table 4.13: ANOVA table for St

Source	DOF	Seq SS	Adj MS	F calc.	F tab.	P	PCR (%)
V	1	97.6	97.6	0.11	5.59	0.752	0.8
f	1	206.9	206.9	0.23	5.59	0.646	1.7
Lay-up	2	5744.1	2872.1	3.19	4.74	0.104	46.5
Error	7	6303.7	900.5				51.0
Total	11	12352					

4.6.5 Delamination factor

Delamination factor (calculated) increased with feed rate which was the most significant factor. This agrees well with results obtained by Davim and Reis [160, 176]. Delamination factor also increases with cutting speed possibly because of tool wear increase and related effect such as rounding of edge and rise in temperature. Type-1 material had the lowest delamination factor while Type-2 despite the good slot wall surface but this may be because high cutting forces. This trend correlates to the cutting temperature results obtained in preliminary work. The PCR of feed rate (the most significant) was 50.1% as shown in Figure 4.107 and Table 4.14. Values of delamination factor and fuzz length are in tabualted in Appendix-G.

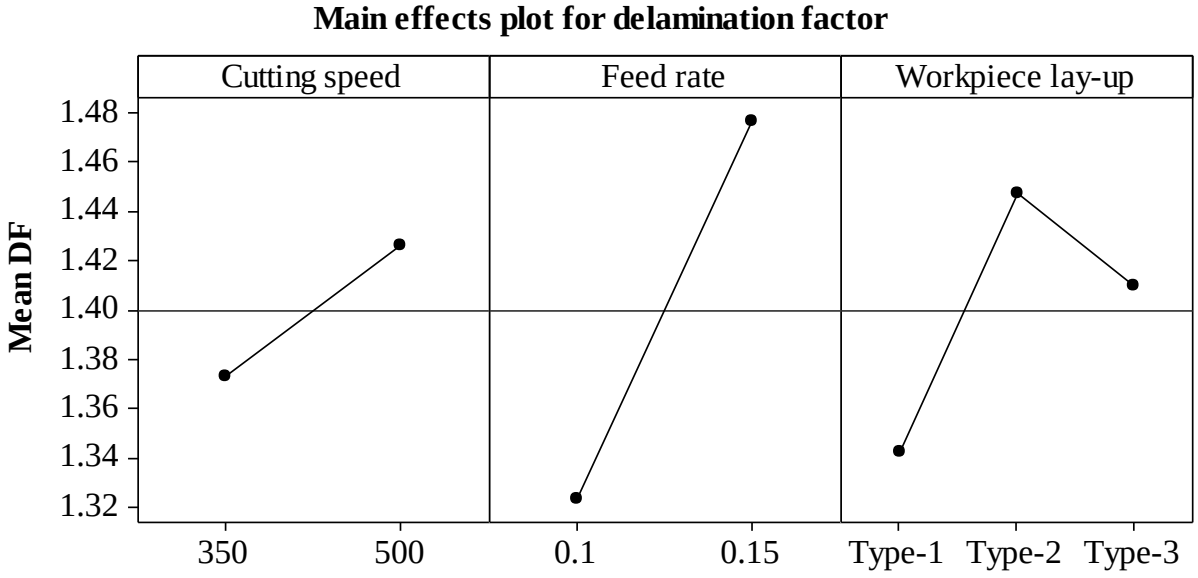

Figure 4.107: Main effects plot for delamination factor

Table 4.14: ANOVA for delamination factor

Source	DOF	Seq SS	Adj MS	F calc.	F tab.	P	PCR (%)
V	1	0.008533	0.008533	1.57	5.59	0.251	6.1
f	1	0.0700533	0.070533	12.96	5.59	0.009	50.1*
Lay-up	2	0.02265	0.011325	2.08	4.74	0.195	16.2
Error	7	0.038083	0.00544				27.6
Total	11	0.1398					

*significant at the 5% level

4.6.6 Fuzz length

Although the tools suffered localised chipping, fuzzing was mainly dependant on the tool condition near the top ply which was relatively smaller compared to the rest of the cutting edge. The length of fuzz measured on up milling side increased with cut length. The main effects plot for fuzz length (Figure 4.108) shows that fuzz length increased with cutting speed and feed rate. The most significant factor affecting the fuzz length was the feed rate. Type-3 material exhibited the longest fuzz, see Table 4.15. The results from delamination factor and fuzz length agree with Colligan and Ramulu [151]. However the amount of fuzz on the up milling was far from the requirements by Airbus [134] and was the reason the up milling side was discarded all the time. Feed rate was the most significant factor affecting fuzz length with 57% PCR.

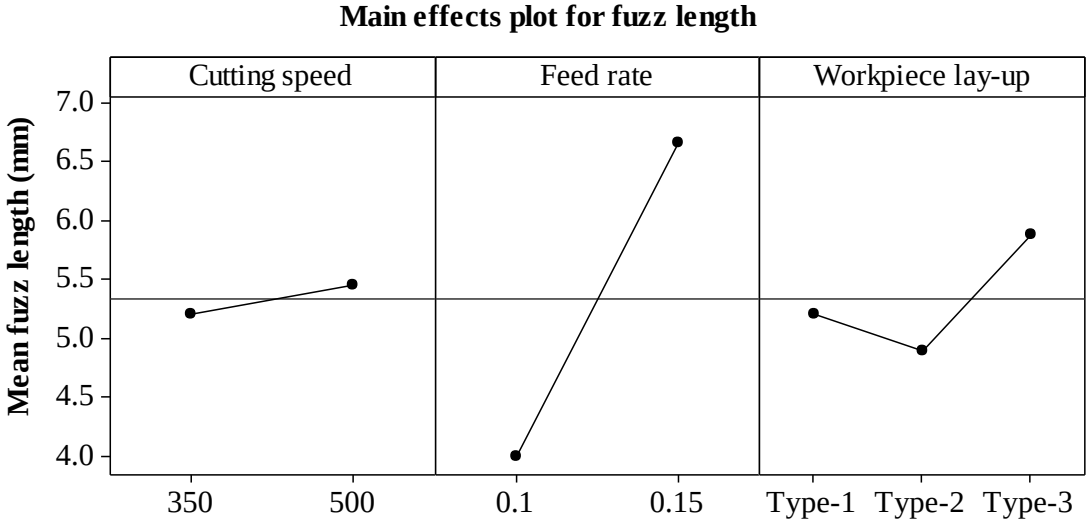

Figure 4.108: Main effects plot for fuzz length

Table 4.15: ANOVA for fuzz length

Source	DOF	Seq SS	Adj MS	F calc.	F tab.	P	PCR (%)
V	1	0.19	0.19	0.1	5.59	0.761	0.5
f	1	21.198	21.198	11.2	5.59	0.012	57.8*
Lay-up	2	2.029	1.015	0.54	4.74	0.607	5.5
Error	7	13.245	1.892				36.1
Total	11	36.662					

*significant at the 5% level

4.7 Phase-2C: Effect of cutting environment

4.7.1 Tool wear

Using the results from Phase-1 Test-11 (dry), Phase-1 confirmation test (twin nozzle) and Phase-2 Test-10 (single nozzle) it was possible to compare the effect of different cutting environment. (Figure 4.109) shows the effect of different environments on flank wear (tool wear following 28000 mm cut length). Use of chilled air (twin nozzle) in confirmation test lead to 30% improvement in tool life compared to dry cutting. Although the single nozzle showed further reduction in tool temperature, there was no tangible difference in tool life using single nozzle.

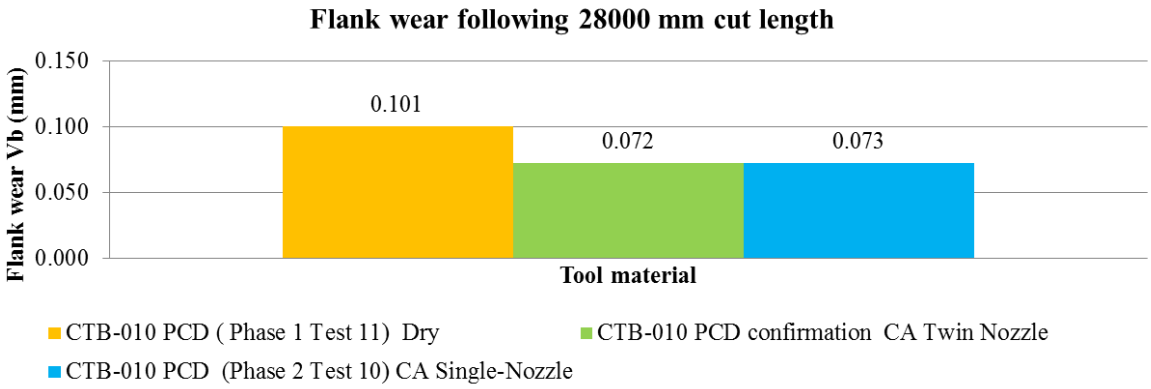

Figure 4.109: Tool wear following 28 m cut length dry, twin nozzle, and single nozzle

Using single nozzle chilled air, the cutting forces were higher possibly because of the reduced temperature leading to reducing the degree of matrix softening. Figure 4.110 shows the effect of cutting environment on Fx and Fy average forces.

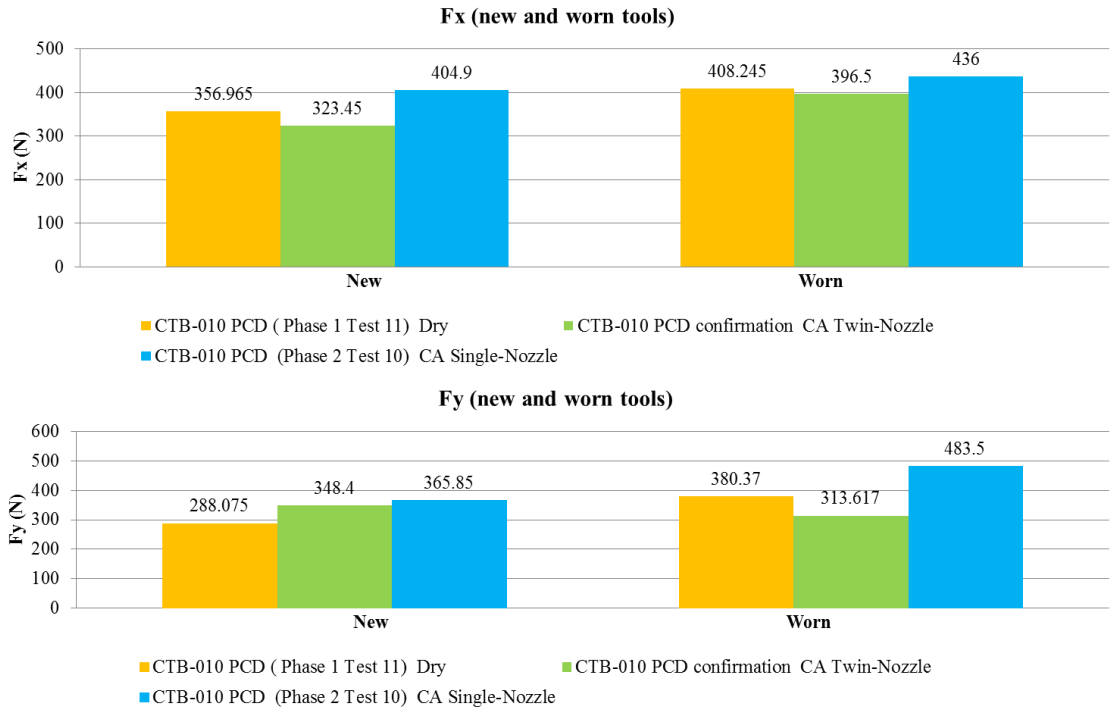

Figure 4.110: Cutting forces (average) for different cutting environments

4.7.2 Delamination factor

Generally, both delamination factor and fuzz length increase with cut length as mentioned earlier due to the increase in tool wear and edge rounding (edge radius) which agree well with Hintze et al observations [171]. Lower delamination factorwas obtained using single nozzle , as shown in Figure 4.111, possibly due to efficient cooling and dust evacuation which reduced the matrix softening and held the fibres to be cut rather than escaping from cutting edge and causing delamination,. The delamination factor, width of damage and fuzz length were respectively (1.6, 20.02 mm, and 9.8 mm) using single-nozzle chilled air compared to (1.8, 21.7 mm and 9.8 mm) for twin-nozzle chilled air when tools were worn following 28000 mm cut length.

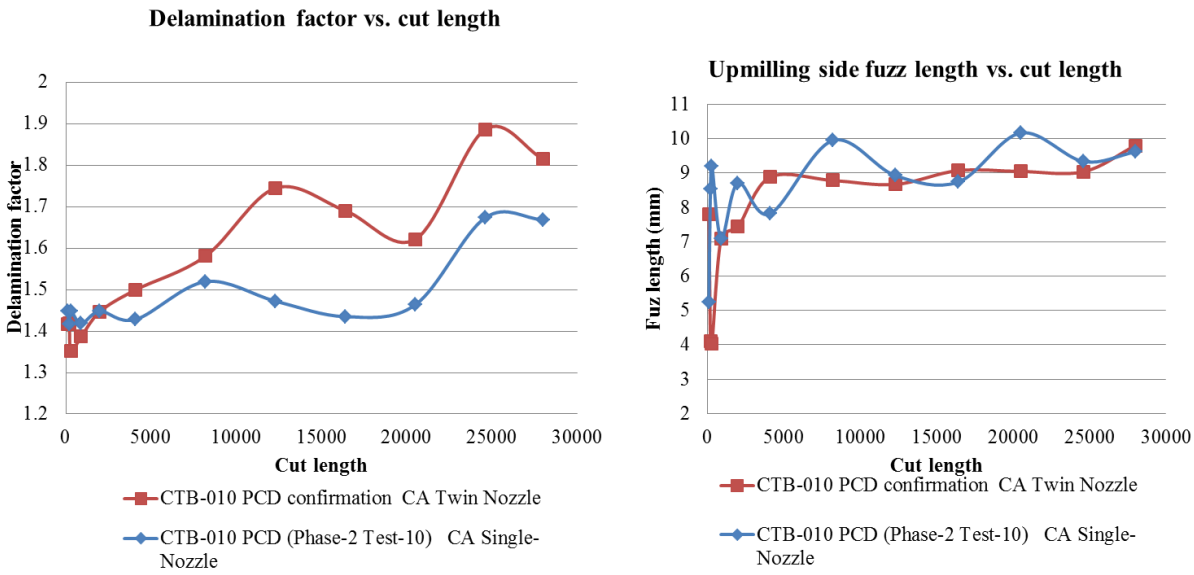

Figure 4.111: Delamination factor and fuzz length

4.7.3 Surface integrity/roughness

Alicona 2D microscope images (Figure 4.112) show that in all cases there were signs of feed marks and there were much more prominent in dry condition may be because of the excessive matrix smearing due to high temperature. It is evident that the use of twin nozzle chilled air maintained a balance between thermal induced damage in dry and mechanical damage in single nozzle as seen in surfaces when tools were worn. Alicona 3D surfaces (Figure 4.113) show that the slightly higher temperature in case of twin nozzle compared to single nozzle may result in a better surface because of matrix smearing which may not have happened in single nozzle mode. Twin-nozzle chilled air resulted in a surface with ~ 50% better in terms of surface roughness when tools were worn.

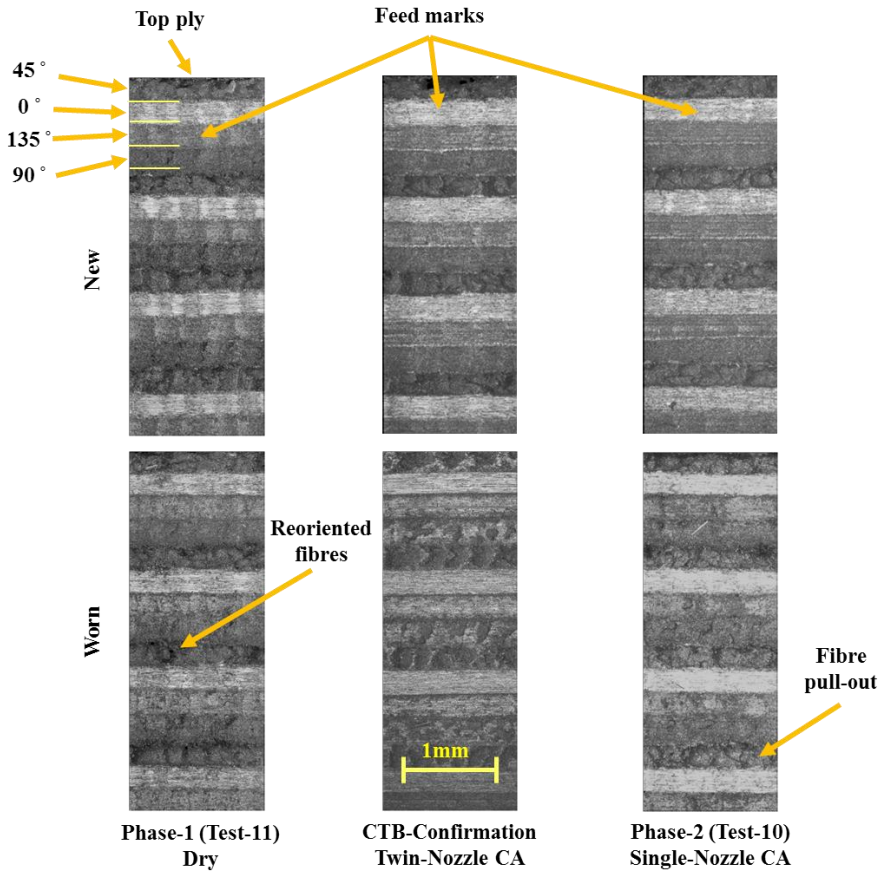

Figure 4.112: Microscope images for down-milling side surfaces different environments.

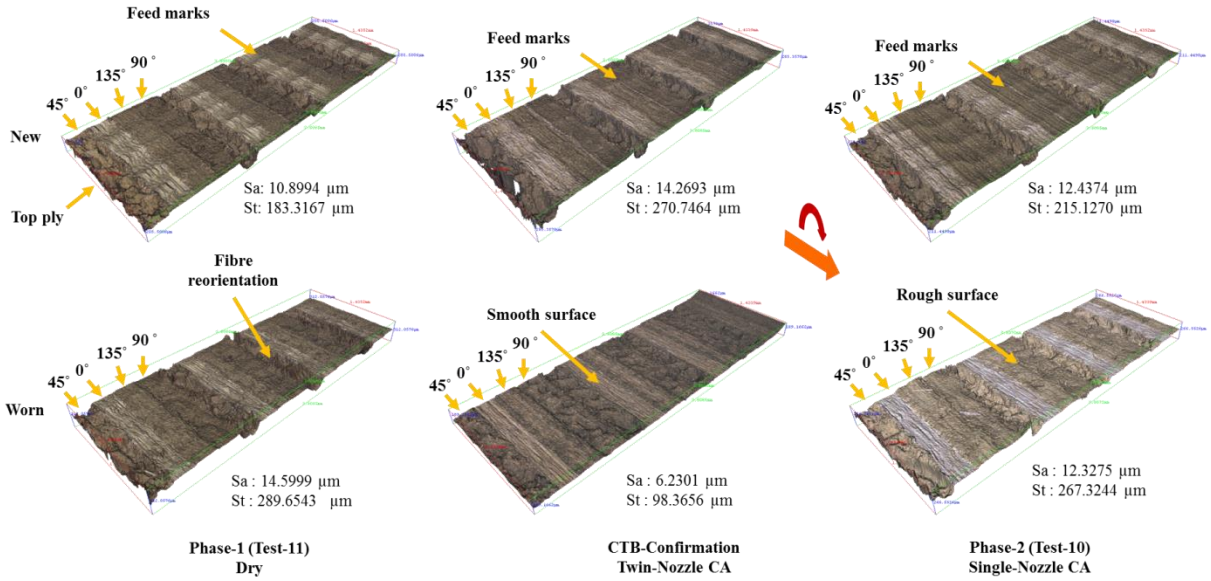

Figure 4.113: Alicona images different environments

4.8 Phase-3A: Influence of router helix angle

Initially, an Exactaform PCD router was used at 500 m/min cutting speed and 0.15 mm/tooth feed rate in chilled air environment but the cutting edge exhibited severe chipping. Examining the PCD grade revealed that the grade was similar to CTM-302 (i.e. coarse grain PCD), therefore, the test was carried out at a lower cutting speed of 200 m/min and feed rate of 0.03 mm/tooth in chilled air environment.

4.8.1 Tool wear

Tool wear against cut length for the three router geometries is shown in Figure 4.114 which indicates that routers had almost the same flank wear at the end of the test. Using either an Exactaform Up-cut, Neutral or Down-cut router did not cause any variation in tool life. In all cases, all cutting edges sustained only gradual abrasion wear possibly due to low cutting speed and feed rate and these continued to cut until a cut length of only 4100 mm reaching ~ 0.1 mm VB flank wear, see Figure 4.115. The performance in terms of tool life was similar and this could be due to the low helix angle and the use of the same PCD grade.

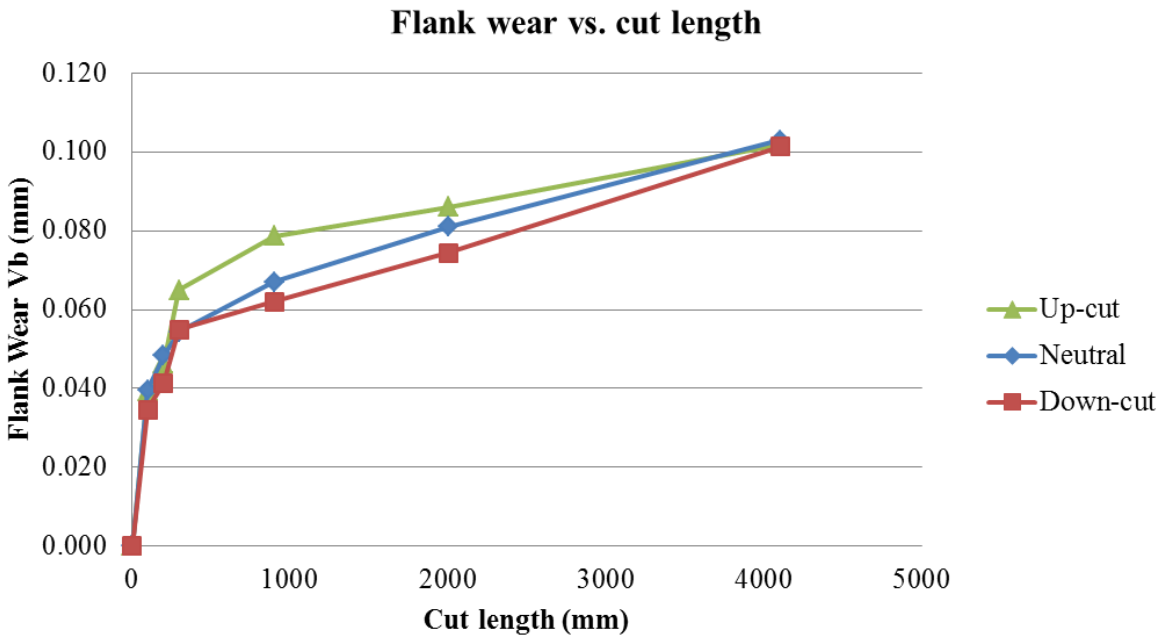

Figure 4.114: Flank wear against time for different router geometries

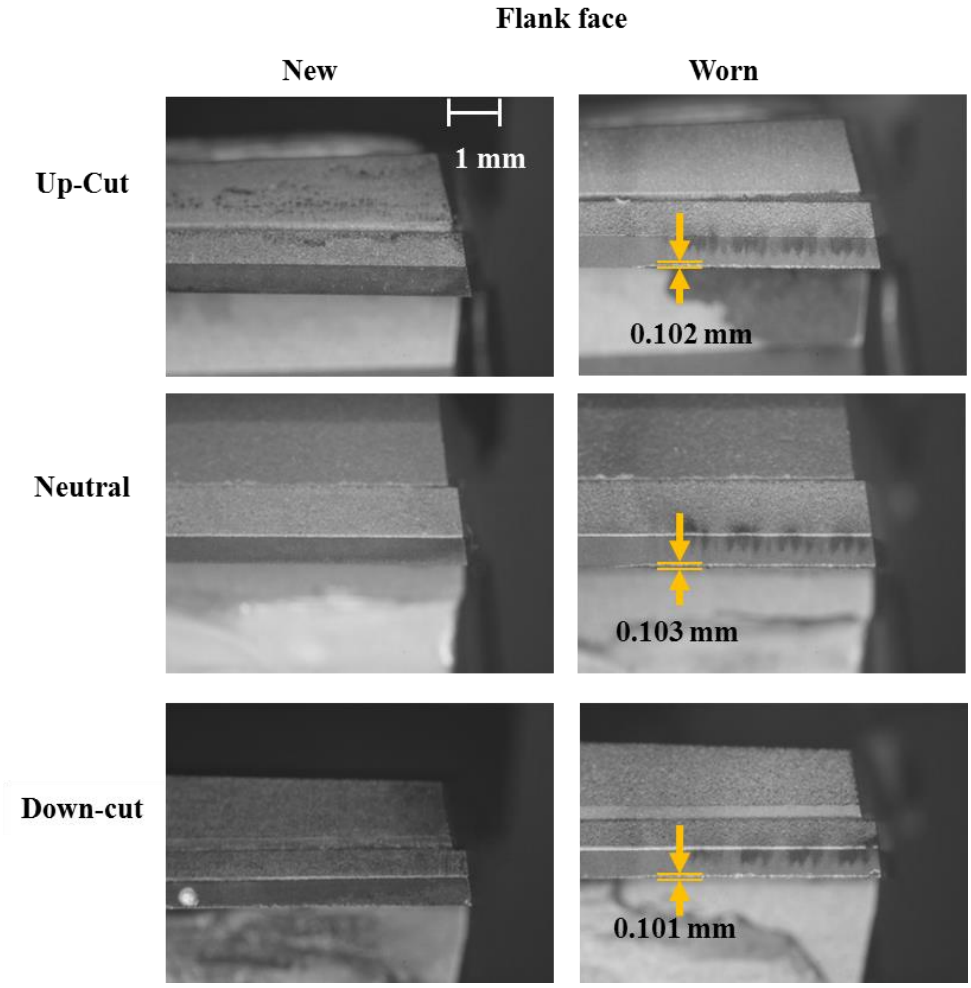

Figure 4.115: Flank wear following 4100 mm cut length at 200 m/min cutting speed and 0.03 mm/tooth feed rate in chilled air environment

4.8.2 Tool temperature

The tool temperature recorded during the cutting of the ¾ engagement coupon was ~ 85 % of the temperature during slotting (full engagement). The temperature when the tool was new was in the region of 200°C. Using Exactaform Up-cut router, the temperature increased from 197 °C to 253 °C following 4100 mm cut length. In the case of Exactaform Neutral router, the temperature was slightly higher as it started from 206 °C and was ~ 260 °C when the tool was worn. On the other hand, the down milling had the lowest temperature 193 ° C when the tool was new and ~ 236 °C when the tool was worn.

Figure 4.116 shows the rate of temperature increase with cut length while Figure 4.117 shows the temperature for the new/worn. Normally, an Up-cut geometry is better for chip evacuation while the down-cut is better for edge quality but chip evacuation was not an issue in the presence of chilled air environment. Generally, helical cutting tool temperature was

lower compared to neutral may be because of the longer tool edge which lowers the temperature per unit length as reported by Sasahara et al.[182].

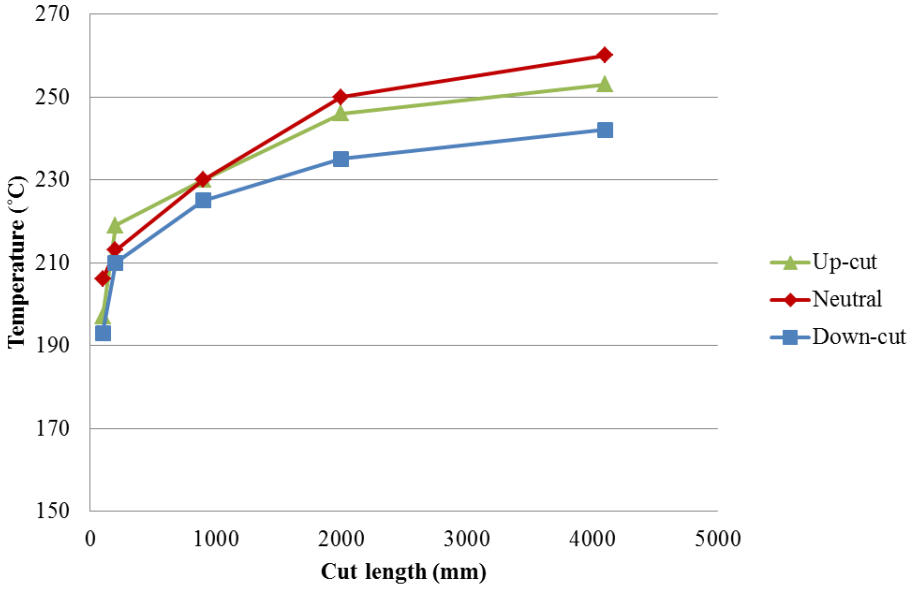

Figure 4.116: Temperature vs. cut length using Exactaform routers

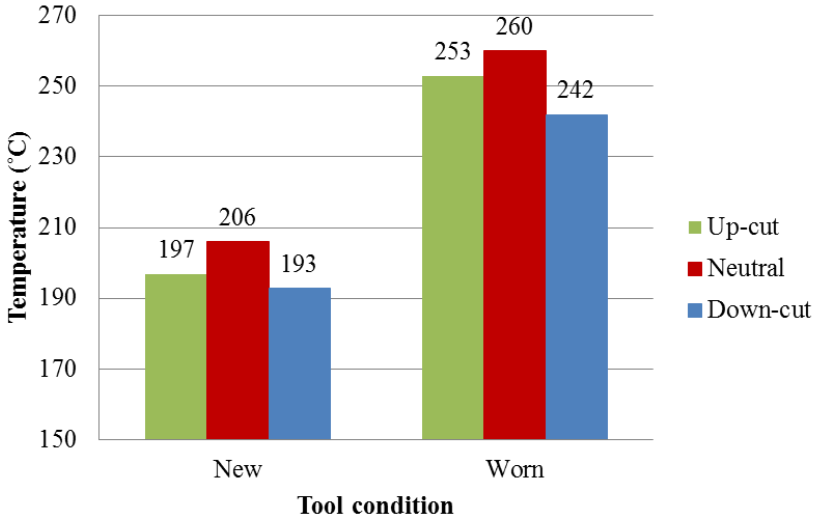

Figure 4.117: Temperature using new and worn Exactaform routers

4.8.3 Cutting forces

Generally the use of helical tools was generating noise possibly due to the fluctuating axial forces compared to the straight fluted Neutral router. The axial force Fz was ~ 30-60 N and the low helix did not cause significant variation in this component compared to high helix in Burr type routers mentioned earlier. Other force components (Fx and Fy) are shown in Figure 4.118 and Figure 4.119 respectively. Using neutral Exactaform Neutral, the high cutting temperature may have contributed to the lower cutting forces especially when the tool was sharp (i.e. new condition) and vice versa in the case of Down-cut (i.e. higher forces due to lower temperature). This was possibly due to the effect of higher temperature in softening of the workpiece matrix lowering frictional forces. This could be the reason that cutting forces Fx were lower when routers were worn. This reduction in forces did not happen in the case of feed force Fy because of the higher feed speed used and the effect of tool wear. This did not apply to Fy (feed force) because a worn tool tends to push the workpiece in feed direction instead of cutting.

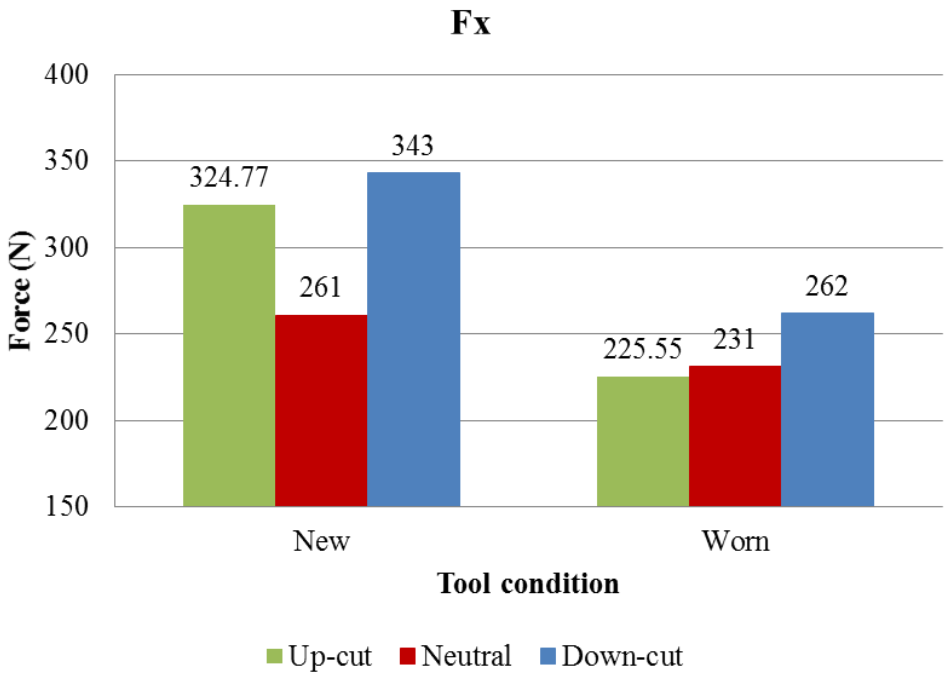

Figure 4.118: Cutting force Fx using Up-cut, Neutral, and Down-cut

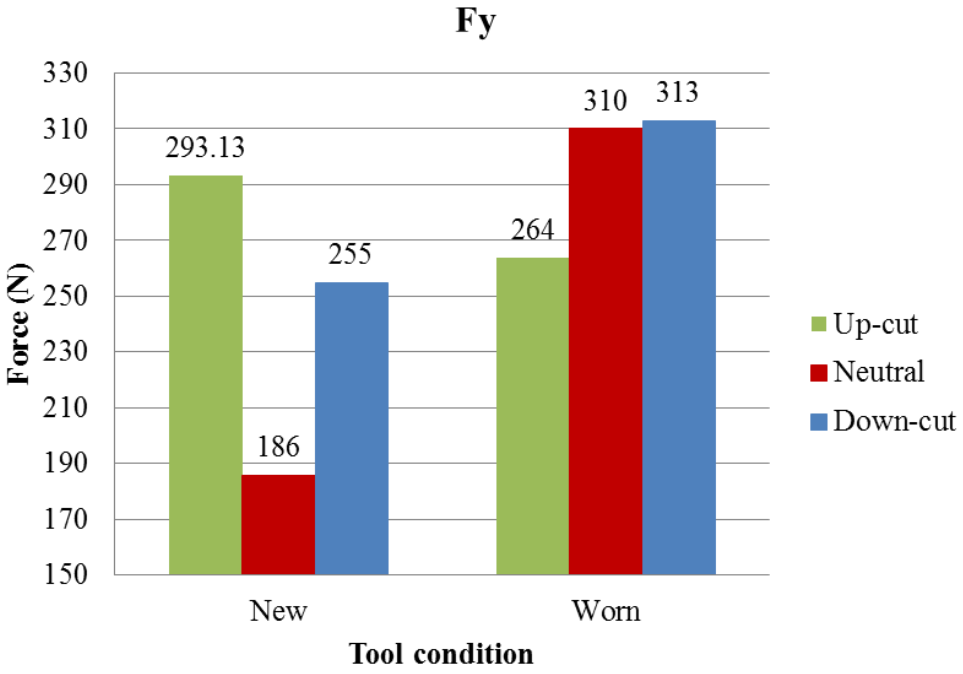

Figure 4.119: Feed force Fx using Up-cut, Neutral, and Down-cut

4.8.4 Surface integrity/roughness

4.8.4.1 4.8.4.1 Slot quality

Cutting started clean on both sides of the slot. Although the routers sustained the same amount of flank wear (~0.1 mm) the tool geometry influenced the occurrence and propagation of fuzzing. For example, using Exactaform Up-cut, an early occurrence of fuzz on up milling side was at a cut length of only ~ 300 mm compared to 550 mm in the case of Neutral and 800 mm in the case of Down-cut possibly due to the Up-cut geometry allowing fibres to escape easily compared to the remaining routers. The density of fuzz on down milling side using neutral tool was higher in comparison which could be a result of the high tool temperature. Fuzz on down milling started following ~2750 mm cut length using Neutral compared to 3500 mm using Down-cut due to the downward cutting action of the later which shear the fibres at the edge, See Figure 4.120 for the slot quality.

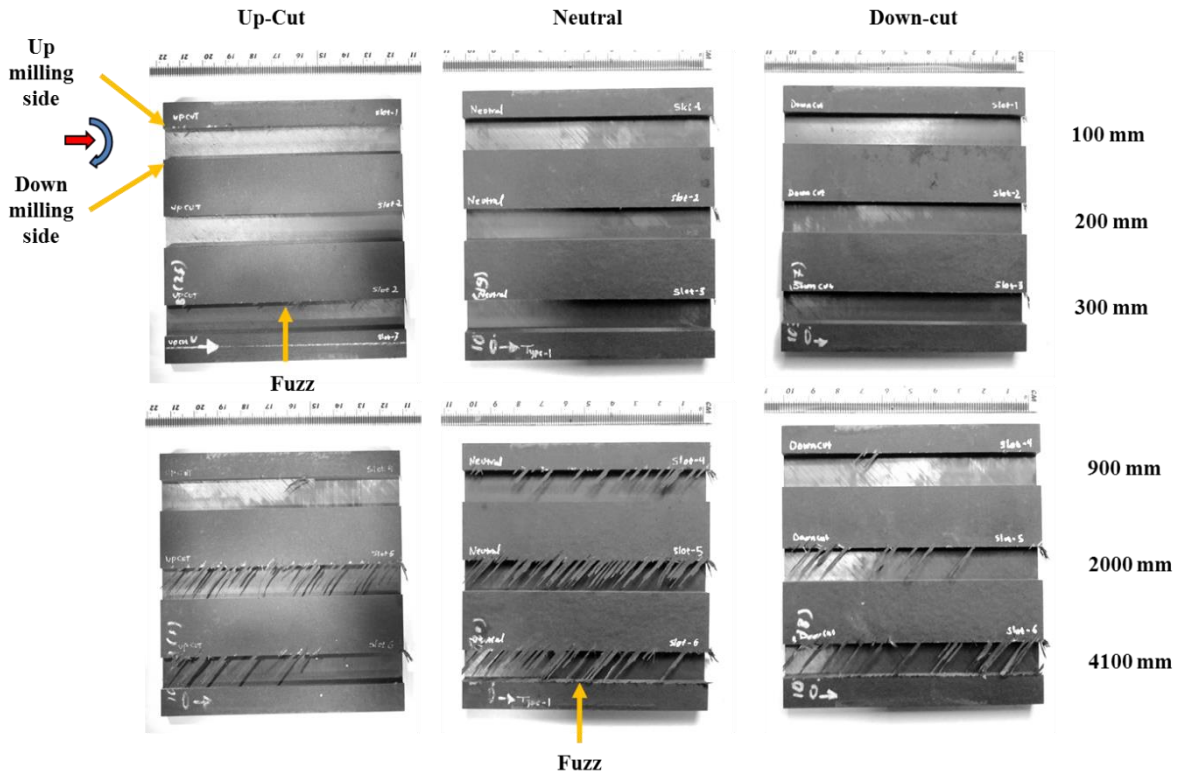

Figure 4.120: Slot quality using different helix angle Exactaform PCD tools

4.8.4.2 4.8.4.2 Surface roughness

Machined surfaces (down milling side) obtained using the Exactaform tools in new condition (shown in Figure 4.121) did not exhibit prominent feed marks compared to 2 fluted routers which may be a result of the stable cutting using tools with more than 2 flutes. Plies in 45° orientation exhibited the usual repetitive wavy pattern. According to stylus measurement using Talysurf (Figure 4.122 left), the Down-cut router produced the roughest surface Sa 8.18 µm and St 102 µm despite the lower temperature measured. At low cutting temperature the cutting was dominated by shearing and when tool was worn the friction and pressure between tool and fibres increased and mechanically induced damage were observed as well as higher cutting forces. Up-cut came second producing a surface with Sa 6.22 µm and St 85.7 µm. On the other hand, the Neutral router produced the finest surface Sa 4.49 µm and St 51.9 µm which may be indicative that high cutting temperature may not be adversely affecting the surface all the time. High temperature (not to the burning level) may promote smoother cutting and smoother surface due to matrix softening and smearing.

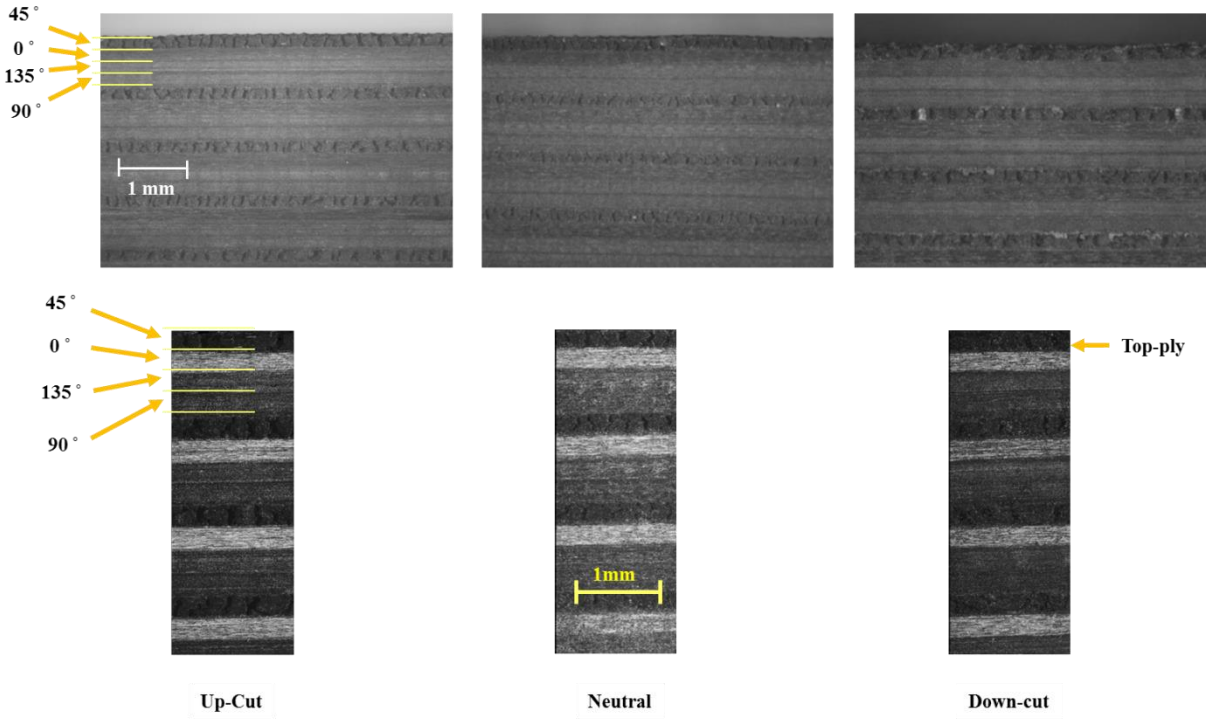

Figure 4.121: Machined surface using Up-cut, Neutral, and Down-cut routers (new tool)

On the other hand, using Alicona to scan the surface (Figure 4.122 right), the Neutral geometry was better in terms of both Sa and St 3D roughness parameters compared to the helical tools regardless of up or down cut.

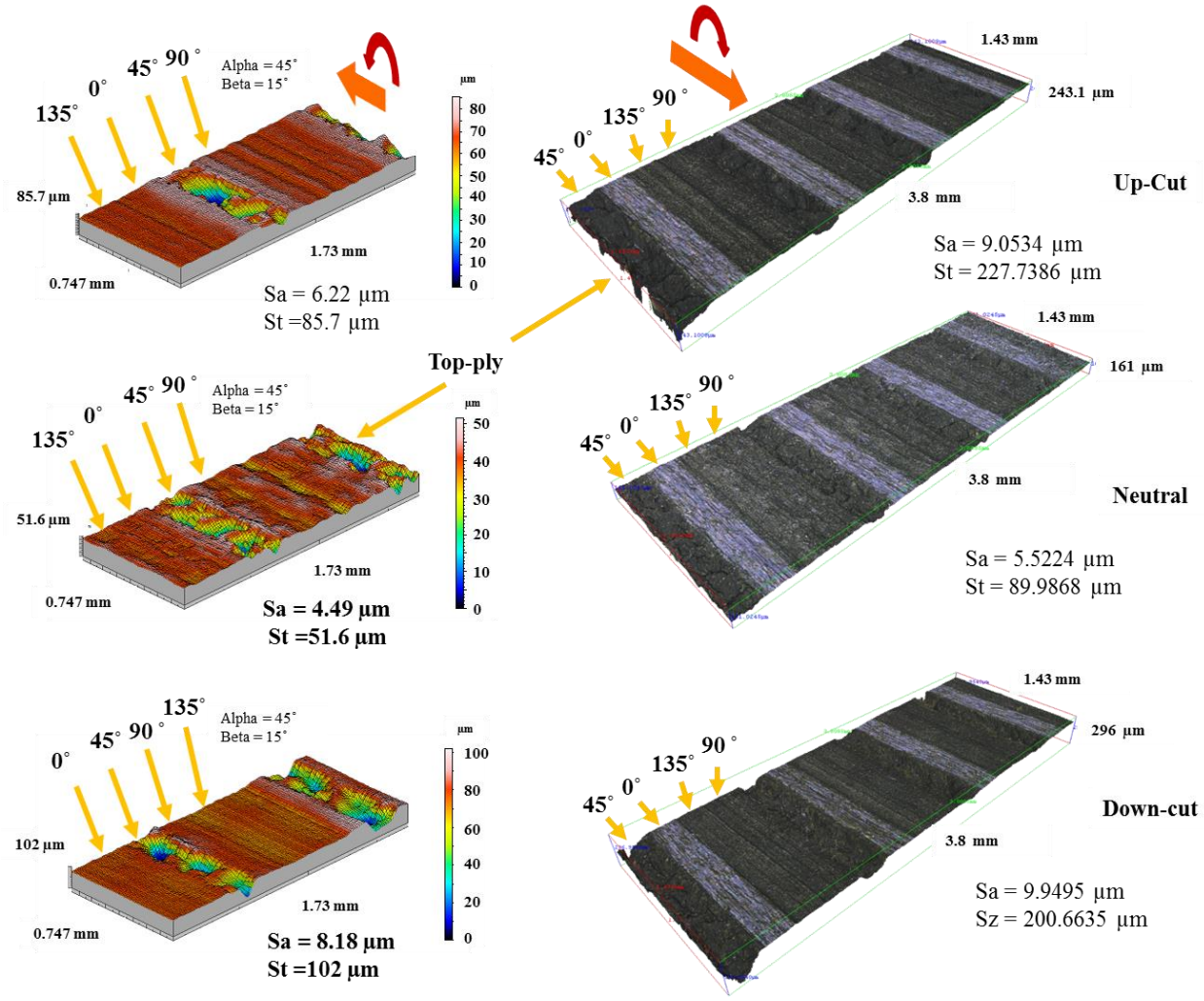

Figure 4.122: 3D surface topography obtained using Talysurf (left) and Alicona (right)

4.9 Phase-3B: Effect of secondary relief angle

This test was to compare the effect of the tool geometry on tool wear, cutting forces, surface integrity/roughness and delamination. The comparison included two test performed previously in Phase-1 using CMX-850 PCD and CTB-010 PCD both with 18° primary relief angle against CMX-850 PCD and MegaDiamond PCD which had with 10° primary relief and 18° secondary relief angles.

4.9.1 Tool wear

The secondary relief angle was reported by Caprino et al to reduce the tool wear [31], in this case the smaller relief angle reduced the tendency to chipping such that the MegaDiamond PCD router sustained minor chipping in comparison to the CTB-010 PCD

regardless that the later showed a slower wear rate in comparison, see Figure 4.123. This flank wear was reported to decrease when larger relief angle is used [31, 184]. In order to use PCD end mills at high cutting speed and feed rate it is hence recommended to use a cutting edge with secondary clearance. Apart from the CMX-850 with primary relief which fractured at a cut length of ~850 mm, the routers were able to cut 28000 mm, see Figure 4.124 for the tool wear against cut length graph.

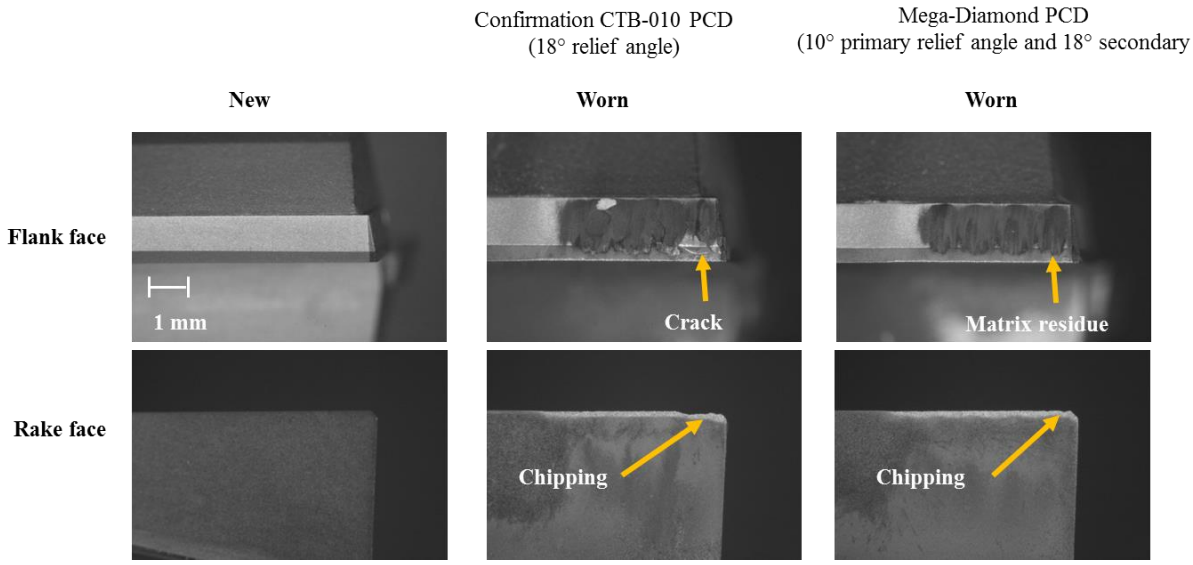

Figure 4.123: Effect of secondary relief on edge chipping

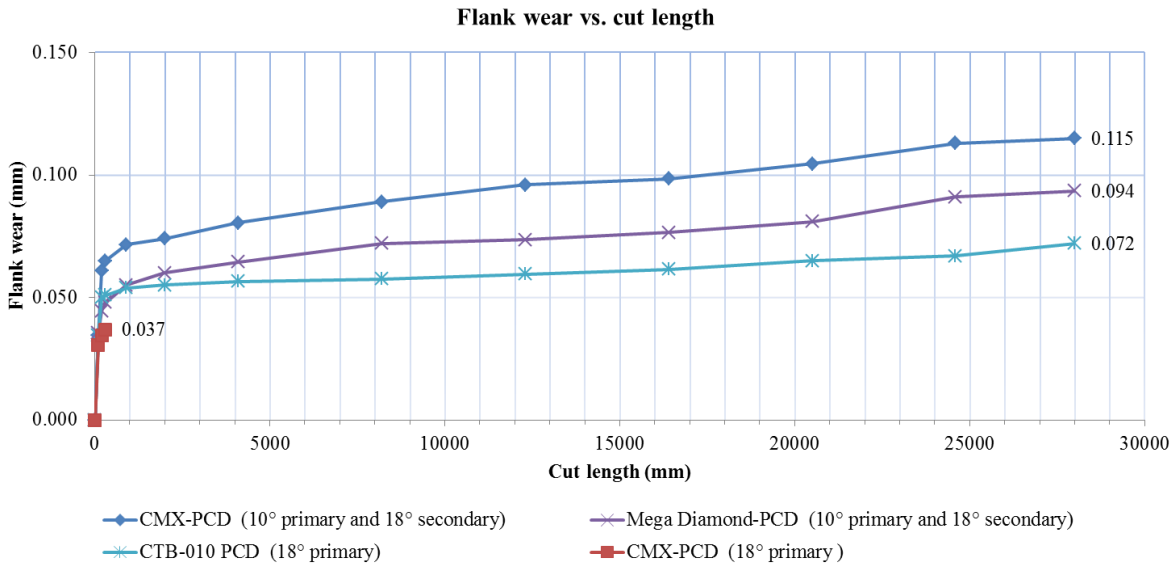

Figure 4.124: Tool wear against cut length at 500 m/min cutting speed and 0.15 mm/tooth feed rate and twin-nozzle chilled air environment

4.9.2 Cutting forces

The CTB-010 PCD had the lowest rate of increase in cutting force from new to worn state due to the steady wear rate. The tools with primary relief only exhibited higher Fx (max) cutting forces when they were new possibly due to the self-induced chatter attributed to such tools which tend to diminish when the tool is worn. Conversely, the tools with primary and secondary relief angles exhibited higher forces when worn due to rubbing against workpiece surface, see Figure 4.125. This contradicted the reported fact that a secondary relief angle was recommended to reduce cutting forces because of bouncing back fibres [29] possibly due to small secondary relief angle used. Increasing the clearance angle was reported to reduce the contact between the tool and workpiece and consequently reduces cutting forces [23, 24, 30]. CMX-850 PCD router with primary relief had the lowest initial Fy feed force possibly due to tool sharpness and smoothness attributed to the fine grain PCD, see Figure 4.126.

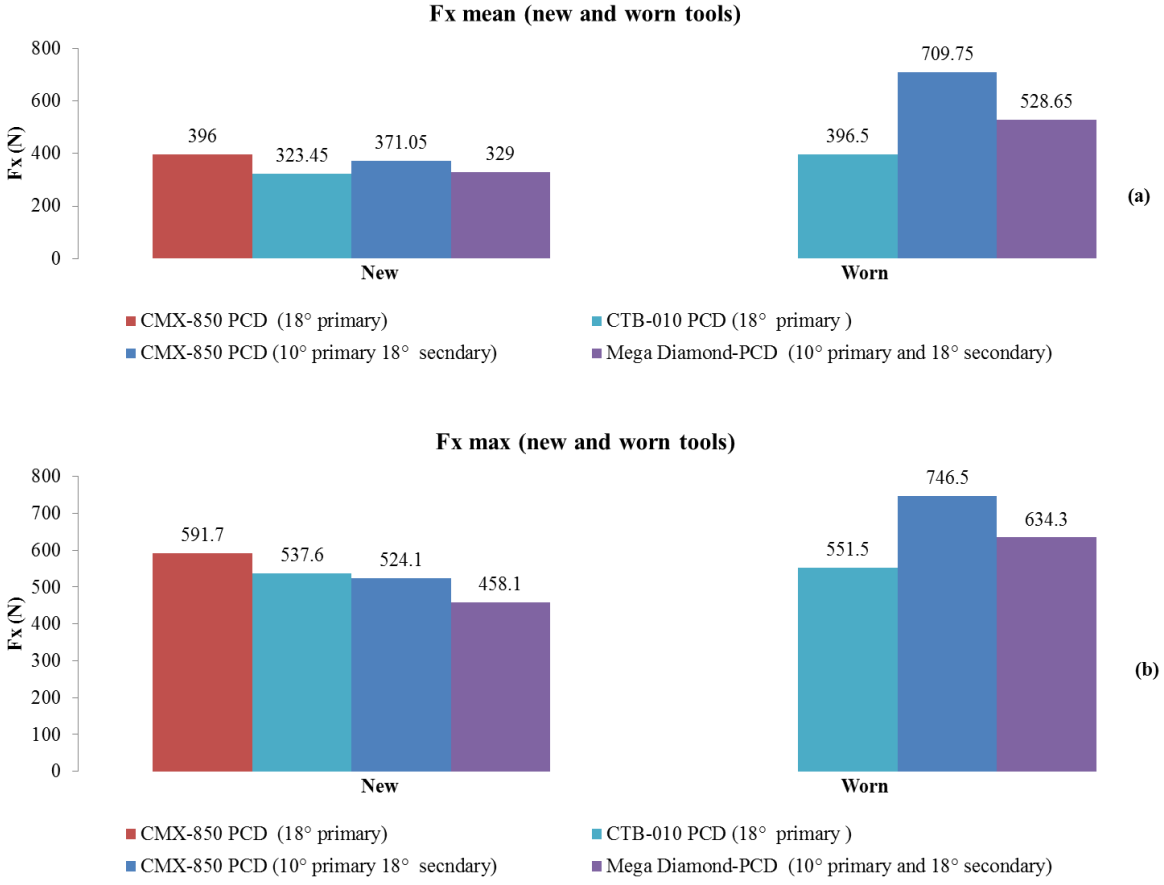

Figure 4.125: Cutting forces Fx for benchmarked tools a) mean b) max

Figure 4.127: Effect of secondary relief on force signal illustrates the recorded force signals for the different tools and how the geometry plays a role in the initial dynamic forces associated with milling process due to varying fibre angles [22]. The fracture of the CMX-850PCD router used at this feed rate was not the first instance, the CMX-850 PCD also fractured in Phase-1 (Test-16) which could be a result of the self-induced chatter. The consequences of such dynamic forces on workpiece surface are discussed in the surface integrity section.

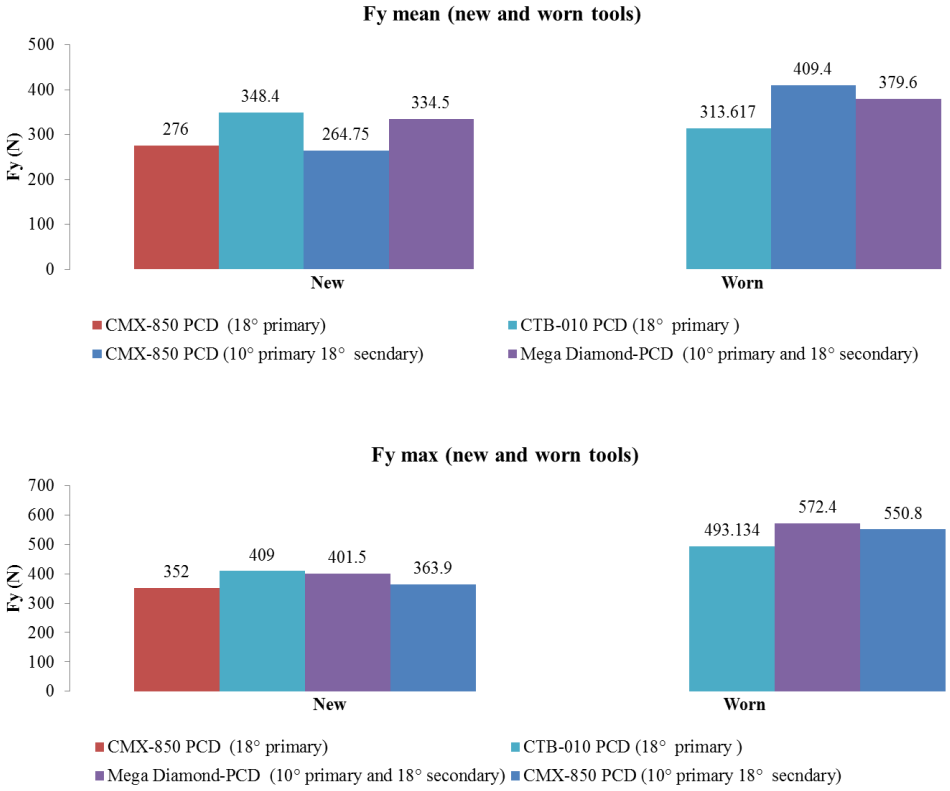

Figure 4.126: Cutting forces Fy for bench marked tools a) mean b) max

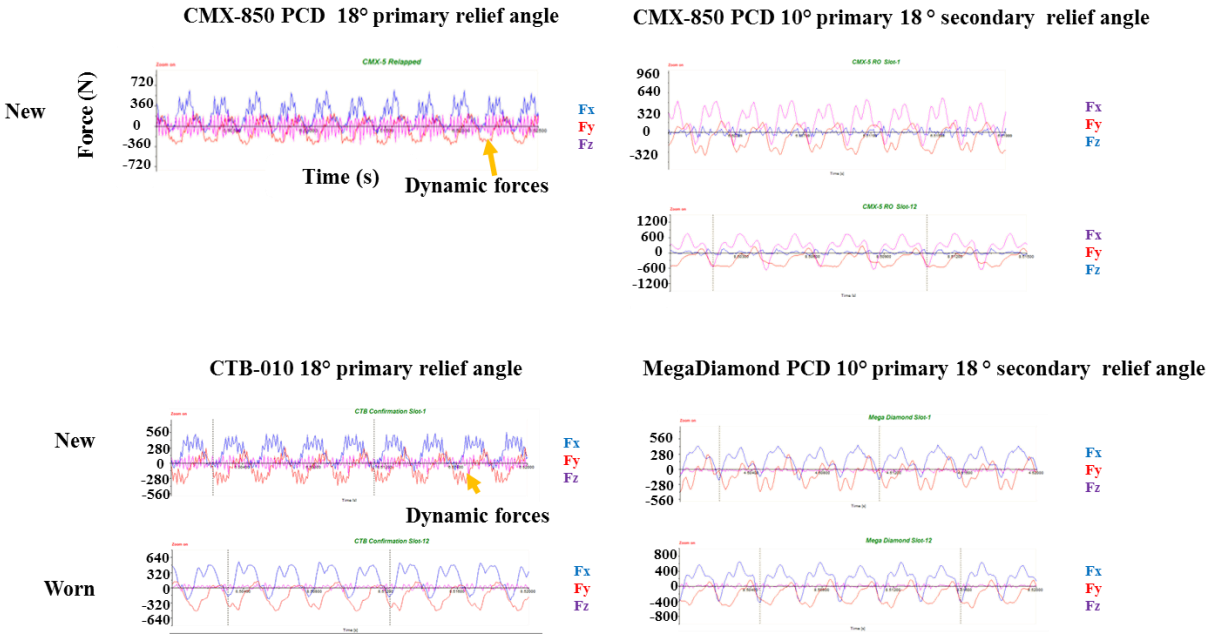

Figure 4.127: Effect of secondary relief on force signal

4.9.3 Surface integrity/roughness

All tools produced slots without fuzz on down-milling side while fuzz was mainly occurring on the up milling side. Figure 4.128 shows the slot obtained, the edge quality using primary and secondary relief angles appeared to be slightly better than a single relief.

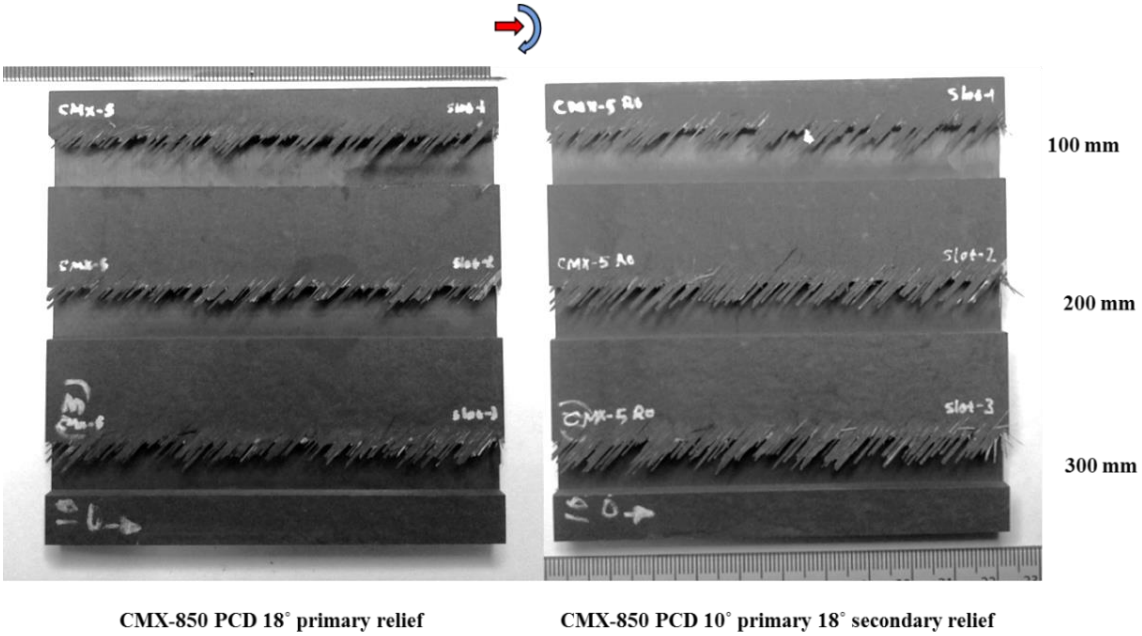

Figure 4.128: Machined slots using different tool geometries

Optical microscope (tool maker's microscope) images showed that the waviness or feed marks were visible when using new tools with primary relief only. Using a tool with primary and secondary relief angles, the marks were barely visible. This could be due to the effect of the cutting edge angles of the later which increased stability and reduced vibration that causes the waviness on the surface resulting in a clean surface. Figure 4.129 shows that surfaces obtained using the worn tools were quite similar in terms of quality.

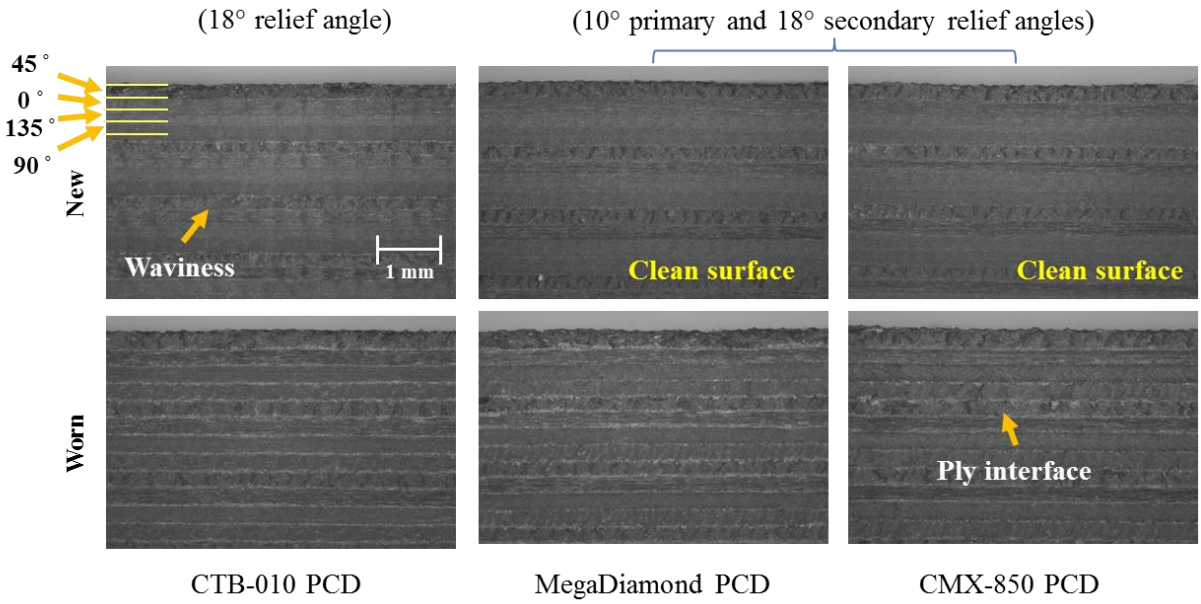

Figure 4.129: Machined surface under tool maker's microscope

The SEM graphs of the down-milling side slot wall (Figure 4.130). The relatively superior wear resistance of the CTB-010 maintained a good surface when the tool was worn. MegaDiamond PCD, the CTB-010 PCD grade equivalent, generated a surface better than that obtained the CMX-850 PCD although they have the same geometry (2 relief angles). The surface when the tool was worn showed some evidence of compressed fibres. Generally, a larger relief angle reduces/eliminates workpiece surface defects caused by tool wear.

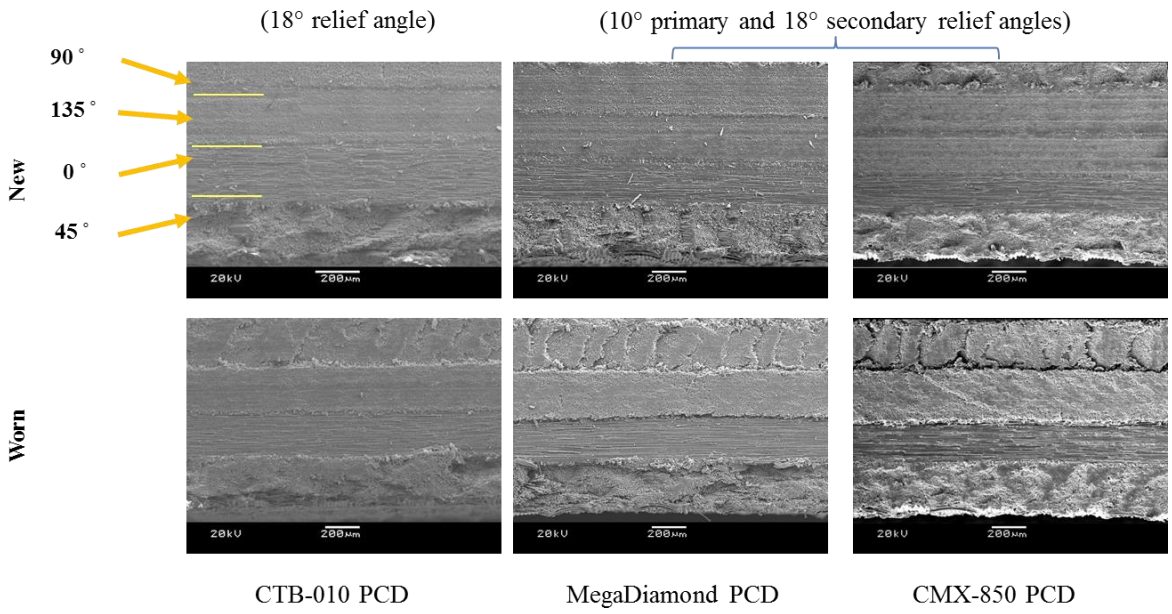

Figure 4.130: SEM images of surfaces obtained using new and worn tools

Surface topography and surface roughness parameters Sa and St are shown in Figure 4.131, Figure 4.132 and Figure 4.133 respectively. Again, CTB-010 PCD with primary relief showed some prominent feed marks in the beginning of the test (tool new) and such feed marks diminished by the end of the test which resulted in surface roughness when tool was worn better than that of the new tool (6.2 µm Sa compared to 14.3 µm Sa) due to the contribution of the feed marks attributed to new tools when cutting is done mostly by shear and mostly visible in case of higher feed rate. Such phenomena may be due to the tool edge flank regrinding by the fibre as noted by Klocke and Wurtz [156] which may provide the tool with a new edge geometry. The damage in 45° layers was the highest as usual and some fibres were pulled out distorting the common wavy pattern of those layers. When the tool was worn the damage extended to the adjacent layer (90°). The 135° layer was easy to compress, this could be the reason they were spread over the neighbouring layers.

There were a lot of similarities between the surfaces generated using both MegaDiamond PCD and CMX-850 PCD possibly because they had the same geometry (10° and 18° primary and secondary relief angles). Although such geometry reduced the tendency of edge chipping, it caused more rubbing and pressure on the machined surface and as a result more spring back phenomenon, noted by Wang and Zhang [29], which occurred at 90° and 135° and were more visible when the tool was worn. Surface roughness parameter Sa for such tools doubled from new to worn condition from 4.8 and 5.4 µm Sa (tool new) to 9.5 and 10 µm Sa (tool worn).

The MegaDiamond grade proved that the 10°/18° primary and secondary relief angle was superior to the single relief angle and resulted in no feed marks at start, which may be a result of dynamic forces as shown in force traces of different tools in Figure 4.127. In addition, the new CMX-850 PCD employing primary and secondary relief angles resulted in surfaces with Sa 5.4331µm and St 112.6945µm which were almost half of the roughness values obtained with a single relief angle tool (10.7725 µm Sa and 185.0971 µm St). When the MegaDiamond and CMX-850 PCD tools with primary and secondary relief were new they produced workpiece surfaces better than CTB-010. If the CTB-010 was ground with equivalent angles it is likely that it would have performed better based on the fact that the CTB-010 was better in terms of wear resistance.

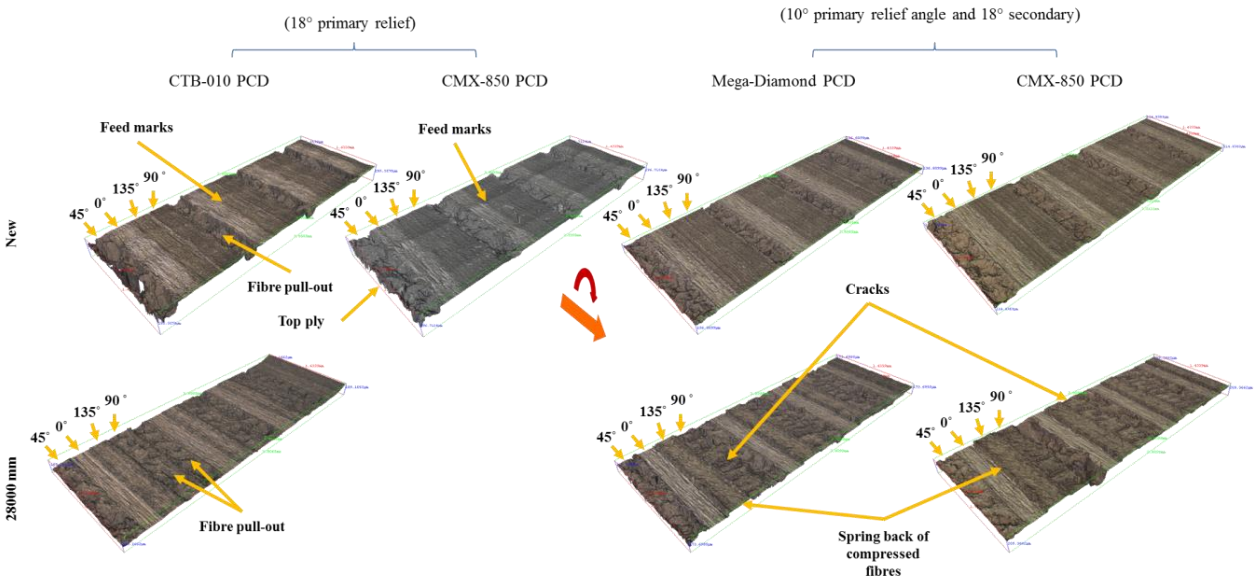

Figure 4.131: Alicona 3D scans of slot wall (down-milling side)

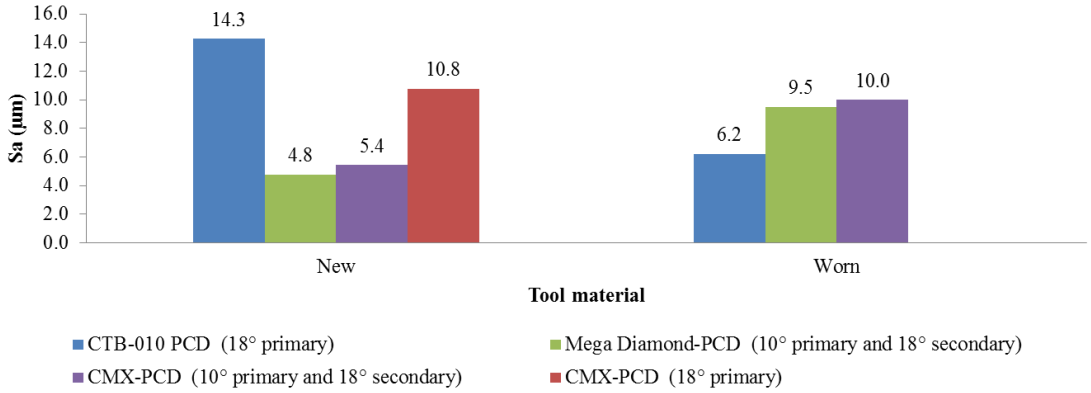

Figure 4.132: 3D surface roughness parameters using different tool

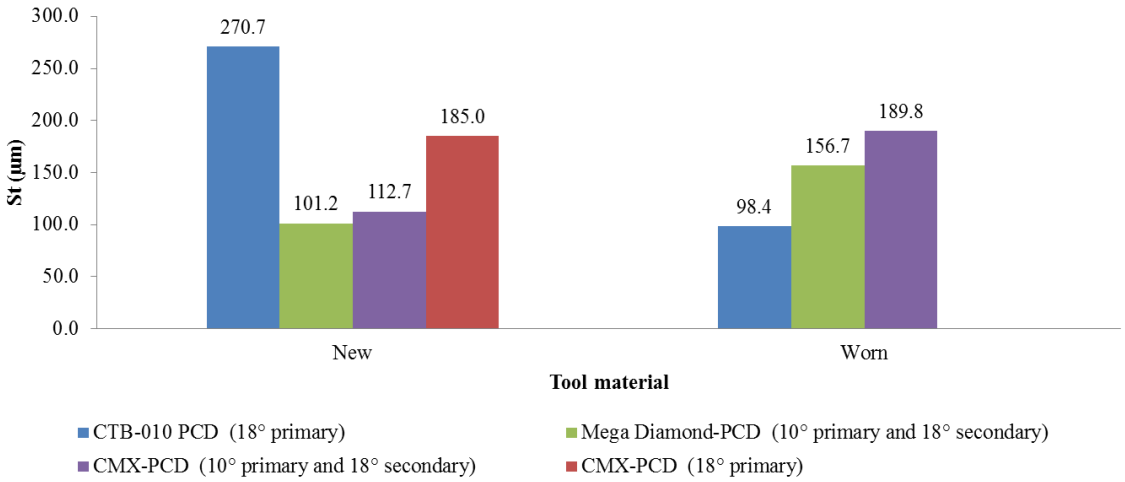

Figure 4.133: 3D surface roughness parameters using different tool

Although Colligan and Ramulu [151] mentioned that Type-I was the most dominant for the 45° top ply, in this test, Type-II delamination was most prevalent which occurred mainly in the 45° top ply on the up milling side. This could be due to the type of fibres used in this test which were flexible enough to escape from the cutting edge without breaking to form Type-I delamination. Alternatively, Colligan and Ramulu's result could have been due to the low temperature associated with the coolant type they used (Freon) which may promoted fracture due to bending. The amount of uncut fibre generally increased with cut length because of the increase in tool wear as the tool became blunt and rounded. This, in turn, caused subsurface delamination the extent of which was measurable using laser scanning. Measuring the length of uncut fibre on the up-milling side, the tools performed similarly apart from MegaDiamond which started and finished the test with relatively lower fuzz length. This may be because of the tool geometry (primary and secondary relief). However the MegaDiamond had little fuzz in down-milling side from 24600 mm cut length, see Figure 4.134. Fuzz length and delamination factor values are listed in Appendix-G.

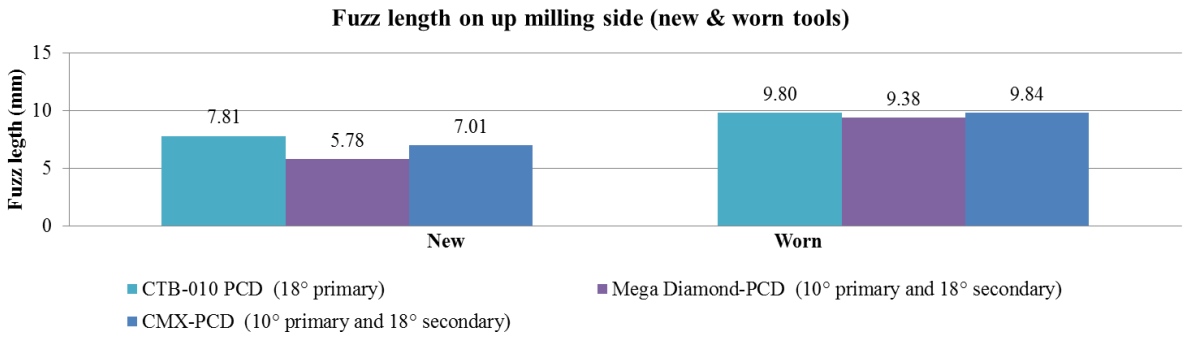

Figure 4.134: Fuzz length for different tools

The MegaDiamond tools showed some good results in terms of delamination factor when the tool was new. This may be related to the tool geometry. CTB PCD came second after MegaDiamond at the same tool conditions but CTB was the last when the tool was worn which may be due to the chipping of the tool edge and high feed forces, see Figure 4.135.

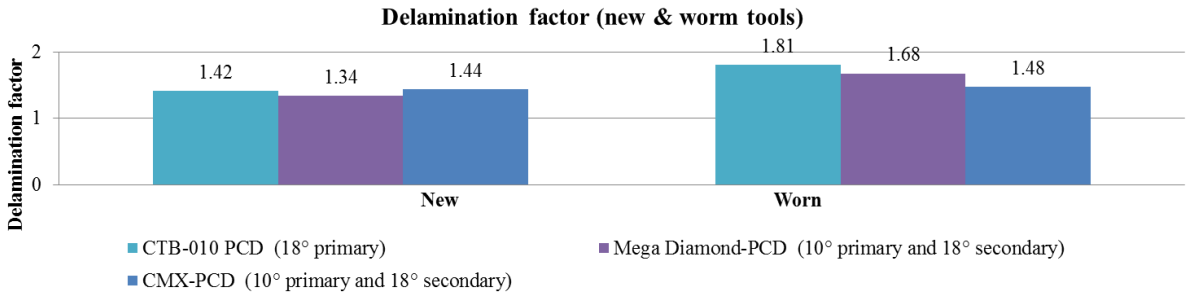

Figure 4.135: Delamination factor for different tools

In summary, the radar graph in Figure 4.136 sorts the tools based on a scale of 1-3 (higher is better) according to responses when these tools were new. The geometry and the mechanical properties of the MegaDiamond together make it a good choice but it was ~17% more expensive per unit. The fabrication of a CTB-010 PCD router with primary and secondary relief angles may result in better performance provided that the edge is ground rather than wire cut.

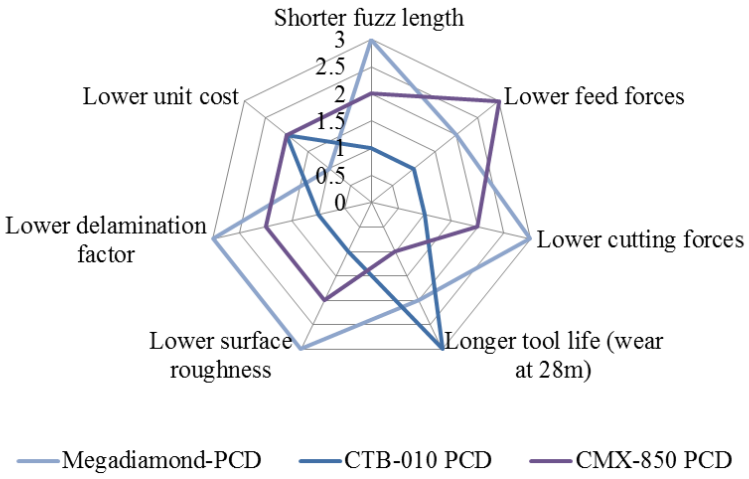

Figure 4.136: Performance of different PCD tools in slotting of CFRP

4.10 Cutting forces, cutting temperature and surface integrity

There were some interactions between cutting forces, and cutting temperature which affected the resulting surface integrity. For example, when milling using different helical tools, the low temperature and high cutting forces associated with using down-cut resulted in rough surfaces while a higher temperature and low forces when using a neutral router resulted in a good surface. This suggested that there was harmless matrix softening which helped reduce friction between the tool and workpiece and consequently reduce cutting forces. The smearing of the softened matrix was beneficial as it added to the surface smoothness. This occurred at a critical temperature of ~200 °C below which the surface deteriorated due to mechanical damage. Above this temperature thermal damage occurred. The critical temperature also influenced the cutting forces. Such a critical temperature was also evident when using different cutting environments such that dry cutting increased thermal damage while the single-nozzle chilled air (low temperature) resulted in higher roughness due to mechanical damage. The best surface roughness was achieved using a twin-nozzle possibly due to cutting at a temperature near the critical temperature.

In case of using a tool with two relief angles, there was no dynamic force which caused feed marks. The stability of this tool geometry contributed to the low delamination factor and fuzz length. The cutting forces using such tools were lower compared to single relief tools. The good surface finish when using twin relief could have resulted from the pressure from the tool flank faces on to the machined surface which was evident in the form of compressed layers. This pressure and rubbing may have caused a rise in temperature which improved the surface.

4.11 Cost/benefit analysis

For the present research work, it was not possible to obtain all the cost variables mentioned in Chapter 2 such machine cost or labour cost due to confidentiality. In addition, the Taylor constant and Taylor exponent for the CFRP material were not available. However, it was possible to provide a comparison between tooling cost using different tool materials/designs. Since the tool life criteria was 28m cut length (equivalent to a length of a wing span) and the tool is used once (not regrindable) to achieve this length of cut, the tooling cost per product C_t becomes the tool price C_{new} minus the tool selvage value C_{scrap}. Assuming the scrap value of the tool was zero the tool cost remained equal to the cost of the new tool as shown in the equation below.

$$Tool\ cost\ \ C_t\ =\ \ C_{new} - C_{scrap} \qquad \text{Equation 4.1}$$

Although many authors find PCD an economic solution for machining composites [154] carbide tools can also offer a versatile solution at lower cost based on test outcomes. For instance, it was possible to obtain 28m cut length using PCD but the quality of the up-milling side was not acceptable due to fuzzing and delamination. On the other hand, at a fraction of the PCD router cost (£59 compared to £310), the uncoated carbide urr router was capable of cutting 28m with no fuzz on either side. The relatively high surface roughness obtained by using uncoated burr routers can be easily accomodated by a subsequent finishing pass using a Dura coated tool which can produce very low surface roughness especially if an up-milling mode is adopted. It was noted by Kauppinen [149] that the wear rate of burr routers was not affected by feed rate which suggests the possibility of using them for high productivity (high feed rate). Assuming that one router will be used for only 28m cut length (although it can be used several time depending on the panel thickness), the total cost then for 28m will be £59 (for the burr router) + £169 (for the Dura coated 2 fluted router) which equals £228, as shown in Table 4.16. This is a 26.5% lower cost than for PCD. Appendix-H lists the unit cost of various tools used in the project.

The cost per meter of cut length, calculated using the equation 4.2, is ~ £8 using WC, compared to £17 per meter using PCD for roughing followed by a finishing pass using a Dura coated tool. The use of a Dura coated burr router is not justified based on the poor performance and the high cost.

$$Cost\ per\ meter\ cut\ length = \frac{Tooling\ cost\ to\ cut\ 28m\ length\ (C_t)}{28}$$ Equation 4.2

Table 4.16: Cost and benefits comparison using PCD and WC

	PCD	**WC**
Tooling cost to cut 28m	£310 (PCD router)	£59 (Uncoated Burr) for roughing + £169 (Dura coated 2 flute) for finishing = £228
Minimum surface roughness in slotting (compared to 3.2 µm Ra or Sa standard for the application)	2.6 µm	1.6 µm
Up-milling side condition	Scrap	Usable
Tooling cost per meter	£17	£8

Considering AWJ process as an alternative, there are a lot of variables that can affect the actual linear cutting speed and cost per meter for a given material such as the properties of material, size and specification of the pump being used, surface finish requirements etc. Assuming the material falls within the range of "generic CFRP" and we are using a 30hp Direct Drive pump rated at 55,000psi/3,800bar, the cut speed range would be 350 – 1,400 mm/min. Therefore, time to cut 1 meter will be 2.8 – 0.7 minutes. The cost per meter then works out at £ 0.75- 0.19/meter. The cost is based upon an overall processing cost for the machine of £16/hour. This cost stays roughly the same irrespective of material or thickness. It should also be considered that as soon as the jet has to go around a corner, then it has to slow down. Piercing of start holes is also a factor that has to be considered when estimating times and costs [235]. At the lower end of the speed range, you will get a nice smooth finish with little evidence of "machining" marks or striations. At the other end of the range, it should be considered a roughing quality cut and will have taper on the cut edge and also evidence of striation lines.

Considering all those aspects, although AWJ can be lower in cost ~ 10% of the milling cost, the milling of CFRP may avoid the water absorption and AWJ related defects. Milling speed using un-coated burr tool was 2547 mm/min which is higher than the roughing speed of the AWJ. As long as the highest productivity requires a quick roughing either by water jet or

by milling, it is much cheaper to use milling rather than installation of AWJ machine which may be costly.

4.12 Summary of results

4.12.1 Phase-1: Effect of operating conditions, tool materials and cutter design

4.12.1.1 Phase-1A: Preliminary work

- Despite a depth of cut of 5 mm, wear on the ITC PCD router was minimal (flank wear < 40 µm after 1860 mm cut length) following slotting of CFRP at a cutting speed and feed rate of 200 m/min and 0.3 mm/tooth respectively. In addition, no major damage modes (e.g. fuzzing, delamination etc.) were apparent on any of the machined surfaces analysed.
- In general, cutting forces increased with both cutting speed and feed rate, which was most likely due to higher wear rates and larger uncut chip thicknesses.
- Workpiece surface roughness typically ranged between 6 to 10 µm Sa (measured using contact stylus). An initial rise followed by a drop in surface roughness was observed as cutting speed increased from 200 to 650 m/min. The opposite trend however was seen with respect to variation in feed rate (0.03 to 0.15 mm/tooth).
- Increasing cutting speed from 200 to 350 m/min led to a ~17% rise in temperature while higher feed rates reduced cutting temperature due to the shorter contact time between the tool and workpiece. Cutting temperature was also observed to vary linearly with increasing depth of cut.

4.12.1.2 Phase-1B: Influence of operating conditions and tool materials

- Rapid wear rates and severe damage in the form of serrated cutting edges (with depth of serration corresponding to ply orientation) were evident when machining with the DLC-coated WC routers. Tool life did not exceed 900 mm, irrespective of the operating conditions. This was caused by the high level of cutting forces (up to 856 N Fx and 1301 N Fy) and abrasive nature of the carbon fibres.
- The use of chilled air prevented accumulation of dust in the slots and reduced the risk of workpiece burning. This was in contrast to tests performed dry where agglomeration of charred matrix material was observed, resulting in poor surface finish and tool life.

- Fuzzing on the machined surfaces was prevalent as tool flank wear exceeded ~ 0.1 mm, irrespective of tool material.
- The combination of low cutting speed and low feed rates generally produced good surface finish (3.6 µm Ra) although signs of burning were still apparent in a number of trials undertaken dry. Conversely, the routers were susceptible to fracture when operating at high cutting speeds and feed rates due to the greater machining forces.
- The use of low cutting speed (200 m/min) together with high feed rate (0.03 mm/tooth) generally resulted in superior workpiece surface integrity/roughness. The nature of workpiece defects however varied according to the ply orientation. Wavy surfaces, fibre reorientation or pull out were prevalent at 45° plies, while loose or spreading of fibres were predominant at 0° and 135° directions with matrix cracking and fibre pull out the dominant damage mechanism in the 90° layers.
- Surface roughness deteriorated as machining progressed due to the increase in tool wear. Workpiece surfaces roughness using CMX-850 PCD was 3.6 µm Ra, 29 µm Rt when new compared to 21 µm Ra and 95 µm Rt when the tool was worn.
- Cutting forces when employing the DLC coated WC tools were significantly higher compared to the PCD routers (Fx and Fy of as low as 159 and 130 N at 200 m/min and 0.03 mm/tooth using PCD compared to as high as 856 N Fx and 1301 N Fy using DLC coated WC). When the angle of the resultant force with respect to cutting direction (perpendicular to feed) was lower than 45°, fuzzing was reduced.
- Tool life was up to 95 times higher when employing PCD compared to the DLC coated WC routers, with the CTB-010 grade showing the best performance according to the ANOVA. None of the factors were significant. A relatively high error level (70%) however was obtained, which was likely due to interactions between factors.
- The coarse grained PCD (CTM-302) was prone to chipping especially at high feed rates due to high mechanical loads and lower fracture toughness of the CTM-302 grade.
- Feed rate was the most significant factor affecting both cutting force (Fx) and surface roughness with PCR's of 38% and 57.47% respectively.
- While the use of chilled air was beneficial for debris removal and prevention of workpiece burning, cutting environment was not statistically significant with respect to all the responses evaluated.

4.12.1.3 Phase-1C: Benchmarking of Element 6 PCD grades at preferred operating parameters

- The performance of the PCD tools fabricated via mechanical grinding was superior to routers manufactured using electrical discharge grinding (EDG). This was possibly due to the generation of tensile residual stresses in the tool material when utilising the non-conventional EDG process.
- The confirmation test involving the CTB-010 grade showed a further 30% improvement in tool wear and corresponding reduction in cutting forces.
- The WPC-102 PCD grade exhibited higher tool wear (~60%), cutting forces (~20%) and surface roughness compared to CTB-010 PCD.

4.12.1.4 Phase-1D: Benchmarking of carbide tooling products

- The Dura coated WC tools suffered peeling/removal of the CVD diamond coating when operating at elevated cutting speeds or feed rates (500 m/min cutting speed and 0.15 mm/tooth feed rate), which was attributed to brittle fracture of the layer.
- Dura coated products outperformed both the DLC-coated and uncoated WC routers in terms of tool life due to its diamond structure containing the stronger sp3 carbon bonds. The workpiece surface generated using the Dura-coated tools were superior in terms of tool life as it was 48 and 16 times longer than DLC-coated and uncoated WC routers respectively. In addition, the surface roughness was better (1.9 µm Sa compared to 9 µm Sa using uncoated) due to the higher wear resistance and lower roughness of the coating surface.
- Uncoated burr type routers generally produced rougher surfaces compared to the 2-fluted cutters (24 µm Sa and 300 µm St) however no fuzzing on either side of the slots were evident even after 28 m cut length, due to its down cutting action.
- No substantial benefit was observed when using the Dura coated burr router due to failure of the coating and subsequent wear on the substrate.

4.12.2 Phase-2: Effect of workpiece material lay-up configuration

4.12.2.1 Phase-2A: Preliminary testing and temperature measurement

- Workpiece material with fibres orientated at 0° (with respect to the tool cutting direction) showed the highest cutting force (Fx) while samples with fibres in the 90° direction generated highest feed force (Fy). This is due to the instantaneous fibre

orientation with respect to the cutting edge at the middle of the slot (i.e. at the point of maximum chip thickness).

- Plies at 45° showed the highest levels of workpiece damage and was generally characterised by a wavy surface due to severe matrix loss or fibre pull out.
- The Type-2 CFRP material generally exhibited the lowest surface roughness (3.4 µm Sa) owing to the higher number of 0° layers in the laminate lay-up. Conversely, the Type-3 configuration resulted in the highest surface roughness due to the greater number of 45° plies.
- Surface roughness (Sa) of the up-milled slot wall (by 70 – 75% depending on the CFRP configuration) was lower compared to surfaces produced by down-milling which was possibly due to the lower temperatures generated in the up-milling direction.
- The layers oriented at 45° were responsible for the highest cutting temperature because of the high friction caused by this layer.
- Cutting temperature was highest when machining the Type-3 material (263°C), which was ~ 4% and 0.7 % greater than Type-1 and Type-2 configurations respectively.
- The Neutral geometry routers resulted in the highest cutting temperature (271°C), with the Down-cut and Up-cut geometry showing reductions of up to ~8% and ~4% respectively.
- Temperature when machining under the ¾ engagement strategy was ~15% lower compared to full engagement slotting.
- Measured temperature was ~100°C higher when machining dry as opposed to employing chilled air. In addition, the use of single-nozzle delivery resulted in 20°C lower cutting temperatures in comparison the twin-nozzle arrangement, due to the higher air speed generated in the former.

4.12.2.2 Phase-2B: Effect of workpiece material lay-up configuration

- Cutting edges prepared using EDG were more prone to chipping due to the high initial cutting forces.
- The Type-3 CFRP configuration generally caused severe chipping of the routers, particularly at locations with higher concentration of 45° orientated layers. Workpiece material configuration was the most significant factor influencing tool life with a PCR of 61.3%.

- Workpiece lay-up was the sole significant factor affecting surface roughness (Sa) with a PCR of 63.7%. Other factors were statistically insignificant.
- In terms of workpiece delamination factor and fuzzing, feed rate had the greatest effect with a PCR of 50.1% and 57.8 % respectively.

4.12.2.3 Phase-2C: Effect of cutting environment

- Although the application of chilled air (in single-nozzle mode) did not have any appreciable effect on tool wear or fuzz length, cutting forces were seen to increase (by 25% for Fx and 5% Fy when tools were new) while workpiece delamination factor was 12.5% lower when using chilled air environment in single-nozzle mode compared to twin-nozzle (1.6 compared to 1.8 when tools were worn).
- Use of twin-nozzle delivery of chilled air was preferred to the single-nozzle mode in terms of surface integrity such that a twin-nozzle chilled air resulted in a surface with ~ 50% better in surface roughness having 6.2 µm Sa and 98 µm St compared to 12.3 µm Sa and 267.3 µm St in case of the single-nozzle configuration.

4.12.3 Phase-3: Effect of varying tool geometry

4.12.3.1 Phase-3A: Influence of router helix angle

- The variation in helix angle did not have any major influence on tool life, possibly due to the relatively low values employed (± 3°).
- The Down-cut geometry generated the lowest cutting temperatures but the highest forces.
- The Neutral geometry router produced the lowest surface roughness (Sa) compared to routers with a positive or negative helix angle.

4.12.3.2 Phase-3B: Effect of secondary clearance angle

- Single relief angle routers were less stable compared with tools having a secondary clearance, especially when the tool was in the new condition/sharp. This was reflected by the force signals showing greater dynamic variation when machining with the single relief tools.
- While feed marks and relatively high surface roughness were initially apparent when employing routers with single relief angles, workpiece quality improved as cutting progressed due to the contact between the cutter and workpiece as tool wear increased.

- In general, the twin relief angle tools generated lower surface roughness (~ 50%), reduced fuzzing and smaller delamination factor compared to single clearance angle routers.

5 CONCLUSIONS & FUTURE WORK

5.1 Conclusions

A- Undertake a comprehensive literature review on the machining of composite materials across different engineering applications, and in particular on the milling/routing of CFRP's.

The literature review highlighted the absence of data on the use of high cutting speeds and high feed rates especially in slotting using polycrystalline diamond (PCD) together with the use of different PCD grades (with cutting edges manufactured by different grinding techniques) or various diamond coatings in the slotting of CFRP. Furthermore, there was no data covering tool temperature during slot milling or the influence of material configuration. The effect of different chilled air flow rates on machined surface quality had not been studied, despite equipment and data for vortex operated chilled air delivery being available with reference to other materials. In addition, delamination assessment using laser techniques was limited. In relation to tool geometry, no details could be found concerning the effect of geometry either on stability of cutting or cutting temperature and consequent effects on surface integrity when milling FRP composites. Cost analysis with respect to tooling when slotting CFRP was similarly not discussed.

B- Identify preferred/optimum tool material, operating parameters and the cutting environment for the machining of specified carbon fibre reinforced composite material.

Cutting force increased with cutting speed and particularly feed rate this latter parameter influencing the cutting force Fx and surface roughness by 38% and 57% PCR respectively. Conversely, increase in the feed rate caused a reduction in cutting temperature due to the reduced contact time between tool and workpiece.

An increase in axial depth of cut (slot depth) resulted in a linear increase in tool temperature. Cutting temperature increased also with cutting speed such that a 17% rise in temperature was observed when cutting speed was increased from 200 to 350 m/min.

Unlike metal cutting, the use of low cutting speed and feed rate resulted in low surface roughness. A surface with 2.6 µm Ra was obtained at 200 m/min cutting speed and 0.15 mm/tooth fed rate.

The use of chilled air reduced the tendency of burning and the thermal induced damage to the workpiece surface. Tool temperature using Twin-nozzle chilled air was 100°C lower than

in dry cutting. Varying the number of nozzles from two to one affected the air flow rate and air temperature and caused a 20 °C reduction in tool temperature and in turn resulted in 12.5% lower delamination factor, 25% lower cutting force Fx and 5% lower feed force Fy. Use of twin-nozzle chilled air improved tool life by 30% in comparison to dry cutting.

Cutting temperature during milling ¾ engagement coupons was 15% less than the tool temperature during slotting at full engagement.

Carbide tools suffered from severe tool wear which was reflected in the cutting forces (1300 N Fx) as well as surface quality especially when milling was undertaken dry environment. The quality deteriorated as the machining progressed.

Tool life using 2-fluted PCD tools was 95 times longer than the DLC-coated WC counterpart due to the higher abrasion resistance of the PCD.

PCD tool life was influenced by edge preparation process such that mechanical grinding was recommended for a tool with higher chipping resistance. The thermal effect of non-conventional EDG promoted cracking of the PCD.

The Dura (CVD diamond) coated tool was the best for finishing as it produced a surface with 1.6 µm Sa surface roughness which was lower than the standard requirement of 3.2 µm. In addition, the Dura-coated router out performed both DLC-coated and uncoated WC routers in terms of wear resistance owing to the stronger Sp3 carbon structure such that it was 48 times better than the uncoated tool in terms of the cut length. Each tool responded differently to the brushing action of the carbon fibres during cutting s resulting in different wear types.

C- Evaluate the effect of workpiece material variables (different unidirectional "UD", and multidirectional workpiece layups etc.) on machinability performance.

The fibre orientation affected cutting forces, cutting temperature and surface roughness. Forces were determined by the instantaneous fibre orientation at point of maximum chip thickness (i.e. middle of the slot). The 0° fibres resulted in the highest cutting force Fx while the highest feed force Fy resulted from cutting 90° layers. Fibres at 45° angle of orientation were responsible for the high levels of surface damage, cutting temperature and tool wear. Lay-up significantly influenced tool wear having a 61.3 % PCR.

Behaviour of a lay-up configuration was affected by its constituents or the number of plies at each direction. Type-2 lay-up for example resulted in the highest cutting forces Fx but resulted in the lowest surface roughness (3.4 µm). Workpiece lay-up was found to be the most significant factor affecting the surface roughness with 63.7 % PCR.

By calculating the cutting force Fx per ply when milling unidirectional lay-up, it was possible to calculate the cutting force for different lay-up configurations.

Cutting temperature was highest when machining the Type-3 material (263°C), which was ~ 4% and 0.7 % greater than Type-1 and Type-2 configurations respectively.

D- Evaluate the effect of varying tool geometry on the machinability of CFRP with reference to the effect of helix angle and secondary clearance on slot milling performance and surface integrity.

Low helix angle variation did not have a major influence on tool life. Down cut geometry resulted in the lowest cutting temperature which was 8% less than neutral geometry. However, the use of neutral geometry was beneficial in terms of surface roughness due to matrix smearing at elevated cutting temperature.

The use of a tool with a secondary clearance resulted in more stable cutting with no dynamic forces or vibration which reduced/eliminated feed marks. The cutting force traces also revealed that cutting stability improved when using a single relief tool. The twin relief cutting edge produced a 50% better surface in terms of surface roughness and resulted in lower fuzz and delamination.

E- Identify operating approaches that minimise / eliminate workpiece surface defects such as delamination, fibre pull-out, matrix chipping / degradation, cracking etc. during milling/routing.

Fuzzing on the machined surfaces was prevalent as tool flank wear exceeded ~ 0.1 mm, irrespective of tool material.

Tool temperature during up-milling was lower than that during down-milling and as a result the surface roughness on the up-milling side was 70% better than the down-milling side. The up-milling mode is suggested for finishing passes to further improve surface quality.

Feed rate was the most statistically significant factor influencing the delamination factor and fuzz length with 50.1% and 57.8% PCR respectively. The use of laser scanning can be used during milling for direct quality monitoring and also as an indirect method to evaluate tool wear.

The use of chilled air was beneficial for debris removal and prevention of workpiece burning. Workpiece delamination factor was 12.5% lower when using chilled air environment

in single-nozzle mode compared to twin-nozzle. However, use of twin-nozzle delivery of chilled air was preferred to the single-nozzle mode in terms of surface roughness.

F- Perform a cost benefit analysis on the proposed machining approach.

The uncoated WC burr router was the ideal choice for roughing due to the ability to cut a 28m fuzz-free cut length (both up milling and down milling sides). The high surface roughness resulting from using the burr tool could be ameliorated by a subsequent finishing pass using a Dura-coated tool. The use of an uncoated burr router followed by a Dura coated 2-flue router for finishing was found economical at £8/m compared to 17£/m using a PCD. The routing of CFRP could be better than AWJ in terms of accuracy and quality. There was no benefit of using a diamond coated burr for slotting due to poor tool life.

5.2 Recommendations for future work

Based on results from the present research, a number of related areas involving the machining of CFRP have been identified for future evaluation:

- Assess the performance of CTB-010 PCD and Dura coated WC routers as well as burr type routers for the edge trimming of CFRP.
- Investigate the use of abrasive point grinding for the routing/trimming of CFRP materials.
- Evaluate the performance benefits of ultrasonic assisted cutting of CFRP in comparison to conventional end milling/trimming.
- Further experimental investigation on the influence of varying tool geometry (larger helix angles, and negative rake angles) and tool design when milling CFRP.
- Investigate the feasibility of employing wire electrical discharge machining (WEDM) for the routing/trimming of CFRP.
- Investigate the performance of trochoidal milling strategy.
- Development of a finite element model to simulate the edge routing/slotting of CFRP in order to predict tool life, cutting forces, cutting temperature and workpiece surface integrity.

6 REFERENCES

1. *Design _ Airbus, a leading aircraft manufacturer*. 2014 [cited 2014 14/03/2014]; Available from: http://www.airbus.com/innovation/ecoefficiency/design/?contentId=%5B_TABLE%3Att_content%3B_FIELD%3Auid%5D%2C&cHash=22935adfac92fcbbd4ba4e1441d13383
2. Marsh, G. *Going stealthy with composites*. 2010 [cited 2014; Available from: http://www.reinforcedplastics.com/view/12162/going-stealthy-with-composites/.
3. Gay, D., S. Hoa, and S. Tsai, *Composite Materials – Design and Applications*. 2003: CRC Press, I S B N 1-58716-084-6.
4. Sheikh-Ahmad, J., *Machining of polymer composites*. 2009: Springer, I S B N 978-0-387-35539-9.
5. Gill, R.M., *Carbon fibres in composite materials*. 1972, I S B N 0-592-00069-9.
6. Callister, W. and D. Rethwisch, *Materials Science and Engineering: An Introduction*. 8th ed. 2010: Wiley, I S B N 978-0-470-41997-7.
7. Mallick, P.K., *Fiber reinforced composites : Materials, manufacturing, and design*. Third Edition. 2008: CRC Press, I S B N 978-0-8493-4205-9.
8. Hexcel *Prepreg Technology*. 2005.
9. Morgan, P., *Carbon fibers and their composites*. 2005: Taylor and Francis, I S B N 978-0-8247-0983-9.
10. *Composite materials handbook* Vol. 5. Ceramic matrix composites. 2002: US Department of Defense, I S B N MIL-HDBK-17-5.
11. Chung, D.D.L., *Carbon Finber Composites*. 1994: Butterworth-Heinemann, I S B N 0-7506-9169-7.
12. *Machining carbon fibre materials : User's guide.* Sandvik Coromant, 2010,C-2920:30.
13. *Introduction to Advanced Composites and Prepreg Technology.* Umeco, 2012,SM1010/03.12/6.
14. Academy, S., *Transitional Composites Training (Material and Process Fsamiliarisation)*. 2006: Airbus, I S B N.
15. Peters, S., *Handbook of Composites*. 2nd ed. 1998: Chapman & Hall, I S B N 0412540207.
16. Choo, V.K.S., *Fundamentals of composite materials*. 1990: Knowen Academic Press, Inc., I S B N 0-929785-00-2.
17. *Composite materials handbook* Vol. 2. Polymer matrix composites materials properties. 2002: US Department of defense, I S B N MIL-HDBK-17-2F.
18. Fournie, L., C. Herve, and F. Fort, *Self-stiffened panels of preimpregnated composite and manufacturing process for components of such panels*. 2008: United States.
19. *Modern Metal Cutting : A Practical Handbook*. 1994: Sandvik Coromant, I S B N 9197229903.
20. Davim, J.P., *Machining of Metal Matrix Composites*. 2011: Springer, I S B N 978-0-85729-937-6.
21. Koplev, A., A. Lystrup, and T. Vorm, *The cutting process, chips, and cutting forces in machining CFRP*. Composites, 1983. 14(4): p. 371-376.
22. Bhatnagar, N., N. Ramakrishnan, N.K. Naik, and R. Komanduri, *On the machining of fiber-reinforced plastic (FRP) composite laminates.* International Journal of Machine Tools & Manufacture, 1995. 35(5): p. 701-716.

23. Wang, D.H., M. Ramulu, and D. Arola, *Orthogonal cutting mechanisms of graphite/epoxy composite. Part I: Unidirectional laminate.* International Journal of Machine Tools and Manufacture, 1995. 35(12): p. 1623-1638.
24. Wang, D.H., M. Ramulu, and D. Arola, *Orthogonal cutting mechanisms of graphite/epoxy composite. Part II: Multi-directional laminate.* International Journal of Machine Tools and Manufacture, 1995. 35(12): p. 1639-1648.
25. Ramulu, M., *Machining and surface integrity of fibre-reinforced plastic composites.* Sadhana-Academy Proceedings in Engineering Sciences, 1997. 22: p. 449-472.
26. Arola, D., M. Ramulu, and D.H. Wang, *Chip formation in orthogonal trimming of graphite/epoxy composite.* Composites Part A: Applied Science and Manufacturing, 1996. 27(2): p. 121-133.
27. Arola, D. and M. Ramulu, *Orthogonal cutting of fiber-reinforced composites: A finite element analysis.* International Journal of Mechanical Sciences, 1997. 39(5): p. 597-&.
28. Arola, D., M.B. Sultan, and M. Ramulu, *Finite element modeling of edge trimming fiber reinforced plastics.* Journal of Manufacturing Science and Engineering-Transactions of the ASME, 2002. 124(1): p. 32-41.
29. Wang, X.M. and L.C. Zhang, *An experimental investigation into the orthogonal cutting of unidirectional fibre reinforced plastics.* International Journal of Machine Tools & Manufacture, 2003. 43(10): p. 1015-1022.
30. Caprino, G. and L. Nele, *Cutting forces in orthogonal cutting of unidirectional GFRP composites.* Journal of Engineering Materials and Technology-Transactions of the Asme, 1996. 118(3): p. 419-425.
31. Caprino, G., I. DeIorio, L. Nele, and L. Santo, *Effect of tool wear on cutting forces in the orthogonal cutting of unidirectional glass fibre-reinforced plastics.* Composites Part a-Applied Science and Manufacturing, 1996. 27(5): p. 409-415.
32. Mkaddem, A., I. Demirci, and M. El Mansori, *A micro-macro combined approach using FEM for modelling of machining of FRP composites: Cutting forces analysis.* Composites Science and Technology, 2008. 68(15-16): p. 3123-3127.
33. Rao, G.V.G., P. Mahajan, and N. Bhatnagar, *Micro-mechanical modeling of machining of FRP composites - Cutting force analysis.* Composites Science and Technology, 2007. 67(3-4): p. 579-593.
34. Rao, G.V.G., P. Mahajan, and N. Bhatnagar, *Three-dimensional macro-mechanical finite element model for machining of unidirectional-fiber reinforced polymer composites.* Materials Science and Engineering: A, 2008. 498(1-2): p. 142-149.
35. Gaitonde, V.N., S.R. Karnik, F. Mata, and J. Paulo Davim, *Study on some aspects of machinability in unreinforced and reinforced polyamides.* Journal of Composite Materials, 2009: p. 725-739.
36. Gaitonde, V.N. and J.P. Davim, *Machinability evaluation in unreinforced and reinforced PEEK composites using response surface models.* Journal of Thermoplastic Composite Materials, 2009: p. 1-14.
37. Palanikumar, K., L. Karunamoorthy, and R. Karthikeyan, *Optimizing the machining parameters for minimum surface roughness in turning of GFRP composites using design of experiments.* Journal of Materials Science & Technology, 2004. 20(4): p. 373-378.
38. Ferreira, J.R., N.L. Coppini, and F.L. Neto, *Characteristics of carbon-carbon composite turning.* Journal of Materials Processing Technology, 2001. 109(1-2): p. 65-71.
39. Rahman, M., S. Ramakrishna, J.R.S. Prakash, and D.C.G. Tan, *Machinability study of carbon fiber reinforced composite.* Journal of Materials Processing Technology, 1999. 89-90: p. 292-297.

40. An, S.O., F.S. Lee, and S.L. Noh, *A study on the cutting characteristics of glass fiber reinforced plastics with respect to tool materials and geometries.* Journal of Materials Processing Technology, 1997. 68(1): p. 60-67.
41. Davim, J.P. and F. Mata, *Chemical vapour deposition (CVD) diamond coated tools performance in machining of PEEK composites.* Materials & Design, 2008. 29(8): p. 1568-1574.
42. Davim, J.P. and F. Mata, *New machinability study of glass fibre reinforced plastics using polycrystalline diamond and cemented carbide (K15) tools.* Materials & Design, 2007. 28(3): p. 1050-1054.
43. Sreejith, P.S., R. Krishnamurthy, S.K. Malhotra, and K. Narayanasamy, *Evaluation of PCD tool performance during machining of carbon/phenolic ablative composites.* Journal of Materials Processing Technology, 2000. 104(1-2): p. 53-58.
44. Ferreira, J.R., N.L. Coppini, and G.W.A. Miranda, *Machining optimisation in carbon fibre reinforced composite materials.* Journal of Materials Processing Technology, 1999. 93: p. 135-140.
45. Silva, L.R. and J.P. Davim, *The Effect of Tool Geometry on the Machinability of Polyamide During Precision Turning.* Journal of Composite Materials, 2009. 43(23): p. 2793-2803.
46. Silva, L.R., J.P. Davim, A.M. Abrao, and P.E. Faria, *Merchant model applied to precision orthogonal cutting of PA66 polyamide with and without glass fiber reinforcing.* Journal of Composite Materials, 2009. 43(23): p. 2727-2737.
47. Masuda, M., Y. Kuroshima, and Y. Chujo, *Failure of tungsten carbide cobalt alloy tools in machining of carbon materials.* Wear, 1993. 169(2): p. 135-140.
48. Santhanakrishnan, G., R. Krishnamurthy, and S.K. Malhotra, *Investigation into the machining of carbon-fiber-reinforced plastics with cemented carbides.* Journal of Materials Processing Technology, 1992. 30(3): p. 263-275.
49. Palanikumar, K. and J.P. Davim, *Mathematical model to predict tool wear on the machining of glass fibre reinforced plastic composites.* Materials & Design, 2007. 28(7): p. 2008-2014.
50. Palanikumar, K. and J.P. Davim, *Assessment of some factors influencing tool wear on the machining of glass fibre-reinforced plastics by coated cemented carbide tools.* Journal of Materials Processing Technology, 2009. 209(1): p. 511-519.
51. Sarma, P.M.M.S., L. Karunamoorthy, and K. Palanikumar, *Surface roughness parameters evaluation in machining GFRP composites by PCD tool using digital image processing.* Journal of Reinforced Plastics and Composites, 2009. 28(13): p. 1567-1585.
52. Palanikumar, K., *Surface roughness model for machining glass fiber reinforced plastics by PCD tool using fuzzy logics.* Journal of Reinforced Plastics and Composites, 2009. 28(18): p. 2273-2286.
53. Palanikumar, K., *Cutting parameters optimization for surface roughness in machining of GFRP composites using Taguchi's method.* Journal of Reinforced Plastics and Composites, 2006. 25(16): p. 1739-1751.
54. Palanikumar, K., F. Mata, and J.P. Davim, *Analysis of surface roughness parameters in turning of FRP tubes by PCD tool.* Journal of Materials Processing Technology, 2008. 204(1-3): p. 469-474.
55. Usuki, H., N. Narutaki, Y. Yamane, S. Karasuno, and T. Ito, *A study on the cutting performance of diamond coated tools - Tool wear of diamond coated tools in machining of CFRP.* Bulletin of the Japan Society of Precision Engineering, 1991. 25(1): p. 35-36.

56. Ramulu, M., M. Faridnia, J.L. Garbini, and J.E. Jorgensen, *Machining of graphite epoxy composite-materials with polycrystalline diamond (PCD) tools.* Journal of Engineering Materials and Technology-Transactions of the ASME, 1991. 113(4): p. 430-436.
57. Davim, J.P. and F. Mata, *A new machinability index in turning fiber reinforced plastics.* Journal of Materials Processing Technology, 2005. 170(1-2): p. 436-440.
58. Kim, J.D. and E.S. Lee, *A study of the ultrasonic-vibration cutting of carbon-fiber-reinforced plastics.* Journal of Materials Processing Technology, 1994. 43(2-4): p. 259-277.
59. Tsao, C.C. and H. Hocheng, *Computerized tomography and C-Scan for measuring delamination in the drilling of composite materials using various drills.* International Journal of Machine Tools & Manufacture, 2005. 45(11): p. 1282-1287.
60. Piquet, R., B. Ferret, F. Lachaud, and P. Swider, *Experimental analysis of drilling damage in thin carbon/epoxy plate using special drills.* Composites Part a-Applied Science and Manufacturing, 2000. 31(10): p. 1107-1115.
61. Hocheng, H. and C.C. Tsao, *Effects of special drill bits on drilling-induced delamination of composite materials.* International Journal of Machine Tools and Manufacture, 2006. 46(12-13): p. 1403-1416.
62. Tsao, C.C. and H. Hocheng. *Parametric study on thrust force of core drill*. Proceddings of 7th Asia Pacific Conference on Materials Processing (APCMP). 2006. Singapore, p. 37-40.
63. Tsao, C.C., *Effect of deviation on delamination by saw drill.* International Journal of Machine Tools & Manufacture, 2007. 47(7-8): p. 1132-1138.
64. Tsao, C.C., *Thrust force and delamination of core-saw drill during drilling of carbon fiber reinforced plastics (CFRP).* International Journal of Advanced Manufacturing Technology, 2008. 37(1-2): p. 23-28.
65. Tsao, C.C., *Experimental study of drilling composite materials with step-core drill.* Materials & Design, 2008. 29(9): p. 1740-1744.
66. Zhang, L.-B., L.-J. Wang, and X.-Y. Liu, *A mechanical model for predicting critical thrust forces in drilling composite laminates* Proceedings of the Institution of Mechanical Engineers, Part B: Journal of Engineering Manufacture, 2001. 215(2).
67. Tsao, C.C., *Prediction of thrust force of step drill in drilling composite material by Taguchi method and radial basis function network.* International Journal of Advanced Manufacturing Technology, 2008. 36(1-2): p. 11-18.
68. Tsao, C.C. and H. Hocheng, *Evaluation of thrust force and surface roughness in drilling composite maternal using Taguchi analysis and neural network.* Journal of Materials Processing Technology, 2008. 203(1-3): p. 342-348.
69. Tsao, C.C., *Investigation into the effects of drilling parameters on delamination by various step-core drills.* Journal of Materials Processing Technology, 2008. 206(1-3): p. 405-411.
70. Enemuoh, E.U., A.S. El-Gizawy, and A.C. Okafor, *An approach for development of damage-free drilling of carbon fiber reinforced thermosets.* International Journal of Machine Tools & Manufacture, 2001. 41(12): p. 1795-1814.
71. Won, M.S. and C.K.H. Dharan, *Chisel edge and pilot hole effects in drilling composite laminates.* Journal of Manufacturing Science and Engineering-Transactions of the ASME, 2002. 124(2): p. 242-247.
72. Won, M.S. and C.K.H. Dharan, *Drilling of aramid and carbon fiber polymer composites.* Journal of Manufacturing Science and Engineering-Transactions of the ASME, 2002. 124(4): p. 778-783.

73. Tsao, C.C. and H. Hocheng, *The effect of chisel length and associated pilot hole on delamination when drilling composite materials.* International Journal of Machine Tools and Manufacture, 2003. 43(11): p. 1087-1092.
74. Khashaba, U.A., *Delamination in drilling GFR-thermoset composites.* Composite Structures, 2004. 63(3-4): p. 313-327.
75. Capello, E., *Workpiece damping and its effect on delamination damage in drilling thin composite laminates.* Journal of Materials Processing Technology, 2004. 148(2): p. 186-195.
76. Davim, J.P., J.C. Rubio, and A.M. Abrao, *A novel approach based on digital image analysis to evaluate the delamination factor after drilling composite laminates.* Composites Science and Technology, 2007. 67(9): p. 1939-1945.
77. Seif, M.A., U.A. Khashaba, and R. Rojas-Oviedo, *Measuring delamination in carbon/epoxy composites using a shadow moire laser based imaging technique.* Composite Structures, 2007. 79(1): p. 113-118.
78. Gaitonde, V.N., S.R. Karnik, J.C. Rubio, A.E. Correia, A.M. Abrao, and J.P. Davim, *Analysis of parametric influence on delamination in high-speed drilling of carbon fiber reinforced plastic composites.* Journal of Materials Processing Technology, 2008. 203(1-3): p. 431-438.
79. Karnik, S.R., V.N. Gaitonde, J.C. Rubio, A.E. Correia, A.M. Abrao, and J.P. Davim, *Delamination analysis in high speed drilling of carbon fiber reinforced plastics (CFRP) using artificial neural network model.* Materials & Design, 2008. 29(9): p. 1768-1776.
80. Palanikumar, K., J.C. Rubio, A.M. Abrao, A.E. Correia, and J.P. Davim, *Influence of drill point angle in high speed drilling of glass fiber reinforced plastics.* Journal of Composite Materials, 2008. 42(24): p. 2585-2597.
81. Campos Rubio, J.C., A.M. Abrao, P. Eustaquio Faria, A.E. Correia, and J.P. Davim, *Delamination in High Speed Drilling of Carbon Fiber Reinforced Plastic (CFRP).* Journal of Composite Materials, 2008. 42(15): p. 1523-1532.
82. Shyha, I.S., D.K. Aspinwall, L.S. Soo, and S. Bradley, *Drill geometry and operating effects when cutting small diameter holes in CFRP*, in *The International conference on Advances in materials and Processing Technologies*. 2008
Manama, Kingdom of Bahrain. p. 12.
83. Lin, S.C. and I.K. Chen, *Drilling carbon fiber-reinforced composite material at high speed.* Wear, 1996. 194(1-2): p. 156-162.
84. Fernandes, M. and C. Cook, *Drilling of carbon composites using a one shot drill bit. Part I: Five stage representation of drilling and factors affecting maximum force and torque.* International Journal of Machine Tools & Manufacture, 2006. 46(1): p. 70-75.
85. Fernandes, M. and C. Cook, *Drilling of carbon composites using a one shot drill bit. Part II: Empirical modeling of maximum thrust force.* International Journal of Machine Tools & Manufacture, 2006. 46(1): p. 76-79.
86. Ni, W., *Orbital Drilling of Aerospace Materials.* SAE International, 2007.
87. Mathew, J., N. Ramakrishnan, and N.K. Naik, *Investigations into the effect of geometry of a trepanning tool on thrust and torque during drilling of GFRP composites.* Journal of Materials Processing Technology, 1999. 91(1-3): p. 1-11.
88. Wang, X., L.J. Wang, and J.P. Tao, *Investigation on thrust in vibration drilling of fiber-reinforced plastics.* Journal of Materials Processing Technology, 2004. 148(2): p. 239-244.
89. Zhang, L.B., L.J. Wang, X.Y. Liu, H.W. Zhao, X. Wang, and H.Y. Luo, *Mechanical model for predicting thrust and torque in vibration drilling fibre-reinforced composite*

materials. International Journal of Machine Tools & Manufacture, 2001. 41(5): p. 641-657.
90. Arul, S., L. Vijayaraghavan, S.K. Malhotra, and R. Krishnamurthy, *The effect of vibratory drilling on hole quality in polymeric composites.* International Journal of Machine Tools and Manufacture, 2006. 46(3-4): p. 252-259.
91. Ramulu, M., T. Branson, and D. Kim, *A study on the drilling of composite and titanium stacks.* Composite Structures, 2001. 54(1): p. 67-77.
92. Garrick, R., *Drilling advanced aircraft structures with PCD (poly-crystalline diamond) drills.* SAE International, 2007.
93. Zitoune, R., V. Krishnaraj, and F. Collombet, *Study of drilling of composite material and aluminium stack.* Composite Structures, 2010. 92(5): p. 1246-1255.
94. Kishore, R.A., R. Tiwari, A. Dvivedi, and I. Singh, *Taguchi analysis of the residual tensile strength after drilling in glass fiber reinforced epoxy composites.* Materials & Design, 2009. 30(6): p. 2186-2190.
95. Pihtili, H. and N. Canpolat, *Investigation of different reinforced composite materials for surface roughness and capacity of being drilled.* Journal of Composite Materials, 2009. 43(19): p. 2071-2080.
96. Shyha, I.S., D.K. Aspinwall, S.L. Soo, and S. Bradley, *Drill geometry and operating effects when cutting small diameter holes in CFRP.* International Journal of Machine Tools & Manufacture, 2009. 49(12-13): p. 1008-1014.
97. Marques, A.T., L.M. Durao, A.G. Magalhaes, J.F. Silva, and J. Tavares, *Delamination analysis of carbon fibre reinforced laminates: Evaluation of a special step drill.* Composites Science and Technology, 2009. 69(14): p. 2376-2382.
98. Krishnamoorthy, A., S.R. Boopathy, and K. Palanikumar, *Delamination analysis in drilling of CFRP composites using response surface methodology.* Journal of Composite Materials, 2009. 43(24): p. 2885-2902.
99. Iliescu, D., D. Gehin, M.E. Gutierrez, and F. Girot, *Modeling and tool wear in drilling of CFRP.* International Journal of Machine Tools & Manufacture, 2010. 50(2): p. 204-213.
100. Hocheng, H. and H.Y. Puw, *On drilling characteristics of fiber-reinforced thermoset and thermoplastics.* International Journal of Machine Tools & Manufacture, 1992. 32(4): p. 583-592.
101. Mohan, N.S., A. Ramachandra, and S.M. Kulkarni, *Machining of fiber-reinforced thermoplastics: Influence of feed and drill size on thrust force and torque during drilling.* Journal of Reinforced Plastics and Composites, 2005. 24(12): p. 1247-1257.
102. El-Sonbaty, I., U.A. Khashaba, and T. Machaly, *Factors affecting the machinability of GFR/epoxy composites.* Composite Structures, 2004. 63(3-4): p. 329-338.
103. Hocheng, H. and H.Y. Puw, *Machinability of fiber-reinforced thermoplastics in drilling.* Journal of Engineering Materials and Technology-Transactions of the Asme, 1993. 115(1): p. 146-149.
104. Durao, L.M.P., M. de Moura, and A.T. Marques, *Numerical simulation of the drilling process on carbon/epoxy composite laminates.* Composites (Part A : Applied Science and Manufacturing), 2006. 37(9): p. 1325-1333.
105. Rahme, P., Y. Landon, P. Lagarrigue, R. Piquet, F. Lachaud, B. Marguet, J. Bourriquet, and C. Le Roy, *Drilling of thick composite structure: State of the art*
SAE International, 2006.
106. Tsao, C.C. and H. Hocheng. *Effects of peripheral drilling moment on delamination using special drill bits*. Proceddings of 10th International Conference on Advances in

Materials and Processing Technologies (AMPT2007). 2007. Daejeon, South Korea, p. 471-476.
107. Zhang, H., W. Chen, D. Chen, and L. Zhang, *Assessment of the exit defects in carbon fibre-reinforced plastic plates caused by drilling.* Key Engineering Materials, 2001. 196: p. 43-52.
108. Park, K.Y., J.H. Choi, and D.G. Lee, *Delamination-free and high-efficiency drilling of carbon-fiber-reinforced plastics.* Journal of Composite Materials, 1995. 29(15): p. 1988-2002.
109. Hocheng, H. and C.C. Tsao. *Comprehensive analysis of delamination in drilling of composite materials with various drill bits*. Proceddings of 6th Asia Pacific Conference on Materials Processing (APCMP). 2003. Taipei, Taiwan, p. 335-339.
110. Tsao, C.C. and H. Hocheng, *Effect of eccentricity of twist drill and candle stick drill on delamination in drilling composite materials.* International Journal of Machine Tools & Manufacture, 2005. 45(2): p. 125-130.
111. Hocheng, H. and C.C. Tsao. *The path towards delamination-free drilling of composite materials*. Proceddings of International Forum on the Advances in Materials Processing Technology. 2005. Glasgow, Scotland, p. 251-264.
112. Persson, E., I. Eriksson, and L. Zackrisson, *Effects of hole machining defects on strength and fatigue life of composite laminates.* Composites Part A: Applied Science and Manufacturing, 1997. 28(2): p. 141-151.
113. Brinksmeier, E. and R. Janssen, *Drilling of multi-layer composite materials consisting of carbon fiber reinforced plastics (CFRP), titanium and aluminum Alloys.* CIRP Annals - Manufacturing Technology, 2002. 51(1): p. 87-90.
114. König, W. and P. Graß, *Quality definition and assessment in drilling of fibre reinforced thermosets.* CIRP Annals - Manufacturing Technology, 1989. 38(1): p. 119-124.
115. Langella, A. and M. Durante, *Comparison of tensile strength of composite material elements with drilled and molded-in holes.* Applied Composite Materials, 2008. 15(4-6): p. 227-239.
116. Murphy, C., G. Byrne, and M.D. Gilchrist, *The performance of coated tungsten carbide drills when machining carbon fibre-reinforced epoxy composite materials.* Proceedings of the Institution of Mechanical Engineers Part B-Journal of Engineering Manufacture, 2002. 216(2): p. 143-152.
117. Dharan, C.K.H. and M.S. Won, *Machining parameters for an intelligent machining system for composite laminates.* International Journal of Machine Tools and Manufacture, 2000. 40(3): p. 415-426.
118. Tsao, C.C. and H. Hocheng, *Taguchi analysis of delamination associated with various drill bits in drilling of composite material.* International Journal of Machine Tools and Manufacture, 2004. 44(10): p. 1085-1090.
119. Mathew, J., N. Ramakrishnan, and N.K. Naik, *Trepanning on unidirectional composites: delamination studies.* Composites Part A: Applied Science and Manufacturing, 1999. 30(8): p. 951-959.
120. Durao, L.M.P., M. de Moura, and A.T. Marques. *Numerical prediction of delamination onset in carbon/epoxy composites drilling*. Proceddings of Euromech Colloquium 473 on Fracture of Composite Materials. 2005. Oporto, Portugal, p. 2767-2778.
121. Guillaumat, L. and Z. Hamdoun, *Reliability model of drilled composite materials.* Composite Structures, 2006. 74(4): p. 467-474.
122. Stone, R. and K. Krishnamurthy, *A neural network thrust force controller to minimize delamination during drilling of graphite-epoxy laminates.* International Journal of Machine Tools & Manufacture, 1996. 36(9): p. 985-1003.

123. Tsao, C.C. and W.C. Chen, *Prediction of the location of delamination in the drilling of composite laminates.* Journal of Materials Processing Technology, 1997. 70(1-3): p. 185-189.
124. Zitoune, R. and F. Collombet, *Numerical prediction of the thrust force responsible of delamination during the drilling of the long-fibre composite structures.* Composites Part a-Applied Science and Manufacturing, 2007. 38(3): p. 858-866.
125. Tsao, C.C. and H. Hocheng, *Effects of exit back-up on delamination in drilling composite materials using a saw drill and a core drill.* International Journal of Machine Tools and Manufacture, 2005. 45(11): p. 1261-1270.
126. Tsao, C.C. and H. Hocheng, *Effect of tool wear on delamination in drilling composite materials.* International Journal of Mechanical Sciences, 2007. 49(8): p. 983-988.
127. Jung, J.P., G.W. Kim, and K.Y. Lee, *Critical thrust force at delamination propagation during drilling of angle-ply laminates.* Composite Structures, 2005. 68(4): p. 391-397.
128. Lachaud, F., R. Piquet, F. Collombet, and L. Surcin, *Drilling of composite structures.* Composite Structures, 2001. 52(3-4): p. 511-516.
129. Hamdoun, Z., L. Guillaumat, and J.L. Lataillade, *Influence of the drilling quality on the fatigue compression behaviour of carbon epoxy laminates.* International Journal of Fatigue, 2006. 28(1): p. 1-8.
130. Mkaddem, A. and M. El Mansori, *Finite element analysis when machining UGF-reinforced PMCs plates: Chip formation, crack propagation and induced-damage.* Materials & Design, 2009. 30(8): p. 3295-3302.
131. Mondelin, A., B. Furet, and J. Rech, *Characterisation of friction properties between a laminated carbon fibres reinforced polymer and a monocrystalline diamond under dry or lubricated conditions.* Tribology International. 43(9): p. 1665-1673.
132. SGS, *Know the drill*, in *Aerospace Manufacturing*. June 2012.
133. Abrate, S. and D.A. Walton, *Machining of composite materials. Part I: Traditional methods.* Composites Manufacturing, 1992. 3(2): p. 75-83.
134. Airbus, *Airbus UK Process Specification.* Machining Composites, 2004. ABP 6-2183(2): p. 36.
135. Denkena, B., D. Boehnke, and J.H. Dege, *Helical milling of CFRPâ€“titanium layer compounds.* CIRP Journal of Manufacturing Science and Technology, 2008. 1(2): p. 64-69.
136. Liu, J., D. Zhang, L. Qin, and L. Yan, *Feasibility study of the rotary ultrasonic elliptical machining of carbon fiber reinforced plastics (CFRP).* International Journal of Machine Tools and Manufacture, 2012. 53(1): p. 141-150.
137. Schulze, V., C. Becke, K. Weidenmann, and S. Dietrich, *Machining strategies for hole making in composites with minimal workpiece damage by directing the process forces inwards.* Journal of Materials Processing Technology. 211(3): p. 329-338.
138. Liu, D., Y. Tang, and W.L. Cong, *A review of mechanical drilling for composite laminates.* Composite Structures, 2012. 94(4): p. 1265-1279.
139. Hocheng, H., H.Y. Puw, and Y. Huang, *Preliminary study on milling of unidirectional carbon fibre-reinforced plastics.* Composites Manufacturing, 1993. 4(2): p. 103-108.
140. Klocke, F., W. Konig, S. Rummenholler, and C. Wurtz, *Milling of advanced composites*, in Machining of ceramics and composites, Jahanmir, Ramulu, and Koshy, Editors. 1999, Marcel Decker. p. 249-325, I S B N 08247-0178-x.
141. Youssef, H. and H. El-Hofy, *Machining technology - Machine tools and operations*. 2008: CRC Press, I S B N 978-1-4200-4339-6.

142. Richards, B., H. K, and W. S, *Lug cutting and trimming of the carbon fibre wing panels of the Airbus A400m with portable hand positioned tools.* SAE International, 2007. 2007-01-3795
143. Schulz, H. and T. Moriwaki, *High-speed Machining.* CIRP Annals - Manufacturing Technology, 1992. 41(2): p. 637-643.
144. *High speed machining and conventional die and mould machining.* Sandvik Coromant, 2003,C-5000 : 329
145. *Tool life testing in milling - Part 2 : End Milling*. 1989, ISO, I S B N ISO-8688-2.
146. Schmitz, T.L., J. Couey, E. Marsh, N. Mauntler, and D. Hughes, *Runout effects in milling: Surface finish, surface location error, and stability.* International Journal of Machine Tools and Manufacture, 2007. 47(5): p. 841-851.
147. Heisel, U. and M. Gringel, *Machine tool design requirements for high-speed machining.* CIRP Annals - Manufacturing Technology, 1996. 45(1): p. 389-392.
148. Nieminen, I., J. Paro, and V. Kauppinen. *High-speed milling of advanced materials*. Proceddings of International Conference on Advances in Materials and Processing Technologies (AMPT 93). 1996. Dublin, Ireland, p. 24-36.
149. Kauppinen, V. *High-speed milling - A new manufacturing technology*. Proceddings of 4th International Conference of the Danube-Adria-Association-for-Automation-Manufacturing (DAAAM). 2004. Tallinn, Estonia, p. 134-137.
150. Shen, B., F.H. Sun, H.G. Xue, M. Chen, and Z.M. Zhang, *Study on fabrication and cutting performance of high quality diamond coated PCB milling tools with complicated geometries.* Surface Engineering, 2009. 25(1): p. 70-76.
151. Colligan, K. and M. Ramulu, *Delamination in surface plies of graphite/epoxy caused by the edge trimming process.* Processing and manufacturing of composite materials (ASME), 1991. PED- Vol. 49/MD-Vol. 27: p. 113-125.
152. Colligan, K. and M. Ramulu, *The effect of edge trimming on composite surface plies* Manufacturing Review (USA) ASME 1992. 5(4): p. 274-283
153. Colligan, K. and M. Ramulu, *Edge trimming of graphite/ epoxy with diamond abrasive cutters.* Machining of advanced composites ASME, 1993. MD-Vol. 45/PED- Vol. 66: p. 19.
154. Ramulu, M. and E. Rogers, *Simulation of router action on a lathe to test the cutting tool performance in edge-trimming of graphite-epoxy composite.* Experimental Techniques, 1994. 18(2): p. 23-28.
155. Wurtz, C., S. Rummenholler, and F. Klocke, *Tool design for milling process of carbon fibre reinforced plastics (CFRP).* Engineering system design and analysis, ASME, 1996. 3: p. 29-32.
156. Klocke, F. and C. Wurtz, *The use of PCD tools for machining fibre reinforced materials*, in *ECCM-8*. 1998: Naples. p. 509-515.
157. Puw, H.Y. and H. Hocheng, *Milling of polymer composites*, in Machining of ceramics and composites, Jahanmir, Ramulu, and Koshy, Editors. 1999, Marcel Dekker. p. 267-294, I S B N 08247-0178-x.
158. Sheikh-Ahmad, J. and G. Sridhar, *Edge trimming of CFRP composites with diamond coated tools: Edge wear and surface characteristics.* SAE International, 2002. 2002-01-1526
159. Horman, S., J. Michael, and M. Collier, *Evaluation of different cutting tool technologies for machining carbon fiber reinforced plastics*, in *Composites Manufacturing 2008*. 2008, SME: 14-16 April, 2008 , Salt Lake City, UT, USA. p. 1-12.

160. Davim, J.P. and P. Reis, *Damage and dimensional precision on milling carbon fiber-reinforced plastics using design experiments.* Journal of Materials Processing Technology, 2005. 160(2): p. 160-167.
161. Ucar, M. and Y. Wang, *End-milling machinability of a carbon fiber reinforced laminated composite.* Journal of Advanced Materials, 2005. 37(4): p. 46-52.
162. Prashanth, J., J. Sheikh-Ahmad, and H. cheraghi, *Edge trimming of CFRP with diamond interlocked tools.* SAE International, 2006. 2006-01-3173
163. Inoue, T., M. Hagino, M. Matsui, and L.W. Gu, *Cutting characteristics of CFRP materials with end milling.* Progress of Machining Technology, 2009. 407-408: p. 710-713.
164. Ramulu, M., C.W. Wern, and J.L. Garbini, *Effect of fibre direction on surface roughness measurements of machined graphite/epoxy composite.* Composites Manufacturing, 1993. 4(1): p. 39-51.
165. Wang, Y., C. Sun, X. Yan, and K. Jiang, *Study on the surface delamination in milling carbon fiber reinforced plastic with PCD tool.* Advanced Materials Research, 2012. 381: p. 1-5.
166. Gao, G., Y. Zhao, and X. Ma, *Research on tool wear and surface characteristics in ultrasonic milling carbon fibre reinforced carbon composite.* Advanced Materials Research, 2011. 497: p. 299-303.
167. Li, Z., X. Wang, and B. Zhao, *An experiment study on milling forces in the ultrasonic milling of CFRP.* Advanced Materials Research, 2012. 472-475: p. 1028-1031.
168. Liu, D., H. Wang, H. Xu, and C. Zhang, *Study of milling force in high speed milling Carbon Fibre Reinforced Plastics(CFRP) using diamond tool.* Applied Mechanics and Materials, 2011. 50-51: p. 368-371.
169. Wang, Y.G., X.P. Yan, X.G. Chen, C.Y. Sun, and G. Liu, *Cutting performance of carbon fiber reinforced plastics using PCD tool*, in *Advanced Materials Research*. Hangzhou City. p. 14-18.
170. Rahim, E.A., Z. Mohid, M.F.M. Jamil, K.C. Mat, R. Koyasu, and H. Sasahara, *Experimental Study of Helical Milling on CFRP (Carbon Fibre Reinforced Polymer) for the Hole Making Process.* Advanced Materials Research, 2012. 576: p. 68-71.
171. Hintze, W., D. Hartmann, and C. Schutte, *Occurrence and propagation of delamination during the machining of carbon fibre reinforced plastics (CFRPs) - An experimental study.* Composites Science and Technology, 2011. 71(15): p. 1719-1726.
172. Iliescu, D., A. Fernandez, M.E. Gutiérrez-Orrantia, L.N.L.d. Lacalle, and F. Girot, *Modeling and Tool Wear in Routing of CFRP*, in *INTERNATIONAL CONFERENCE ON ADVANCES IN MATERIALS AND PROCESSING TECHNOLOGIES (AMPT2010)*. 2010, American Institute of Physics: Paris, France.
173. Seikh-Ahmad, J., J. Twomey, D. Kalla, and P. Lodhia, *Multiple regression and committee neural network force prediction models in milling FRP.* Machining science and technology, 2007. 11(3): p. 391-412.
174. Sheikh-Ahmad, J. and R. Yadav, *Model for predicting cutting forces in machining CFRP.* international Journal of Materials and Product Technology, 2008. 32(2/3): p. 152-167.
175. Rahman, M., S. Ramakrishna, and H.C. Thoo, *Machinability study of carbon/peek composites.* Machining Science and Technology, 1999. 3(1): p. 49-59.
176. Davim, J.P. and P. Reis, *Multiple regression analysis (MRA) in modelling milling of glass fibre reinforced plastics (GFRP).* International Journal of Manufacturing Technology and Management (IJMTM), 2004. 6(1/2): p. 185-197.

177. Davim, J.P., P. Reis, and C.C. Antonio, *A study on milling of glass fiber reinforced plastics manufactured by hand-lay-up using statistical analysis (ANOVA).* Composite Structures, 2004. 64(3-4): p. 493-500.
178. Lopez de Lacalle, N., A. Lamikiz, F.J. Campa, A.F. Valdivielso, and I. Etxeberria, *Design and test of a multitooth tool for CFRP milling.* Journal of Composite Materials, 2009. 43(26): p. 3275-3290.
179. Azmi, A., R. Lin, and D. Bhattacharyya, *Parametric study of end milling glass fibre reinforced composites.* AIP conference proceedings, International conference on advances in materials and processing technologies (AMPT2010), 2010: p. 1083-1088.
180. Azmi, A., R. Lin, and D. Bhattacharyya, *Machinability study of glass fibre-reinforced polymer composites during end milling.* The International Journal of Advanced Manufacturing Technology, 2012: p. 1-15.
181. Kalla, D., J. Sheikh-Ahmad, and J. Twomey, *Prediction of cutting forces in helical end milling fiber reinforced polymers.* International Journal of Machine Tools and Manufacture, 2010. 50(10): p. 882-891.
182. Sasahara, H., T. Nitta, and K. Nishi. *Analysis of tool temperature in high-speed milling*. Proceddings of 10th International Conference on Precision Engineering (ICPE). 2001. Yokohama, Japan, p. 279-283.
183. Schulz, H., *Hochgeschwindigkeits-bearbeitung*. 1996, Carl Hanser, Munich.
184. Ramulu, M., *Cutting-edge wear of polycrystalline diamond inserts in machining of fibrous composite material*, in Machining of ceramics and composites, Jahanmir, Ramulu, and Koshy, Editors. 1999, Marcel Dekker. p. 357-409, I S B N 08247-0178-x.
185. Konig, W., P. Grass, A. Heintze, F. Okey, and C. Schmitz-Justin, *Development in drilling & contouring composites containing Kevlar.* Production Engineer, 1984. 63(8): p. 56-61.
186. Reineck, I., M.E. Sjostrand, J. Karner, and M. Pedrazzini, *HCDCA diamond-coated cutting tools.* Diamond and Related Materials, 1996. 5(6-8): p. 819-824.
187. Davim, J.P., *Machining of Hard Materials*. 2011: Springer, I S B N 978-1-84996-449-4.
188. *Diamond tool materials for metalworking.* Element 6,
189. Dold, C., M. Henerichs, L. Bochmann, and K. Wegener, *Comparison of Ground and Laser Machined Polycrystalline Diamond (PCD) Tools in Cutting Carbon Fiber Reinforced Plastics (CFRP) for Aircraft Structures.* Procedia CIRP. 1(0): p. 178-183.
190. Deuerler, F., H. van den Berg, R. Tabersky, A. Freundlieb, M. Pies, and V. Buck, *Pretreatment of substrate surface for improved adhesion of diamond films on hard metal cutting tools.* Diamond and Related Materials, 1996. 5(12): p. 1478-1489.
191. Oles, E.J., A. Inspektor, and C.E. Bauer, *The new diamond-coated carbide cutting tools.* Diamond and Related Materials, 1996. 5(6-8): p. 617-624.
192. Holmberg, K. and A. mathews, *Coatings Tribology*, ed. D. Dowson. 1994: Elsevier, I S B N 0 444 88870 5.
193. Olsen, R.H., R.C. Dewes, and D.K. Aspinwall, *Machining of electrically conductive CVD diamond tool blanks using EDM.* Journal of Materials Processing Technology, 2004. 149(1-3): p. 627-632.
194. Stephan, P.M., R.A. Hay, and C.D. Dean, *The new diamond technology and its application in cutting tools.* Diamond and Related Materials, 1992. 1(5-6): p. 710-716.
195. Kennedy, B., *Competently cutting composites*, in *Cutting Tool Engineering*. 2008. p. 7-11.
196. Prashanth, J., *Tool wear of diamond interlocked tools in routing of CFRP composites.*, in *College of Engineering*. 2005, Wichita State University. p. 146.

197. Soo, S.L., I.S. Shyha, T. Barnett, D.K. Aspinwall, and W.-M. Sim, *Grinding performance and workpiece integrity when superabrasive edge routing carbon fibre reinforced plastic (CFRP) composites.* CIRP Annals - Manufacturing Technology, 2012. 61(1): p. 295-298.
198. Astakhov, V.P., *Ecological machining: Near-dry machining* in Machining, J.P. Davim, Editor. 2008, Springer. p. 195-223, I S B N 978-1-84800-212-8.
199. Su, Y., N. He, L. Li, and X.L. Li, *An experimental investigation of effects of cooling/lubrication conditions on tool wear in high-speed end milling of Ti-6Al-4V.* Wear, 2006. 261(7-8): p. 760-766.
200. Liao, Y.S., H.M. Lin, and Y.C. Chen, *Feasibility study of the minimum quantity lubrication in high-speed end milling of NAK80 hardened steel by coated carbide tool.* International Journal of Machine Tools and Manufacture, 2007. 47(11): p. 1667-1676.
201. Ueda, T., A. Hosokawa, and K. Yamada, *Effect of oil mist on tool temperature in cutting.* Journal of Manufacturing Science and Engineering-Transactions of the Asme, 2006. 128(1): p. 130-135.
202. Ko, T.J., H.S. Kim, and B.G. Chung, *Air-oil cooling method for turning of hardened material.* International Journal of Advanced Manufacturing Technology, 1999. 15(7): p. 470-477.
203. Rahman, M., A.S. Kumar, S. Manzoor Ul, and M.S. Ling, *Effect of chilled air on machining performance in end milling.* International Journal of Advanced Manufacturing Technology, 2003. 21(10-11): p. 787-795.
204. Su, Y., N. He, L. Li, A. Iqbal, M.H. Xiao, S. Xu, and B.G. Qu, *Refrigerated cooling air cutting of difficult-to-cut materials.* International Journal of Machine Tools & Manufacture, 2007. 47(6): p. 927-933.
205. Le Coz, G., M. Marinescu, A. Devillez, D. Dudzinski, and L. Velnom, *Measuring temperature of rotating cutting tools: Application to MQL drilling and dry milling of aerospace alloys.* Applied Thermal Engineering, 2012. 36(0): p. 434-441.
206. *Metal cutting Technology - Technical Guide* 2010: Sandvik Coromant, I S B N 1-800-726-3845.
207. *Tool cooling system : How it works*. 2013 30-04-2014]; Available from: http://nexflowair.com/tool_cooler_large_how_they_work.php#.UcdpB_nVDpU.
208. Davim, J.P., *Surface Integrity in Machining*. 2010: Springer, I S B N 978-1-84882-873-5.
209. Lou, S.J. and J.C. Chen, *In-process surface roughness recognition (ISRR) system in end-milling operations.* International Journal of Advanced Manufacturing Technology, 1999. 15(3): p. 200-209.
210. Ramulu, M., *Characterization of surface quality in machining of composites*, in Machining of ceramics and composites, Jahanmir, Ramulu, and Koshy, Editors. 1999, Marcel Dekker. p. 575-648, I S B N 08247-0178-x.
211. *Composites international news.* Composites, 1982. 13(3): p. 330-336.
212. Rusinek, R., *Cutting process of composite materials: An experimental study.* International Journal of Non-Linear Mechanics, 2010. 45(4): p. 458-462.
213. Kalla, D. and J. Twomey, *Committee Network (CN) force prediction model in milling of carbon fiber reinforced polymers*, in *2nd Annual Symposium on Graduate Research and Scholarly Projects.* . 2006, Wichita State University. Graduate School: Wichita, KS. p. 54-55.
214. Simulia, *Analysis of composite material uning Abaqus*. 2011, Dassult Systemes.

215. Rentsch, R., O. Pecat, and E. Brinksmeier, *Macro and micro process modeling of the cutting of carbon fiber reinforced plastics using FEM.* Procedia Engineering, 2011. 10(0): p. 1823-1828.
216. Karpat, Y., O. Bahtiyar, and B. Deger, *Mechanistic force modeling for milling of unidirectional carbon fiber reinforced polymer laminates.* International Journal of Machine Tools and Manufacture, 2012. 56: p. 79–93.
217. Karpat, Y., O. Bahtiyar, and B. Değer, *Milling Force Modelling of Multidirectional Carbon Fiber Reinforced Polymer Laminates.* Procedia CIRP, 2012. 1(0): p. 460-465.
218. El-Hofy, H., *Fundamentals of Machining Processes : Conventional and Nonconventional Processes*. Second Edition. 2014: CRC Press, I S B N 978-1-4665-7702-2.
219. Abrate, S. and D. Walton, *Machining of composite materials. Part II: Non-traditional methods.* Composites Manufacturing, 1992. 3(2): p. 85-94.
220. Negarestani, R., M. Sundar, M.A. Sheikh, P. Mativenga, L. Li, Z.L. Li, P.L. Chu, C.C. Khin, H.Y. Zheng, and G.C. Lim, *Numerical simulation of laser machining of carbon-fibre-reinforced composites.* Proceedings of the Institution of Mechanical Engineers Part B-Journal of Engineering Manufacture, 2009. 224(B7): p. 1017-1027.
221. Folkes, J., *Waterjet-An innovative tool for manufacturing.* Journal of Materials Processing Technology, 2009. 209(20): p. 6181-6189.
222. Shanmugam, D.K., F.L. Chen, E. Siores, and M. Brandt. *Comparative study of jetting machining technologies over laser machining technology for cutting composite materials*. Proceddings of 11th International Conference on Composite Structures (ICCS 11). 2001. Melbourne, Australia, p. 289-296.
223. Shanmugam, D.K., T. Nguyen, and J. Wang, *A study of delamination on graphite/epoxy composites in abrasive waterjet machining.* Composites Part a-Applied Science and Manufacturing, 2008. 39(6): p. 923-929.
224. El-Hofy, H., *Advanced Machining Processes : Nontraditional and Hybrid Machining Processes*. 2005: McGraw-Hill, I S B N 9780071453349.
225. Grove, D.M. and T.P. Davis, *Engineering Quality and Experimental Design*. 1992: Longman Scientific & Technical, I S B N 0582066875.
226. Spur, G. and U. Lachmund, *Turning of fibre rinforced plastics*, in Machining of ceramics and composites, Jahanmir, Ramulu, and Koshy, Editors. 1999, Marcel Dekker. p. 209-248, I S B N 08247-0178-x.
227. Ross, P.J., *Taguchi Techniques for Quality Engineering*. Second edition. 1996: McGraw-Hill, I S B N 0070539588.
228. Davim, J.P., *Machining Composite Material*. 2010: ISTES Ltd, I S B N 1848211708.
229. Denkena, B., M. Krüger, D. Bachrathy, and G. Stepan, *Model based reconstruction of milled surface topography from measured cutting forces.* International Journal of Machine Tools and Manufacture, 2012. 54–55(0): p. 25-33.
230. Bissacco, G., H.N. Hansen, and L. De Chiffre. *Size Effects on Surface Generation in Micro Milling Hardened Tool Steel*. Proceddings of 2006. Elsevier BV, p. 593-596.
231. Zaghbani, I., J.F. Chatelain, V. Songmene, S. Berube, and A. Atarsia, *A comprehensive analysis of cutting forces during routing of multilayer carbon fiber-reinforced polymer laminates.* Journal of Composite Materials. 46(16): p. 1955-1971.
232. Ronkainen, H., S. Varjus, J. Koskinen, and K. Holmberg, *Differentiating the tribological performance of hydrogenated and hydrogen-free DLC coatings.* Wear, 2001. 249(3-4): p. 260-266.
233. Konig, W., P. Grass, C. Wulf, and H. Willerscheid, *Machining of fibre reinforced plastics.* CIRP Annals, 1985. Manufacturing Technology 34(No.2): p. 537-548.

234. Sato, M., N. Tamura, and H. Tanaka, *Temperature Variation in the Cutting Tool in End Milling.* Journal of Manufacturing Science and Engineering, 2011. 133(2): p. 021005-021005.
235. Davis, G., *Abrasive water jet (AWJ) cutting cost for 10 mm thick CFRP*, M. El-Hofy, Editor. 2013.

7 APPENDICES

Appendix-A: Material properties

Table 7.1: Properties of various fibres and whiskers [11]

Material	Density (g/cm^3)	Tensile strength (GPa)	Modulus of elasticity (GPa)	Ductility (%)	Melting temperature (°C)	Specific modulus (10^6 m)	Specific strength (10^4 m)
E-glass	2.55	3.4	72.4	4.7	<1725	2.90	14
S-glass	2.50	4.5	86.9	5.2	<1725	3.56	18
SiO_2	2.19	5.9	72.4	8.1	1728	3.38	27.4
Al_2O_3	3.95	2.1	86.9	0.55	2015	9.86	5.3
ZrO_2	4.84	2.1	42.4	0.62	2677	7.26	4.3
Carbon (high strength)	1.5	5.7	340	2.0	3700	18.8	19
Carbon (high modulus)	1.5	1.9	280	0.36	3700	36.3	13
BN	1.9	1.4	530	1.6	2730	4.87	7.4
Boron	2.36	3.4	90	0.89	2030	16.4	12
B_4C	2.36	2.3	480	0.48	2450	20.9	9.9
SiC	4.09	2.1	480	0.44	2700	12.0	5.1
TiB_2	4.48	0.10	510	0.02	2980	11.6	0.3
Be	1.83	1.28	300	0.4	1277	19.7	7.1
W	19.4	4.0	410	0.95	3410	2.2	2
Polyethelene	0.97	2.59	120	2.2	147	12.4	27.4
Kevlar	1.44	4.5	120	3.8	500	8.81	25.7
Al_2O_3whiskers	3.96	21	430	4.9	1982	11.0	53.3
BeO whiskers	2.85	13	340	3.8	2550	12.3	47.0
B_4C whiskers	2.52	14	480	2.9	2450	19.5	56.1
SiC whiskers	3.18	21	480	4.4	2700	15.4	66.5
Si_3N_4 whiskers	3.18	14	380	3.7		12.1	44.5
Graphite whiskers	1.66	21	703	3.0	3700	43	128
Cr whiskers	7.2	8.90	240	3.7	1890	3.40	12

Appendix-B: Laminate fabrication procedure (lay-up)

Manual layup: the layup process was carried out in clean room at regulated and controlled temperature and humidity on a special table with a glass surface with a bar to hold the roll of prepreg material. A roll of prepreg (130 m long × 0.6 m wide) stored in a freezer (at -16˚) needed to defrost in its sealed bag for use, otherwise they were stored to maintain shelf life (30 days). The typical layup sequence included defrosting of the material for 24 hours at room temperature (20˚C), preparing a table for cutting by adding guide cork, use of the steel triangle, steel ruler, and a knife to cut plies to size, then sorting the cut plies according to the manufacturing instructions sheet (MIS). Plies with 90˚ and 0˚ are directly to size, while those with 45˚ or 135˚ required cutting at angle the stitching the plies from the release film side using flash tape then finally cutting to size, see Figure 7.1.

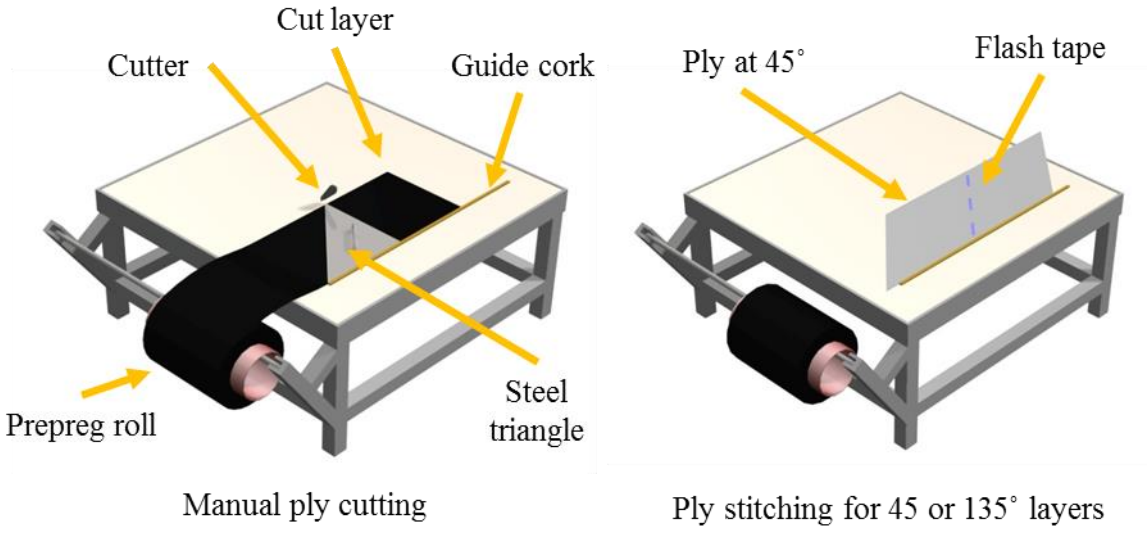

Figure 7.1: Manual ply cutting (left), stitching of plies (right)

A layup vacuum bag is prepared using layers of different materials to ensure extraction of any excess air entrapped in-between the plies. Each laid up ply is then pressed with a square Teflon edge squeegee to remove any entrapped air and to achieve good adhesion. After each 4 plies, the vacuum bag is sealed and vacuum is applied for 4 minutes for ‘debulking’ and removing any trapped air, see Figure 7.2 .

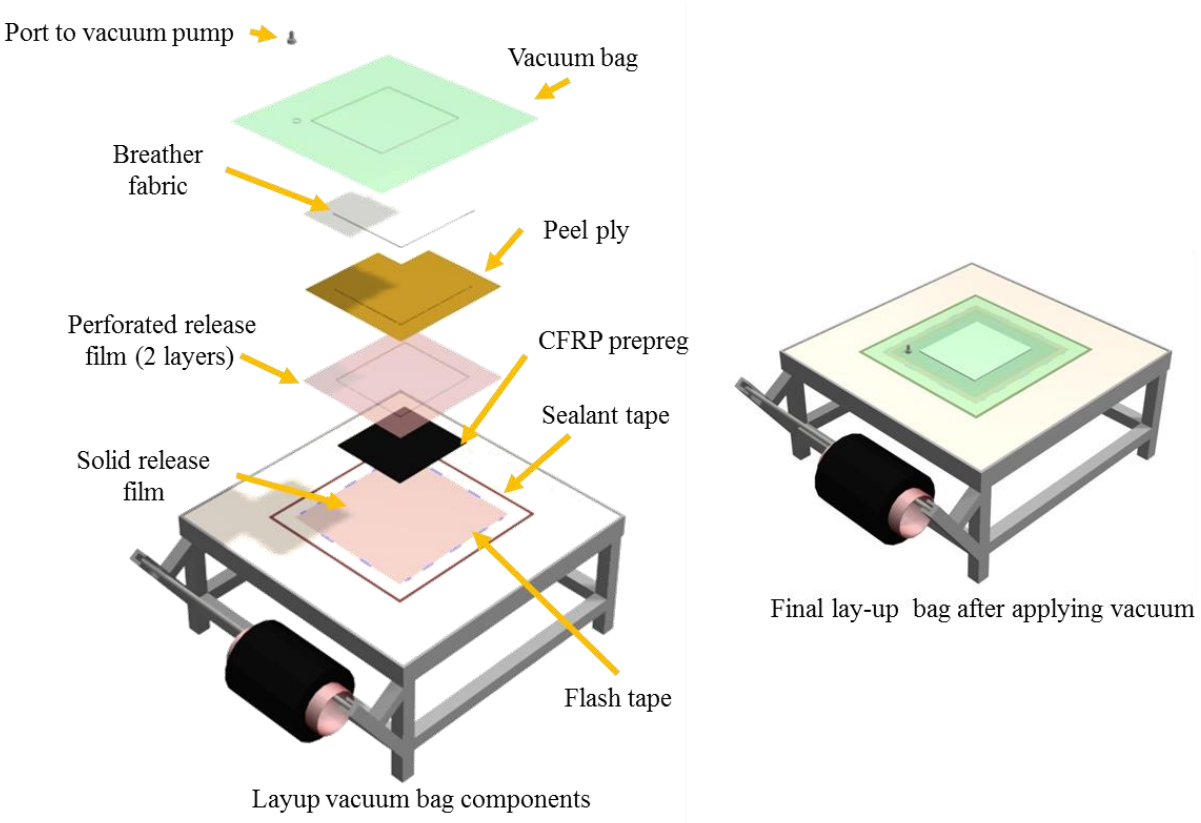

Figure 7.2: components of layup vacuum bag and a final layup under vacuum

Autoclave curing process: it is recommended to store the laid up panel to maintain shelf life and cure sooner after the layup. A flat aluminium plate is cleaned using a chemical release agent (solvent) to remove any residues from previous cures a step requires safety precautions such as special glove and heavy duty face mask to avoid toxic fumes. Laminated panels are bagged up for curing in the autoclave, surrounded with cork, and thermocouples are embedded to monitor the instantaneous temperature of panels. Figure 7.3 shows typical components of a vacuum bag while Figure 7.4 shows the cork dam, thermocouple, and the final bag ready for curing in an autoclave. Autoclave cycle and typical process parameters are shown in Figure 7.5. Panel testing: Following the curing process, cured panels are sent to NDT to be checked for defects using a gantry Ultrasonic C-scan machine. Figure 7.5 shows a typical C-scan test results.

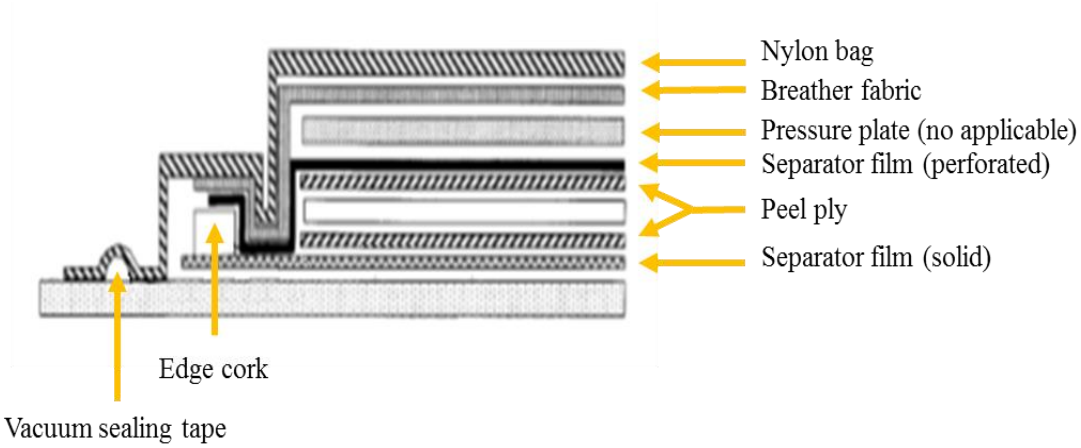

Figure 7.3: Typical curing bag components (Courtesy of Airbus)

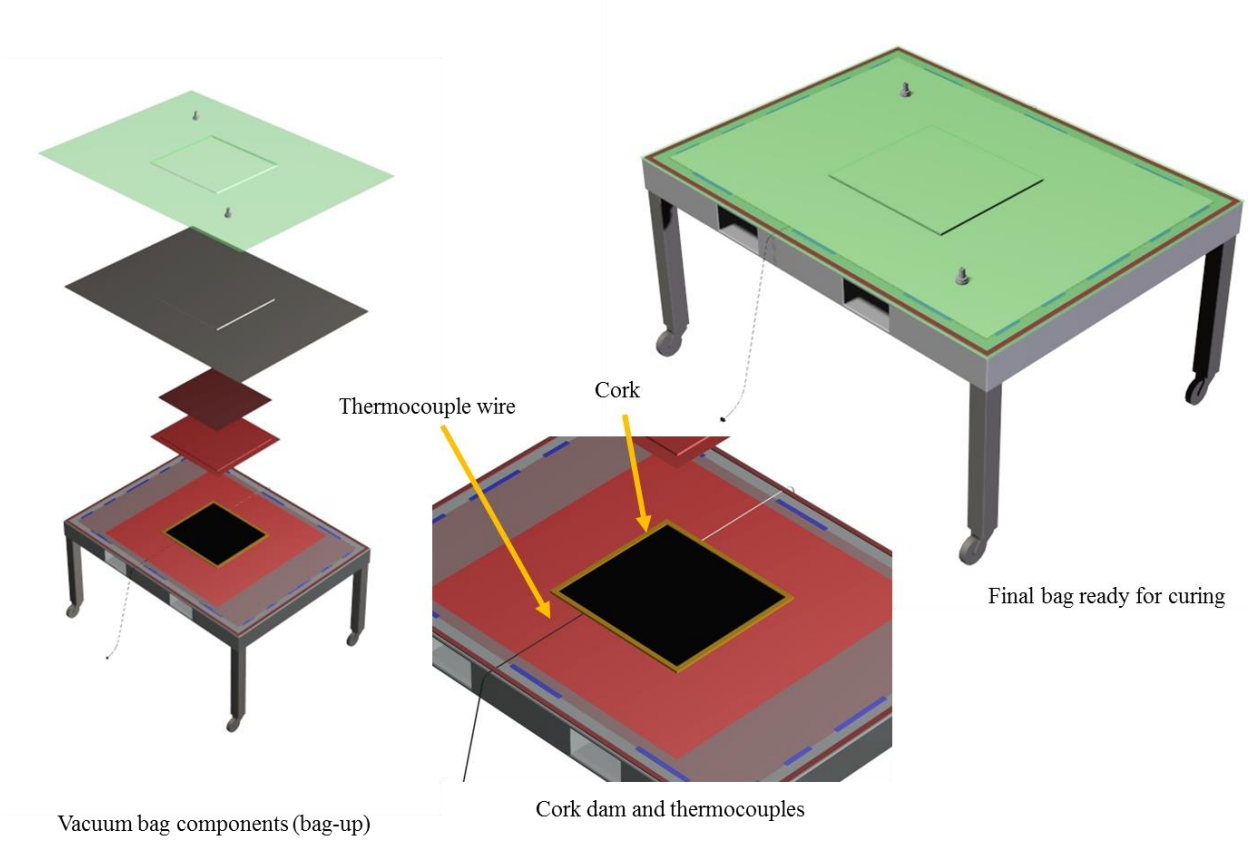

Figure 7.4: Vacuum bag prepared for autoclave curing

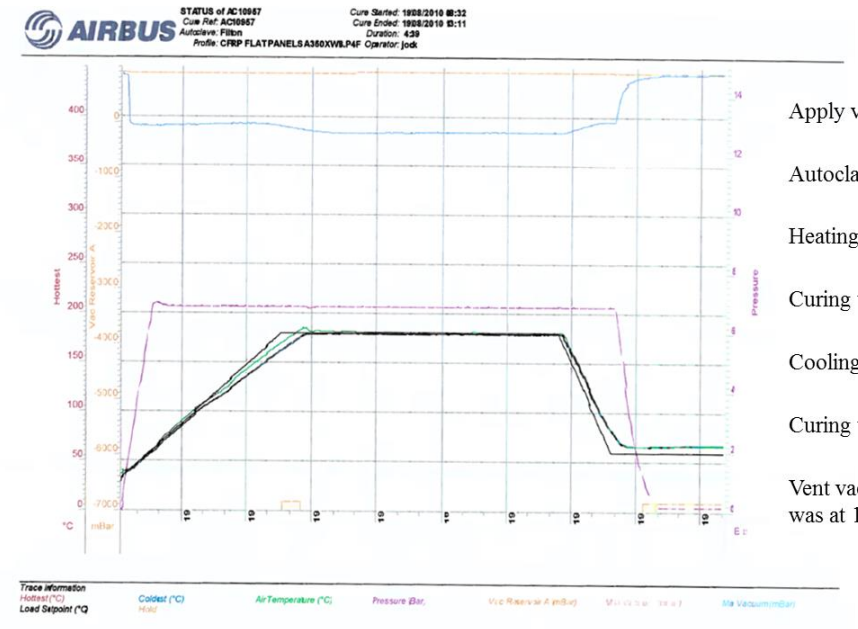

Figure 7.5: Curing cycle pressure-temperature over time graph

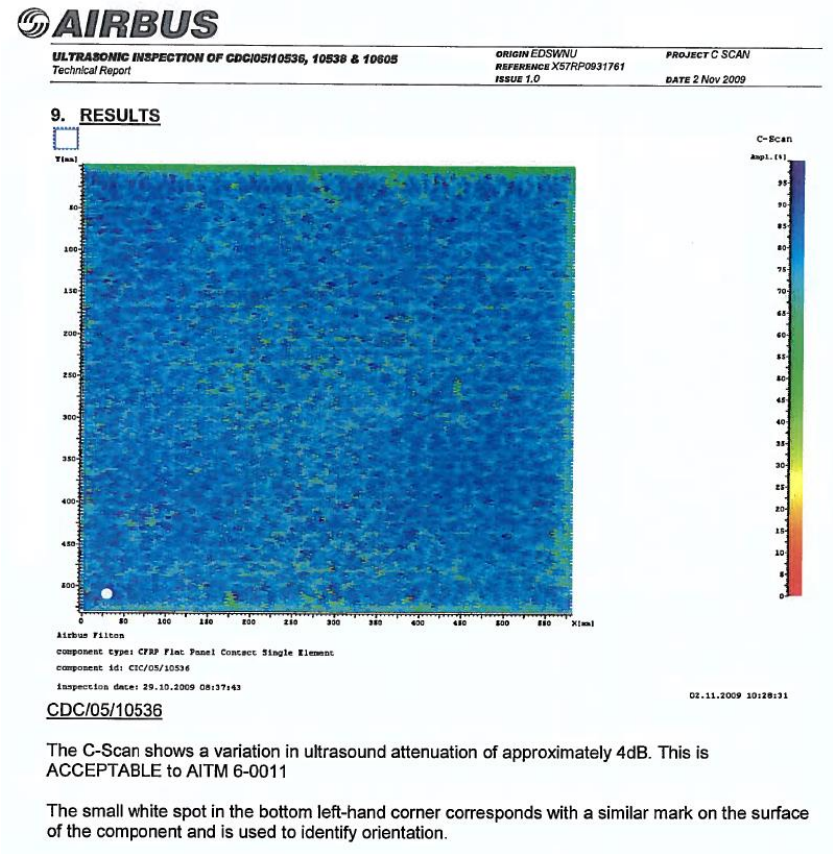

Figure 7.6: Typical C-scan result showing a defect free panel

Appendix-C: Material safety datasheet (sample)

SOFICAR	MATERIAL SAFETY DATA SHEET (ISO DIS 11014)	No.	AQ.999
	TORAYCA® CARBON FIBRE PREPREG	Date	Sept. 2005

1. Chemical Product and Company Identification.

Product name: **TORAYCA CARBON FIBRE PREPREG 180° Cure** (Group 6 Resin #3910, #3911)
Manufacturer name: **TORAY Industries, Inc.**
Address: 2-1 Nihonbashi-Muromachi 2-Chome, CHUO-KU TOKYO 103 JAPAN

Contacts:

- in Europe: **Société des Fibres de Carbone S.A. - SOFICAR**
  Technical Customer Support
  Telephone N°: +33 145 111 280
- in Japan: **ACM Technology Dept.**
  Gal Manager of ACM Technology Dept.
  Telephone N°: +81 332 455 762

2. Composition/Information on ingredients

Chemical name: **TORAYCA CARBON FIBRE PREPREG 180° Cure** (Resin #3910, #3911)
Common chemical name: Prepreg
Substance/mixture: Mixture

Hazardous Components	*WT%*
Fiber or woven fabric Carbon fiber (PAN based)	50 – 70
Thermoplastic resin	5 – 15
Bisphenol F type epoxy resin, CAS N°: 58421-55-9, R36 R38 R43	2 - 10
Hardener	15 - 25
Polymer additive	5 - 15

3. Hazards Identification

Main Routes of Entry: Dermal contact, ingestion
Carcinogenicity inds: NA

Adverse human health effects:

- Irritating to eyes
- Irritating to skin
- May cause sensitization by skin contact.

Environmental effects:

- The dust of hardened prepreg or carbon fiber fuzz may cause short circuit when contacted to electrical apparatus.

Appendix-D: Carbon fibre properties

Toray carbon fibres T800S can be supplied in 3 different twist configurations (A= twisted yarn, B= untwisted yarn from twisted yarn by untwisting process and C= never twisted).

TECHNICAL DATA SHEET
No. CFA-019

TORAYCA®
T800S DATA SHEET

Intermediate modulus, high tensile strength fiber, developed as a cost effective alternative to T800H. This never twisted fiber has excellent tensile composite properties and is specifically designed to meet the weight saving demand of aircraft and high performance recreational products.

FIBER PROPERTIES

	English	Metric	Test Method
Tensile Strength	850 ksi	5,880 MPa	TY-030B-01
Tensile Modulus	42.7 Msi	294 GPa	TY-030B-01
Strain	2.0 %	2.0 %	TY-030B-01
Density	0.065 lbs/in^3	1.80 g/cm^3	TY-030B-02
Filament Diameter	2.0E-04 in.	5 µm	
Yield 24K	1,446 ft/lbs	1,030 g/1000m	TY-030B-03
Sizing Type & Amount	10E	0.5 %	TY-030B-05
Twist	Never twisted		

PRELIMINARY COMPOSITE PROPERTIES*

Tensile Strength (RT)	430 ksi	2,950 MPa
Tensile Strength (-75°F)	415 ksi	2,860 MPa
Tensile Modulus (RT)	22.5 Msi	154 GPa
Open Hole Tensile Strength	70.5 ksi	487 MPa
Open Hole Compressive Strength (RT)	42.0 ksi	291 MPa
Open Hole Compressive Strength (180°F/wet)	33.0 ksi	229 MPa
CAI	43.5 ksi	300 MPa
CILS	12.5 ksi	85 MPa

* Toray 350°F Toughened Epoxy Resin. Normalized to 60% fiber volume.

See Section 4 for Safety & Handling Information. The above properties do not constitute any warranty or guarantee of values. These values are for material selection purposes only. For applications requiring guaranteed values, contact our sales and technical team to establish a material specification document.

TORAY CARBON FIBERS AMERICA, INC.

Appendix-E: ANOVA analysis equations

Percentage contribution (PCR) was calculated using Equation 1 [227] where SSA is the sum of squares for a factor, DOFA is the degree of freedom of that factor, MSE is the mean square of error, and SST is the sum of squares total. The error percentage was calculated using Equation 2.

$$PCR = 100\ [SSA\text{-}DOFA(MSE)]/\ SST \qquad \text{Equation 7.1}$$

$$\text{Error \%} = 100 - \%\ PCR\ of\ all\ factors \qquad \text{Equation 7.2}$$

Appendix-F: CNC program code

Slotting full engagement coupon

The CNC code for slotting (full engagement of 12 mm) is detailed in Table 7.2 while the tool path is shown in Figure 7.7.

Table 7.2: CNC program for slotting

Main CNC code (P500)	**Subroutine for slotting (P501)**
G21 ; M98 P9007 T19 ; M6 ; G59 G90 X16.0 Y–10.0 G43 H19 Z10.0 F1000 ; S 9289 M01 ; M03 ; G0 Z–5.0 ; M98 P501 L3 ;	G90 G1 Y110.0 F1858 ; G0 Z100.0 ; Y–10.0 ; G91 X34.0 ; M01 ; M03 ; G90 Z-5.0 ; M99 ;

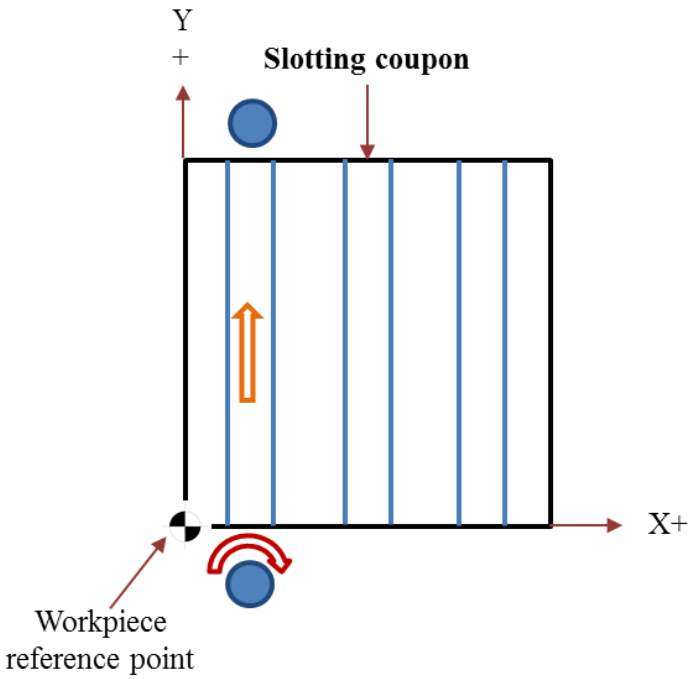

Figure 7.7: Router path in slotting of surface integrity coupon

Tool life ¾ engagement

Table 7.3 shows the machine program for milling the tool life coupon using ¾ engagement (9 mm width of cut) either cutting 250 mm by 250 mm length or continuously. Figure 7.8 shows the tools path.

Table 7.3: CNC program for milling tool life coupon

Main CNC code (P510)	**Subroutine for desecrate cut (P511)**	**Subroutine for continuous cut (P511)**
G21 ; M98 P9007 T19 ; M6 ; G58 G90 X10.0 Y-8.0 ; G43 H19 Z10.0 F1000 ; S5308 M03 ; G0 Z-5.0 ; G1 Y3.0 F2548 ; M98 P511 L13 ; G0 Z 200.0 ; Y50.0 ; M30 ;	G90 G1 X250.0 ; G0 Z100.0 ; M01 ; M03 ; Z 5.0 ; G1 Z-5.0 ; G91 Y9.0 ; G90 X10.0 ; G0 Z100.0 M01 ; M03 ; Z5.0 ; G1 Z-5.0 ; G91 Y9.0 ; M99 ;	G 90 G1 X250.0 ; G91 X250.0 ; G91 Y9.0 ; G90 X10.0 ; G91 Y9.0 ; M99 ;

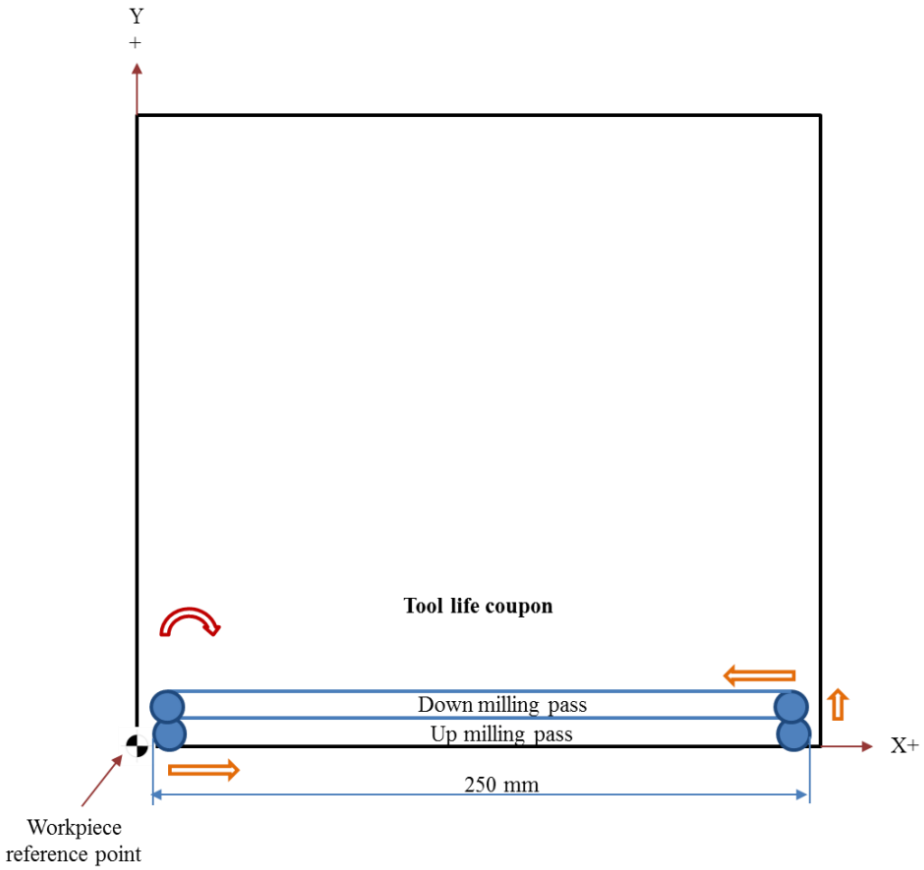

Figure 7.8: Router path in milling of tool life coupon

Appendix-G: Fuzz and delamination measurements

Table 7.4: Benchmarking test at 500 m/min cutting speed 0.15 mm/tooth in Twin-Nozzle CA environment (Phase-1C)

	Width of damage		**DF**		**Fuzz length**		**Slot width**	
	New	Worn	New	Worn	New	Worn	New	Worn
WPC-102 PCD	17.56	18.84	1.46	1.57	7.02	9.72	12.04	11.97
CTB-010 PCD	17.01	21.77	1.42	1.81	7.81	9.80	12.04	11.78

Table 7.5: CTB-010 PCD confirmation test at 500 m/min cutting speed, 0.15 mm/tooth and CA Twin-Nozzle environment

	Slot-1	**Slot-2**	**Slot-3**	**Slot-4**	**Slot-5**	**Slot-6**
Damage width	17.01	17.03	16.23	16.64	17.37	17.10
DF	1.417	1.42	1.352	1.39	1.45	1.49
Slot width	12.04	12.05	11.96	12.03	12.05	11.97
Fuzz length	7.81	4.11	4.03	7.10	7.44	8.88
	Slot-7	**Slot-8**	**Slot-9**	**Slot-10**	**Slot-11**	**Slot-12**
Damage width	18.97	20.94	20.28	19.46	22.63	21.77
DF	1.58	1.74	1.69	1.62	1.89	1.81
Slot width	11.97	12	11.82	11.96	11.91	11.78
Fuzz length	8.79	8.67	9.07	9.05	9.04	9.80

Table 7.6: Phase-2B tests delamination (new tool)

	Width of damage	**DF**	**Width of slot**	**Fuzz length**
Test-1	15.03	1.25	12.08	2.80
Test-2	16.04	1.34	12.15	4.52
Test-3	16.19	1.35	12.12	4.93
Test-4	17.09	1.42	12.10	7.19
Test-5	16.99	1.42	12.02	5.32
Test-6	17.51	1.46	11.96	6.47
Test-7	15.04	1.25	12.21	5.62
Test-8	16.22	1.35	12.02	2.59
Test-9	16.77	1.40	12.02	3.55
Test-10	17.38	1.45	12.04	5.24
Test-11	20.17	1.68	11.96	7.16
Test-12	17.18	1.43	12.06	8.58

Table 7.7: CTB-010 PCD (Phase-2 Test-10) Single-Nozzle CA

	Slot-1	**Slot-2**	**Slot-3**	**Slot-4**	**Slot-5**	**Slot-6**
Damage width	17.38	16.99	17.37	17.02	17.37	17.13
DF	1.448	1.42	1.45	1.42	1.45	1.42
Slot width	12.035	12.01	12.05	12.09	12.01	12.09
Fuzz length	5.24	8.54	9.19	7.09	8.71	7.81
	Slot-7	**Slot-8**	**Slot-9**	**Slot-10**	**Slot-11**	**Slot-12**
Damage width	18.23	17.66	17.22	17.56	20.08	20.02
DF	1.52	1.47	1.43	1.46	1.67	1.66
Slot width	11.95	12.02	11.96	11.97	11.95	12.02
Fuzz length	9.95	8.93	8.73	10.17	9.34	9.67

Table 7.8: Benchmarking at 500 m/min cutting speed and 0.15 mm/tooth feed rate in Twin-Nozzle CA environment (Phase-3B)

	Width of damage		**DF**		**Fuzz length**		**Slot width**	
	New	**Worn**	**New**	**Worn**	**New**	**Worn**	**New**	**Worn**
CMX-850	17.32	17.71	1.44	1.47	7.01	9.84	12.01	11.96
MegaDiamond	16.09	20.17	1.34	1.68	5.77	9.37	12.31	11.82

Appendix-H: Routers unit cost

Table 7.9: Routers, codes and unit cost

Router	**Code**	**Unit cost**
Element-6 CTM-302 PCD	Seco Reaming 28108-928	£310.00
Element-6 CTB-010 PCD (mechanically ground)	Seco Reaming 28156-928	£310.00
Element-6 CMX-850 PCD	Seco Reaming 28155-928	£310.00
Element-6 WPC-102 PCD	Seco 02692693	£310.00
Seco-Mega-Diamond PCD router	SECO 890120E35.0Z2A 8002081-0018 DC-12	£361.00
Element-6 CTB-010 PCD (wire cut)	SECO BR28155 02692693 4361079 020/026	£310.00
Uncoated Burr router	SECO 871120.0 4486035-014	£59.90
Diamond coated (DURA) Burr router	SECO 871120.0 – Dura 4431601 - 011	£144.00
Uncoated carbide router	Jabro tools 94120 d=12 87250 AMG	£72.30
Diamond like carbon (DLC) coated WC	Seco Jabro A033798-02696031	£155.37
Diamond coated (DURA) WC	Seco 02692693	£169.00